THIAMIN DIPHOSPHATE CATALYSIS IN *ESCHERICHIA COLI* PYRUVATE DEHYDROGENASE MULTI-ENZYME COMPLEX: ACTIVATION, COVALENT ELECTROPHILIC CATALYSIS, AND SUBSTRATE CHANNELING

By

ANAND BALAKRISHNAN

A Dissertation submitted to the

Graduate School-Newark

Rutgers, The State University of New Jersey

in partial fulfillment of the requirements

for the degree of

Doctor of Philosophy

Graduate Program in Chemistry

written under the direction of

Professor Frank Jordan

and approved by

_____

_____

_____

_____

Newark, New Jersey

May, 2011

ABSTRACT OF THE THESIS

Thiamin Diphosphate Catalysis in *Escherichia coli* Pyruvate Dehydrogenase Multi-enzyme Complex: Activation, Covalent Electrophilic Catalysis, and Substrate Channeling

By

Anand Balakrishnan

Thesis Director: Professor Frank Jordan

Spectroscopic identification and characterization of covalent and non-covalent intermediates on large enzyme complexes is an exciting and challenging area of modern enzymology. While nuclear magnetic resonance (NMR) methods which provide detailed chemical insights have been successfully employed previously, limited examples are available in the literature for large enzyme complexes. Enzymes utilizing cofactors provide promising examples for such studies when synthetic routes to labeled cofactor analogs and protocols for reconstitution of apo-enzymes with such analogs are readily available.

Syntheses of key isotope enriched thiamin diphosphate (ThDP) analogs – [C2, C6' – $^{13}C_2$] ThDP, [N4' – ^{15}N]ThDP and [C2 – ^{13}C]ThDP – enabled first detection of (i) various ionization/tautomerization states of ThDP during the catalytic cycle of three ThDP dependent enzymes using cross polarization magic angle spinning (CPMAS) solid state NMR (SSNMR) spectroscopy and (ii) [C2, C6' – $^{13}C_2$] ThDP covalent intermediates on the E1 component (E1p) during the catalytic cycle of *E. coli* pyruvate dehydrogenase multi-enzyme complex (PDHc) by filter experiments including solution 1-D ^{1}H-^{13}C HSQC NMR.

Direct evidence was gathered for the 4'-aminopyrimidinium form (APH^+) on ThDP molecules bound to (i) *S. cerevisiae* yeast pyruvate decarboxylase (YPDC) (ii) E1p and (iii) the E1 component of *E. coli* 2-oxoglutarate dehydrogenase complex (E1o) using ^{13}C and ^{15}N CPMAS SSNMR. The thiazolium C2-H bond was found to be slightly acidic in the cofactor bound to these enzymes. ^{15}N SSNMR experiments confirmed the formation of the 1',4'-iminopyrimidine tautomer in presence of substrate analogs; a mechanism is proposed for the stabilization of this biologically rare tautomer in enzyme active-sites.

Using rapid chemical quench in conjunction with solution NMR, pre-steady state analyses were performed on the native PDHc and PDH complexes reconstituted with E1p active-site loop variants of very low PDHc activity. The C2-α-lactylThDP intermediate could not be detected under any of the conditions used, indicating that its formation is slower than its decarboxylation. The enamine intermediate accumulates at a rate 110 s^{-1} on E1p and PDHc, while the rates are 100-fold slower for the PDHc variants. 2-acetylThDP could be detected on E1p only during its reaction with pyruvate and the artificial electron acceptor DCPIP. Reductive acetylation of the lipoyl domain in a pre-steady state single turn-over experiment (a model for the E1p-E2p reductive acetyl transfer reaction) was determined by mass spectrometry. Combined, these kinetic results from artificial oxidation reactions suggest the enamine is very well stabilized by E1p and oxidation of the enamine and substrate channeling to E2p are favored by intact PDHc.

These studies provide unprecedented insight into the acid-base and covalent electrophilic roles of ThDP in enzyme catalysis and the methods described herein are applicable to all such complexes.

ACKNOWLEDGEMENTS

Professor Jordan, my mentor, has been my primary source of strength and encouragement throughout the course of my graduate research work. His kind guidance - marked by his unbounded patience, incisive scientific insights, and the complete freedom to test new ideas – presented abundant opportunities for learning and my overall scientific development. I will cherish forever his kind and encouraging words when I was disheartened and our chats about everything under the sun during more contented times. Being his protégé is an honor and a cause of great pride.

I thank my thesis committee members for their valuable inputs during the course of my research and for their constructive remarks during my pre-oral presentation, dissertation defense, and for their critical review of this thesis. I thank Prof. Huskey for the helpful discussions on enzyme kinetics and equilibria in Chapter 3. I thank Prof. Farinas for the many helpful discussions during the course of my research and for his insightful remarks.

My very special thanks are due to Dr. Natalia Nemeria. Her constant support, encouragement and training were instrumental in my scientific development. Studies on the reductive acetylation reaction of PDHc using lipoyl domain construct and Mass Spectrometry were performed in collaboration with her.

This work was made possible by the alliance with various researchers. I take great pleasure in acknowledging their collaboration and feel honored to be part of such a team. I express my immense gratitude to Dr. Sumit Chakraborty for his support, encouragement and training during my initial years of graduate study. His synthesis of [C2, C6' – $^{13}C_2$]ThDP served as the starting point for this work. All the Solid State NMR

experimental work and Density Functional Theory calculations were performed under the expert guidance of Prof. Tatyana Polenova at the Department of Chemistry and Biochemistry, University of Delaware, Newark, DE. Solid State NMR experiments on model compounds and enzymes were performed by my colleague, Mr. Sivakumar Paramasivam, and all figures in this thesis illustrating the SS NMR spectra were produced by him. I thank Dr. Olga Dmitrenko for help with performing Density Functional Theory calculations. Special thanks are owed to Dr. Sachin Kale for his work on the E1p active-site dynamic loops. Initial ideas for the studies described in Chapter 2 originated during our discussions, and plasmids encoding the E1p variants used during the course of this work were created by him. Special thanks are also due to Dr. Ahmet T. Baykal for his synthesis and NMR work on the models for 1'4'-iminopyrimidine. I thank Dr. Lazaros Kakalis for help with the design and setup of various NMR experiments. [C2 – ^{13}C]Thiamin was a generous gift from Dr. John Schloss.

Special thanks go to my friend, Jaeyoung Song, for providing a constant source of friendship, encouragement and support, and for being there for me at all times. I consider it my fortune to be his friend. I am grateful to all my colleagues at the Chemistry Department for their valuable discussions and suggestions. I thank Dr. Roman Brukh, Ms. Maria Araujo, Mr. Paulo Vares, Ms. Judy Slocum, Ms. Louise Curry, Ms. Lorraine McClendon, and Ms. Monika Dabrowsky for their continued help.

Financial support during the course of this work by the Chemistry Department, Rutgers University, Newark, NJ, and by the National Institutes of Health, Bethesda, MD, is gratefully acknowledged.

Finally, I humbly express my gratitude to my parents for their infinite love, and for being the source and the sustenance of me and my dreams.

DEDICATIONS

Humbly dedicated to My Parents, and All My Teachers

and in fond memory of My Grandfather, Mr. T.S. Sundaram

TABLE OF CONTENTS

LIST OF TABLES

LIST OF FIGURES

LIST OF SCHEMES

ABBREVIATIONS

1-lip E2p	Dihydrolipoamide acetyltrasferase (single lipoyl domain)
3-lip E2p	Dihydrolipoamide acetyltrasferase (three lipoyl domain)
AcPhi	Sodium acetylphosphinate
AcThDP	C2-acetylthiamin diphosphate
ADH	Alcohol dehydrogenase
AEBSF	4-(2-aminoetyl) Benzensulfonyl fluoride
Acetyl CoA	Acetylcoenzyme A
ADP	Adenosine diphosphate
APH$^+$	4'-aminopyrimidine form of thiamindiphosphate bound to enzymes
APH$^+$	4'-aminopyrimidinium form of thiamin diphosphate bound to enzymes
ATP	Adenosine triphosphate
CD	Circular Dichroism
CoA	Coenzyme A
CPMAS	Cross polarization magic angle spinning
DCPIP	1,6-dichlorophenolindophenol
DEAE	Dietylaminoethyl
DFT	Density functional theory
DMSO	Dimethyl sulfoxide
DTT	Dithiothreitol
E1p	E1 component of *E. Coli* pyruvate dehydrogenase multienzyme complex
E1o	E1 component of *E. Coli* 2-oxoglutarate dehydrogenase multienzyme complex
E2p	*E. Coli* dihydrolipo-amide acetyltrasferase
E3p	*E. Coli* dihydrolipo-amide dehyrogenase
EDTA	Ethylenediamine tetraacetic acid
ESI	Electrospray ionization
FAD	Flavin adenine dinucleotide
FPLC	Fast protein liquid chromatography
FTMS	Fourier Transform Mass spectrometry

gCHSQC	gradient Carbon heteronuclear single quantum coherence
GC-MS	Gas chromatography - mass spectrometry
HEThDP	C2-α-hydroxyethylthiamin diphosphate
HLADH	horse liver alcohol dehydrogenase
HPLC	High performance liquid chromatography
HSQC	Heteronuclear single quantum coherence
IP	1',4'-iminopyrimidine form of thiamin diphosphate bound to enzymes
IPTG	Isopropyl-β-D-1-thiogalactopyranoside
K_d	Dissociation constant
$K_{d(ThDP)}$	Apparent coenzyme dissociation constant
K_m	Michaelis constant
$K_{m(ThDP)}$	Michaelis constant with respect to ThDP
LD	Lipoyl domain of *E. Coli* dihydrolipoamide acetyltrasferase
LThDP	C2-α-lactylthiamin diphosphate
MAP	Methyl acetylphos-phonate
MES	2-(N-morpholino) ethanesulfonic acid
MSP	methyl succinylphosphonate, disodium
mTPK	mouse thiaminpyrophospho kinase
NAD^+	Nicotinamide adenine dinucleotide (oxidized)
NADH	Nicotinamide adenine dinucleotide (reduced)
NMR	Nuclear magnetic resonance spectroscopy
PCR	Polymerase chain reaction
PDHc	Pyruvate dehydrogenase multienzyme complex
PDA	Photo diode array detector
PEG	Polyethylene glycol
PhiLThDP	C2-α-phosphinolactyl thiamin diphosphate
PLThDP	C2-α-phosphonolactyl thiamin diphosphate
PMSF	Phenylmethyl-sulfonyl fluoride
PP	Propionylphosphinate, sodium
ROCSA	Recoupling of chemical shift anisotropy

SDS	Sodium dodecyl sulfate
SDS-PAGE	SDS-polyacrylamide gel electrophoresis
SSNMR	Solid state nuclear magnetic resonance spectroscopy
TCA	Trichloroacetic acid
Th	Thiamin
Th.HCl	Thiamin chloride hydrochloride
ThDP	Thiamin diphosphate
THF	Tetrahydrofuran
TMS	Tetramethyl silane
Tris	2-amino-2-hydroxymethyl-1,3-propanediol
UV/Vis	Ultraviolet - visible
n_H	Hill coefficient
***Y*PDC**	Yeast pyruvate decarboxylase

CHAPTER 1 Elucidation of Proton Positions in Various Ionization and Tautomerization States of the Thiamin Coenzyme Bound to Enzymes Using Solid State Nuclear Magnetic Resonance

1. 1 INTRODUCTION

Over the past seven decades our understanding of thiamin diphosphate (ThDP) catalysis in biology has produced the current picture of its mechanism which is a fascinating synthesis of ideas ranging from acid-base catalysis to zwitterionic stabilization in the active centers. As prominent examples of electrophilic covalent catalysis, the ThDP superfamily of enzymes utilize to the full extent the bifunctionality of ThDP – acid-base catalysis via the 4'-aminopyrimidine ring, and umpohlung catalysis of the thiazolium ring – to catalyze both 2-oxoacid decarboxylation and C-C carboligation reactions (*1-14*). At the heart of the proposed catalytic mechanism common to all members of the ThDP superfamily of enzymes, are some critical protonation/deprotonation steps which lead to the activation of the aromatic rings of the cofactor (Scheme 1.1, left side). Protonation at the N1' position of the 4'-aminopyrimidine ring precedes its tautomerization to the 1',4'-iminopyrimidine form which assists deprotonation of the thiazolium C2-H proton producing the thiazolium Ylide, a central intermediate in all ThDP dependent catalysis (1). The Rutgers group has shown that circular dichroism (CD) spectroscopy could address some of these questions since all states of the coenzyme are chiral when enzyme bound. But, CD spectroscopy also has its limitations. Of the four species of ThDP postulated to co-exist prior to the arrival of substrate, CD signatures were characterized for the 4'-aminopyrimidine (AP) and 1',4'-

iminopyrimidine (IP) tautomers of the coenzyme on several enzymes, and the assignments were supported with corresponding chemical models (*15-20*). However, there is no conclusive spectroscopic evidence for the enzyme bound 4'-aminopyrimidinium ionization state (APH^+) or for the ylide (Yl).

Thiamin is protonated at the N1' position with a pKa of 4.85 units for this titration in water (*21*). However, various members of the ThDP superfamily of enzymes show optimal activity in the pH range 6 – 8 units. To achieve this optimal activity the enzymes have to perturb the pKa of the N1' position in enzyme bound forms of ThDP. As illustrated in (Scheme 1.1, left side), this essential step is key to the tautomerization of the 4'-aminopyrimidine ring to the more basic IP tautomer. Incorporation of ThDP analogs with C substitution at the 1' position and 3' position into apo YPDC produce inactive holo-enzyme for the 1' substituted analog, indicating the importance of the N atom (*3*). Substitution of the conserved Glu residue close to the N1' atom produced variants with compromised activities in many members of the ThDP superfamily; these experiments provide indirect support for protonation at N1' position on enzymes. One of the aims of the current study is to gather direct spectroscopic evidence for the enzyme bound APH^+ state.

Scheme 1.1 Catalytic cycle of YPDC.

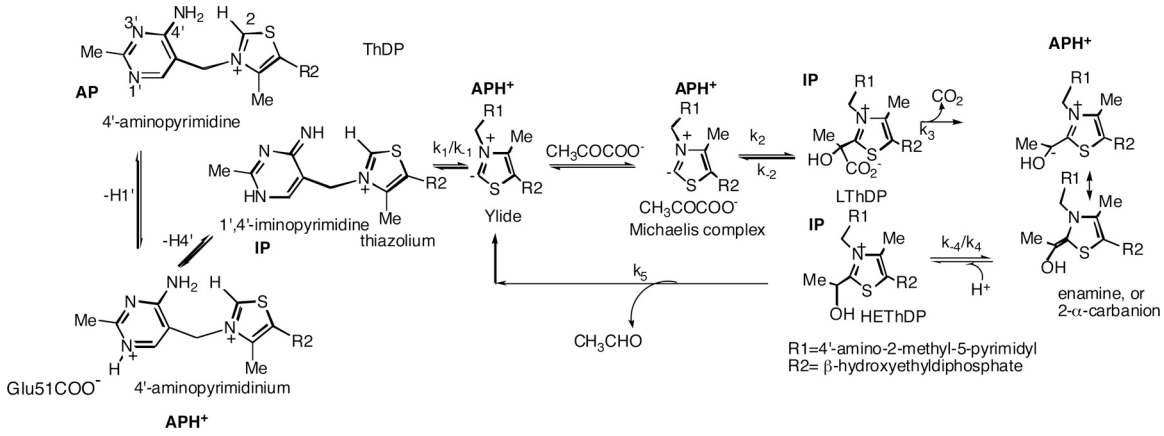

The ionization/tautomeric states of the 4'-aminopyrimidine ring are indicated in bold font.

While the IP tautomer has been shown to be stabilized in some enzymes prior to substrate addition, (E1 component of human pyruvate dehydrogenase complex, and pyruvate oxidase from *lactobacillus plantarum*) the IP tautomer was found to be the predominant tautomeric state accompanying tetrahederal substituent at the C2 position in ThDP bound to enzymes (*16, 17*). The proposed chemical steps leading to the formation of the IP tautomeric form of the 4-aminopyrimidine ring involve protonation of the incipient C2α-oxyanion by 4'-aminopyrimidine ring, now in the APH^+ state as illustrated in Scheme 1.2. X-ray structures of ThDP dependent enzymes containing the pre-decarboxylation intermediate analogs in the active-site show the C2α-O atom positioned closer to the N4' atom (*6, 13, 22, 23*) thus lending structural support for this proposed mechanism. Inter-atomic distances measured between C2α-O and N4' atoms in the E1 component of *E. coli* pyruvate dehydrogenase complex (E1p) and C2α-phosphonolactyl ThDP (PLThDP) complex (Figure 1.1) and on some similar such complexes are unusually short (see Table 1.1) as compared to the normal range for O···N H bonding distances (2.7 – 3.0Å). Conversely, migration of the proton from C2α-OH to N4' atom precedes the decomposition of C2α-tetrahederal intermediates; accumulation of the post-decarboxylation intermediate, 1',4'-imino-C2α-HEThDP, in YPDC also point toward the role of this stabilization during steps preceding product release (*24, 25*). However the chemical basis for this thermodynamic stabilization of this intermediate is not well understood. Direct experimental detection of the ionization/tautomerization states at the N4' atom could provide independent spectroscopic evidence for the IP tautomer and provide information about how this unique stabilization is achieved on enzymes.

Scheme 1.2 Mechanism of formation of pre-decarboxylation intermediate and its stable analog

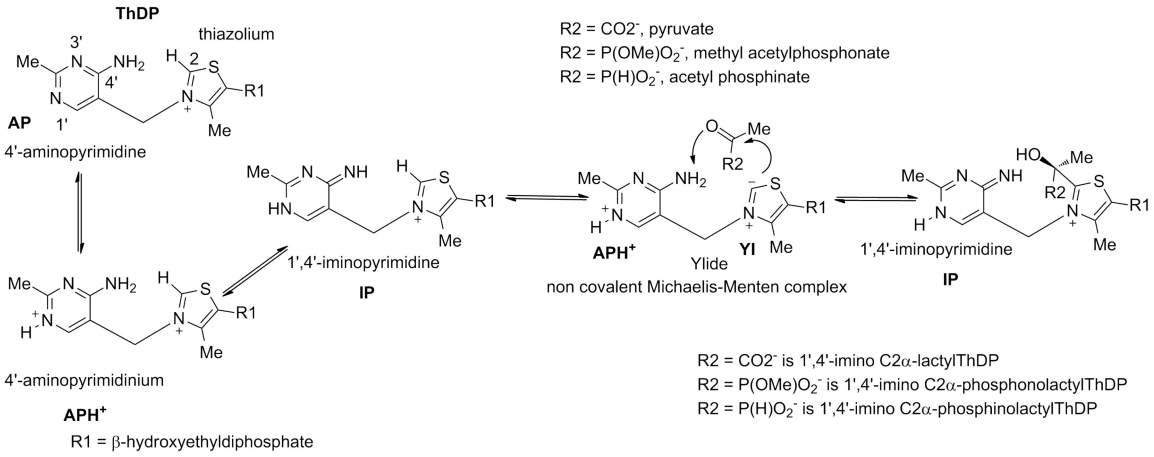

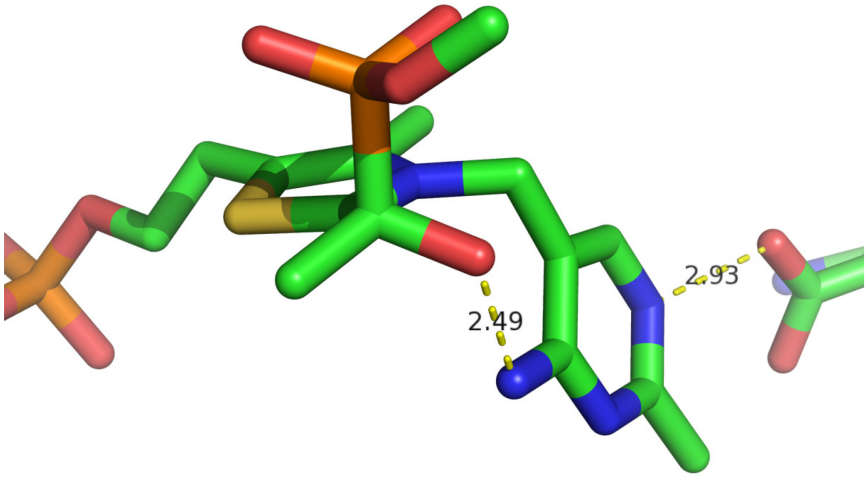

Figure 1.1 C2-α-phosphonolactyl ThDP (PLThDP), a tetrahederal intermediate analog bound to the active site of E1p.

Interatomic distances between N4' and C2α-O atoms (2.49 Å) and N1' and terminal COO^- of Glu571 (2.93 Å). Illustration created using the graphics program PyMOL from the PDB file PDB ID: 2G25 (*22*). Distances were measured using the distance measurement tool in the software.

Table 1.1 Distance between N4' atom and C2α – O atom in tetrahederal intermediate analogs bound to some ThDP dependent enzymes

Enzyme-Intermediate complex	**N – O distances (Å)**
E1p – PLThDP	2.45 – 2.49 (*22*)
H407A E1p – PLThDP	2.54 – 2.68 (*22*)
Benzaldehyde lyase – PMThDP	2.55 – 2.56 (13)
Benzoylformate decarboxylase – PMThDP	2.53 – 2.67 (*23*)
Pyruvate oxidase – PLThDP	2.38 (6)
Pyruvate oxidase – C2-α-lactyl ThDP	2.52 (6)
D28A YPDC - C2-α-lactyl ThDP	2.57 – 2.61 (*26*)

PLThDP is a stable adduct of methyl acetylphosphonate and ThDP and is a C2α-lactylThDP analog. PMThDP is a stable adduct of methyl benzoylphosphonate and ThDP and is a C2α-mandelylThDP analog. Distances are minimum and maximum distances in different active-sites all containing the intermediate in these multimeric enzymes. Distances were measured using the distance measurement tool in the graphics program PyMOL used to display and analyse X-ray data from respective PDB files.

Defining the position of labile protons on aromatic cofactors such as ThDP is essential to a fundamental understanding of acid-base catalysis on enzymes and the current state of the art in X-ray crystallography precludes such understanding, as does solution state NMR studies on large proteins (*Mr* >100,000). NMR chemical shifts are a very sensitive probe of both ionization and tautomeric states (*27-29*). While isotropic chemical shifts available from solution NMR spectra are in many cases sufficient to infer the ionization and tautomeric states (*30, 31*), chemical shift anisotropy (CSA) tensors recorded in the solid state provide much more detailed insight (*32-36*). Furthermore, Density Functional Theory (DFT) calculations of the magnetic shielding anisotropy tensors and their analysis in light of the experimental NMR results yield comprehensive understanding of the electronic structure of a molecule (*37-39*). Solid-state NMR measurements are often the only way to record chemical shifts and CSA tensors, for example, in large proteins, where solution lines are broadened beyond detection. The large molecular weight of the ThDP-dependent enzymes (varying between 160,000 and 250,000) has so far limited their solution NMR studies, while solid-state NMR spectroscopy presents a promising alternative for investigation of their catalytic mechanisms. In order to define the ionization and tautomeric states of ThDP cofactor in these enzymes solid-state NMR characterization of ThDP free and bound to the proteins was undertaken.

In the recent decade, biological solid-state NMR spectroscopy has developed rapidly to become one of the essential biophysics and structural biology techniques (*40, 41*). The wealth of structural and dynamics information that can be derived from various NMR observables with unprecedented atomic-level detail, in conjunction with the independence of resonance linewidths on the molecular size, make solid-state NMR an especially

powerful and attractive tool for investigations of large proteins and protein assemblies (*42-44*). The potential of solid-state NMR in enzymology has remained relatively unexplored, and only few examples to date have been reported applying this method to studies of enzymatic mechanisms (*45-52*).

The ^{13}C and ^{15}N isotropic chemical shifts as well as the complete chemical shift anisotropy tensors of key atoms of ThDP using specifically labeled thiamin analogs (Scheme 1.3) in different states of ionization of the 4'-aminopyrimidine ring were assigned. Aided by these assignments, the ^{13}C and ^{15}N NMR results on ThDP bound to yeast pyruvate decarboxylase (YPDC, EC 4.1.1.1), and to the E1 components of the pyruvate (E1p, EC 1.2.4.1) and 2-oxoglutarate (E1o, EC 1.2.4.2) dehydrogenase complexes from *Escherichia coli* were interpreted. Evidence was gathered for: (1) Assignment of the resonances pertinent to bound C2 and C6' atoms – the latter being a reporter for the state of ionization/tautomerization of the 4'-aminopyrimidine ring; (2) The chemical shift experienced by the thiazolium C2 resonance on binding to the enzymes, not readily accessible by solution NMR studies (*53*) (3) Formation of a pre-decarboxylation intermediate analogs on addition of methyl acetylphosphonate (MAP) to E1p and acetyl phosphinate (AcPhi) to YPDC according to the chemical shifts of the C2 atoms; and (4) Assignment of ^{15}N resonances pertinent to the bound N4' atom in APH^+, AP and IP forms. In this study, the enzyme complexes were prepared as hydrated precipitates under crystallization conditions, but at the pH optimum of the respective enzymes, and the intermediates are observed while enzyme-bound.

Scheme 1.3 Isotope enriched thiamin used for model studies

A

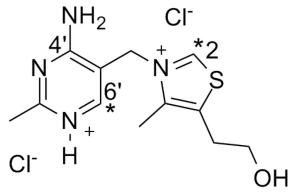

[C2, C6' - $^{13}C_2$] Thiamin chloride hydrochloride

B

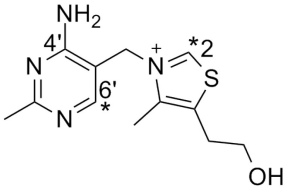

[C2, C6' - $^{13}C_2$] Thiamin

C

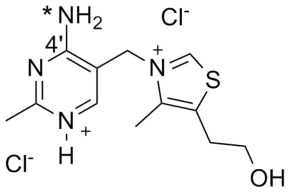

[N4' - ^{15}N] Thiamin chloride hydrochloride

D

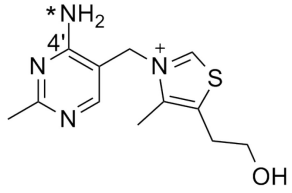

[N4' - ^{15}N] Thiamin

E

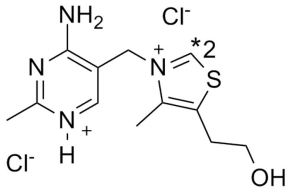

[C2 - ^{13}C] Thiamin chloride hydrochloride

F → **G**

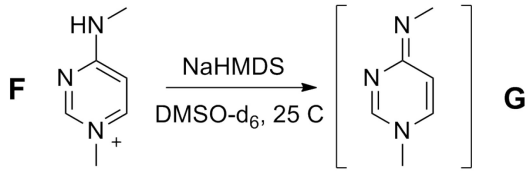

N1,N4-Dimethyl-4-aminopyrimidinium

N1,N4-Dimethyl-4-iminopyrimidine

* denotes position of isotopic enrichment.

1. 2 MATERIALS AND METHODS

1.2.1 Materials

All chemicals were purchased from Sigma-Aldrich (St.Louis, MO). All the chemicals purchased were of the highest purity grade available and were used without any further purification unless otherwise specified. Anhydrous solvents were either purchased from Acros Organics USA (Morris Plains, NJ) in anhydrous grade or were dried according to literature procedures (*54*). ^{15}N-NH_4Cl (99.9%) was purchased from Cambridge Isotope Laboratories, Inc (Andover, MA). 3-Chloro-4-oxopentyl acetate, a gift from Hoffmann-La Roche Inc (Nutley, NJ) was purified immediately prior to use by distillation under reduced pressure (0.1 mm Hg) at 85 °C.

Biochemicals and buffers - MES, Tris.HCl, ThDP, and DTT were from USB. ATP was from Sigma-Aldrich. Optimized for crystallization, Polyethylene glycol (PEG) 8000 (flakes), PEG 4000 (flakes), PEG monomethyl ether 2000 (50% solution), and 2-propanol were from Hampton Research. PEG 2000 monomethyl ether 2000 (flakes) was from Fluka Analytical crystallization grade.

Substrate analogues methyl acetylphosphonate, acetyl phosphinate and pyruvamide were synthesized previously at Rutgers (*55*).

[C2 – ^{13}C] Thiamin chloride hydrochloride was a generous gift from Dr. John Schloss.

[C2, C6' – $^{13}C_2$] Thiamin chloride hydrochloride was synthesized previously at Rutgers, and the synthetic route is reported elsewhere (*55*).

1.2.2 Synthesis of [N4' – ^{15}N] thiamin chloride hydrochloride

Compounds I, II & III (refer Scheme 1.4) were synthesized with some minor modifications to the previously described methods by Todd et al (*56*). Compound IV was synthesized according to a method described by Uray et al (*57*). Compounds V, VI & VII were synthesized with minor modifications to the methods described by Contant et al (*58*) and Nicewonger et al (*59*).

Synthesis of 4-hydroxy-5-cyano-2-methylpyrimidine (I)

To a solution of sodium ethoxide (12.07 g, 177.5 mmol) in absolute ethanol (200 mL) acetamidine hydrochloride (16.75 g, 177.5 mmol) was added with stirring. The mixture was allowed to stir at 0 °C for 30 min. and the precipitate was filtered off. To the filtrate ethyl α-ethoxymethylene-α-cyanoacetate (10.0 g, 59.17 mmol) was added with stirring. After complete addition the mixture was allowed to stir 12 hours at 0 °C. A crystalline precipitate (5 g) was observed which was filtered off. The precipitate (5 g) was treated with aqueous acetic acid (50% v/v, 10 mL) and the mixture was allowed to stir over night. A solid (colorless needles) was observed which was filtered off and the filtrate evaporated to obtain a white solid which could be crystallized into colorless needles from either water of aqueous acetic acid. Yield (3 g, 30%). ^{1}H NMR (500 MHz, D_2O): δ 8.558 (s, 1H); 2.584 (s, 3H)

Scheme 1.4 Synthesis of [N4' – ^{15}N] Thiamin diphosphate

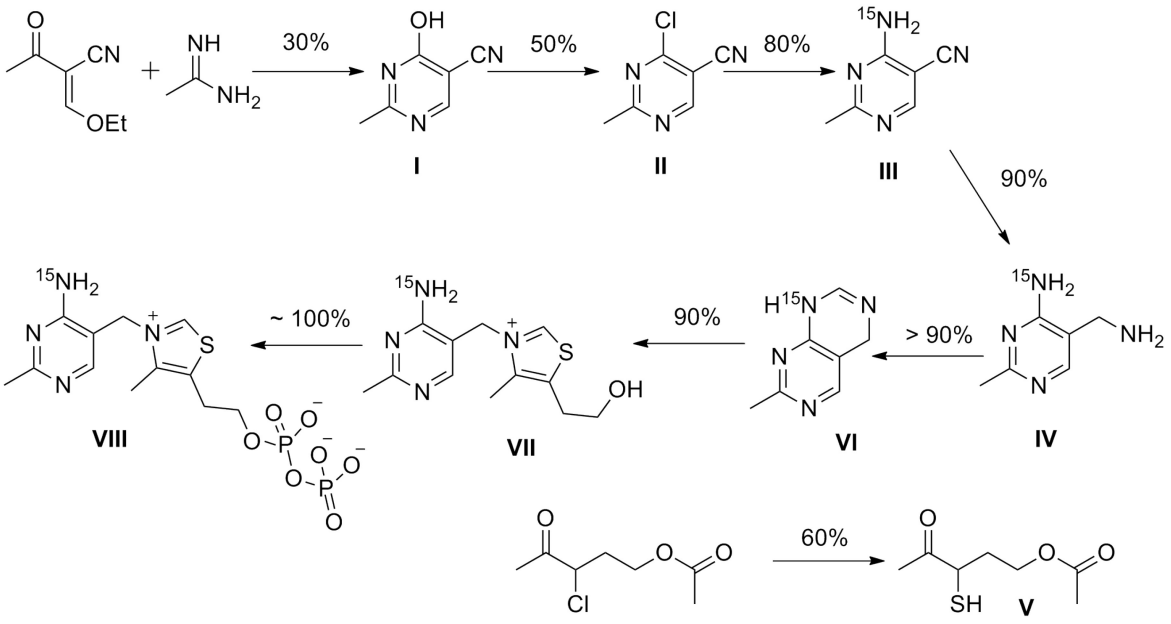

Reaction conditions are described in detail in the text. Percentage yields for individual transformations were calculated based on amount of material isolated after each step. Conversion of IV to VII was a one-pot reaction, and conversion of VII to VIII was achieved enzymatically; percentage conversions as determined by ^{1}H-NMR are reported for these transformations.

Synthesis of 4-chloro-5-cyano-2-methylpyrimidine (II)

To compound I (2 g 14.82 mmol) was added 8 mL of phosphorous oxychloride. The mixture was refluxed at 115 °C with vigorous stirring for 30 minutes or until the mixture turned a dark reddish brown. The stirring was stopped, the mixture was allowed to cool to RT and the excess phosphorous oxychloride was removed under reduced pressure (0.1 mm Hg). The remaining thick paste was taken into ice-cold water. The solution was neutralized with saturated potassium carbonate solution and the pH was adjusted to 10.0 units. Then the aqueous solution was extracted with diethyl ether (200 mL) three times. The combined extracts were dried over anhydrous sodium sulfate and solvent removed under reduced pressure. A reddish yellow oily liquid which solidifies upon cooling was obtained. Product could be recrystallized from petroleum ether. Yield (1.14 g, 50%).

^{1}H NMR (500 MHz, D_2O): δ 8.364 (s, 1H); 2.388 (s, 3H). MS (EI): m/z 153, 118, 91, 85, 51.

Synthesis of [4-^{15}N] 4-amino-5-cyano-2-methylpyrimidine (III)

To an ice-cold solution of sodium hydroxide (2.10 g, 52.5 mmol) in 3 mL water, ^{15}N-NH_4Cl (3 g, 55 mmol) was added in parts. After complete addition the mixture was allowed to stir in ice-bath with the reaction flask sealed. To this solution, a solution of compound II (0.500 g, 3.26 mmol) in ice-cold absolute ethanol (25 mL) was added drop-wise over 30 min. with stirring. After complete addition, the mixture was stirred for another 60 min. The solvents were removed under reduced pressure and the residue was triturated with boiling

methylene chloride (100 mL). The dry solid obtained could be recrystallized from anhydrous methanol.

Yield (0.352 g., 80%). ^{1}H NMR (500 MHz, d6-DMSO): δ 8.499 (s, 1H); 7.756 (br. d, J = 89 Hz, 2H); 2.382 (s, 3H).

Synthesis of [4-^{15}N] 4-amino-5-aminomethyl-2-methylpyrimidine (IV)

To a solution of Raney-Nickel (250 mg.) in 20mL dimethyl formamide (saturated with ammonia) compound III (0.400 g, 2.97 mmol) was added. The yellowish-orange mixture was hydrogenated in a bomb reactor at 60 °C under 3 bar hydrogen gas pressure with vigorous stirring overnight. After completion, the catalyst was filtered out and the solvent from the filtrate was removed under reduced pressure (0.1 mm Hg). The yellowish precipitate obtained was sublimed at 115 °C under reduced pressure (0.1 mm Hg) to obtain a white powder.

Yield (0.372 g, 90%). ^{1}H NMR (500 MHz, d6-DMSO): δ 7.875 (s, 1H); 6.672 (d, J = 88.5 Hz, 2H); 3.523 (s, 2H); 2.277 (s, 3H); 1.891 (br. s, 2H).

Synthesis of 3-mercapto-4-oxopentyl acetate (V)

To a suspension of sodium hydrogensulfide (0.941 g, 16.8 mmol) in anhydrous methanol (7 mL) maintained at 0 °C, a solution of 3-chloro-4-oxopentyl acetate (3.0 g, 16.81 mmol) in anhydrous methanol (7 mL) was added drop-wise under N_2 protection. The temperature

was maintained between 0 °C – 2 °C and the mixture was stirred vigorously during addition. After the addition was complete the reaction mixture was allowed to warm up to RT slowly and while stirring for 2.5 hours. White precipitate was observed and the mixture was filtered under N_2 and the filtrate evaporated. The oily residue was dissolved in anhydrous methylene chloride and filtered again under N_2 to remove any insoluble material. The filtrate was evaporated under reduced pressure to yield slightly yellow oil. Upon distillation under reduced pressure at 90 °C a clear liquid was obtained. Yield (1.78 g, 60%).

^{1}H NMR (500 MHz, $CDCl_3$): δ 4.201 (t, J = 6 Hz, 2H); 3.411 (dt, J = 7.5 Hz, 11 Hz, 1H); 2.332 (s, 3H); 2.270 (m, J = 6Hz, 7.5 Hz, 15 Hz, 1H); 2.033 (s, 3H); 1.937 (m, J = 6 Hz, 7.5 Hz, 15 Hz, 1H); 1.726 (d, J = 11 Hz, 1H). MS (EI): m/z 134, 116, 73, 43.

Synthesis of [1-^{15}N] 7-methyl-1,4-dihydropyrimido [4,5-d]pyrimidine (VI)

In a round bottom flask under N_2 equipped with a vigreux column Hickman still head, compound IV (0.420 g, 3.04 mmol) and freshly distilled toluene sulfonicacid (10 mg) were placed. Anhydrous triethyl orthoformate (1.2 mL, 7.3 mmol) was added. The mixture was heated at 110 °C with stirring, and the ethanol produced was distilled of until a thick white paste was observed. This was left to stand at 110 °C for an additional 45 min. Then 2 mL of anhydrous toluene was added and the mixture was refluxed at 90 °C for 2.5 hours. The solvent was removed in the apparatus and the residue dried for half hour under reduced pressure (0.1 mm Hg). At this point a small sample was collected for NMR analysis. Yield (>90%). ^{1}H NMR (500 MHz, d6-DMSO): δ 8.019 (s, 1H); 7.209 (s, 1H); 4.501 (s, 2H); 2.384 (s, 3H).

Synthesis of [N4' – ^{15}N] thiamin chloride hydrochloride (VII)

To compound VI in the same pot, anhydrous formic acid (15 mL) was added. Compound V (0.558 g, 3.17 mmol) was added drop-wise and temperature was maintained below 35 °C. The mixture was stirred at RT under N_2 for 45 min. A freshly prepared solution of HCl in absolute ethanol (3 mL) was added slowly to the mixture. The mixture was stirred at RT for 45 min. The volatiles were removed under reduced pressure and the solid green residue was suspended in 5 mL absolute ethanol. 2 mL aqueous HCl (25 %) was added and the reaction mixture was slowly warmed until a clear solution was obtained. The solution was cooled to room temperature and then kept at 4 °C overnight for crystallization. The white crystals formed were collected by filtration and the filtrate was evaporated under reduced pressure. The residue was dissolved in 2 mL distilled water and was washed three times with 4 mL chloroform. The aqueous phase was evaporated under reduced pressure and the resultant dark green solid was recrystallized as above. The crystals were collected by filtration and dried under vacuum. Yield (0.830 g, 90%).

^{1}H NMR (500 MHz, d6-DMSO): δ 9.930 (s, 1H); 9.106 (br. d, J = 91.5 Hz, 2H); 8.345 (s, 1H); 5.572 (s, 2H); 3.660 (t, J = 5.5 Hz, 2H); 3.071 (t, J = 5.5 Hz, 2H); 2.565 (s, 3H); 2.524 (s, 3H).

1.2.3 Thiamin models – protonated and unprotonated states, imino tautomer

The protonation site for thiamin is known to be the N1' atom (*21*). Hence, crystalline thiamin chloride hydrochloride (Th•HCl) synthesized as above was used in its present form

as a model for the N1' protonated form. Neutralization of this compound yielded thiamin (Th) which was used as a model for the unprotonated thiamin (Th) (N1' unprotonated form). The neutralization procedure is described below for the [N4'- ^{15}N] thiamin chloride hydrochloride.

[N4' – ^{15}N] thiamin

To a suspension of [N4' – ^{15}N] thiamin chloride hydrochloride (0.020 g., 0.06 mmol) in 5 mL absolute ethanol under N_2 protection, triethyl amine (0.022 g., 0.20 mmol) was added drop-wise. The clear solution obtained was now stirred for 10 min. To this solution anhydrous diethyl ether was added and immediate precipitation was observed. The addition of diethyl ether was continued until no further precipitation was observed. The precipitate was collected by filtration and washed with anhydrous diethyl ether and dried under vacuum. Similar procedure was used for preparing [C2, C6' -$^{13}C_2$] thiamin from [C2, C6' -$^{13}C_2$] thiamin chloride hydrochloride.

N1, N4 – Dimethyl-N4-iminopyrimidine

N1, N4 – Dimethyliminopyrimidine (see structures F and G in Scheme 1.3), a model of the imino tautomeric form of ThDP was generated *in situ* in an NMR tube by titration with sodium bis(trimethylsilyl)amide as described previously (*19*). To a solution of N1,N4 – dimethyl-4-aminopyrimidinium iodide (20 mg, 0.08 mmol) in 500 µL anhydrous d_6-DMSO in a NMR tube flushed with N_2, sodium bis(trimethylsilyl)amide (16.2 mg, 0.09 mmol) dissolved in 100 µL anhydrous d_6-DMSO was added. After thorough mixing with pipette

under N_2 protection, the NMR tube was capped and sealed. ^{1}H, ^{13}C and ^{1}H-^{13}C HMQC spectra were acquired on the sample. All ^{1}H resonances were previously assigned for both the starting material and N1,N4–dimethyl-4-iminopyrimidine. This information aided in comparision and assignment of cross peaks in the ^{1}H-^{13}C HMQC spectrum to individual carbon atoms.

1.2.4 Enzymatic synthesis of labeled ThDP from labeled thiamin

Conversion of thiamin to ThDP (VIII) in presence of ATP and Mg^{2+} catalysed by the enzyme *mouse* thiamin pyrophosphokinase (*60*) was used as a mild and efficient method to synthesize labeled ThDP molecules. The reaction conditions were optimized to achieve 100% conversion, as determined by ^{1}H NMR, in preparative scale quantities.

To 650 μL of a solution containing labeled thiamin (6.8 mg, 20.1 μmol), ATP (20.4 mg, 37.0 μmol) and $MgCl_2$ (9.2 mg, 45.3 μmol) made in 20 mM KH_2PO_4 buffer (pH 7.1), 55 μL of *mouse* Thiamin pyrophosphokinase (55 mg/mL) was added. The reaction mixture was incubated for 12 h at 20 °C. The reaction was stopped by adding 300 μL 3N HCl to precipitate the enzyme. After centrifugation at 14000 rpm for 30 min at 4 °C, the pelleted protein was discarded and the supernatant was filtered through Gelman Nylon acrodisc 0.45 μm. The pH of the supernatant was adjusted to 5.5-6.0 and the product was stored at –80 °C in small aliquots. Under these conditions 100% conversion of thiamin to ThDP was consistently realized as determined by ^{1}H NMR analysis. Conversion of ThDP was confirmed by ^{1}H NMR analysis. Under these conditions (50 μL of the supernatant mixed with 550 μL D_2O) the C6'-H, and -CH_2- for β-hydroxyethylene group, exhibit unique

chemical shifts for thiamin and ThDP and are the most well resolved for purposes of quantitation via peak integration.

Thiamin: ^{1}H NMR (500 MHz, D_2O/H_2O): δ C6'-H 8.051 (s, 1H); -CH_2-OH 3.926 (t, J = 5.5 Hz, 2H); -Tz-CH_2- 3.232 (t, J = 5.75 Hz, 2H)

ThDP: ^{1}H NMR (500 MHz, D_2O/H_2O): δ C6'-H 7.977 (s, 1H); -CH_2-OPP (q, J = 5.75 Hz, 6 Hz, 2H); -Tz-CH_2- 3.375 (t, J = 5.5 Hz, 2H)

1.2.5 Protein purification and apoenzyme preparations

Yeast PDC (YPDC) from *S. cervisiae* was purified as detailed in Chapter 3. *E. coli* E1p was purified as detailed in Chapter 2 and *E. coli* E1o was purified as detailed in Appendix.

Preparation of apo E1p

E1p could be easily converted to the apoenzyme form by extensive dialysis against 2L of 20 mM KH_2PO_4 buffer pH 7.0.

Preparation of apo E1o

E1o was purified in the apoenzyme form while avoiding thiamin and Mg^{2+} during the protein overexpression, and avoiding use of ThDP and Mg^{2+} in all buffers during purification steps and storage.

Preparation of apo YPDC

YPDC was purified as holoenzyme and converted into the apoenzyme by following the procedure from earlier reports (*61*) with some minor modifications.

To 4 mL YPDC (20mg/mL) was added 12 mL of dissociation buffer (DB),containing 0.1 M Tris-HCl, 1 mM Na_2-EDTA, 0.1 N NaOH (pH 8.9) and the solution was incubated on ice for 15 min. The sample was then centrifuged in a Amicon-30K 5 mL centrifugal unit at 4,000 rpm to reduce total volume to 2 mL. This sample was diluted with 8 mL of DB followed by centrifugation to reduce volume to 2 mL. This washing step was repeated three more times. Trace amounts of ThDP could be removed by passing the treated enzyme solution through a Sephadex G-25 M mini column, PD-10 Columns (Pharmacia Biotech. Piscataway, NJ). The PD-10 column was first equilibrated with two bed volumes of the DB buffer passed through by gravity, then the DB buffer-treated enzyme preparation was loaded and eluted by about one and half volume of the same DB buffer by gravity. The eluent was again concentrated in a Amicon-30K 5 mL device at 4,000 rpm to reduce the volume to about 2 mL. No enzyme activity should be detected after this step. This preparation was diluted with 8 mL of the reconstitution buffer (RB), containing 0.1 M sodium phosphate, 1 mM Mg^{2+} (pH 6.0) and the sample was then centrifuged at 4,000 rpm to reduce the volume to about 2 mL. This washing step was repeated 3 more times. This apo YPDC preparation did not show any pyruvate decarboxylase activity in the assay.

1.2.6 Reconstitution of apoenzymes with labeled ThDP

Labeled ThDP refers to [C2, C6' – $^{13}C_2$] ThDP, [C2 – ^{13}C] ThDP or [N4' -^{15}N] ThDP. Same procedure as described below was used for reconstitution of the apo-enzymes with these labeled ThDP analogs.

E. coli E1p was incubated with 3 active-site equivalents of labeled ThDP and 2.5 mM Mg^{2+} in 20 mM KH_2PO_4 buffer pH 7.0 or 20 mM Tris buffer pH 8.0.

E. coli E1o was incubated with 3 active-site equivalents of labeled ThDP and 2.5 mM Mg^{2+} in 20 mM KH_2PO_4 buffer pH 7.0 or 20 mM Tris buffer pH 8.0. The excess unbound cofactor was separated by passing the enzyme preparation through a Sephadex G-25 M mini column, PD-10 Column. For solution NMR experiments 0.95 active-site equivalents of cofactor was used instead.

YPDC

Fresh YPDC apoenzyme was immediately reconstituted with labeled ThDP as follows: 60 mg of apoenzyme in 20 mM MES buffer pH 6.0 was concentrated to 1 mL volume in Amicon 30K 5 mL centrifugal unit. To this was added 1 mL of the labeled ThDP stock (20 mM ThDP), and 10 mM Mg^{2+}. This mixture was incubated at 4 °C for 3-4 h. Now, the mixture was concentrated to 1 mL and 4 mL of buffer with 10 mM Mg^{2+} was added and concentrated again to 1 mL, this washing step was performed 2 more times. After the final wash, the labeled enzyme mixture was loaded onto a PD-10 column equilibrated with 20 mM MES pH 6.0 buffer and eluted with the same buffer. 500 µL fractions containing the labeled enzyme were combined and concentrated to 1 mL. This was again loaded into a

PD-10 column and the steps were repeated to ensure complete removal of trace amounts of labeled ThDP. Finally the labeled enzyme was diluted to 3 mL total volume (recovered concentration 15-17 mg/mL). 10 μL enzyme solution was used to assay for activity.

1.2.7 Estimation of protein content

Protein concentrations were determined by the method described by Bradford et al. (*62*). Dilutions of proteins were added to 1X Bradford reagent (BioRad, CA) and the absorbance at 595 nm was used to estimate the concentration from a standard curve prepared with BSA.

1.2.8 Enzyme activity measurements

YPDC enzyme activity was determined using NADH/ADH coupled assay (*63*). Conversion of acetaldehyde to ethanol by yeast alcohol dehydrogenase in presence of NADH was coupled to YPDC catalyzed production of acetaldehyde from sodium pyruvate. The disappearance of NADH is monitored at 340 nm using a UV-VIS. The activity was measured in the presence of 20 mM pyruvate in standard assay buffer (50 mM MES, 1 mM ThDP, 2 mM $MgCl_2$, 0.2 mg/mL NADH, 0.08 mg/mL ADH, pH 6.0) at 30°C. The reaction was started with addition of 3 μg/mL YPDC.

Enzyme activity for E1p and E1o was determined using the E1 specific assay with 2,6-dichlorophenol-indophenol (DCPIP) reduction by the enamine at 600 nm. E1p assay conditions are described in detail in Chapter 2, and E1o assay conditions are essentially similar with the exception of 2-oxoglutarate as substrate instead of pyruvate.

1.2.9 Solid state NMR sample preparation

Model compounds

Crystalline [C2, C6'-$^{13}C_2$] thiamin chloride hydrochloride (10.4 mg, 0.031 mmol) or [N4'-^{15}N] thiamin chloride hydrochloride (9.0 mg, 0.027 mmol) were packed into 3.2 mm MAS rotors and used in the subsequent MAS NMR experiments as models for the N1' protonated form (see Scheme 1.3 A, C).

[C2, C6'- $^{13}C_2$] thiamin (8.0 mg, 0.027 mmol) or [N4'- ^{15}N] thiamin (6.7 mg, 0.022 mmol) were packed into 3.2 mm MAS rotors and used in the subsequent MAS NMR experiments as models for the N1' un-protonated form (see Scheme 1.3 B,D).

Enzyme samples

Individual enzymes were prepared as hydrated precipitates from the reaction buffers under their respective crystallization conditions. Individual enzyme precipitation solution composition is derived from reservoir solution composition used for crystallization of respective enzymes (*64-66*). The microcrystals obtained as described below were collected and transferred into 3.2 mm MAS rotors by centrifugation.

***E. coli* E1p**

450 μL of enzyme with labeled ThDP (70 mg/mL) was divided into two aliquots. To one aliquot 10 mM MAP was added and the mixture was incubated for 30 min at 4 °C, Next, enzyme precipitation solution (25 μL of 40% PEG 2000 mme, 20% isopropanol in 15 mM HEPES buffer pH 7.05) was added. This mixture was incubated at 4 °C for 10 min. This

addition/incubation cycle continued until no further precipitation could be observed. The final concentration of PEG was ~ 27%. For samples at pH 8.0 the enzyme preparation and precipitation buffer were made up in 20 mM MES buffer pH 8.0. The suspension was incubated for 3-4 h at 4 °C. Next, the suspension was loaded into a 1 mL flame-sealed pipet tip and centrifuged at 6000 rpm at 4 °C. The supernatant was separated; the pellet was transferred into a 200 µL flame-sealed pipet tip by centrifugation and finally transferred into a NMR rotor by centrifugation at 6000 rpm.

***E. coli* E1o**

The same procedure as above was followed with two changes (i) 24% w/v PEG 4000 in 20 mM KH_2PO_4 (pH 7.0) was used as precipitation solution (ii) The final concentration of PEG 4000 was 16%.

YPDC

3 mL total volume (recovered concentration 15-17 mg/mL), was divided into 3 aliquots of 1 mL each. To the second, pyruvamide (100 mM and 200 mM final concentrations for ^{13}C and ^{15}N experiments respectively) was added; to the third, acetyl phosphinate (60 mM final concentration) was added. These samples were incubated for 15 min at 4 °C. The precipitation solution used was 20% PEG 8000, and 0.5 mM DTT in 20 mM MES pH 6.0. The final concentration of PEG 8000 was 13.3%.

Control samples of enzymes containing unlabeled ThDP were prepared similarly.

1.2.10 Carbon-13 solution NMR of enzymes labeled with [C2, C6'- $^{13}C_2$]ThDP

To 540 µL *E. coli* E1p (25 mg/mL) samples 60 µL of D_2O was added and 1D-^{13}C NMR spectra were recorded on a 600 MHz Varian instrument; 131,000 scans were collected at 20 °C. The preparation was incubated with 10 mM MAP (final concentration) to acquire spectra of enzyme with substrate analogue MAP bound to the enzyme.

The above preparations were quenched with 200 µL of 12.5% TCA in 1M DCl/D_2O, and centrifuged at 14000 rpm to precipitate the protein. The clear supernatant was filtered through a Gelman Nylon Acrodisc (0.45 µm) and analyzed by 1D-^{1}H gCHSQC NMR spectroscopy to selectively detect protons attached to ^{13}C nuclei. 32,000 scans were collected at 25 °C.

For YPDC, the enzyme reconstituted with labeled ThDP was concentrated to 25 mg/mL and the two experiments mentioned above were performed using 20 mM acetyl phosphinate instead of MAP.

1.2.11 CD spectroscopy with NMR sample preparations

Near UV (280 nm – 400 nm) CD spectra were acquired on E1p samples incubated with MAP before precipitation for solid state NMR on an Applied Photophysics (Leatherhead, Surrey, UK) Chirascan instrument. After NMR experiments, the protein pellet was redissolved in 20 mM KH_2PO_4 (pH 7.0) or 20 mM Tris (pH 8.0) buffer and Near UV CD spectra were acquired on the clear solution.

1.2.12 ^{13}C and ^{15}N CPMAS Solid State NMR experiments

Experimental setup for model compounds

All ^{13}C and ^{15}N MAS spectra presented in this work were acquired at 9.4 T (400.17 MHz ^{1}H Larmor frequency) on a Tecmag Discovery spectrometer outfitted with a 3.2 mm wide bore Varian HXY T3 probe. The actual sample temperature includes a correction of about $+5^{o}$ C arising from sample spinning at 10 kHz spinning speed. The temperature was calibrated for this probe at different MAS frequencies using a $PbNO_3$ temperature sensor (*67*), and the actual temperature at the sample was 18 ^{o}C maintained to within ±0.5 °C throughout the experiments using the Varian temperature controller. ^{13}C chemical shifts were referenced to the downfield peak of adamantane (38.56 ppm with respect TMS). ^{15}N chemical shifts were referenced to ammonium chloride (39.2 ppm with respect to liquid NH_3).

The low spinning-frequency ^{13}C CPMAS spectra were acquired on Th•HCl at ω_r = 2900, 4070 and 5980 Hz. The MAS frequency was controlled with Tecmag MAS controller: within ±5 Hz at 2900 kHz, while at 4070 and 5980 Hz the variation was up to ±100 Hz. The standard CP sequence was used with 1 ms contact time; the ^{1}H radio frequency field strength was 60 kHz, the ^{13}C field was linearly ramped 80-100% with the center of the ramp being 50 kHz. The ^{1}H 90^{o} pulse width was 2.5 μs. The same experimental parameters were used at every spinning speed. The ^{1}H decoupling was performed using TPPM (*68*) with 100 kHz ^{1}H radio frequency field strength maintained for the duration of the acquisition period, 25.6 ms. The CPMAS spectra were acquired with either 32 scans (at ω_r = 2900 Hz) or with 4 scans (ω_r = 4070 and 5080 Hz); the recycle delay was 10 s. The

spectra were processed without any line broadening, and the intensities of each sideband were extracted for the two carbons in the 2, 6'-^{13}C Th•HCl sample.

The low spinning-frequency ^{13}C CP-MAS spectra of 2, 6'-^{13}C Th were acquired at ω_r = 2075, 3810, and 5973 Hz. The rest of the experimental conditions were the same as for the thiamin hydrochloride sample. At all MAS frequencies, 16 scans were used with 10 sec pulse delay.

Herzfeld-Berger analysis (*69*) was performed to calculate the CSA parameters from the intensities of the spinning side-band envelopes for the two carbon atoms in both forms of thiamin.

The ^{15}N CP-MAS NMR spectra of 4'-^{15}N Th•HCl and Th were acquired at the spinning frequency of 10 kHz. The standard CP sequence was used with 1 ms contact; the ^{1}H radio frequency field strength was 60 kHz, the ^{15}N field was linearly ramped 80-100% with the center of the ramp being 50 kHz.100 kHz. TPPM decoupling was applied during the acquisition time (30 ms); ^{1}H radio frequency field strength was 100 kHz. 32 scans were acquired with a recycle delay of 10 s.

ROCSA (Recoupling Of Chemical Shift Anisotropy) pulse sequence (*70*) was used to recouple the ^{13}C and ^{15}N CSA interaction at MAS frequencies above 10 kHz. The ^{13}C ROCSA spectra were collected at the MAS frequency of 12 kHz. The ^{13}C radio frequency field strength during the ROCSA period was 51.3 kHz, and that of the ^{1}H decoupling was 122 kHz. The ^{15}N ROCSA spectra were collected at the MAS frequency of 10 kHz. The ^{15}N rf field strength during the ROCSA period was 42.8 kHz and that of the ^{1}H decoupling was 100 kHz. 16 transients were added up with a recycle delay of 10 sec for each t_1 point.

32 and 24 t_1 points were acquired using the States method (*71*) for ^{15}N and ^{13}C ROCSA spectra, respectively. The CSA dimension was zero-filled to 512 points; no apodization was applied prior to the Fourier transformation.

Experimental setup for enzymes reconstituted with labeled ThDP

All ^{13}C CPMAS were acquired at 9.4 T (400.17 MHz ^{1}H Larmor frequency) on a Tecmag Discovery spectrometer outfitted with a 3.2 mm wide bore Varian HXY T3 probe. The MAS frequency was 10.000±0.010 kHz controlled by a Tecmag MAS controller. The temperature calibration was done using a $PbNO_3$ temperature sensor. For both ^{13}C and ^{15}N CPMAS experiments, the actual sample temperature includes a correction of +5 ^{o}C taking into account sample spinning. ^{13}C chemical shifts were referenced to the downfield peak of adamantane (38.56 ppm with respect to TMS). The ramped CP sequence was used with 1.0-1.5 ms contact time. The ^{1}H radio frequency field strength was 50-60 kHz, and the ^{13}C field was linearly ramped from 80-100% with the center of the ramp being $\omega_{rf}(^{13}C) = \omega_{rf}(^{1}H) \pm \omega_r$. The ^{1}H 90^{o} pulse length was 2.5-3.65 μs. The ^{1}H decoupling was performed using TPPM with ω_{rf} = 70-100 kHz. The number of transients and the recycle delay for each spectrum are given in the figure captions. All ^{13}C spectra were processed with 20 Hz exponential broadening.

All ^{15}N CPMAS spectra were acquired at 14.1 T (599.78 MHz ^{1}H Larmor frequency) on a Varian InfinityPlus spectrometer outfitted with a standard bore 3.2 mm HXY T3 probe. The MAS frequency was 10.000±0.001 kHz controlled by a Varian MAS controller. ^{15}N chemical shifts were referenced to ammonium chloride (39.2 ppm with respect to liquid

NH_3). The ramped CP sequence was used with 1.5-1.6 ms contact time. The ^1H radio frequency field strength was 50-60 kHz and the ^{15}N field was linearly ramped from 80-100% with the center of the ramp being $\omega_{rf}(^{15}N) = \omega_{rf}(^1H) \pm \omega_r$.. The ^1H 90^o pulse length was 2.50-2.78 μs. The ^1H decoupling was performed using TPPM (*68*) with ω_{rf} = 90-100 kHz. The number of transients, the recycle delay, and the apodization parameters for each spectrum are given in the figure captions.

1. 3 RESULTS AND DISCUSSION

1.3.1 Assignments of ^{13}C resonances in different ionization states of thiamin

Since there are two ^{13}C isotopically labeled sites (C2 and C6') in thiamin ambiguity arises in the resonance assignment of ^{13}C spectra of samples in the absence of *a priori* knowledge about the two carbon chemical shifts. In order to resolve this ambiguity, the $^{1}J_{13C\text{-}1H}$ coupling constant for these two carbons was measured by solution NMR and compared with DFT computed *J*-couplings in thiamin chloride hydrochloride and thiamin. The results are summarized in Table 1.2. Based on the DFT calculations, $^{1}J_{C2\text{-}H}$ is larger than $^{1}J_{C6'\text{-}H}$ by more than 22 Hz in thiamin chloride hydrochloride and by 35 Hz in thiamin. The experimental *J*-couplings obtained from the proton-coupled ^{13}C solution NMR spectra are in excellent agreement with the theoretical predictions, and immediately permit assignment of the two carbons in both ionization states; the corresponding isotropic solution chemical shifts are also indicated in Table 1.2.

.

1.3.2 ^{13}C and ^{15}N Chemical Shift Anisotropies (CSA) in different ionization states of thiamin: Solid-State NMR

The ^{13}C CSA tensors were recorded by two methods: i) slow-MAS spectra at three different spinning speeds with subsequent Herzfeld-Berger analysis to extract the CSA tensor components; (*69*) ii) symmetry-based Recoupling Of Chemical Shift Anisotropy (ROCSA) method suitable for high MAS frequencies (*70*). The ^{15}N CSA parameters were determined

using ROCSA because the much smaller ^{15}N CSA tensor resulted in rather weak side-band intensities even at slow-MAS frequencies and prohibit their accurate measurement.

The ^{13}C spectra, slow-MAS and ROCSA, are illustrated in Figure 1.2. From (Table A1, in Appendix) it becomes evident that the two methods give consistent results for ^{13}C CSA tensors in both ionization states. The C2 CSA tensor is not very different in the two ionization forms. The three principal components (δ_{11}, δ_{22} and δ_{33}) display a small shift of ca. 3 ppm in the upfield direction upon protonation, from Th to Th•HCl. As a result, the net change is only in the isotropic chemical shift, from 156.5 ppm to 153.4 ppm, while the reduced anisotropy δ_σ and the asymmetry parameter η_σ remain nearly the same in the two states. As expected, the CSA parameters of C6' are significantly different in the two protonation states. The C6' isotropic chemical shift changes by about 12.5 ppm upfield upon protonation, from Th to Th•HCl. The principal components of the CSA tensor, δ_{11} and δ_{33} also move upfield by 17 and 15 ppm, respectively. The δ_{22} component displays only a small shift of 6 ppm. The resulting change in the reduced anisotropy δ_σ and the asymmetry parameter η_σ is negligible- these remain the same within the error bars in the two protonation states, as the difference between the relative shifts of δ_{iso} and δ_{33} is small.

Table 1.2 Experimental and computed $^{1}J_{13C\text{-}1H}$ coupling constants for [C2, C6' – $^{13}C_2$] thiamin chloride hydrochloride and [C2, C6' – $^{13}C_2$] thiamin.

Sample	Atom	J_{CH} (Hz)		δ_{iso} (ppm)
		Solution NMR	**DFT**	**Solution NMR**
Thiamin HCl	C2	214.1	208.8	154.6
	C6'	185.6	186.7	145.1
Thiamin	C2	213.6	210.0	157.8
	C6'	177.5	175.3	161.0

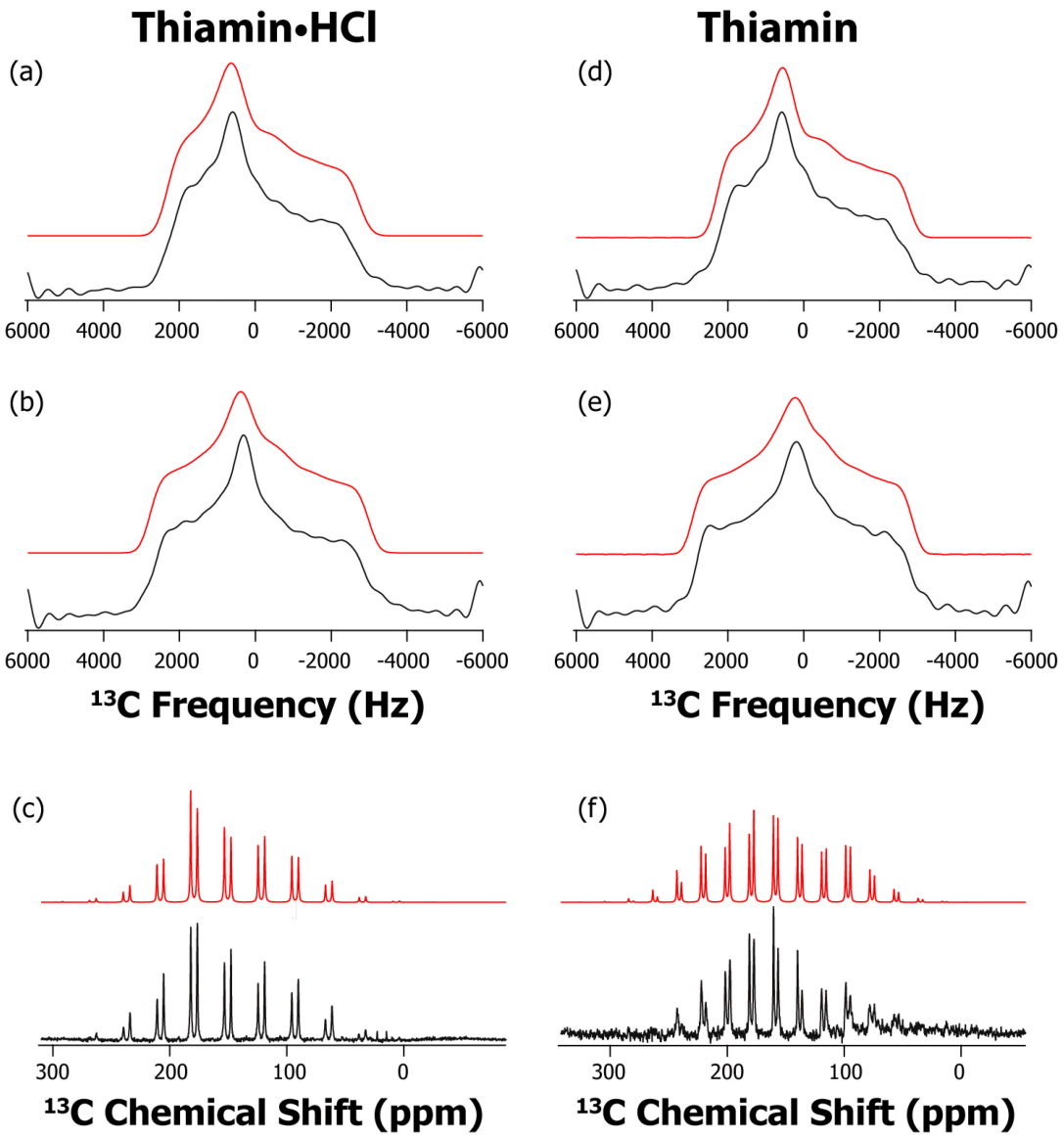

Figure 1.2 ^{13}C ROCSA and slow-MAS spectra of Th•HCl and Th

experimental (black) and simulated (red). a) ROCSA spectrum of C2 of Th•HCl; b) ROCSA spectrum C6' of Th•HCl; c) slow-MAS spectrum C2 and C6' of Th•HCl at 2900 Hz rotor frequency; d) ROCSA spectrum of C2 of Th; e) ROCSA spectrum of C6' of Th; and f) slow-MAS spectrum of C2 and C6' of Th at 2075 Hz rotor frequency.

The ^{15}N ROCSA spectra are presented in Figure 1.3. The N4' CSA parameters are found to be even more sensitive to the protonation state than C6'. The isotropic chemical shift, δ_{iso}, differs by more than 25 ppm in the two forms. Of the three principal components of the CSA tensor, the δ_{11} component of N4' CSA tensor is observed to be the most sensitive to the protonation, moving downfield by ca. 40 ppm from Th to Th•HCl. As a result, the reduced anisotropy, δ_σ, increases by 15 ppm in Th•HCl. The δ_{22} and δ_{33} principal components also display considerable downfield shift of 20 and 16 ppm, respectively. It is not possible to accurately measure η_σ in these experiments, because this parameter has a strong correlation with the line-broadening parameter used in fitting the experimental ^{15}N ROCSA lineshapes with nearly axial symmetry. As a consequence, the position of both δ_{22} and δ_{33} is not as well defined as that of δ_{11} especially when η_σ is in the range of 0.1 - 0.4 (*72*).

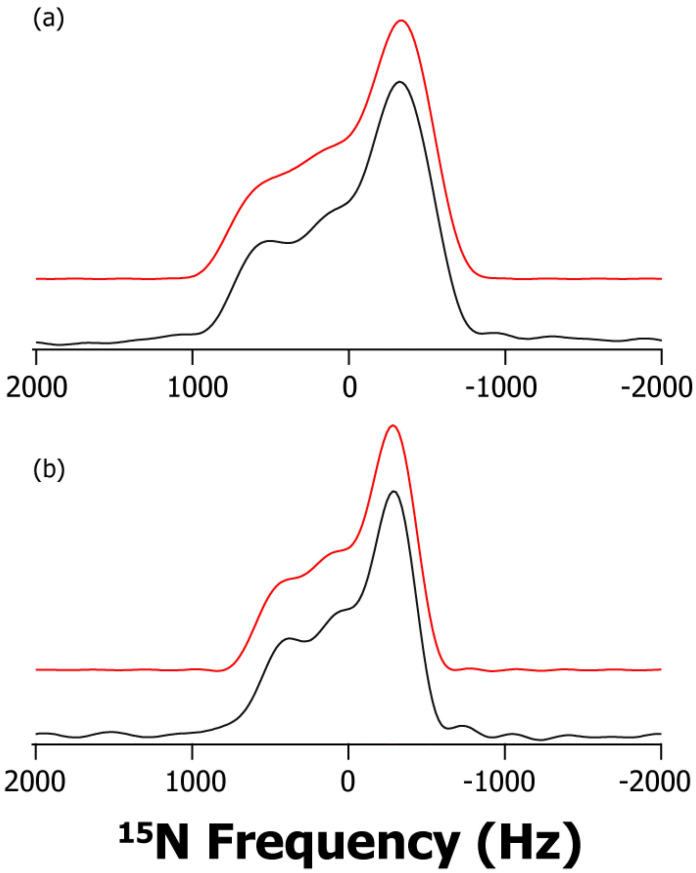

Figure 1.3 ^{15}N ROCSA spectra of Th•HCl and Th:

experimental (black) and simulated (red). a) N4' of Th•HCl; b) N4' of Th.

1.3.3 ^{13}C and ^{15}N Chemical Shift Anisotropies (CSA) in Thiamin hydrochloride: Density Functional Theory (DFT)

Experimental results and DFT calculations are summarized in (Table A1, in Appendix). DFT calculations performed on the geometry-optimized structure of Th•HCl predict the experimental trend very well in the following respects: i) C6' is more shielded than C2; and ii) δ_σ of C6' is larger than that of C2.

The calculations predict the principal components of the C2 CSA tensor to within 9 ppm. The calculated isotropic chemical shift of C2, 154.9 ppm, agrees well with the experimental value of 153.4 ppm. Maximum deviation is observed for δ_{11} (13 ppm) and δ_{22} (-8 ppm) with δ_{33} showing no deviation at all. For C6', the computed principal components of the magnetic shielding anisotropy tensor are in even better agreement with experiment, with the difference being only of the order of 7 ppm. Since for C6' the three computed principal components deviate in the same direction (downfield) with respect to the experimental values, the isotropic chemical shift also differs by 6 ppm.

For N4' CSA, the agreement between experiment and theory is excellent, and even tighter agreement is observed than for the ^{13}C tensors. The average deviation of the three principal components is less than 7 ppm. The computed δ_{11} and δ_{22} are 7.5 ppm upfield, while the calculated δ_{33} is downfield by 5 ppm compared with experiment. The calculated isotropic chemical shift is therefore only 3.4 ppm different from the experimental value.

The effect of the presence of two chloride anions in the DFT calculations was also addressed. During additional round of calculations performed with geometry optimization

on the twice positively charged Th•HCl without the two chloride anions the following trends were observed:

1. The predicted C6' CSA tensor is in much better agreement with experiment without the two chloride anions, with the average deviations between experiment and theory of less than 4 ppm for the three principal components. The predicted isotropic chemical shift of 149.7 ppm is in much better agreement with the experimental value of 147.8 ppm.
2. At the same time, the computed principal components of the C2 CSA tensor show greater deviations from the experimental values (by more than 20 ppm on average). As observed in the calculations with chloride anions, this deviation can be largely attributed to changes in δ_{11} (30 ppm) and to a lesser extent to δ_{22} (-15 ppm) with δ_{33} showing no deviation at all.
3. The computed N4' CSA tensor deviates more from the experimental values without the chloride anions with an average difference of 13 ppm for the individual principal components. Both δ_{22} and δ_{33} display the maximum deviation from experiments as well as from their computed values in the presence of chloride ions. The δ_{11} component of N4' remains relatively unchanged upon the removal of the chloride ions.

1.3.4 ^{13}C and ^{15}N Chemical Shift Anisotropies (CSA) in thiamin: Density Functional Theory (DFT)

For the DFT calculations on thiamin, a starting model derived from the Th•HCl X-ray structure by removing the HCl was used and further geometry optimization was performed to obtain the final structure for magnetic shielding anisotropy tensor calculations.

As in the case of Th•HCl, DFT calculations on the geometry-optimized Th structure correctly predict that C6' is more deshielded than C2, which is consistent with the experimental results. The calculated reduced anisotropy, δ_σ, of C6' is higher than that of C2, as observed in experiments.

The calculated principal components of the C2 CSA tensor agree with their experimental values to within 7 ppm. As in the Th•HCl calculation, δ_{11} of C2 shows greater deviation from experiment (9 ppm downfield), while δ_{22} and δ_{33} are upfield compared with experiment. As a result, the calculated isotropic chemical shift is different by only 1 ppm from experiment. For C6', the average deviation of the calculated principal components is also less than 7 ppm. δ_{11} and δ_{33} are downfield compared with experiment (by 6.2 and 6.8 ppm, respectively), while δ_{22} is upfield by 7.5 ppm. This results in the calculated isotropic chemical shift (162.2 ppm) in close agreement with the experimental value (160.4 ppm).

The calculated N4' CSA components are also in close agreement with experiment, to within 9 ppm. As observed in the Th•HCl calculations, both δ_{11} and δ_{22} contribute to the difference between calculations and experiment with δ_{33} showing no deviation.

The perturbation of the carbon CSA tensors due to the removal of the chloride anions in Th is nearly the same as in Th•HCl. The C6' CSA tensor is observed to agree more closely with the experimental values, while C2 CSA tends to deviate to a greater extent from the experiment; nevertheless, the agreement between theory and experiment is still very good.

Conversely, the absence of the two chloride anions has a great effect on the N4' CSA tensor in Th. The δ_{11} and δ_{33} components differ from their experimental values by -27 and -39 ppm, respectively. As a result, the computed isotropic chemical shift is off by more than 20 ppm upfield. Moreover, the calculations predict an almost rhombic tensor (η_δ = 0.90), whereas in experiments the tensor is close to axial (η_δ = 0.28).

The sensitivity of the C2 and N4' CSA tensors to the absence of the chloride ions in both AP and APH^+ forms can be attributed to the chloride ion located close to the sulfur atom in the thiazolium ring (Figure A1 in Appendix). The interatomic C2-Cl and N4'-Cl distances are ca. 3.7 Å and 3.2 Å, respectively, in the X-ray structure as well as in the geometry optimized structures used in our shielding tensor calculations.

In summary, the calculations predict accurately the C2 and N4' CSA tensors in the presence of the chloride anions, and the C6' CSA tensor in the absence of chloride anions. This trend is observed to be the same for both Th as well as Th•HCl. The correlation between the computed and the experimental CSA components is shown in Figure 1.4 for both ^{13}C and ^{15}N atoms. As discussed, the correlation between the ^{15}N CSA predictions and the experimental values is much better in the presence of the chloride anions than without chloride anions (see Figure 1.4 b, c, respectively).

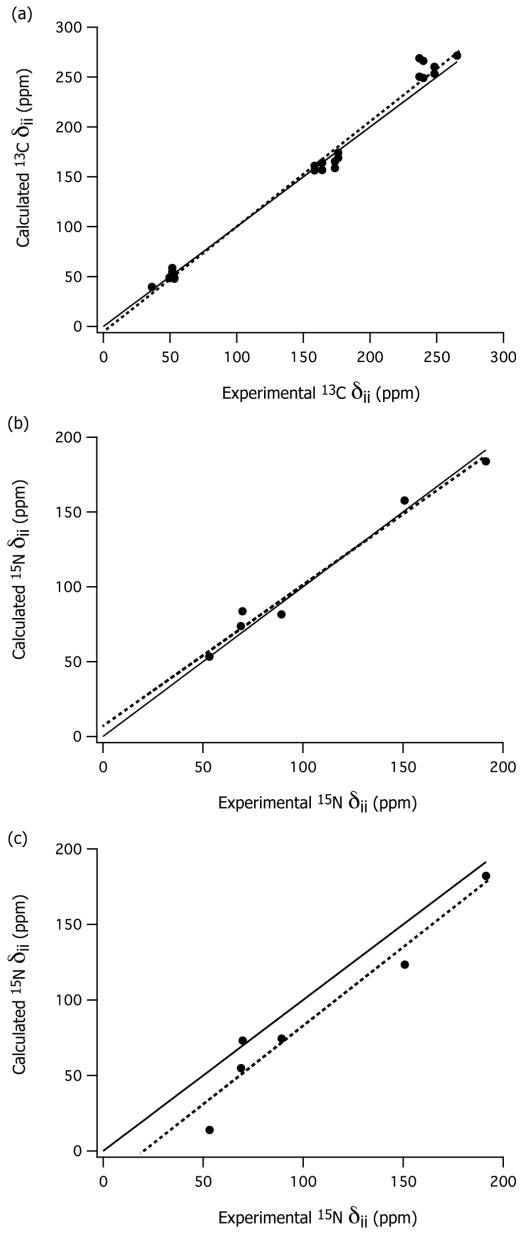

Figure 1.4 Correlation between the principal components δ_{ii} of the calculated (DFT) and experimental (NMR) chemical shift anisotropy tensors of Th•HCl and Th:

a) ^{13}C of C2 and C6'; b) ^{15}N of N4' with chloride anions; and c) ^{15}N of N4' without chloride anions. The solid lines in both figures indicate perfect agreement ($\delta_{cal} = \delta_{exp}$), and the dotted lines are the least-square fits: (a) $\delta_{cal} = 1.05 * \delta_{\exp} - 4.88$, $R^2 = 0.99$; (b) $\delta_{cal} = 0.94 * \delta_{\exp} + 7.86$, $R^2 = 0.98$; and (c) $\delta_{cal} = 1.03 * \delta_{\exp} - 20.28$, $R^2 = 0.94$.

1.3.5 ^{13}C and ^{15}N solution NMR chemical shifts of N4 and C6 atoms from the IP model compound

N1, N4-dimethyl-4-iminopyrimidine was shown to be an appropriate model for the enzyme bound IP tautomer by Jordan et al., (*20*). Baykal et al. determined the ^{15}N NMR chemical shift for the N4 atom and also determined the ^{1}H NMR chemical shifts ^{1}H atoms using [N4 – ^{15}N] N1, N4-dimethyl-4-iminopyrimidine generated *in situ* in the NMR tube (*19*).

The natural abundance ^{13}C NMR chemical shift for the C6 atom in N1,N4-dimethyl-4-aminopyrimidinium iodide and N1, N4-dimethyl-4-iminopyrimidine were determined as follows:

Firstly, the ^{1}H NMR, natural abundance ^{13}C NMR and ^{1}H-^{13}C hmqc spectra were acquired. The ^{1}H NMR spectrum was in excellent agreement with previously reported data enabling specific assignment of the C2-H, C5-H and C6-H resonances. Next, a single cross peak corresponding to the C6-H in the ^{1}H dimension of the ^{1}H-^{13}C hmqc spectrum allowed assignment of the C6 carbon resonance in the ^{13}C dimension. This assignment was confirmed by identification of a resonance at 145.54 ppm in the ^{13}C NMR spectrum (see Table 1.3). Next, the broad resonance at 9.42 ppm in ^{1}H NMR spectrum pertaining to N4-H was used as a reporter for the generation of N1, N4-dimethyl-4-iminopyrimidine. Upon titration, the ^{1}H NMR resonance diminishes and at ~1:1 molar ratio with base it is absent. Similar ^{1}H NMR, natural abundance ^{13}C NMR and ^{1}H-^{13}C hmqc NMR spectra were acquired. These spectra enabled assignment of the C6 atom resonances in ^{13}C dimension (see Table 1.3). This assignment was confirmed by identification of a resonance at 135.99 ppm in the ^{13}C NMR spectrum.

Table 1.3 Assignment of aromatic ^{1}H and ^{13}C resonances for the IP model compound

Ref. TMS δ, 0.00 ppm	N1,N4-Dimethyl-4-aminopyrimidinium		N1,N4-Dimethyl-4-iminopyrimidine	
	^{1}H, δ ppm	^{13}C , δ ppm	^{1}H, δ ppm	^{13}C , δ ppm
C2-H	8.815 (d)	154.922	7.705 (d)	150.303
C5-H	6.802 (d)	106.515	5.678 (d)	110.744
C6-H	8.117 (dd)	145.537	6.862 (dd)	135.989
N4-H	9.412 (br, s)	---	---	---

Table 1.4 Model NMR chemical shifts of the key C2, C6' and N4' atoms in various enzyme bound ionization and tautomeric states of ThDP

Model compound	*Thiamin hydrochloride*	*Thiamin*	*1,4 – Dimethyl-4-iminopyrimidine*
Enzyme bound ThDP state	4'-Aminopyrimidinium **(APH^+)** (δ ppm)	4'-Aminopyrimidine **(AP)** (δ ppm)	1',4'-Iminopyrimidine **(IP)** (δ ppm)
C2 (a, d)	153.5	156.8	--
C6' (b, e)	147.9	160.7	135.9†
N4' (c, f)	114.2	89.3	212.0†
C2 carbanion or the ylide **(YI)** (δ ppm)		253‡	

(a, b, c, d, e, f) = Labels used in Scheme 1.5 to depict these atoms in enzyme bound ThDP. Chemical shifts reported for thiamin hydrochloride and thiamin are from Solid-state CPMAS NMR experiments. See Table 1.2 for solution NMR chemical shifts.† = Solution NMR chemical shifts of 1,4–Dimethyl-4-iminopyrimidine, a model for the IP form, generated *in situ* in an NMR tube by titration of 1,4–dimethyl-4-aminopyrimidinium iodide with sodium(bistrimethylsilyl)amide (*19*). ‡ = Solution NMR chemical shift of a stable thiazol-2-ylidene, used as a guide for the enzyme bound YI resonance (*73*).

Scheme 1.5 Assignment of NMR resonances to individual ThDP atoms in enzyme bound species.

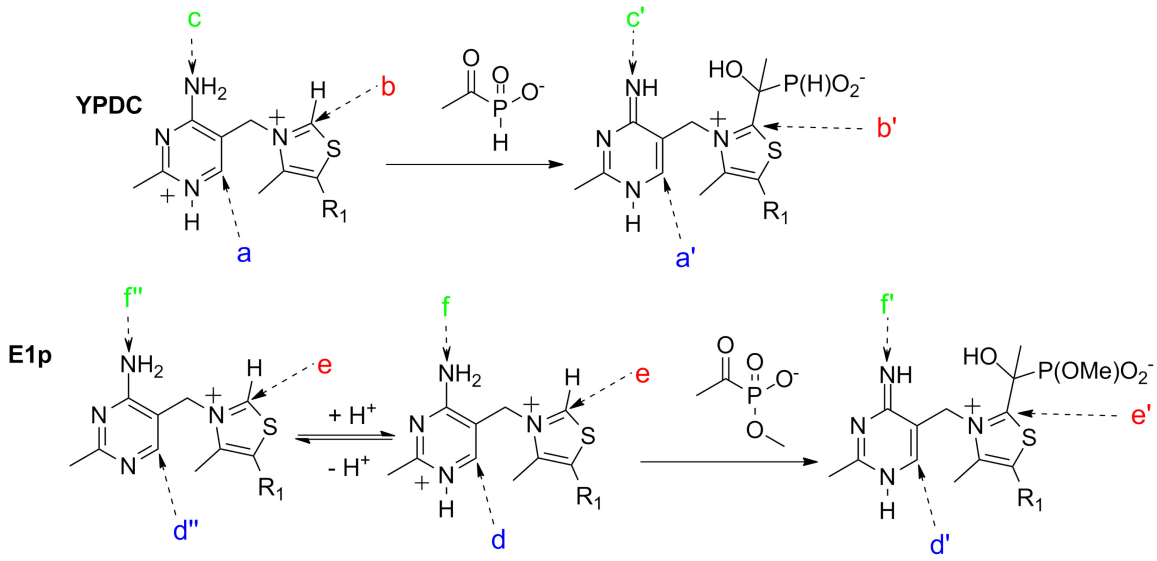

Labels in: (Blue) correspond to C6' atom and (Red) correspond to C2 atom observed in ^{13}C CPMAS SSNMR experiments (Figure 1.5, Figure 1.7, and Figure 1.10); (Green) correspond to N4' atom observed in ^{15}N NMR experiments (Figure 1.11, Figure 1.12, and Figure 1.13).

1.3.6 The chemical shift of C2 is perturbed on enzyme bound ThDP

A ^{13}C CPMAS SSNMR spectrum acquired with YPDC (unlabeled ThDP) sample was used as control spectrum for ^{13}C resonances originating from enzyme residues. In the 100 – 200 ppm region illustrated in Figure 1.5d, the anticipated region for ThDP C2 and C6' atoms, resonances pertaining to (i) the backbone and side-chain carbonyl carbons, and carboxylate carbons (170 – 180 ppm), (ii) aromatic carbons originating from aromatic amino acid side chains (120 – 140 ppm) and (iii) Cζ carbon atoms from tyrosine and arginine residues (157 – 160 ppm) were observed. Apart from these regions, no other resonances which could potentially interfere with ^{13}C ThDP resonances were observed (see model chemical shifts from Table 1.4). Similar control spectra were acquired for E1p and E1o samples and the same general features were observed.

When the ^{13}C CPMAS SSNMR spectrum of YPDC reconstituted with [C2,C6'–$^{13}C_2$]ThDP, a sample containing 4 labeled ThDP molecules per tetrameric enzyme molecule (Mr 250,000), was compared with the YPDC (with unlabeled ThDP) spectrum, two new resonances stood out: One resonance at 162.2 ppm; and another at 146.8 ppm, reminiscent of the C6' carbon in protonated form of thiamin (Figure 1.5 c, d). On the basis of this experiment, and experiments on E1o reconstituted with [C2,C6'–$^{13}C_2$]ThDP (Figure 1.7 a) and E1p reconstituted with [C2–^{13}C]ThDP (Figure 1.10 a) discussed later in this section, the resonances could be assigned to individual atoms of ThDP bound to YPDC, the one at 162.2 ppm to C2 and the one at 146.8 ppm to C6' (refer to Scheme 1.5 for assignment of NMR resonances to enzyme bound ThDP atoms, and to Table 1.4 for relevant model chemical shifts for comparison).

Based on these observations the following conclusions can be drawn:

a. ThDP is in its APH^+ form according to the chemical shift of the C6' atom on all three enzymes. All of the enzyme-bound thiamin pK_a values are higher than that in water (4.85 units, (*21*)), presumably raised by the conserved glutamate within short H-bond of the N1' atom of bound ThDP.
b. The C2-H bond of the thiazolium ring is in its un-dissociated form, not in the ylide form. No evidence could be found for any resonances near 250 ppm previously assigned to a YI model by solution NMR (*73*).
c. In the SSNMR experiments, there is a small but measurable chemical shift revealing a ca. 6-9 ppm deshielding of the thiazolium C2 atom by the enzymes. This perturbation is within experimental error the same on YPDC, E1p and E1o.

In an earlier solution NMR study using [C2-^{13}C]ThDP with YPDC (*53*), evidence was presented that the C2 chemical shift is virtually unchanged compared to free ThDP.

Solution NMR experiments using YPDC reconstituted with [C2,C6'-$^{13}C_2$]ThDP did not yield conclusive results. Spectra of YPDC and apo-YPDC reconstituted with labeled ThDP appeared similar, with no discernible changes at either the ~146 ppm (C6') or ~162 ppm (C2) region. Acid quench of the sample and NMR analysis of supernatant confirmed the presence of labeled ThDP in the supernatant. Acid quench of a similar sample containing additional acetyl phosphinate, followed by NMR analysis of supernatant revealed the presence mostly (~ 85%) of C2α-phoshinolactylThDP (PhiLThDP) and some ThDP (Figure 1.6), confirming the success of the reconstitution procedure, and also the ability of the reconstituted enzyme to form reaction intermediates.

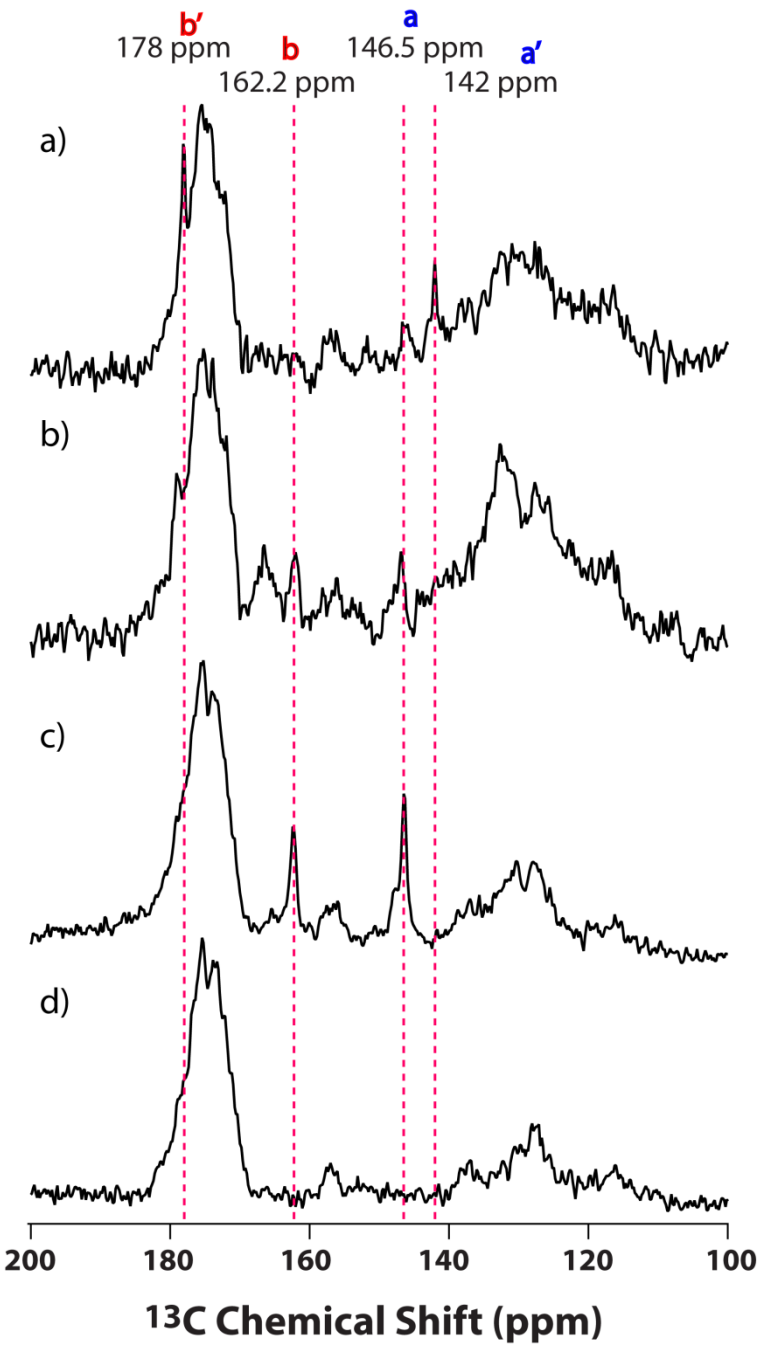

Figure 1.5 ^{13}C CPMAS SSNMR spectra of YPDC with [C2,C6'–$^{13}C_2$]ThDP.

a) [C2,C6'–$^{13}C_2$]ThDP and acetyl phosphinate (60 mM) **b)** [C2,C6'–$^{13}C_2$]ThDP and pyruvamide (100 mM). The broad resonance at ~166 ppm is from pyruvamide **c)** only [C2,C6'–$^{13}C_2$]ThDP **d)** YPDC with unlabeled ThDP. control spectrum. All the spectra were acquired at 5 ºC with 16,384 transients and 5 s recycle delay.

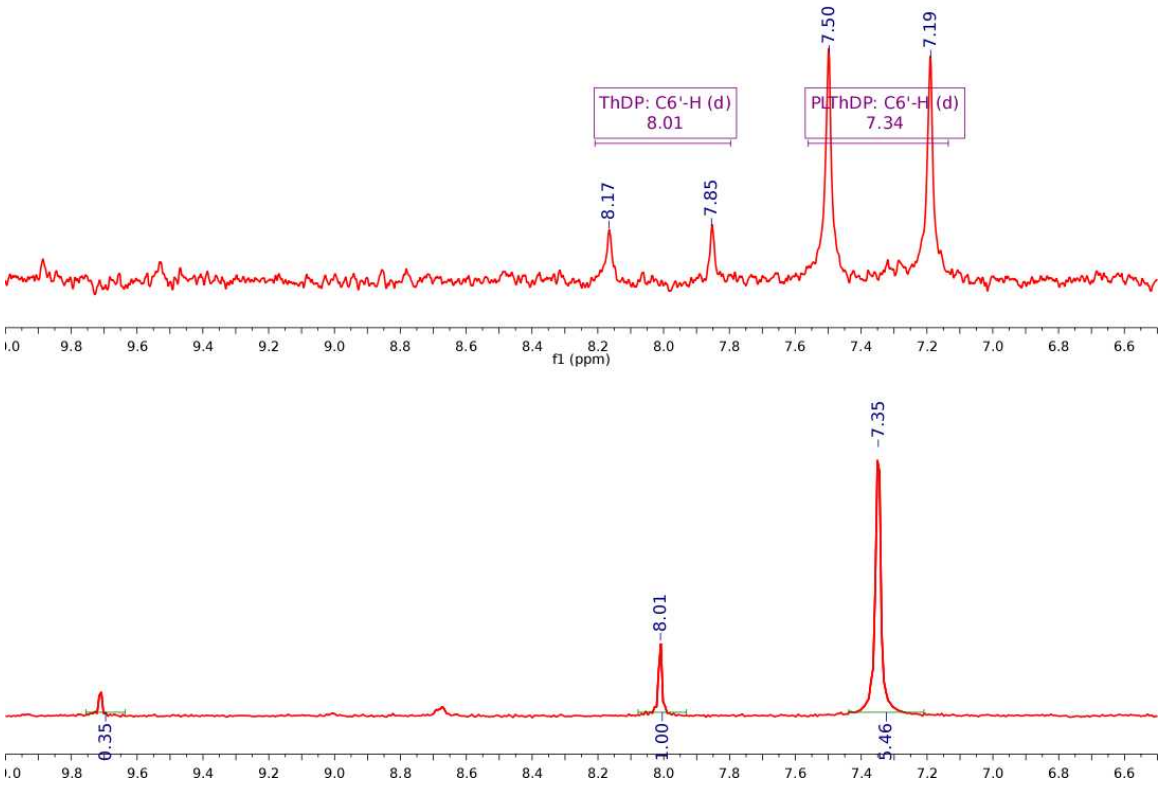

Figure 1.6 ^{1}H-^{13}C HSQC(1D-^{1}H) NMR analysis of ThDP covalent intermediates.

C6'-H fingerprint region in spectra obtained after chemical quench NMR analysis of the supernatant from a mixture containing YPDC reconstituted with [C2, C6' – $^{13}C_2$] ThDP and incubated with 40 mM acetyl phosphinate. **Bottom:** ^{1}H decoupled spectrum showing (i) $^{13}C6'$-H resonance of ThDP from active-sites containing the Michaelis complex (according to CD spectroscopy) at 8.01 ppm and (ii) the $^{13}C6'$-H resonance of C2-α-PhiLThDP. Relative integration of signals yields an estimate of filled active-sites (~ 85%). **Top:** ^{1}H non-decoupled spectrum showing the $^{13}C6'$-^{1}H coupling. The coupling constant is 186 Hz for both signals confirming the resonance at 7.35 ppm originates from a ThDP adduct.

1.3.7 Internal equilibrium on enzymes prior to substrate binding.

The solid-state isotropic chemical shift of the C6' atom provided direct evidence for the presence of the APH^+ form on all three enzymes tested. The current SSNMR findings - with the C6' atom - are complementary to the CD results where only the AP and IP forms could be detected, pH titration of the AP form affords a titration curve enabling calculation of the pK_a of the APH^+ form on several enzymes (see Figure 1.8 for an example of such a pH titration on E1o), and indirectly implies the presence of the APH^+ form (*15*).

Consequently, in a corresponding SSNMR experiment, increasing the pH should decrease the relative concentration of the APH^+ form, and only the C6' resonance should be affected. To test this idea ^{13}C CPMAS SSNMR spectra of E1o reconstituted with [C2,C6'–$^{13}C_2$]ThDP at pH 7.0 and at pH 8.0 were acquired (Figure 1.7).

Increasing the pH from 7.0 to 8.0, the resonance at 146 – 147 ppm pertaining to the C6' carbon diminishes in intensity significantly (relative to protein backbone), whereas the resonance at ~ 161 ppm pertaining to the C2 carbon is relatively unaffected. Moreover, a broad new resonance is seen at 167.2 ppm which is assigned to C6' of enzyme bound ThDP in the AP form. Results from ^{15}N CPMAS SSNMR experiments on E1p to be discussed later in this section support these conclusions.

1.3.8 Substrate surrogate activation of YPDC does not affect ionization/tautomeric states of 4'-aminopyrimidine moiety of enzyme bound ThDP.

YPDC activity is known to be regulated by substrate binding at a distinct regulatory site Cys221 (*74-76*). Pyruvamide a non-decarboxylating analog is a known substrate activator surrogate (*77*). X-ray crystallography studies provide evidence for large scale rearrangements in conformations of two loop regions (101 – 113, and 292 – 301) in presence of pyruvamide and also pyruvate leading to a sequestered active-site (*26*). H/D exchange experiments at the thiazolium C2 position on activated and unactivated YPDC point clearly to the cofactor C2-H bond as the locus of activation and as much as a 1000-fold enhancement of the exchange rate in the presence of pyruvamide was observed (*53*).

In a spectrum of apo-YPDC reconstituted with [C2,C6'–$^{13}C_2$]ThDP and pyruvamide (100 mM) (Figure 1.5 b), there was no change in chemical shift of the C2 and C6' resonances, which were again found at 162 ppm and 146 ppm, respectively. However, the intensities for these resonances were diminished as compared to the sample in the absence of pyruvamide (unactivated) (Figure 1.5 c). This apparent reduction in intensities could arise possibly due to some conformational exchange broadening of the lines in the presence of pyruvamide.

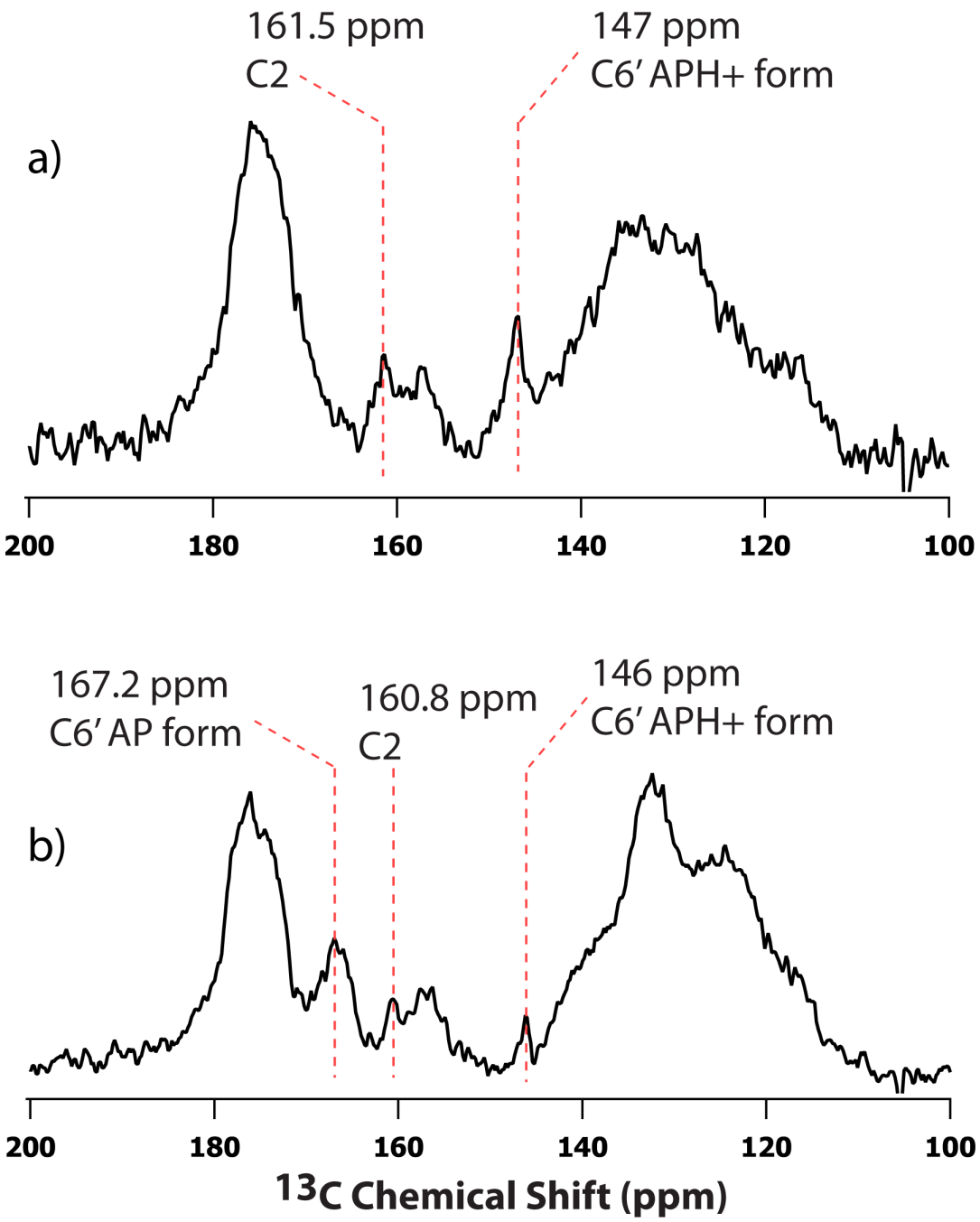

Figure 1.7 *^{13}C CPMAS SSNMR spectra of* **E. coli** *2-oxoglutarate dehydrogenase E1 reconstituted with [C2,C6' –$^{13}C_2$]ThDP.*

a) Spectrum acquired at pH 7.0 at 8 ºC with 32,768 transients. **b)** Spectrum acquired at pH 8.0 at 10 ºC with 28,900 transients. Recycle delay was 5 s for acquiring both spectra.

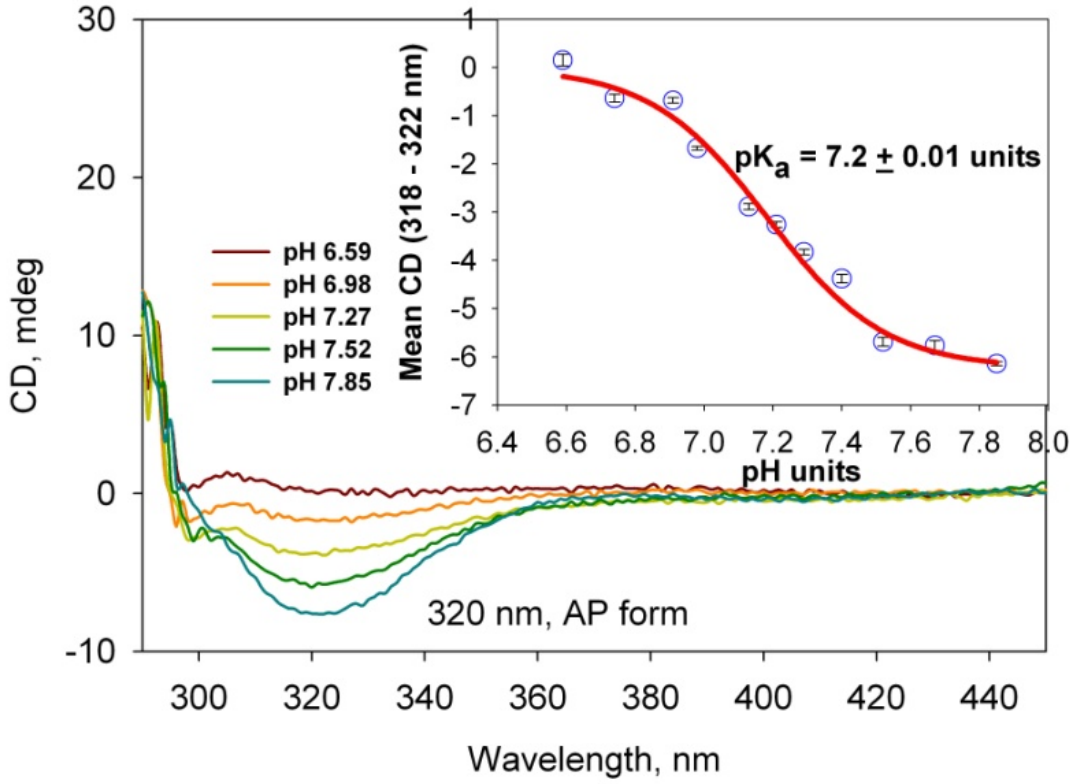

Figure 1.8 Near UV CD spectra of E1o at varying pH values.

Representative CD spectra of the E1o component. (inset) pH dependence of the CD bands at 320 nm reflecting AP formation. E1o (5 mg/mL) was diluted in a triple buffer (15 mM MES, 15 mM KH_2PO_4, and 15 mM Tris) containing additional 0.5 mM ThDP, and 2.5 mM $Mg2^+$ at pH 7.0. To study the pH dependence of the spectral bands, the pH of the protein solution was adjusted to the desired value with either 1M acetic acid or 1M Tris base monitored using a sympHony pH electrode (VWR) and CD spectra were recorded after each adjustment. The pK_a was determined using the equation: $\log(Y) = \log(Y_{max}) - \log(1 + 10^{(pKa-X)})$ where Y and Y_{max} are CD and CD_{max}.

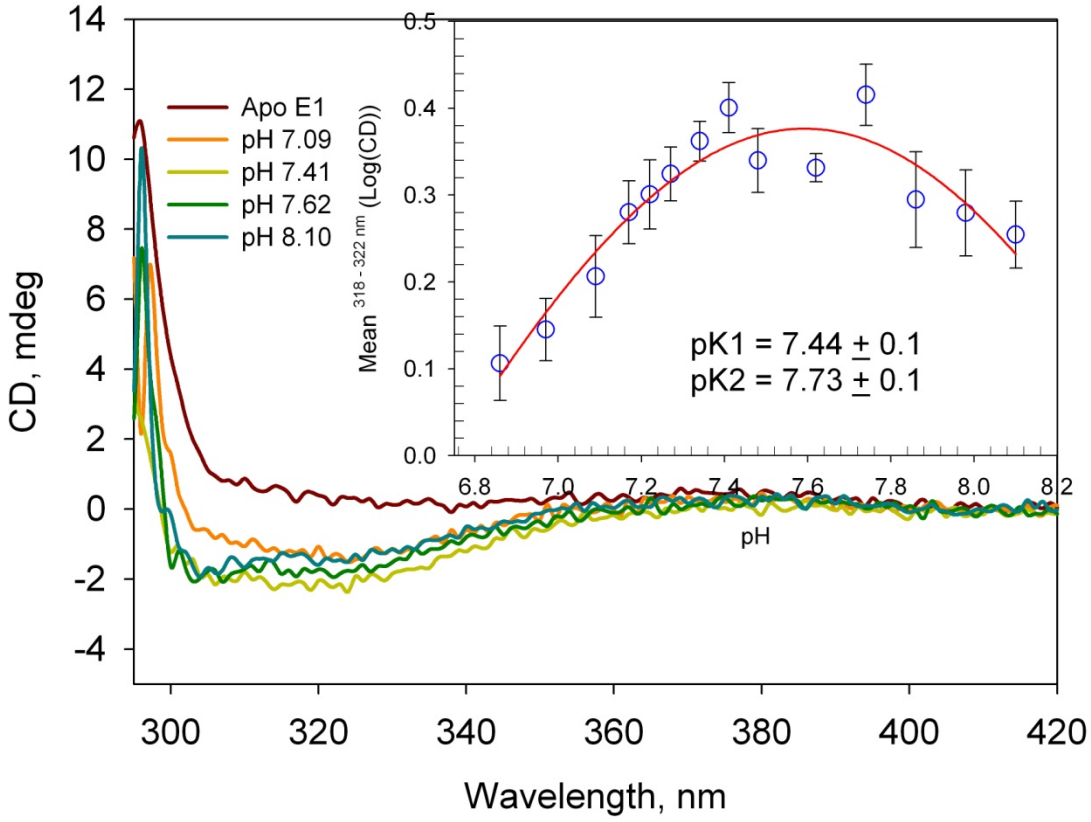

Figure 1.9 Near UV CD spectra of E1p at varying pH values.

Representative CD spectra of the E1p component. (inset) pH dependence of the CD bands at 320 nm reflecting AP formation. E1p (5 mg/mL) was diluted in a triple buffer (15 mM MES, 15 mM KH_2PO_4, and 15 mM Tris) containing additional 0.5 mM ThDP, and 2.5 mM $Mg2^+$ at pH 7.0. To study the pH dependence of the spectral bands, the pH of the protein solution was adjusted to the desired value with either 1M acetic acid or 1M Tris base monitored using a sympHony pH electrode (VWR) and CD spectra were recorded after each adjustment. The pKs were determined using the equation: $\log(Y) = \log(Y_{max}) - \log(1 + 10^{(pK1-X)} + 10^{(X - pK2)})$ where Y and Y_{max} are CD and CD_{max}. Apo E1p spectrum was recorded in buffer containing no ThDP.

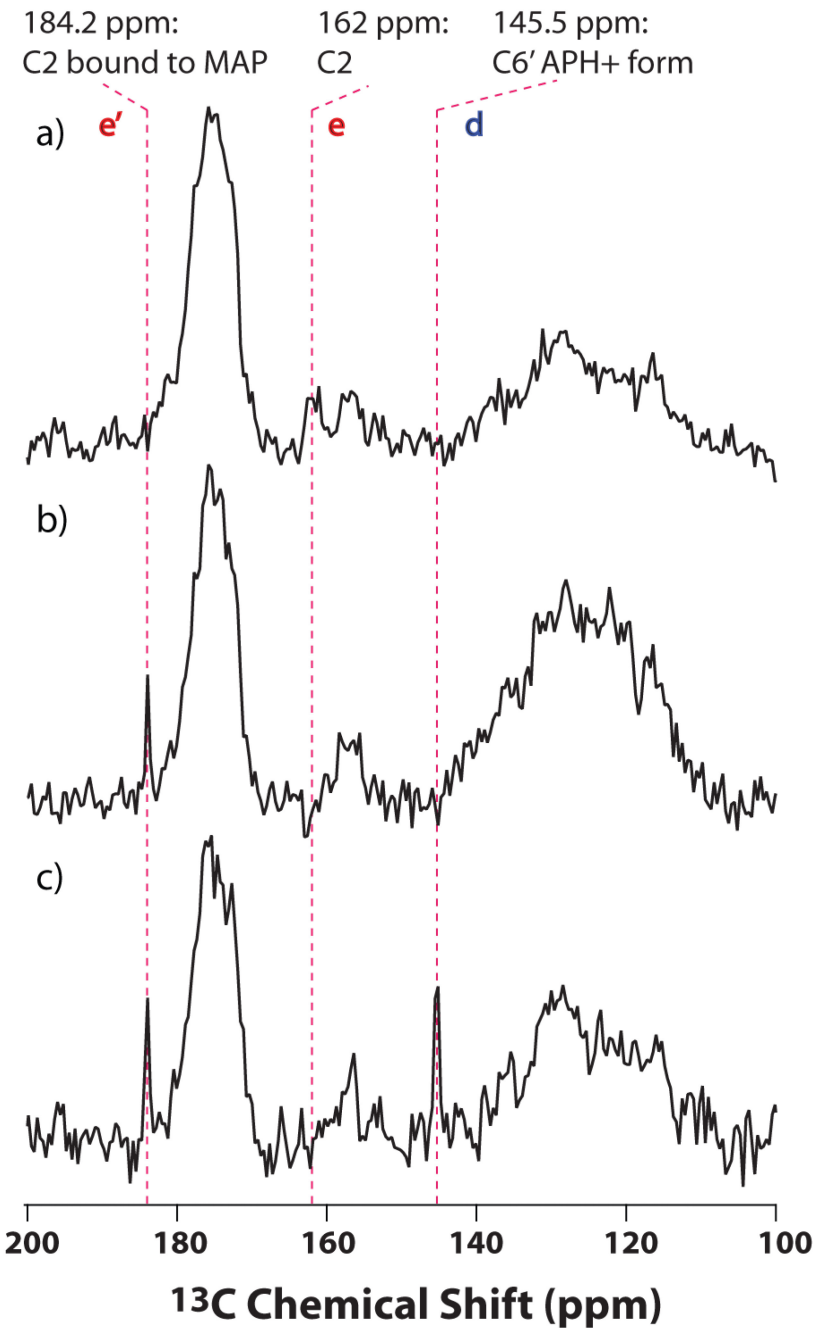

Figure 1.10 ^{13}C CPMAS SSNMR spectra of E1p reconstituted with [C2,C6'–$^{13}C_2$]ThDP and [C2–^{13}C]ThDP

E1p reconstituted with: **a)** [C2–^{13}C]ThDP. **b)** [C2–^{13}C]ThDP and additional 10 mM methyl acetylphosphonate. **c)** [C2,C6'–$^{13}C_2$]ThDP and additional 10 mM methyl acetylphosphonate. The spectra were acquired at 15 ºC with 16,384 transients; the recycle delay was 10 s (spectrum a) and 5 s (spectra b and c).

1.3.9 The thiazolium C2 resonance reports formation of a stable pre-decarboxylation intermediate derived from a substrate analog.

At Rutgers, advantage has been taken of the fact that 2-oxophosphonates and 2-oxophosphinates are excellent 2-oxoacid analogs that form stable pre-decarboxylation intermediate analogs (*78, 79*). In the first instance, methyl acetylphosphonate (MAP, single negative charge at the phosphonate monoester) was used on several enzymes and with E1p *from E. coli* the covalent pre-decarboxylation analog intermediate 2-phosphonolactylThDP (PLThDP) (Scheme 1.2) could be identified by x-ray crystallography. Also, acetyl phosphinate (AcPhi), an even better steric approximation to pyruvate was shown on several enzymes to not only form such complexes but to also act as potent inhibitor (*80*). Both of these pyruvate analogs gave strong indication that in their covalent adducts with ThDP on enzymes, the IP tautomeric form predominates. Further evidence for the environment around individual C2, C6', and N4' atoms in these covalent intermediate analogs was gathered using SSNMR spectroscopy.

Addition of MAP to E1p resulted in the spectra in (Figure 1.10 b, c). First, a weak signal at 162 ppm in the bottom spectrum in the absence of MAP confirms the bound C2 resonance also seen in Figure 1.5 c and Figure 1.7. Two experiments were carried out in the presence of MAP to facilitate the assignments: spectrum b is with the single ^{13}C2 label, spectrum c with the [C2,C6'-$^{13}C_2$]ThDP. The spectra provide unambiguous assignment of C2 and C6' - 183 ppm for the former and 146 ppm for the latter - in the presence of MAP.

The C2 resonance at 183 ppm displays a 21 ppm deshielding on formation of the tetrahedral PLThDP, appropriate for replacement of H by C (*81*). The following experiment confirmed formation of PLThDP. Chemical quench with acid, followed by solution NMR analysis of the supernatant from a mixture of E1p reconstituted with [C2,C6'-$^{13}C_2$]ThDP and MAP revealed the presence of PLThDP at ~80% occupancy in the active site.

While the enzyme bound PLThDP adduct is anticipated to exist in the IP tautomeric state and the corresponding C6' resonance is predicted by model studies to appear around 136 ppm, the major resonance for the C6' atom appears at around 146 ppm and is assigned to the APH^+ state. Since the ^{13}C resonance for the IP tautomer falls in the envelope of enzyme aromatic residues, conclusive evidence is not available from this experiment for the IP form.

Addition of AcPhi to YPDC resulted in the spectrum in Figure 1.5 b. Three prominent changes were observed. (1) The C2 resonance at 162 ppm disappears. (2) Two new resonances at 142 ppm and 179 ppm appear. (3) The resonance at 146 ppm for the C6' in the APH^+ form of ThDP is significantly diminished**.** Similar to the E1p-MAP experiment, the disappearance of the 162 ppm resonance and the appearance of a new one at 178 ppm could be attributed to the C2 atom in the enzyme-bound C2-α-phosphinolactylThDP intermediate. The most novel finding is the strong resonance at 142 ppm, seen along with the weaker yet clear resonance at 146 ppm. Firstly, the resonance at 146 ppm corresponds to a fraction of unreacted enzyme-bound ThDP, seen as a Michaelis complex in CD experiments on YPDC, while the resonance at 142 ppm most likely pertains to the 4'-aminopyrimidine ring of C2α-phosphinolactylThDP. The chemical shift for C6' resonance

in the IP form is 136 ppm from model studies, and the chemical shift observed is a value in between the IP (136 ppm) and the APH^+ (147.9 ppm) suggesting a possible averaging due to fast exchange between these two forms in the active-sites containing the tetrahederal intermediate analog as depicted in Scheme 1.6. No unambiguous evidence was obtained for the IP tautomeric form from the C6' chemical shifts, however, the C2 chemical shifts provided evidence for direct detection of enzyme bound tetrahedral intermediate of ThDP by NMR.

1.3.10 Nitrogen - 15 chemical shifts on addition of substrate analogs confirm protolytic equilibria under various conditions

It was anticipated that observation of the ^{15}N resonance from ThDP specifically ^{15}N-labeled at the 4' position may provide the most direct evidence for the state of tautomerization/ionization of the 4'-aminopyrimidine ring. Therefore, [N4'-^{15}N] ThDP was synthesized and E1p was reconstituted with this compound. This experiment is even more challenging than the ^{13}C experiments above because of the lower sensitivity of the ^{15}N nuclide and the ensuing lower S/N ratios even at 14.1 T (^1H Larmor frequency of 600 MHz). A ^{15}N CPMAS SSNMR spectrum acquired with E1p (unlabeled ThDP) sample showed no prominent features other than some broad resonances in the backbone amide region (105 – 135 ppm). Similar control spectra were acquired for YPDC sample and the same general features were observed. Importantly, the ^{15}N resonance of the N4' atom of ThDP in the APH^+ ionization state appears at 116.5 ppm which falls within the envelope of the enzyme backbone amide resonances. Nevertheless, the CPMAS ^{15}N SSNMR spectra

acquired with E1p reconstituted with [N4'-^{15}N] ThDP presented in Figure 1.11 and Figure 1.12 do provide important insight.

Internal equilibrium in E1p active-sites prior to substrate binding.

The enzyme bound ThDP is predicted to be in the APH^{+} form according to the ^{13}C experiments with E1p at pH 7.0. Due to the overlap of resonances from enzyme residues with the ThDP N4' resonance no clear indication of enzyme bound ThDP in ^{15}N CPMAS SSNMR experiments at pH 7.0 could be obtained (Figure 1.11 b). However, ^{13}C experiments with E1o and CD experiments on many members of the ThDP superfamily suggest a shift in equilibrium to the AP form, which can be detected at 89 ppm (according to model chemical shifts), in enzyme bound ThDP at higher pH values. A spectrum of the sample containing E1p reconstituted with [N4'-^{15}N] ThDP at pH 8.0 (Figure 1.12 b) indeed shows clear evidence for a resonance at 84.6 ppm corresponding to the AP form of enzyme bound ThDP.

A spike on the high field side of the protein backbone band at ~107 ppm in the spectrum of E1p with [N4'-^{15}N] ThDP at pH 7.0 as illustrated in (Figure 1.11 b) is a likely candidate for the N4' atom of enzyme-bound ThDP in the APH^{+} form for the following reasons. The spike is not observed in the sample at pH 7.0 with MAP, consistent with the conversion of ThDP to PLThDP in this sample. In the spectra of pH 8.0 samples, this spike is not observed in the spectrum of the sample with MAP, and is observed in lesser prominence in the spectrum of the sample without MAP, where the enzyme bound ThDP exists in equilibrium between APH^{+} and AP forms.

Observation of the N4' atom in the presence of MAP

In a spectrum of the sample containing E1p reconstituted with [N4'-^{15}N] ThDP at pH 8.0 containing additional MAP clear indication of a new signal around 141.2 ppm could be observed. This chemical shift is in-between the 212 ppm for the IP form and APH^{+} at 114.2 ppm (89.3 ppm for the AP form) - values from models in the absence of the enzyme (Figure 1.11 a). Also, a spectrum of the sample containing E1p reconstituted with [N4'-^{15}N] ThDP at pH 8.0 containing additional MAP shows clear evidence for resonances at (i) 84.6 ppm pertaining to the fraction of enzyme bound ThDP in AP form and at (ii) 141.2 ppm pertaining to the form.

Considering the CD and SSNMR data *in toto*, a plausible explanation for the observed value of 141 ppm at pH 7.0 is as follows. According to the positive CD signal observed on complexes of ThDP enzymes with phosphonate or phosphinate based substrate analogs, the tetrahederal adduct formed between the ThDP and these analogs in predominantly in the IP form (presumably in a fast exchange equilibrium with the APH^{+} form, for which we have not identified a CD signature). At the higher pH of 8.0, we observe the additional resonance at 84.6 ppm pertaining to the active-sites with ThDP in the AP form presumably in a slow equilibrium with the other forms. Similar chemical shift averaging due to fast exchange on pyridoxal model systems and also between two-site and three-site equilibria are seen by solid-state NMR studies on the pyridoxal-5'-phosphate dependent tryptophan synthase when the active-site is occupied by a quinonoid intermediate (*52, 82-84*). While the model chemical shifts for these three environments are good, the impact of the enzyme environment on the chemical shift of ^{15}N resonances, especially for strongly hydrogen bonded systems, is difficult to predict, and equally difficult to model.

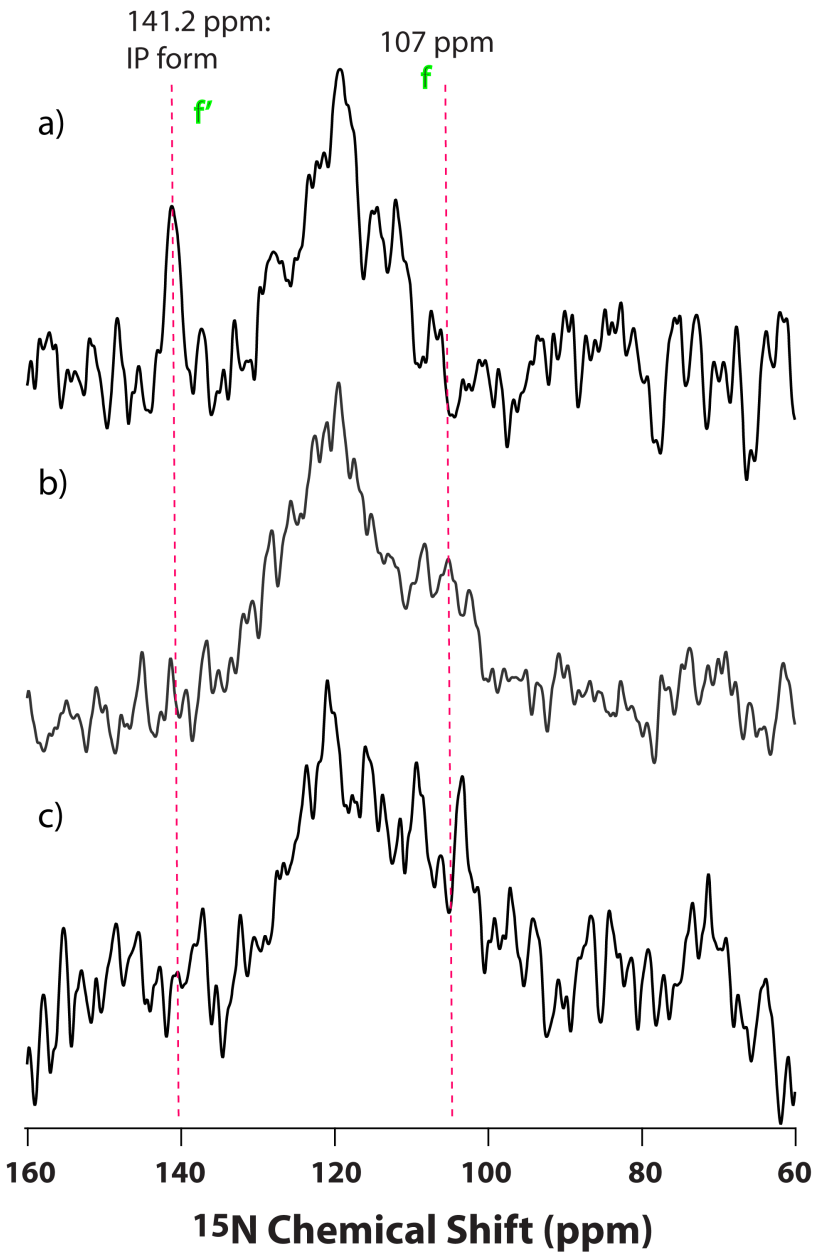

Figure 1.11 ^{15}N CPMAS SSNMR spectra of E1p reconstituted with [N4'–^{15}N]ThDP at pH 7.0.

E1p reconstituted with: **a)** 3 eq. [N4'–^{15}N]ThDP and additional 10 mM methyl acetylphosphonate at -25 ^{o}C. **b)** 3 eq. [N4'–^{15}N]ThDP at -25 ^{o}C. **c)** 1 eq. [N4'–^{15}N]ThDP at -23 ^{o}C. The spectra are a sum of 30,720 transients (spectrum a), 16,384 transients (spectrum b), and 14,336 transients (spectrum c); the recycle delay was 5 s. All spectra were processed with 50 Hz exponential broadening.

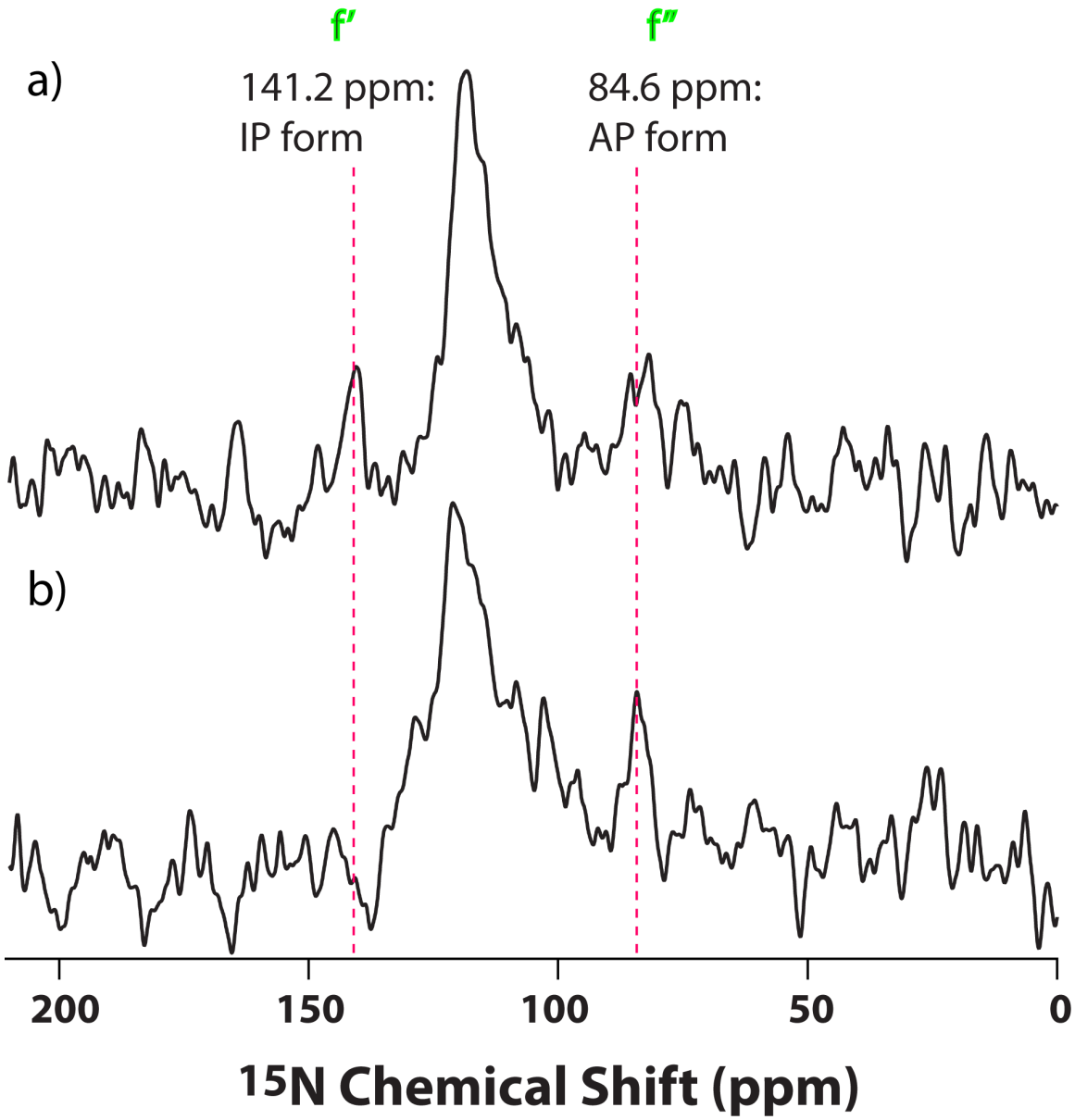

Figure 1.12 ^{15}N CPMAS SSNMR spectra of E1p reconstituted with [N4'–^{15}N]ThDP at pH 8.0.

E1p reconstituted with **a)** 3 eq. [N4'–^{15}N]ThDP and additional 10 mM methyl acetylphosphonate. **b)** Reconstituted with 3 eq. [N4'–^{15}N]ThDP. The spectra were acquired at -25 ^{o}C with 32,768 scans and 5 s recycle delay. Both spectra were processed with 100 Hz exponential broadening.

Scheme 1.6 Likely explanations for $^{15}N4'$ chemical shift of ThDP in active-centers with tetrahederal intermediates

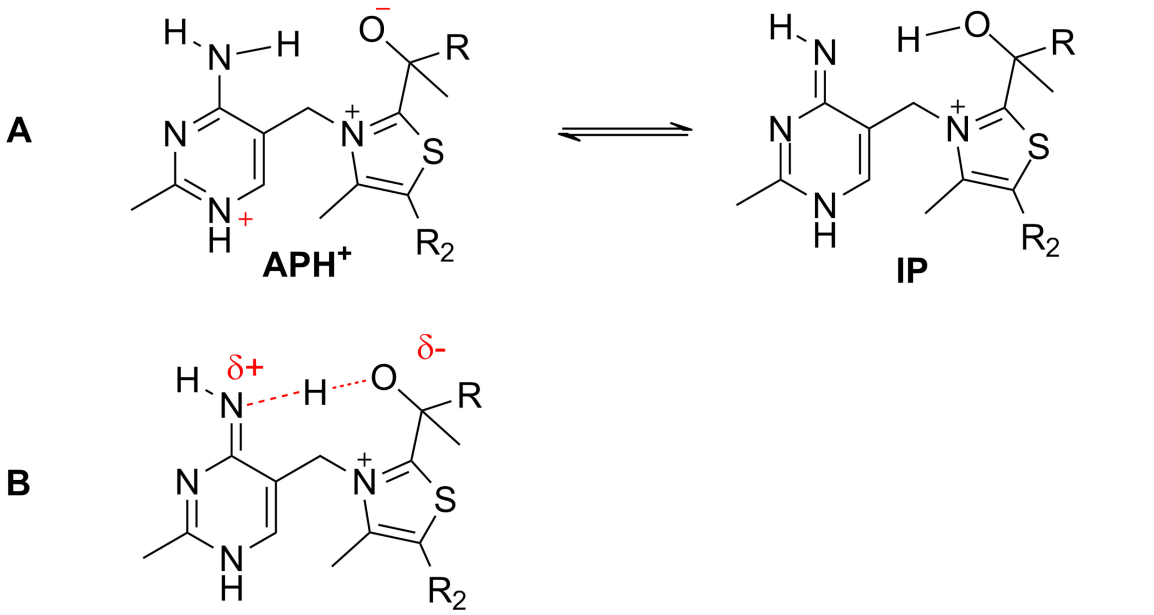

R = $P(OMe)O_2^-$, C2-α-phosphonolactylThDP
R = $P(H)O_2^-$, C2-α-phosphinolactylThDP
R = CO_2^-, C2-α-lactylThDP
R = H, C2-α-hydroxyethylThDP
R_2 = β-hydroxyethyl diphosphate

A) Fast exchange equilibrium between the APH+ and IP states. The resonance structure of the APH^+ form is shown with the formal + charge placed on N1' position. **B)** Tetrahederal intermediate with a proton forming intramolecular strong H bonds (represented by dashed red lines) with two electronegative atoms.

Observation of the N4' atom on YPDC.

In the CPMAS ^{15}N SSNMR spectrum of a sample containing YPDC reconstituted with [N4'-^{15}N] ThDP at pH 6.0 a broad signal pertaining to enzyme backbone resonances is observed (Figure 1.13). The spectrum of a sample containing additional pyruvamide is essentially similar. There are no observable differences between these spectra. No clear evidence for the N4' atom of enzyme bound ThDP at pH 6.0 could be obtained from these experiments.

However, in a spectrum of a sample also containing acetylphosphinate, there is in evidence for a signal centered at 176 ppm, assigned to the IP form which is in protolytic equilibrium as discussed earlier.

We could propose two possible explanations for the observed chemical shift:

(a) Assuming that the observed signal represents a weighted average of IP (212 ppm in models) and APH^+ (116 ppm in models) in a fast exchange (Scheme 1.6 A), the observed NMR chemical shift under these conditions would be a 'weighted average' based on the mole fraction of each species in equilibrium. The NMR chemical shift would vary among enzymes based on the fraction species stabilized in either form by the enzymes.

(b) Alternatively, the proton affecting the ^{15}N chemical shift is located between the N4' atom and the C2α-O oxygen atom as illustrated in Scheme 1.6 B. The particular chemical shift value observed with different enzymes would depend on the location of this proton, the closer it is to oxygen, the more the observed value resembles the chemical shift of the imino tautomeric form generated in models. The observed short distances between the N4' atom and C2-α-O atom in the x-ray structure as noted in Table 1.1 indicate possibility of a

strong H-bond between these atoms which could facilitate such a H bond. Other residues hydrogen bonding to the N4' could also affect its chemical shift. The short hydrogen bond observed in the PLThDP-E1p complex (2.49 Å) certainly would not preclude such a 'bridging' proton (Figure 1.1). This explanation could also account for the observation of the IP form by CD in various members of the ThDP superfamily with a tetrahedral C2α substitution. Such an intermediate proton location would also be mechanistically useful, as this proton has to constantly shuttle during the reaction.

While the above two cases cannot be distinguished from the current experimental results, low field ^{1}H SSNMR experiments especially in the 14 - 18 ppm region, could provide evidence for intermediates containing strong H bonds.

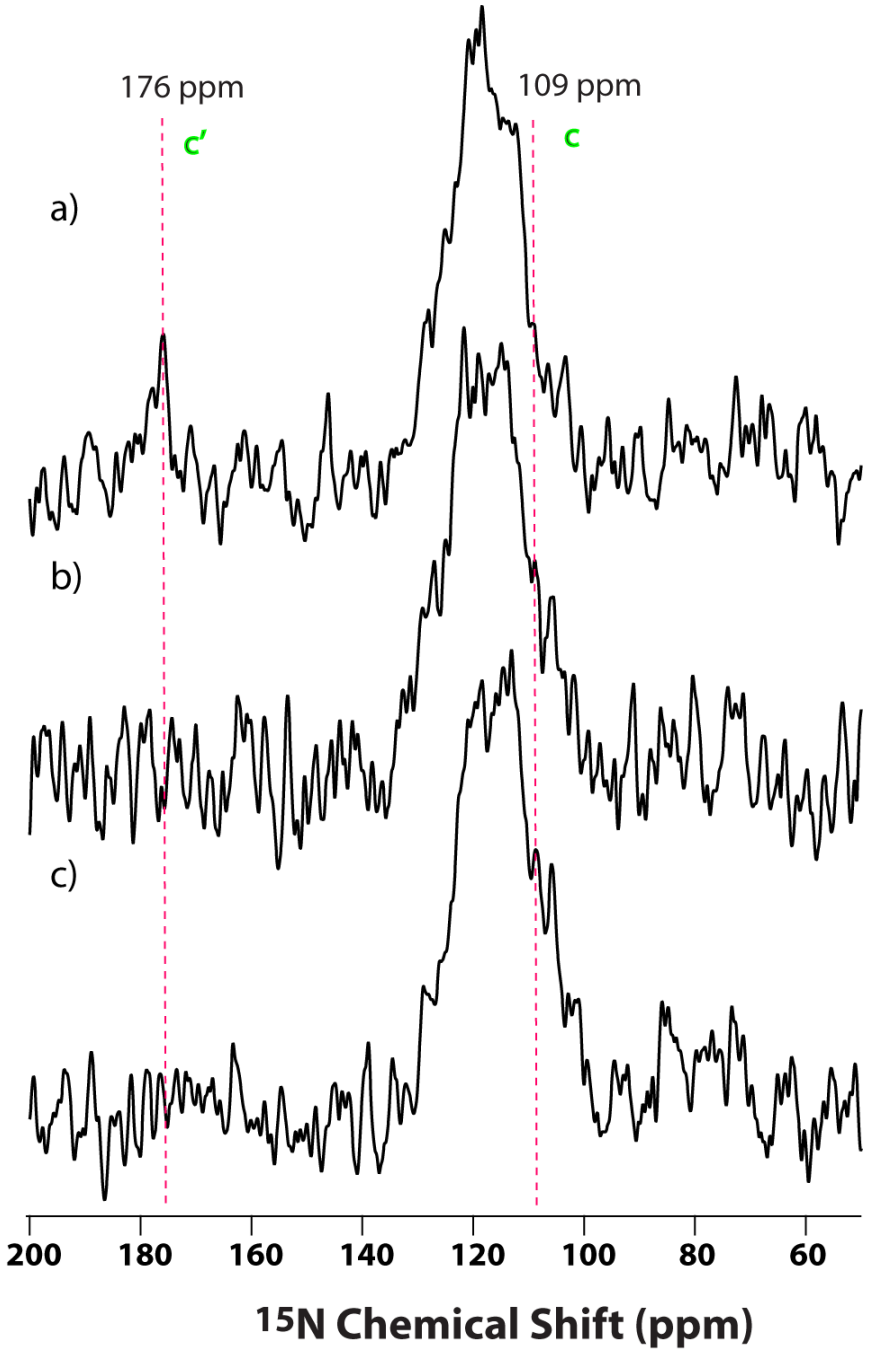

Figure 1.13 ^{15}N CPMAS SSNMR spectra of YPDC reconstituted with [N4'–^{15}N]ThDP.

YPDC reconstituted with [N4'–^{15}N]ThDP **a)** In the presence of 60 mM acetyl phosphinate at -25 ^{o}C. **b)** In the presence of 300 mM pyruvamide -25 ^{o}C. **c)** [N4'–^{15}N]ThDP -25 ^{o}C. To obtain **a)** 57,344 transients with 4 s recycle delay. **b)** 23,552 transients with 5 s recycle delay. **c)** 27,648 transients with 5 s recycle delay. 50 Hz exponential broadening was used.

1. 4 CONCLUSIONS

This study presents the first observation by solid-state NMR experiments of the states of ionization and tautomerization of ThDP bound to three enzymes by monitoring the key carbon and nitrogen atoms specifically introduced into the coenzyme. The ThDP bound to enzymes is stabilized in the protonated APH^+ state in all three enzymes in the absence of substrate near the optimal pH of the enzymes. This finding provides the first direct evidence for the initial step in the proposed mechanism of ThDP activation. On E1o and E1p, the C6' resonance and N4' resonance, respectively, respond to pH change. This is consistent with the idea that the pK_a for the 4'-aminopyrimidinium ion is significantly elevated on the enzymes (it is 4.85 in water) due to (i) An electrostatic interaction with the highly conserved glutamate residue within hydrogen bonding distance of the N1' atom and (ii) The active sites favoring a positive charge at the N1' position. Compelling evidence for active-site stabilization of a positive charge at N1' (the APH^+ form) is also derived from experiments in which the conserved glutamate is replaced by alanine on E1p and YPDC (*85, 86*) , resulting in a protein that binds N1'-methylthiaminium diphosphate (an electrostatic analog of the APH^+ form) more firmly than ThDP itself. This pK_a elevation is also a requirement for catalytic efficiency since the other forms (AP, IP and indeed Yl) all must be derived from APH^+ chemically (Scheme 1.1).

The chemical shift for the C2 atom of the enzyme bound ThDP is 162 ppm as compared to free ThDP at 153.5–156.8 ppm, suggesting that the catalytic centers induce modestly increased acidity (according to the deshielding) at this important C2 carbon on all three enzymes.

The changes in chemical shift at C2 on addition of the substrate analogs provide strong independent evidence for the formation of a tetrahedral intermediate on all three enzymes, previously deduced from X-ray structures. Other covalent intermediates such as the enamine, could also be studied by this method, if stabilized using conjugated substrates and slow variants (*11, 25, 87*), as the results of x-ray studies could use independent support. While the CD results enabled the detection of the AP and IP forms, the SSMAS NMR results for the first time also enabled observation of the APH^+ form. Based on these findings an important former conclusion can be updated. Previously, CD spectroscopy results implied that in all cases studied (10 enzymes to date), on the reaction pathway, tetrahedral substitution at the C2 atom is accompanied by the IP tautomer. Due to lack of a CD signature identified for APH^+, the presence or absence of APH^+ could not be established. The MAS NMR results suggest, as an update to the earlier conclusion, the idea that tetrahedral substitution at C2 could be accompanied by the IP and the APH^+ form, with the understanding that these forms are at protolytic equilibrium with each other. Parenthetically, this conclusion is also supported by the 'averaged' ^{15}N chemical shift observed when MAP is added to E1p and acetylphosphinate is added to YPDC.

This study demonstrates that the states of ionization and tautomerization can indeed be ascertained on even rather large enzymes (E1p and E1o of ca. 200,000 Da, and YPDC of ca. 250,000 Da) by a combination of MAS NMR and CD methods, the two techniques that appear to be complementary to each other for this purpose on ThDP enzymes.

The current findings open exciting opportunities for future investigations. To gain further insights on the electronic structure and the nature of the intermediates of ThDP enzymes, quantum chemical calculations of the ^{13}C and ^{15}N magnetic shielding anisotropy tensors

need to be performed. These are challenging due to the large size of the proteins, and therefore likely need to be conducted at the QM/MM level. While sensitivity of the MAS NMR experiments remains an issue at 9.4 and 14.1 T, measurements at higher magnetic field strengths could provide better signal-to-noise ratios, and therefore open opportunities for recording ^{13}C and ^{15}N chemical shift anisotropy tensors (rather than isotropic chemical shifts only), which in turn provide much more detail on the electronic environments of the molecule. Finally, detection of specific cofactor-protein interaction by multidimensional MAS NMR correlation spectroscopy will be realistic with the high magnetic fields, and can provide additional insights on the structure of the intermediates and catalytic mechanisms of ThDP-dependent enzymes.

CHAPTER 2 Transient State Kinetic Analysis of Various Covalent Intermediates in *E. coli* Pyruvate Dehydrogenase Multi-enzyme complex Catalysis

2. 1 INTRODUCTION

The pyruvate dehydrogenase multienzyme complex (PDHc) is a 4500 kDa exquisite molecular machine that belongs to a family of enzymes that catalyze oxidative decarboxylation of 2-oxo acids generating respective acyl-coenzyme A and NADH. The *E. coli* pyruvate dehydrogenase multienzyme complex is comprised of three enzyme components; (1) E1p or pyruvate decarboxylase (EC 1.2.4.1) is present in 24 copies and has a size of 99,474 Da, (2) E2p or dihydrolipoyl acetyltransferase (EC 2.3.1.12) is also present in 24 copies and has a size of 65,959 Da and (3) E3p or dihydrolipoyl dehydrogenase (EC 1.8.1.4) is present in 12 copies and has a size of 50554 Da.(*88-90*) The complex catalyzes the oxidative decarboxylation of pyruvate according to equation 1 (*91*):

$$\text{pyruvate} + \text{CoA} + \text{NAD}^+ \longrightarrow \text{acetyl-CoA} + \text{CO}_2 + \text{NADH} + \text{H}^+ \quad \text{.....(1)}$$

The components catalyze parts of the overall reaction (*92-94*) as shown in equations 2-6.

$$\text{pyruvate} + \text{E1-ThDP-Mg}^{2+} \longrightarrow \text{E1-hydroxyethylidene-ThDP-Mg}^{2+} + \text{CO}_2 \quad \text{.....(2)}$$

$$\text{E1-hydroxyethylidene-ThDP-Mg}^{2+} + \text{E2-lipoamide} \longrightarrow \text{E1-ThDP-Mg}^{2+} + \text{E2-acetyldihydrolipoamide} \quad \text{.....(3)}$$

$$\text{E2-acetyldihydrolipoamide} + \text{CoA} \longrightarrow \text{E2-dihydrolipoamide} + \text{acetyl-CoA} \quad \text{.....(4)}$$

$$\text{E2-dihydrolipoamide} + \text{E3-FAD} \longrightarrow \text{E2-lipoamide} + \text{E3-FADH}_2 \quad \text{.....(5)}$$

$$\text{E3-FADH}_2 + \text{NAD}^+ \longrightarrow \text{E3-FAD} + \text{NADH} + \text{H}^+ \quad \text{.....(6)}$$

Scheme 2.1 Mechanism of Pyruvate Dehydrogenase multi-enzyme complex

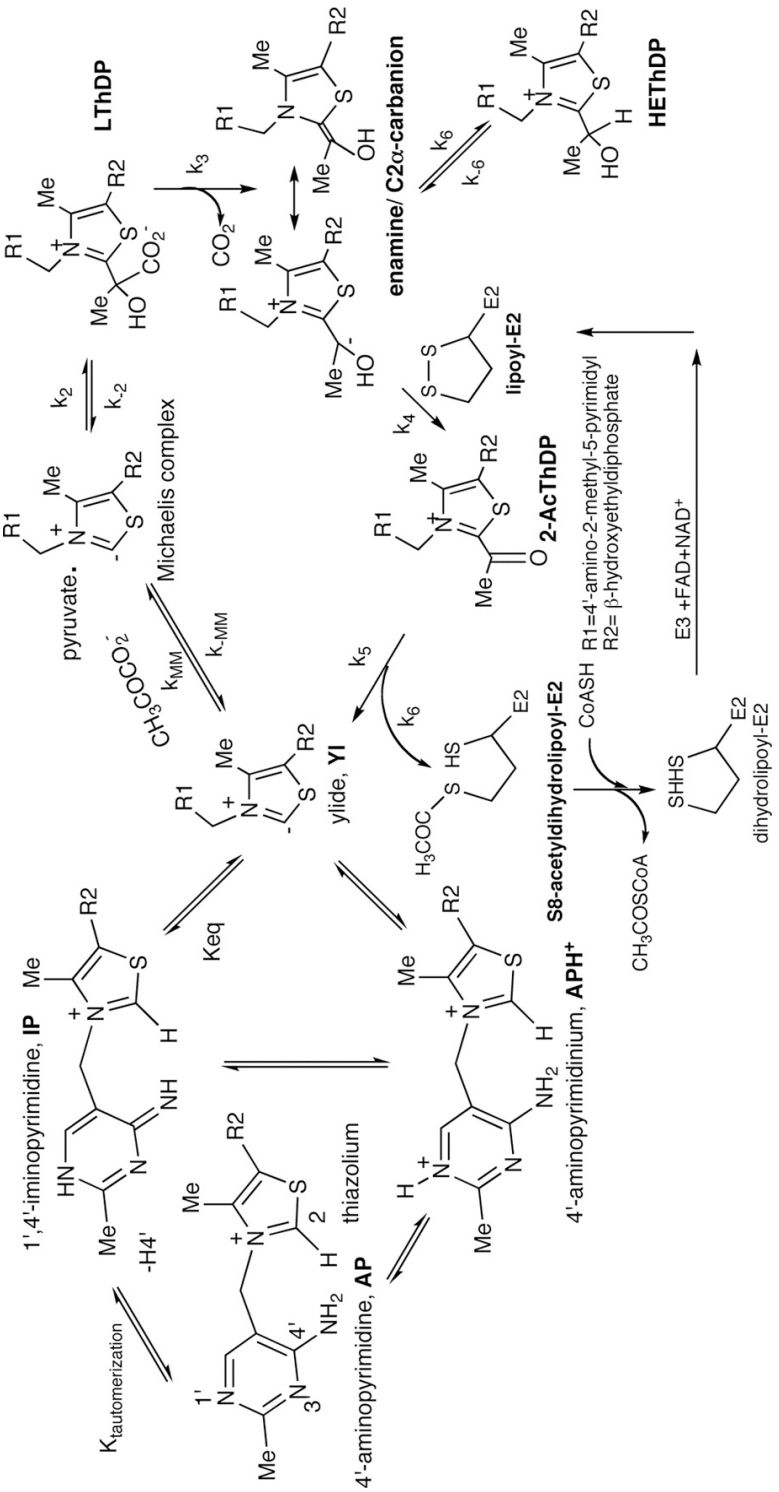

PDHc catalyzes this sequence of reactions using an array of coenzymes covalently and non-covalently bound to the various components.

The E1p component catalyzes thiamin diphosphate (ThDP) dependent decarboxylation of pyruvate whose product reductively acetylates the covalently bound lipoamide group on E2p. The lipoamide group transfers the acetyl moiety to a coenzyme A molecule bound at the catalytic domain and is subsequently reversibly oxidized by a FAD group bound to the E3p component.

Obtaining net forward rate constants for the various reactions is challenging in view of the fact that there are multiple covalent intermediates formed between the thiamin diphosphate (ThDP) cofactor associated with the E1p component and the substrate derived moieties as seen in Scheme 2.1. An ingenious method to detect and quantify these ThDP covalent intermediates was invented by Tittmann and Hübner (TH) using NMR detection (*4*), with the realization that **(*i*)** all of the intermediates are stable in acid and **(*ii*)** the chemical shifts of the C6' proton resonances for ThDP and the intermediates are sufficiently distinct subsequent to acid chemical quench of the reaction mixture and hence can be used as a finger-print region for distinguishing the various intermediates (Table 2.1) and **(*iii*)** relative integrals of the various C6' proton resonances provides a quantitative estimate of relative abundance of the various intermediates. While this method has been successfully employed to gain detailed insights into the mechanisms of other pyruvate dependent enzymes and also the isolated E1p components from human PDHc (*95, 96*) and *E. coli* PDHc (*97*), presence of aromatic substrates and/or cofactors in overwhelming amounts thwarts interpretation of ^{1}H NMR spectra in the C6' fingerprint region (7.1 – 8.7 ppm) (see Table 2.1 for chemical shifts).

Table 2.1 ^{1}H NMR finger-print region for C6' proton of ThDP covalent intermediates

ThDP covalent intermediate	C6' proton chemical shift(s), (ppm)
ThDP	8.01
LThDP	7.26
Enamine/HEThDP†	7.34
AcThDP‡	7.36, 7.37 and 8.61

Refer to Scheme 2.1 for abbreviations. † Due to the acid quench conditions, the enamine intermediate is detected as C2-α-hydroxyethylThDP (HEThDP). ‡ C2-α-acetylThDP (AcThDP) is in its keto, hydrate and internal-carbinolamine forms under acidic conditions.

The current study aims at taking the method to the next step and **(*i*)** to determine the effects of PDH complex assembly on the various forward rate constants in the overall PDHc reaction, **(*ii*)** and to determine the rate-limiting steps in a variety of E1p variants shown earlier to have structural importance in assembly of E1p and E2p. To evaluate the effects of assembly, we needed to simplify the aromatic region of the ^{1}H spectrum as in the overall complex reaction mixture several other cofactors (FAD, coenzyme A, NAD^{+}) also have resonances in this chemical shift region, in addition to those due to the ThDP. Using PDHc (and its E1p variants) reconstituted with specifically labeled [C2,C6'-$^{13}C_2$]ThDP we could carry out 1D ^{1}H-^{13}C gCHSQC NMR experiments in which only protons attached to ^{13}C would be prominent, allowing for the large differential in concentrations of substrate and cofactors.

Detection of the ThDP-bound covalent intermediates was supplemented by direct mass spectral detection of E1p catalysed acetylation of the independently expressed lipoyl domain and measurement of the rate of reductive acetylation so that communication between the E1 active center and the first lipoyl domain of the E2 component could be assessed.

X-ray crystallographic studies revealed a disorder-to-order transition of two dynamic loops spanning residues 401 – 413 (inner loop) and 541 – 557 (outer loop) in the presence of intermediate analog C2-α-phosphonolactylThDP in the E1p active-site (*22*). The intermediate analog interacts with a conserved histidine residue His407 thus ordering the inner-loop and interaction between residues Asn404 and Asp549 further order the outer-loop over the active-site (Figure 2.1). Site-directed mutagenesis studies showed His407 to

be important for reductive acetylation, i.e., in steps leading to transfer of acetyl moiety from E1p active-site to the lipoyl group on E2p (*98*).

Extensive biochemical and biophysical studies by Kale et al. showed the active-center dynamic loops (i) modulate catalysis in *E. coli* PDH complex by forming a new surface during the closed state enabling interaction between E1p and the lipoyl domain on E2p and (ii) also sequester the E1p active-sites to prevent undesirable side reactions (*99-101*). E1p variants containing substitutions at Glu401 and Asp549, created during the course of the above studies, interestingly stabilize the Michaelis complex intermediate as opposed to the parental enzyme. Pre-decarboxylation steps were also found to be rate-limiting in these variants with highly compromised overall PDHc activity. In conclusion they point out a modulation of the overall catalytic cycle by these dynamic loops and an 'efficient coupling of dynamics and catalysis.'

This study presents results on E1p and on several slower variants, created on three loops (residues 177-179, residues 401-413, the inner active center loop, and residues 541-557, the outer active center loop) which were previously identified as being important in the mechanism. The results suggest that formation of the first covalent (pre-decarboxylation) intermediate C2α-lactylThDP (LThDP in Scheme 2.1) is rate limiting for the initial series of steps leading to the enamine intermediate, while reductive acetylation is rate limiting in the overall reaction. Decarboxylation of LThDP appears to be faster than its formation in all variants tested. Combining kinetic data obtained from NMR and mass spectrometry methods provided a complete picture of the covalent intermediates in PDHc catalysis and finally, the affects of complex assembly on rates could be assessed for the first time.

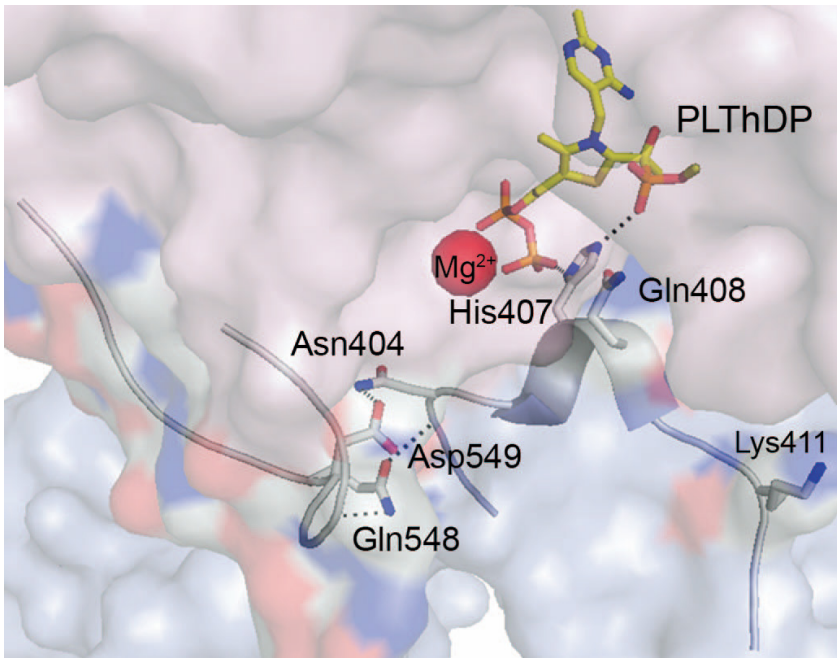

Figure 2.1 Active-site loops ordered over the E1p active-site containing PLThDP

2. 2 MATERIALS AND METHODS

2.2.1 Materials

Thiamin diphosphate ThDP, NAD^+, coenzyme A, dithiothreitol (DTT) and isopropyl β-D-1-thiogalactopyranoside (IPTG) were from USB (Cleveland, OH); dichlorophenol-indophenol (DCPIP) from Sigma (St.Louis, MO). Wizard® *Plus* Minipreps DNA Purification System was from Promega (Madison, WI).

2.2.2 Bacteria and Plasmids

E. coli strain JRG 3456 deficient in native E1p gene transformed with pGS878 plasmid containing *aceE* gene encoding the E1p was used for overexpression of E1p. For the E1p active-site loop variants, *E. coli* strain JRG 3456 containing *aceE* gene encoding for the E1p variant created previously was used for overexpression (*99, 101*).

E. coli strain JRG 1342 carrying plasmid encoding 1-lip PDHc (pGS501) was used for overexpression of 1-lip pyruvate dehydrogenase multi-enzyme complex (1-Lip PDHc).

The pET-22b (+)-1-lip E2p vector transformed in *E. coli* BL21(DE3) cells was used for overexpression of 1-lip E2p (*102*). This single lipoyl E2p construct is virtually indistinguishable in its biochemical behavior from the three-lipoyl wild-type E2p and is mechanistically useful.

The pET-22b (+)-E3p vector transformed in *E. coli* BL21(DE3) cells was used for overexpression of E3p (*102*).

2.2.3 Purification of *E. coli* E1p variants

Protein overexpression

A LB plate containing ampicillin (50 µg/mL) was streaked with cells from the working cell bank stored at -80 ^{o}C. After approximately 16 h of incubation at 37 °C, single colonies from the plate were used to inoculate 15 mL LB medium containing 0.2 mM sodium acetate, 50µg/mL ampicillin and 0.2% glucose. The culture was grown overnight at 37 ^{o}C while shaking at 250 rpm (New Brunswick Scientific, NJ). This overnight culture was then transferred into 700 mL of LB medium containing ampicillin (50 µg/mL). The scale of culture was increased as desired by increasing number of flasks. After the culture had reached the early log phase (OD_{600} = 0.6-0.8) protein expression was induced with 1.0 mM of IPTG dissolved in sterile water. The cell culture was then allowed to grow overnight. The induced culture was harvested by centrifuging at 5000 rpm for 5 min. The pellet was washed in phosphate buffered saline (20 mM KH_2PO_4, 100 mM NaCl, pH 7.5) combined to a single fraction and stored at -20 ^{o}C for at least 5 h or until further use.

Cell lysis

All operations were performed on ice or at 4 °C. The frozen cell pellet was thawed and immediately resuspended in 40 mL sonication buffer (20 mM KH_2PO_4, 2.0 mM ThDP, 5.0 mM $MgCl_2$, 1.0 mM DTT, 1.0 mM EDTA and 1.0 mM benzamidine HCl. pH 7.0) using a cell homogenizer and combined in a 100 mL beaker. Subsequently, 1.0 mM PMSF and 0.6 mg/mL of lysozyme were added and incubated on ice with intermittent stirring. After 15 min, 1000 U of DNase and 500 U of RNase were added to disrupt the cellular DNA released as a result of freeze-thawing and lysozyme treatment. After 30 min on ice with

intermittent stirring the cleared lysate was sonicated on ice with 10 s ON and 20 s OFF pulses for 4 min on the sonicator. The clarified lysate was then centrifuged for 20 min at 17,000 rpm at 0^{o}C. Appropriate amount of sonication buffer was then added to the supernatant according to ratio 10 mL/g wet cell weight. This solution was then used for ammonium sulfate fractionation.

Ammonium sulfate fractionation

The cooled lysate was made 30% in $(NH_4)_2SO_4$ gradually over 10 min with gentle stirring. Stirring was continued after complete addition of salt, after 15 min the precipitate was removed by centrifuging the suspension for 15 min at 17,000 rpm. The resultant supernatant was made 65% in $(NH_4)_2SO_4$ and stirred for 15 min on ice. The heavy precipitate that resulted at this step was separated by again centrifuging the suspension for 15 min at 17,000 rpm. The pellet containing the major fraction of E1p was then dissolved in ice cold dialysis buffer (20 mM KH_2PO_4, 0.2 mM ThDP, 2.0 mM $MgCl_2$, 1.0 mM DTT, 0.60 mM EDTA and 1.0 mM benzamidine HCl. pH 7.0) and dialyzed for the minimum of 3 h (usually 16 h) using 12,000-14,000 MWCO membrane (Spectrapor). Subsequently the protein fraction was centrifuged to remove unfolded protein and stored at -20 ^{o}C until further use.

Anion exchange chromatography using FPLC

Anion exchange chromatography was used to purify the E1p from enriched protein fraction resulting from ammonium sulfate fractionation. The protein fraction was filtered through 0.22micron syringe filter (Millipore, MA) and about 15 mL (max total protein 1600 mg) was loaded on Hiload HQ 26/10 column containing a quaternary ammonium gel

matrix on an AKTA FPLC (GE Healthcare, NJ). The sample was then eluted with a linear gradient of 20 to 100 % of Buffer B (Buffer A 20 mM KH_2PO_4, pH 7.5; Buffer B 20 mM KH_2PO_4, 1.0 M NaCl, pH 7.5). The peaks of interest were then analyzed with SDS-PAGE (see Materials and Methods in Appendix). Fractions showing greater than 90 % purity were pooled, concentrated and subsequently applied on the HPLC for final polishing.

Anion exchange chromatography using HPLC

Additional purification to homogeneity was achieved by applying the protein on a TSK DEAE-5PW HPLC column and eluting with a linear gradient (0.075-0.5 M) of NaCl in 20 mM KH_2PO_4 buffer (pH 7.5). Pure fractions (>98%) as judged by SDS-PAGE were combined and dialyzed against dialysis buffer (20 mM KH_2PO_4, 0.2 mM ThDP, 2.0 mM $MgCl_2$, 1.0 mM DTT, 0.50 mM EDTA and 1.0 mM benzamidine HCl. pH 7.0). Purified E1p in dialysis buffer after concentration to 1-2 mL was stored at -20 °C until further use.

2.2.4 Purification of *E. coli* 1-Lip E2p

Protein overexpression

A LB plate containing ampicillin (50 µg/mL) was streaked with cells from the working cell bank stored at -80^{o}C. After approximately 16 h of incubation at 37 °C, single colonies from the plate were used to inoculate 15 mL LB medium containing ampicillin (50µg/mL). The culture was grown overnight at 37 ^{o}C while shaking at 250 rpm (New Brunswick Scientific, NJ). This overnight culture was then transferred into 700 mL of LB medium containing ampicillin (50 µg/mL). The scale of culture was increased as desired by increasing the

number of flasks. After the culture had reached the early log phase (OD_{600} = 0.6-0.8) protein expression was induced with 1.0 mM of IPTG and 0.3 mM DL-α-lipoic acid. The cell culture was allowed to grow for an additional 6 h. The induced cells were then harvested by centrifugation (5000 rpm for 5 min) and washed with washing buffer (20 mM KH_2PO_4, 0.10 M NaCl, 0.25 mM EDTA, pH 7.5). The washed pellet was stored at -20 ^{o}C until further use.

Cell lysis

All operations were performed on ice or at 4 °C. The frozen cell pellet was thawed and immediately resuspended in 40 mL sonication buffer (20 mM KH_2PO_4, 0.10 M NaCl, 1.0 mM DTT and 1 complete protease inhibitor cocktail tablet (Roche Diagnostics). pH 7.5) using a cell homogenizer and combined in a 100 mL beaker. Subsequently, 1.0 mM PMSF and 0.6 mg/mL of lysozyme were added and the mixture was incubated on ice with intermittent stirring. After 15 min, 1000 U of DNase and 500 U of RNase were added. After 30 min on ice with intermittent stirring the cleared lysate was sonicated on ice with 10 s ON and 20 s OFF pulses for 4 min. The clarified lysate was then centrifuged for 20 min at 17,000 rpm at 0^{o}C. Appropriate amount of sonication buffer was then added to the supernatant according to ratio; 10 mL/g wet cell weight. This solution was then used for ammonium sulfate fractionation.

Ammonium sulfate fractionation

The cooled lysate was made 25% in $(NH_4)_2SO_4$ gradually over 10 min with gentle stirring. Stirring was continued after complete addition of salt, after 15 min the precipitate was removed by centrifuging the suspension for 15 min at 17,000 rpm. The resultant

supernatant was made 55% in $(NH_4)_2SO_4$ and stirred for 15 min on ice. The heavy precipitate that resulted at this step was separated by again centrifuging the suspension for 15 min at 17,000 rpm. The pellet containing the major fraction of E2p was then dissolved in ice cold dialysis buffer (20 mM KH_2PO_4, 1.0 mM EDTA, 1.0 mM benzamidine HCl, 2 mM leupeptin, 0.20 M NaCl, 1.0 mM DTT and 25 μM AEBSF. pH 7.5) and dialyzed for the minimum of 3 h (usually 16 h) using 12,000-14,000 MWCO membrane (Spectrapor). Subsequently the protein fraction was centrifuged to remove unfolded protein and stored at -20 ^oC until further use.

Gel filtration column chromatography

Gel filtration chromatography was used to purify the E2p from enriched protein fraction resulting from ammonium sulfate fractionation. The protein fraction was filtered through 0.22micron syringe filter (Millipore, MA) and about 8 mL (recommended sample volume 0.5%-4% column volume) was loaded on to HiPrep 26 x 60 Sephacryl S-300 High Resolution gel-filtration column pre-equilibrated with two column volumes of Buffer C (20 mM KH_2PO_4, 0.5 mM EDTA, 0.20 M NaCl, 1.0 mM DTT, 1.0 mM benzamidine HCl. pH 7.2) at a flow rate of 1.5 mL/min. The protein was eluted at 1 mL/min (or 0.12 mL/min for overnight runs) and 4 mL fractions were collected. The fractions were checked for protein content by UV/Vis and purity was assessed by SDS-PAGE. Fractions containing pure E2p were combined and centrifuged on an ultracentrifuge for 4 h at 46,000 rpm. The pellets obtained were resuspended in 1.0 mL each of buffer C containing additional 0.30 M NaCl (total 0.50 M) and kept on ice in the cold room for 15 h. The undissolved protein was separated by centrifugation (17,000 rpm for 20 min) and the supernatant was analyzed by

SDS-PAGE. The 1-lip E2p was stored at -80 °C until further use in buffer C after concentration to 1-2 mL.

2.2.5 Purification of *E. coli* E3p

The cell growth and expression of E3 were the same as described above for 1-lip E2p, except the DL-α-lipoic acid was not included in the LB medium during induction.

Cell lysis

The cell lysis procedure is as described above for 1-lip E2 with some minor modifications: The DNase and RNase treatment step was excluded.

Ammonium sulfate fractionation

To the cooled lysate ammonium sulfate was added to 40% of saturation over 10 min with gentle stirring. Stirring was continued after complete addition of salt, after 15 min the precipitate was removed by centrifuging the suspension for 15 min at 17,000 rpm.

Hydrophobic column chromatography using FPLC

The clarified supernatant was applied to a phenyl-Sepharose High Performance hydrophobic column (Amersham Pharmacia Biotech, Piscataway, NJ) at room temperature, pre-equilibrated with column buffer (50 mM KH_2PO_4 1mM EDTA and 40% ammonium sulfate. pH 8.0). A decreasing gradient of ammonium sulfate was applied and E3 was eluted at 15% saturation of ammonium sulfate. Fractions containing E3p were collected

and analyzed using SDS–PAGE. Fractions containing major amount of E3 were pooled and dialyzed against dialysis buffer (50 mM KH_2PO_4, 1mM EDTA, 10 μM FAD, pH 8.0).

Anion exchange chromatography using HPLC

Additional purification to homogeneity was achieved by applying the protein on a TSK DEAE-5PW HPLC column and eluting with a linear gradient (0.075-0.5 M) of NaCl in 20 mM KH_2PO_4 buffer pH 7.5. Pure fractions (>98%) as judged by SDS-PAGE were combined and dialyzed against dialysis buffer (50 mM KH_2PO_4, 1mM EDTA, 10 μM FAD, pH 8.0). The final product was concentrated to 1-2 mL and stored frozen at – 20 °C.

2.2.6 Purification of 1-Lip PDH complex

Protein overexpression

A LB plate containing ampicillin (50 μg/mL) was streaked with cells from the working cell bank stored at -80 ^{o}C. After approximately 16 h of incubation at 37 °C, single colonies from the plate were used to inoculate 15 mL LB medium containing 0.2 mM sodium acetate, 50μg/mL ampicillin and 0.2% glucose. The culture was grown overnight at 37 ^{o}C while shaking at 250 rpm (New Brunswick Scientific, NJ). This overnight culture was then transferred into 700 mL of LB medium containing ampicillin (50 μg/mL). The scale of culture was increased as desired by increasing the number of flasks. After the culture had reached the early log phase (OD_{600} = 0.6-0.8) protein expression was induced with 0.5 mM IPTG and 0.3 mM DL-α-lipoic acid. The cell culture was grown for further 6 h. The induced culture was harvested by centrifuging at 5000 rpm for 5 min. The pellet was

washed in phosphate buffered saline (20 mM KH_2PO_4, 100 mM NaCl, pH 7.5) combined to a single fraction and stored at -20 ^oC for at least 5 h or until further use.

Cell lysis

The cell lysis procedure is as described above for E1p with some minor modifications: The DNase and RNase treatment step was excluded.

PDH complex sedimentation

The clear lysate was centrifuged on an ultracentrifuge for 20 min at 46000 rpm to remove insoluble debris and further centrifuged for 4 h at 46000 rpm to sediment the 1-lip PDHc. The pellets were suspended in Buffer A (20 mM KH_2PO_4, 0.5 mM DTT, 0.5 mM benzamidine.HCl, 0.5 mM EDTA, pH 7.5) and allowed to go into solution overnight. A clear PDHc solution was obtained after centrifugation at 17000 rpm for 20 min to remove undissolved protein.

Anion exchange chromatography using HPLC

Additional purification to homogeneity was achieved by applying the protein solution on a TSK DEAE-5PW HPLC column and eluting with a linear gradient (0.075-0.5 M) of NaCl in 20 mM KH_2PO_4 buffer (pH 7.5). Pure fractions (>98%) as judged by SDS-PAGE were combined and dialyzed against dialysis buffer (20 mM KH_2PO_4, 0.2 mM ThDP, 2.0 mM $MgCl_2$, 1.0 mM DTT, 0.50 mM EDTA and 1.0 mM benzamidine HCl. pH 7.0). The 1-lip PDHc was stored at -20 °C until further use in dialysis buffer after concentration to 1-2 mL.

2.2.7 Estimation of protein content

Protein concentrations were determined by the method described by Bradford et al. (*62*). Dilutions of proteins were added to 1X Bradford reagent (BioRad, CA) and the absorbance at 595 nm was used to estimate the concentration from a standard curve prepared with BSA.

2.2.8 Enzyme activity measurements

Overall PDHc activity was measured by reconstitution of E1p or its variants with independently expressed 1-lip E2p and E3p (*103*) components. The individual components were mixed in a 1:1:1 mass ratio and incubated at 4 ºC for 0.5 h to generate PDHc. Varian 300 DMS spectrophotometer was used to monitor the pyruvate-dependent reduction of NAD^+ catalyzed by PDHc at 340 nm. The reaction medium contained in 1 mL of 0.1 M Tris-HCl buffer (pH 8.0) - 1 mM $MgCl_2$, 2 mM sodium pyruvate, 2.5 mM NAD^+, 0.2 mM ThDP, and 2.6 mM DTT. The reaction was initiated by adding 0.1 mM CoA and 3 μg of PDHc and the temperature was maintained at 30 ºC during the procedure. Steady-state velocities were taken from the linear portion of the progress curve. One unit of activity is defined as the amount of NADH produced (μM/min/mg E1p).

The E1p component-specific activity was determined by monitoring the reduction of 2,6-dichlorophenolindophenol (DCPIP) at 600 nm (*104*). The reaction medium contained in 1 mL of 50 mM KH_2PO_4 buffer (pH 7.0) - 1 mM $MgCl_2$, 2.0 mM sodium pyruvate as substrate, 0.2 mM ThDP, and 0.1 mM DCPIP at 30 °C. The reaction was initiated by adding the enzyme. One unit of activity is defined as the amount of DCPIP reduced

(μmol/min/mg of E1p). Percent activities reported for variants are compared with similarly treated E1ec. All activity measurements were carried out at 30 ^{o}C.

2.2.9 Reconstitution of apoenzymes with [C2, C6' – $^{13}C_2$] ThDP

E1p and 1-lip PDHc could be purified in the apoenzyme form by extensive dialysis - two dialysis runs in series against 2L of the reaction buffer for 4 hours each - of the holoenzyme against reaction buffer (20 mM KH_2PO_4, 0.1 mM DTT, 0.1 mM benzamidine.HCl, pH 7.0) without the cofactors (ThDP and Mg^{2+}).

All stock solutions and dilutions were made in the reaction buffer. [C2, C6' – $^{13}C_2$] ThDP stock solution (10 mM) prepared as mentioned in Chapter 1 was used as is.

E1p or variant (0.20 mM active sites) purified in the apo-enzyme form was incubated with one equivalent of [C2, C6' – $^{13}C_2$] ThDP (0.20 mM) and Mg^{2+} (2.5 mM) for 30 min at 4 °C. The final volume was usually 2.5 mL. Small aliquots were withdrawn to perform steady-state activity assay using DCPIP to confirm formation of the holoenzyme. This sample was used for further experiments.

1-lip PDHc purified in the apoenzyme form (0.20 mM active sites of E1) was incubated with one equivalent of [C2, C6' – $^{13}C_2$] (0.20 mM) ThDP and Mg^{2+} (2.5 mM) for 30 min at 4 °C. Small aliquots were withdrawn to perform steady-state oxidoreductase activity assay using pyruvate, NAD^+ and Coenzyme A to confirm formation of the holo multi-enzyme complex. The final volume was usually 2.5 mL. This sample was used for further experiments.

1-lip PDHc reconstituted with E1p variant was assembled from components as follows. E1p variant (0.20 mM) purified in the apoenzyme form was incubated with one equal part by protein content (1 mg :1 mg :1 mg :: E1:E2:E3) of 1-lip E2p and E3p added from stock. This assembled complex was incubated for 30 min at 4 °C. Next, this mixture was loaded into an Amicon Centriprep 5 mL unit and diluted with the reaction buffer. This diluted mixture was centrifuged at 6000 rpm at 4 °C for 20 min. This washing step was repeated 3 more times. The final concentration of the reconstituted apo 1-lip PDHc was adjusted to 0.20 mM with reaction buffer and was incubated with one equivalent of [C2, C6' – $^{13}C_2$] (0.20 mM) ThDP and Mg^{2+} (2.5 mM) for 30 min at 4 °C. Small aliquots were withdrawn to perform steady-state oxidoreductase activity assay using pyruvate, NAD^+ and Coenzyme A to confirm assembly of the holo multi-enzyme complex. The final volume was usually 2.5 mL. This sample was used for further experiments.

2.2.10 Rapid chemical quench and NMR analysis methods

Pre-steady state experiments were performed to monitor covalent ThDP intermediates on (i) E1p and variants with pyruvate (ii) E1p and variants with pyruvate and DCPIP artificial oxidation reaction and (iii) oxidoreductase reaction of 1-lip PDH complex - or assembled 1-lip PDH complex with E1 variants - in presence the of all substrates.

The experiments were discontinuous assays i.e., individual reactions were stopped at different time points. Samples at various time points were prepared as follows. [C2, C6' – $^{13}C_2$] ThDP labeled enzyme was loaded into syringe A and pyruvate was loaded into syringe B in a rapid chemical quench apparatus (Kintek RQF-3 model, Kintek Corp.). A

quench solution (12.5% TCA in 1M DCl/D_2O) was loaded into syringe C. Enzyme and pyruvate solutions were mixed rapidly in a 1:1 volume ratio by a computer controlled drive-plate and incubated for predetermined times in a reaction loop. After this incubation period the reaction mixture was mixed rapidly with the quench solution from syringe C and the resulting mixture was collected. The mixture was centrifuged at 13000 rpm for 30 min, the supernatant was collected and filtered through a Gelman 0.45 μM disc and the filtrate was used for analysis by 1D-^{1}H gradient carbon HSQC NMR.

For longer time scales, 10 s and longer, the samples were assembled similarly into three different solutions. First, equal volumes of the enzyme (200 μL) and substrate (200 μL) solutions were mixed in an eppendorf and after a predetermined time period (monitored using a stop-clock) the reaction was stopped by addition of quench solution (200 μL). The mixture was centrifuged at 13000 rpm for 30 min, the supernatant was collected and filtered through a Gelman 0.45 μM disc and the filtrate was used for analysis by 1D-^{1}H gradient carbon HSQC (gCHSQC) NMR.

The contents of the syringes were varied to monitor the different reactions:

i. For E1p with pyruvate single turn-over, syringe A contained E1p (0.20 mM) reconstituted with [C2, C6' – $^{13}C_2$] ThDP in reaction buffer; syringe B contained pyruvate (20 mM) in reaction buffer; and syringe C contained the quench solution.
ii. For E1p and DCPIP dependent artificial oxidation, syringe A contained E1p (0.20 mM) reconstituted with [C2, C6' – $^{13}C_2$] ThDP (0.20 mM) in reaction buffer; syringe B contained pyruvate (20 mM) and DCPIP (4 mM) in reaction buffer; and syringe C contained the quench solution.

iii. For the overall PDHc oxidoreductase reaction, syringe A contained 1-lip PDHc (0.20 mM) reconstituted with [C2, C6' – $^{13}C_2$] ThDP (0.20 mM), NAD^+ (5 mM), and coenzyme A (2 mM) in reaction buffer; syringe B contained pyruvate (20 mM); and syringe C contained the quench solution.

All NMR experiments were performed on a Varian model 600 MHz NMR instrument. Data acquisition was at 25 ºC and sample pH was ~ 0.75. 16384 transients in the ^1H dimension were collected with recycle delay time of 2 s.

The relative integrals of C6'-H signals of respective ThDP intermediates represent relative ratios of ThDP covalent intermediates in the NMR sample after correction for amount of unbound ThDP estimated using the following equations (2.1).

$$[E-ThDP] = \frac{[ThDP]_0 + [E]_0 + K_D}{2} - \sqrt{\frac{([ThDP]_0 + [E]_0 + K_D)^2}{4} - [ThDP]_0[E]_0} \qquad (2.1)$$
$$[ThDP] = [ThDP]_0 - [E-ThDP]$$

Here, [E-ThDP] represents concentration of E-ThDP complex; [ThDP] and $[ThDP]_0$ represent concentrations of free and total ThDP; K_D is the dissociation constant.

Time course of the fraction abundance of an intermediate over the total active-sites present (sum total of ThDP and all ThDP covalent intermediates C6'-H signals) was fit to single exponential equation (2.2) or double exponential equations of the form (2.3) for intermediates which increase to reach a steady-state level and of the form (2.4) for intermediates with an increase to reach a steady-state followed by a decrease.

$$f = f_1 \times (1 - e^{-k_1 t}) \qquad (2.2)$$

$$f = f_1 \times (1 - e^{-k_1 t}) + f_2 \times (1 - e^{-k_2 t}) \quad (2.3)$$

$$f = f_0 + f_1 \times (e^{-k_1 t}) - f_2 \times (e^{-k_2 t}) \quad (2.4)$$

In a similar presteady state experiment for detection of S-acetylcoenzyme A, [C3 - ^{13}C] pyruvate was used and the product [C2 - ^{13}C] S-acetylcoenzyme A was detected using 1D-^{1}H gradient carbon HSQC NMR method. The overall PDHc reaction as mentioned above was performed with minor modifications. Unlabeled ThDP was used and [C3 - ^{13}C] pyruvate was used. All reagent concentrations are provided in Table 2.2.

The C3-H signals from pyruvate in both forms (ketone and hydrate) and C2-H signal from S-acetylconenzyme A were integrated and the time course of fraction relative abundance of product over total acetyl groups (from pyruvate and acetyl coenzyme A; acetyl groups attached to ThDP are in low abundance compared to the substrate and product forms) was plotted and fit to a single-exponential equation (2.5).

$$f = f_0 + f_1 \times (1 - e^{-k_1 t}) \quad (2.5)$$

An experiment to detect distribution of ThDP intermediates during the steady state of the reverse reaction catalyzed by 1-lip PDHc using S-acetylcoenzyme A and NADH as substrates was performed as follows: 1-lip PDHc (0.10 mM) reconstituted with [C2, C6' – $^{13}C_2$] ThDP (0.10 mM) was incubated for 2 min on ice in reaction medium (400 μL) containing Mg^{2+} (2 mM), NAD^+ (3.6 mM), NADH (1.08 mM), and S-acetylcoenzyme A (3 mM). After 2 min the reaction was quenched with 12.5% TCA in 1M DCl/D_2O and the mixture was treated as mentioned earlier and analyzed by 1D-^{1}H gCHSQC NMR.

2.2.11 Stop-flow UV/Vis analysis of 1-lip PDHc catalyzed oxidative decarboxylation reaction

E. coli 1-lip PDHc was loaded into syringe A; pyruvate, NAD^+ and Coenzyme A, were loaded into syringe B in a SX-18MV stopped flow spectrophotometer equipped with a photo diode array (PDA) detector (Applied Photophysics, Leatherhead, U.K.). The contents of the syringes were mixed in a cuvette hosted in a chamber with the temperature control at 25 ºC and the reaction was monitored over the 200-700 nm wavelength range for time periods of 1 - 4 s and data were collected every 2.5 ms along the 10 mm path length. Global analysis and single vector decomposition were performed using Pro-K© (Applied Photophysics, Leatherhead, U.K.) a part of the software package accompanying the instrument. Data fitting was also performed using the software SigmaPlot© version 10.0 (Systat Software, Inc., San Jose, CA).

The data were fit to the following equations.

$$A = A_0 + A_1 \times (e^{-k_1 t}) + A_2 \times (e^{-k_2 t}) \quad (2.6)$$

$$A = A_0 + A_1 \times (e^{-k_1 t}) + v \times t \quad (2.7)$$

$$A = A_0 + A_1 \times (e^{-k_1 t}) + A_2 \times (1 - e^{-k_2 t}) + v \times t \quad (2.8)$$

Scheme 2.2 Process flow-chart for Rapid chemical quench/ NMR method

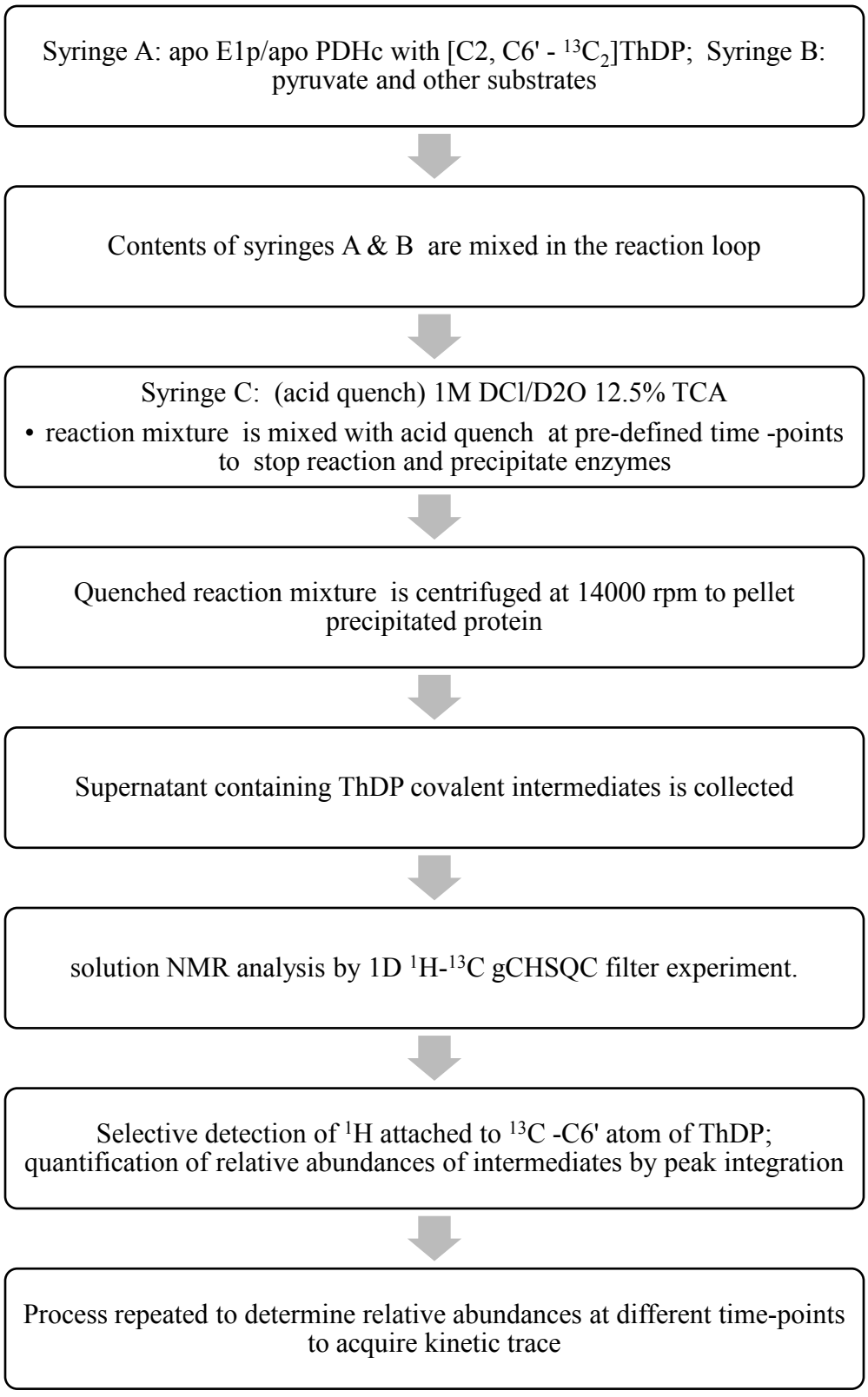

Table 2.2 Reaction conditions for various pre-steady state experiments

Reagents	**ThDP Intermediates**	**S-acetylcoA**	**Flavin Intermediates**
Method	*RCQ, NMR*	*RCQ, NMR*	*SF-PDA UV/Vis*
(Syringe A)			
PDH complex†	0.20 mM	0.02 mM	0.02 mM
[C2, C6' – $^{13}C_2$]ThDP/ ThDP	0.20 mM	2 mM	2 mM
Mg^{2+}	2.5 mM	2.5 mM	2.5 mM
NAD^+	5 mM	5 mM	5 mM
Coenzyme A	2 mM	2 mM	2 mM
(Syringe B)			
pyruvate/[C3 - ^{13}C] pyruvate	20 mM	5 mM	20 mM
(Syringe C)	12.5% TCA in 1M	12.5% TCA 1M	N/A
Quench solution	DCl/D_2O	DCl/D_2O	

Experiments were performed using enzyme and biochemicals at noted concentrations at 25 °C in reaction buffer (20 mM KH_2PO_4, 0.1 mM DTT, 0.1 mM benzamidine.HCl, pH 7.0). † PDHc concentration in terms of E1 active-sites concentration. RCQ = Rapid chemical quench. SF-PDA = Stopped-flow Photo Diode Array Detector.

2.2.12 Reductive acetylation of lipoyl domain

Lipoylation of the lipoyl domain in vitro by E. coli lipoyl protein ligase

According to ESI MS, the lipoyl domain expressed in BL21 (DE3) cells in the presence of lipoic acid (0.3 mM) represents a mixture of the lipoylated and unlipoylated fractions. To achieve uniform lipoylation, enzymatic lipoylation reaction was performed *in vitro*. A reaction mixture consisting of 50 mM $(NH_4)_2CO_3$ buffer pH 7.0, lipoyl domain mixture (60 μM), ATP (1.2 mM), $MgCl_2$ (1.2 mM), lipoic acid (0.6 mM) and *E. coli* lipoyl protein ligase (10 μM) was incubated for one hour at 25^oC followed by incubation at 4^oC for overnight. Next, the mixture was dialyzed against 50 mM $(NH_4)_2CO_3$ buffer pH 7.0 for 3 hours and a small aliquot was analyzed by ESI MS.

Acetylation of the lipoyl domain by E1ec under steady-state conditions

For reductive acetylation of the lipoyl domain, the chemical-quench-flow experiment was employed using KinTek Quench-Flow instrument (KinTek Corp.,) with the following composition of the reactants (the final concentrations are presented in parenthesis): In syringe A lipoyl domain (40 μM) in 50 mM $(NH_4)_2CO_3$ pH 7.0 buffer was mixed with E1p (0.05-0.2 μM active-sites), ThDP (0.4 mM) and $MgCl_2$ (4 mM) in a total volume of 1 mL. Syringe B contained pyruvate (2 mM) in 1 mL of 50 mM $(NH_4)_2CO_3$ pH 7.0 buffer. In the KinTek Quench-Flow instrument, 15 μL of the reaction mixture from syringe A was mixed with 15 μL of pyruvate from syringe B leading to a estimated concentration of reactants in the reaction loop: lipoyl domain (20 μM), E1 (0.025 – 0.1 μM), ThDP (0.20 mM), $MgCl_2$ (2 mM) and pyruvate (1 mM). The reaction was stopped at various time points in the range

of 0.1-10 s by mixing with a quench solution (83 μL) containing 50% methanol and 2% formic acid. Samples were immediately analyzed by ESI MS.

Single-turnover experiment

For a single-turnover experiment in syringe A were mixed lipoyl domain (40 μM) and E1p (concentration of active centers/subunits = 40 μM) in 50 mM $(NH_4)_2CO_3$ pH 7.0 buffer containing $MgCl_2$ (4 mM) and ThDP (0.40 mM). Syringe B contained pyruvate (2 or 4 mM). In KinTek Quench-Flow instrument, 15 μL of the reaction mixture from syringe A was mixed with 15 μL of pyruvate from syringe B leading to an estimated concentration of reactants in the reaction loop: lipoyl domain (20 μM), E1 (20 μM), ThDP (0.20 mM), $MgCl_2$ (2 mM) and pyruvate (1 or 2 mM). The reaction was stopped at 0.005-0.15 s by mixing with a quench solution (83 μL) containing 50% methanol and 2% formic acid. Samples were immediately analyzed by ESI-MS.

Scheme 2.3 Process flow-chart for Rapid chemical quench/ ESI-MS method

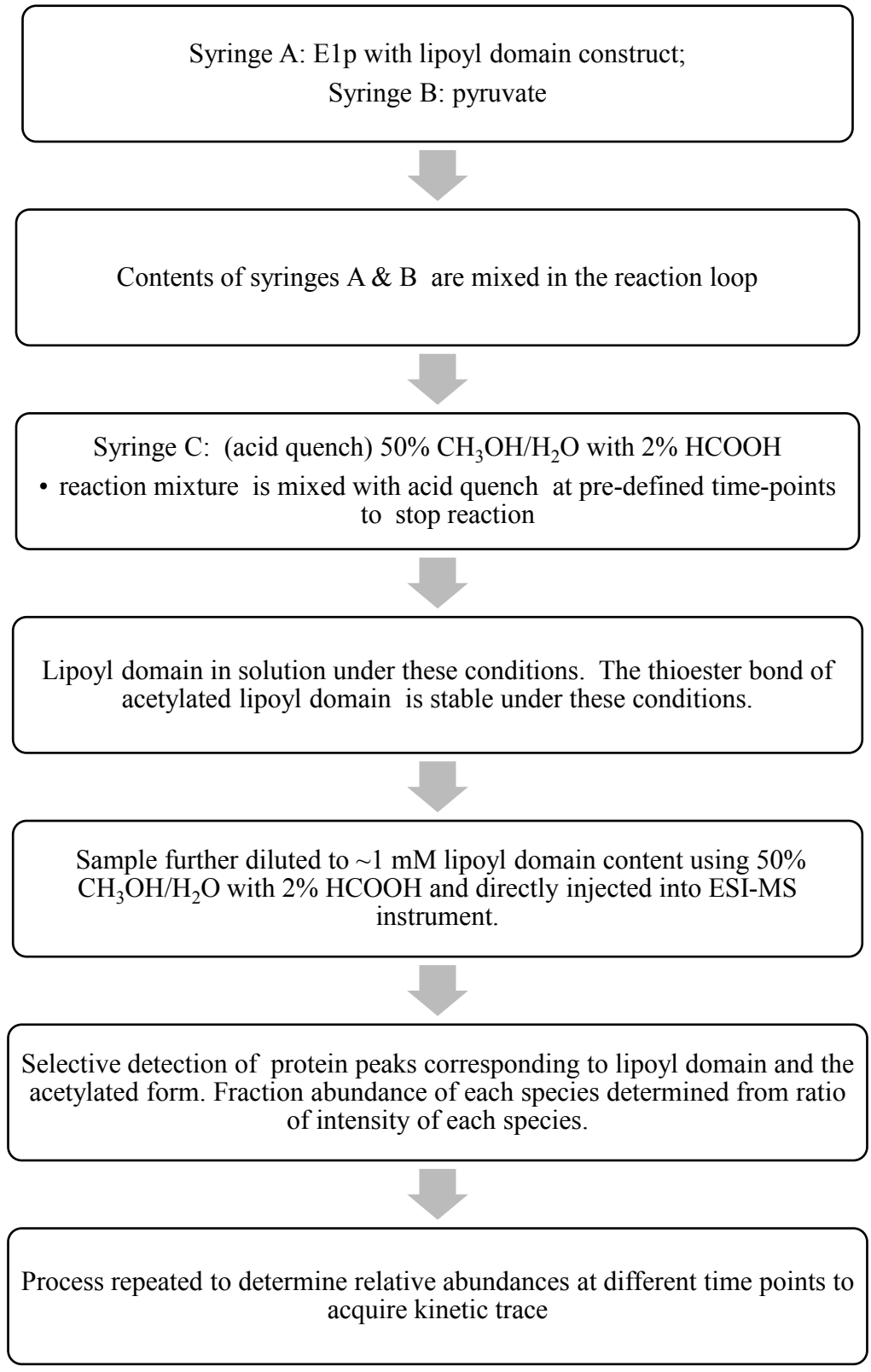

2. 3 RESULTS AND DISCUSSION

2.3.1 Detection of covalent ThDP intermediates by NMR

While the method developed at Halle involving detection of covalent ThDP intermediates using the C6'-H signatures in ^{1}H NMR spectra was successfully employed to study many members of the ThDP superfamily (*4, 96, 97, 105-107*), it is still limited by interference from resonances of aromatic substrates in the C6'-H fingerprint region. To overcome this problem and further extend the applications to monitor reactions which typically involve aromatic substrates such as PDH complex reactions [C2,C6' – $^{13}C_2$]ThDP was used during the course of these studies. This enabled selective detection of [C2,C6' – $^{13}C_2$]ThDP covalent intermediates using 1D ^{1}H-^{13}C gradient carbon heteronuclear single quantum coherence (gCHSQC) experiments. In a typical ^{1}H–decoupled experiment, data are collected only in the ^{1}H dimension and only protons attached directly to ^{13}C atoms are detected. Given the natural abundance of ^{13}C of 1%, [C2,C6' – $^{13}C_2$]ThDP covalent intermediates can be detected and quantified even with the presence of 100-fold excess of aromatic substrates over enzymes, with the exception of cases where ^{1}H resonances from the substrates and intermediates occur at nearly the same frequencies. Some typical spectra are illustrated in Figure 2.2 which provide evidence for the successful detection of some major ThDP covalent intermediates under various conditions. The LThDP intermediate however was not detected, presumably due to it not accumulating under the various reaction conditions tested. The [C2,C6' – $^{13}C_2$]ThDP covalent intermediates show resonances in ^{1}H dimension at the same positions as their unlabeled counterparts show in ^{1}H NMR spectra (refer to Table 2.1 for chemical shifts). In addition, integration of areas under these peaks could provide a quantitative estimate of their fractional abundance as in

^{1}H NMR experiments. Like the previous chemical quench/NMR methods, the current method cannot distinguish between the enamine and HEThDP intermediates. The central enamine intermediate is detected as HEThDP due to the acid quench conditions.

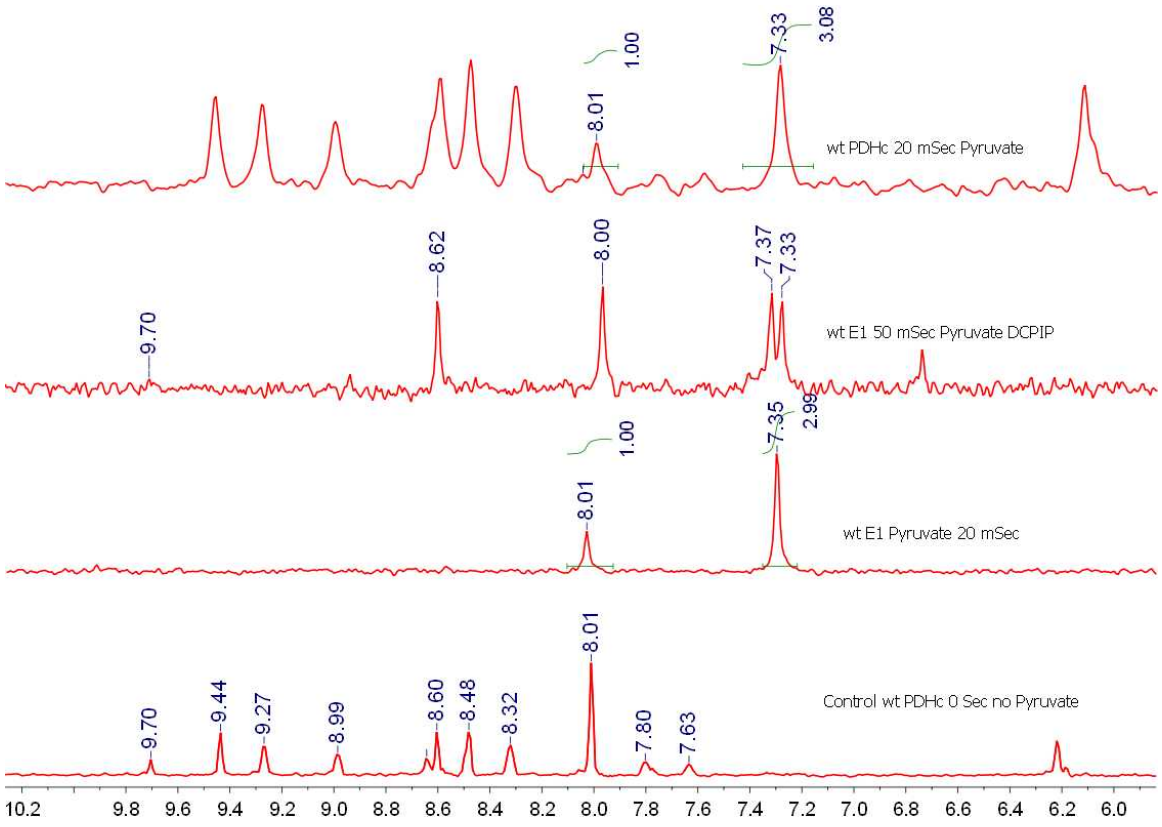

Figure 2.2 Distribution of ThDP intermediates in reactions of E1p and PDH complex

1D ^{1}H-^{13}C HSQC NMR spectra of the supernatant after acid quench removal of protein from the reaction of PDH multi-enzyme complex. From bottom (i) control sample: PDHc reaction mixture quenched before addition of pyruvate (ii) 20 ms: Reaction of PDHc-E1 with pyruvate (iii) 50 ms: Reaction of PDHc-E1 with pyruvate and DCPIP (iv) 20 ms: Reaction of PDH complex overall reaction. Thiamin derived peaks are marked at 9.71 ppm (C2-H), 8.62 ppm (AcThDP), 8.01 ppm (C6'-H), 7.37 ppm (AcThDP) and 7.34 ppm (HEThDP). The other peaks are due to the substrates NAD^{+}, coenzyme A, or DCPIP and the products NADH and S-acetylcoenzyme A or reduced form of DCPIP.

2.3.2 Covalent ThDP intermediates during E1p catalysis

The E1p component in the absence of E2p-E3p sub-complex converts pyruvate to acetaldehyde where the acetaldehyde release is known to be the rate determining step for the reaction (*108*). To determine the formation of the ThDP covalent intermediates in the presence of pyruvate, E1p reconstituted with [C2, C6' – $^{13}C_2$]ThDP was mixed with pyruvate and the reaction was stopped at various time points (0.005 to 30 s). Samples collected were analyzed by the 1D-^{1}H gCHSQC NMR experiment and some resultant spectra are shown in Figure 2.3. Only resonances at 7.34 ppm pertaining to the HEThDP intermediate could be detected during the various time scales. Qualitatively, these spectra suggest that the LThDP intermediate does not accumulate at detectable levels during the reaction. The decarboxylation of LThDP is much faster than its formation. The signal corresponding to the HEThDP intermediate at 7.34 ppm shows a time-dependent increase reaching a steady-state while the signal corresponding to ThDP at 8.01 ppm shows a time-dependent decrease, indicating a conversion of ThDP to HEThDP and the accumulation of HEThDP in E1p active-sites reminiscent of a single-turn over experiment.

Integration of the signals and a correction for fraction unbound ThDP determined using the equation 2.1 at various time points yields fraction relative abundance of HEThDP plotted as a kinetic trace in Figure 2.4. These values were fit to a single exponential process as described by equation 2.2 to yield an apparent first-order rate constant of 117 $\pm$ 14 s^{-1} for the formation of HEThDP in E1p active-sites. The rate of formation of HEThDP is 5-6 orders of magnitude larger than the steady-state conversion of HEThDP to ThDP (0.007 s^{-1}) by E1p (*108*). This result suggests that E1p in isolation is kinetically incompetent toward non-oxidative decarboxylation as performed by YPDC or other 2-oxoacid decarboxylases.

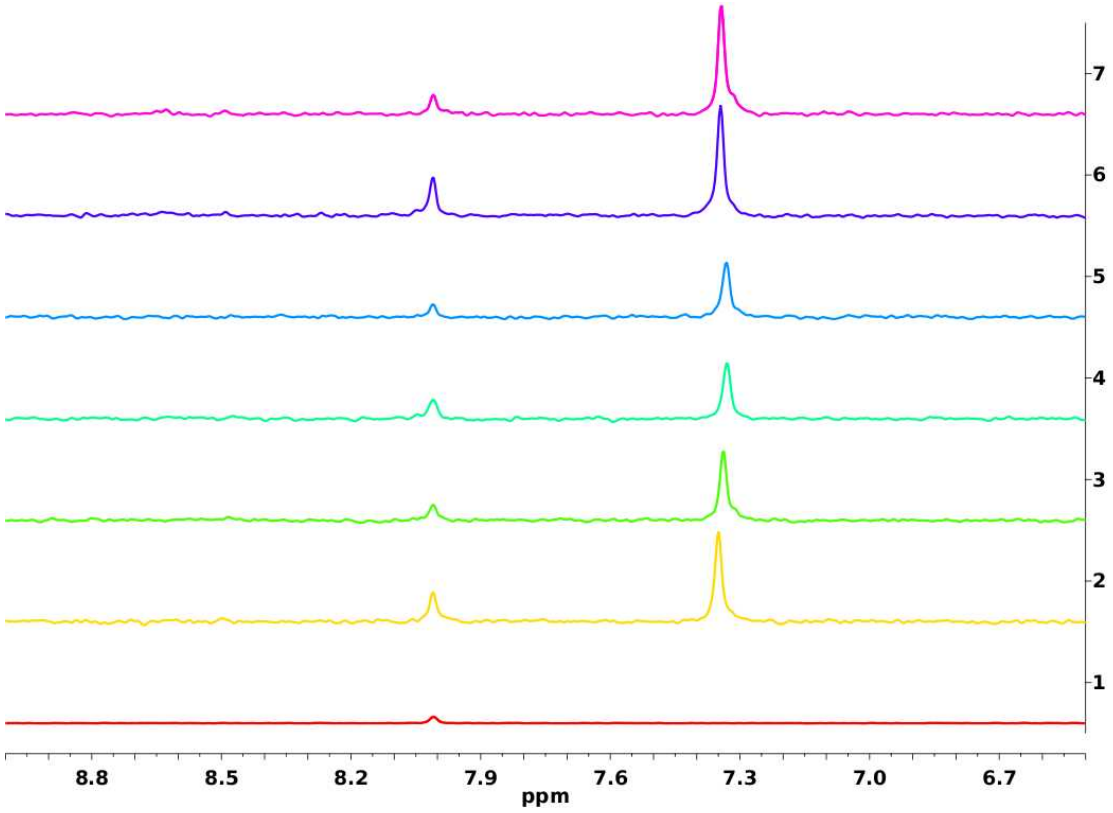

Figure 2.3 Distribution of covalent ThDP intermediates during reaction of E1p with pyruvate.

C6'-H ThDP intermediates fingerprint region (6.5 – 9.0 ppm) in 1D ^{1}H-^{13}C HSQC NMR spectra. Reaction of E1p with pyruvate was quenched in acid at various time points to obtain supernatant containing ThDP intermediates. (1) Control sample: no pyruvate (2) 0.02 s (3) 0.05 s (4) 0.1 s (5) 0.5 s (6) 5 s (7) 30 s. ThDP (C6'-H): δ 8.01 ppm; HEThDP (C6'-H): δ 7.34 ppm.

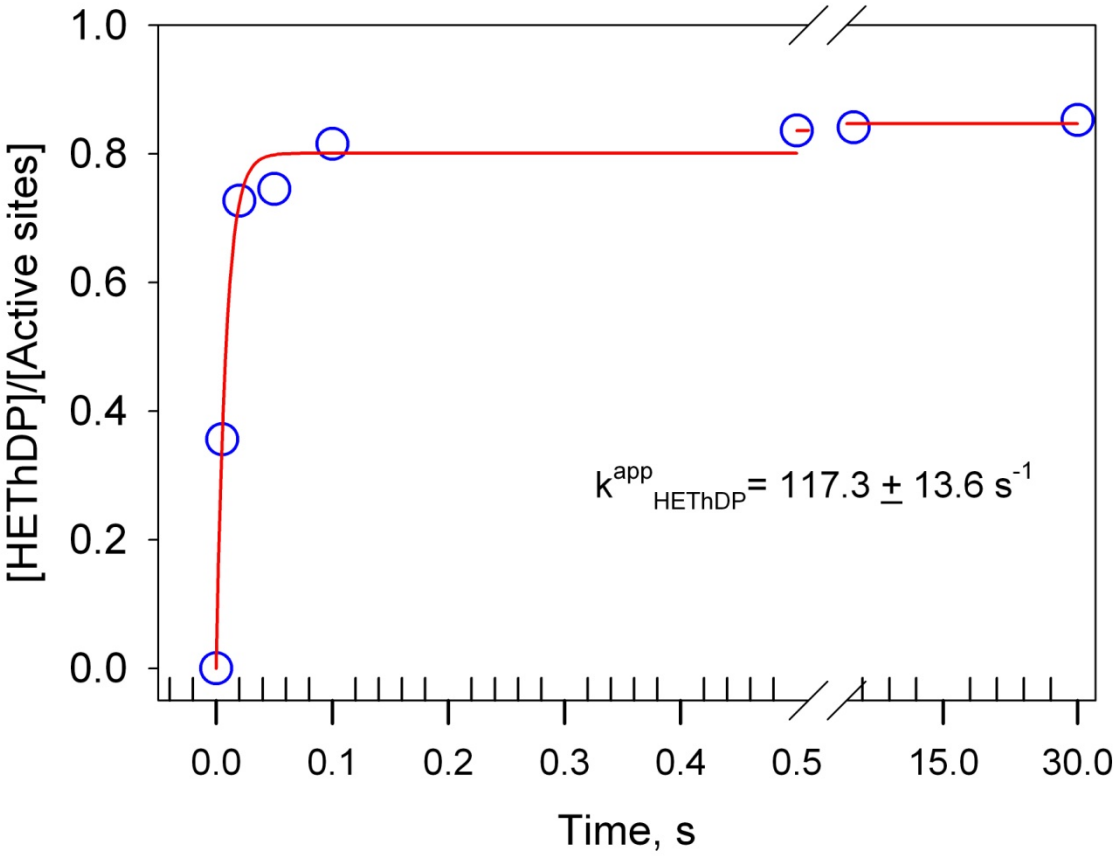

Figure 2.4 Time dependence of fraction HEThDP in E1p reaction with pyruvate

Fraction HEThDP (blue) calculated using ratio of C6'-H signal of HEThDP to total C6'-H signals from HEThDP and ThDP determined at various time points (0, 0.005, 0.02, 0.05, 0.1, 0.5, 5, 30 s) during E1p reaction with pyruvate. The data points were fit using equation 2.2 and the red line is the regression fit trace. The first-order rate constant is an apparent rate constant for formation of HEThDP.

2.3.3 Covalent intermediates in the artificial oxidative decarboxylation reaction of E1p

2,6-Dichlorophenolindophenol (DCPIP) is an oxidizing agent used as a two-electron acceptor to assay most famously for Vitamin C. It has been employed as specific assay for ThDP dependent oxidative decarboxylases by detecting reduction of DCPIP (λ_{max} = 600 nm) by the central enamine intermediate (*104, 109*) as illustrated in Scheme 2.4. While the k_{cat} of 0.65 $\pm$ 0.16 s^{-1} determined by this assay is 100-fold lower than the k_{cat} of 95 $\pm$ 12 s^{-1} determined by PDH activity assay, the DCPIP artificial oxidation reaction was employed as a good model reaction and a quick and efficient assay to study the enzyme bound enamine oxidation for isolated E1p variants as the NADH coupled acetaldehyde reduction assay is limited by the very low conversion rates of pyruvate to acetaldehyde by E1p.

To determine the formation of the ThDP covalent intermediates in the presence of pyruvate and DCPIP, E1p reconstituted with [C2, C6' – $^{13}C_2$]ThDP was mixed with pyruvate and DCPIP and the reaction was stopped at various time points (0.005 to 30 s). Samples collected were analyzed by the 1D-^{1}H gCHSQC NMR experiment and some resultant spectra are shown in Figure 2.5. Resonances at 7.34 ppm pertaining to the HEThDP intermediate and at 7.36, 7.37 and 8.62 ppm pertaining to the acetyl, hydrate and internal carbinolamine forms of AcThDP could be detected during the various time scales. Qualitatively, these spectra suggest that the LThDP intermediate does not accumulate at detectable levels during the reaction. The decarboxylation of LThDP is much faster than its formation. The signal corresponding to the HEThDP intermediate at 7.34 ppm shows a time-dependent increase reaching a steady-state during early time scales (0 – 0.05 s) followed by a decrease corresponding to the conversion of the enamine to AcThDP (0.05 –

5 s) and finally an increase due to the complete consumption of DCPIP at longer time points (5 – 30 s). The signals corresponding to AcThDP show a time-dependent rapid increase during short time scales (0 – 0.5 s) and a decrease at longer time scales (0.5 – 30 s) corresponding to the total consumption of DCPIP. The signal corresponding to ThDP at 8.01 ppm shows a time-dependent decrease, indicating a conversion of ThDP to enamine and AcThDP leading to the accumulation of either the enamine or AcThDP in E1p active-sites.

Integration of the signals and a correction for fraction unbound ThDP determined using equation 2.1 at various time points yields the fraction of relative abundance of HEThDP and AcThDP at various time points plotted as a kinetic trace as shown in Figure 2.6 . The relative fractions during the short time scales were fit to a single exponential process as described by equation 2.2 to yield an apparent first-order rate of formation of $57 \pm 6\ s^{-1}$ for AcThDP and $73.2 \pm 8.8\ s^{-1}$ for the enamine, assuming the total amount of enamine during any time point is the sum total of AcThDP and HEThDP. The fractional abundance of AcThDP was also fit to a bi-exponential process as described by equation (2.4) to yield an apparent rate of formation of $52 \pm 7.5\ s^{-1}$ and a pseudo first-order rate of hydrolysis of $0.23 \pm 0.05\ s^{-1}$.

These kinetic data provide clear evidence for the notion that the enamine intermediate is favorably stabilized on E1p and is susceptible toward oxidation rather than protonation. In studies using HEThDP as a substrate for E1p Zhang et al. estimated upto 10^7 fold rate acceleration for ionization of the C2α-H bond of HEThDP bound to E1p which corresponds to a 10 kcal/mol stabilization of the enamine intermediate on the enzyme (*110*).

The detection of AcThDP during the reaction of E1p with DCPIP also provides conclusive evidence for the mechanism of oxidation as proposed in Scheme 2.4. However, interesting questions still remain about the whether DCPIP binds at any specific locus on the enzyme and if the oxidation proceeds via two single electron steps or a concerted two-electron process. The slow rate of hydrolysis of AcThDP indicates that the last step in the mechanism is the slow step. This finding could possibly explain the discrepancy between the k_{cat} values derived from DCPIP based assay and PDH activity based assay. While, the enamine is oxidized at a rate comparable to its formation, the AcThDP intermediate thus generated is hydrolyzed at a very slow rate since such a reaction is not a part of the natural catalytic cycle for E1p. The hydrolysis rate of 0.23 ± 0.05 s^{-1} of enzyme bound 2-acetylThDP determined here is similar to hydrolysis rate of synthetic 2-acetylThDP off the enzyme at pH values 7-7.5 (*111*) i.e., even when bound to enzyme, the rate of hydrolysis is unaffected. Since the hydrolysis is necessary a step to regenerate the active enzyme, the k_{cat} values are very low. However, the DCPIP based artificial oxidation reaction is indeed a very good model for studying the oxidation of enamine on such oxidative-decarboxylases at the active-sites level using pre-steady state kinetics.

Scheme 2.4 Oxidation of the enamine by 2,6-dichlorophenolindophenol in E1p

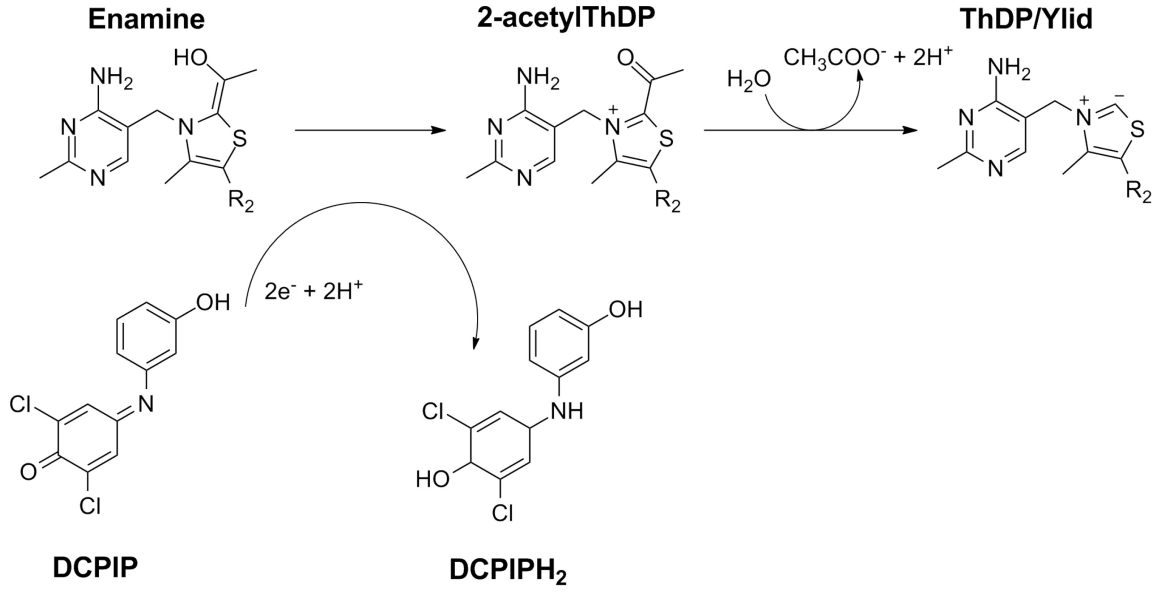

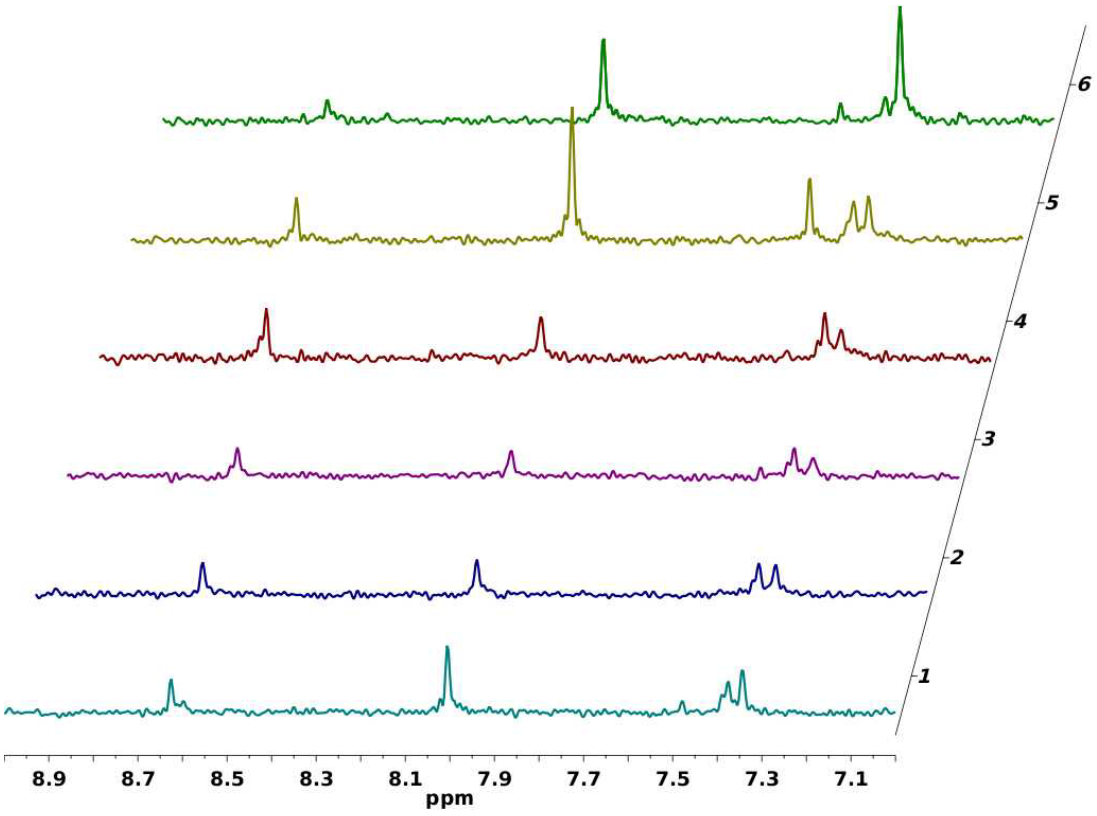

Figure 2.5 Distribution of ThDP intermediates during the reaction of E1p with pyruvate and DCPIP.

C6'-H ThDP intermediates fingerprint region (7.0 – 9.0 ppm) in 1D ^{1}H-^{13}C HSQC NMR spectra. DCPIP dependent oxidation reaction of enamine on E1p was quenched in acid at various time points to obtain supernatant containing ThDP intermediates. (1) 0.02 s (2) 0.05 s (3) 0.1 s (4) 0.5 s (5) 5 s (6) 30 s. ThDP (C6'-H): δ 8.01 ppm; HEThDP (C6'-H): δ 7.34 ppm; 2-acetylThDP (C6'-H): δ 8.62 ppm (carbinolamine), 7.38 & 7.37 ppm (hydrate and keto forms).

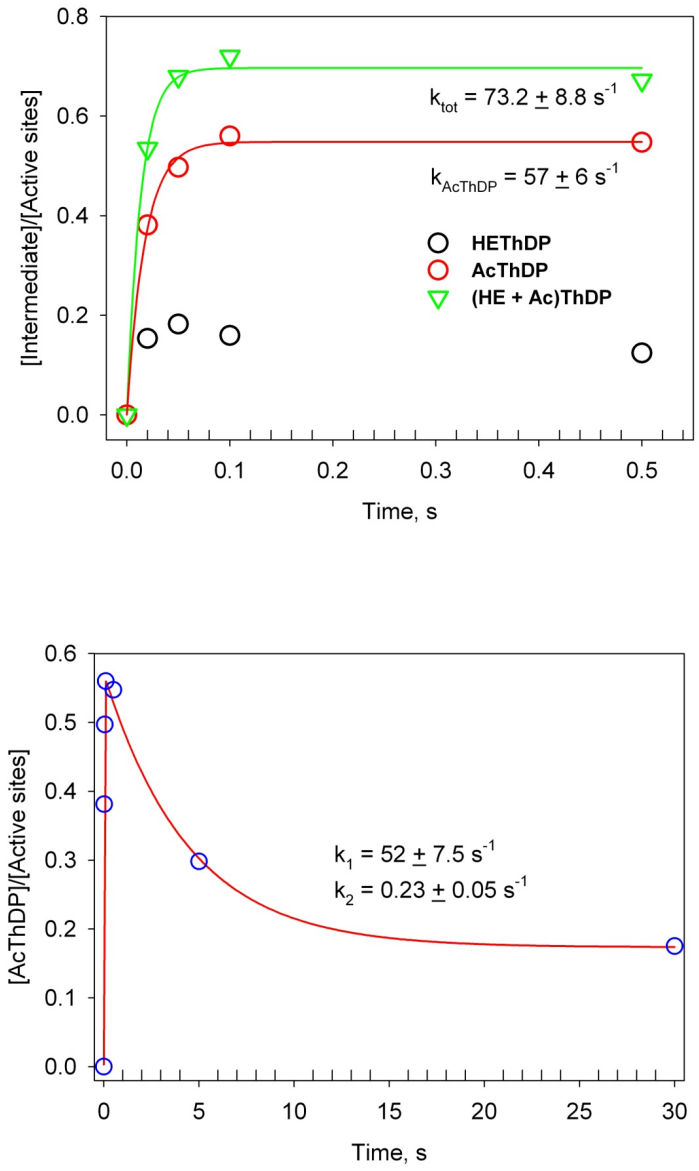

Figure 2.6 Time dependence of HEThDP and AcThDP during the reaction of E1p with pyruvate and DCPIP

Fraction intermediate (AcThDP (red), HEThDP (black)) calculated using ratio of C6'-H signals of intermediate to total C6'-H signals from AcThDP, HEThDP and ThDP determined during first 0.5 s. Bottom: time course of AcThDP - Steady state is reached within 0.5 s; next, consumption of DCPIP leads to depletion of AcThDP and formation of HEThDP. The red trace is the regression fit line.

2.3.4 Covalent intermediates during PDHc reaction

Some covalent intermediates such as the enamine and its subsequent oxidation to 2-acetylThDP by the artificial electron acceptor DCPIP were determined by using E1p in isolation in model reactions. Experiments using the PDH complex in the presence of all substrates were performed to determine the fate of these covalent intermediates during the catalytic cycle of the reconstituted PDHc, and to determine if complex assembly has any effect on catalysis in the E1p active-sites.

To determine the formation of the ThDP covalent intermediates in the presence of substrates (pyruvate, coenzyme A, and NAD^+) PDHc reconstituted with [C2, C6' – $^{13}C_2$]ThDP was mixed with the substrates and the reaction was stopped at various time points (0.005 to 30 s). Samples collected were analyzed by a 1D-^{1}H gCHSQC NMR experiment and some resultant spectra are shown in Figure 2.7. Surprisingly, similar to the observations with E1p alone, only resonances at 7.34 ppm pertaining to the HEThDP intermediate could be detected during the various time scales.

Qualitatively, these spectra suggest that the LThDP intermediate does not accumulate at detectable levels during the reaction. The decarboxylation of LThDP is much faster than its formation. 2-AcetylThDP, the intermediate generated after oxidation of the enamine, could not be detected at any time. Two studies on the transient nature of the 2-acetylThDP intermediate during PDHc catalysis showed that it was (i) chemically competent and could be transferred to the reduced form of the lipoate (dihydrolipoate form) moiety when generated on the enzyme using 3-fluoropyruvate and (ii) using [C3 - ^{14}C]pyruvate labeling 0.5% of PDHc active-sites were found to contain 2-acetylThDP during the overall PDHc

reaction, while up to 12% of active-sites were found to contain the intermediate in an artificial enamine oxidation reaction using ferricyanide (*111, 112*). These results are similar to the current findings using the NMR method. While, 2-acetylThDP could be exquisitely detected during the artificial oxidation reaction, it presumably does not accumulate at detectable levels (by NMR) during the overall PDH complex reaction in E1p active-sites. This in-turn could indicate that the rate of transfer to lipoyl moiety is higher than the rate of oxidation of the enamine.

The signal corresponding to the HEThDP intermediate at 7.34 ppm shows a time-dependent increase reaching a steady-state while the signal corresponding to ThDP at 8.01 ppm shows a time-dependent decrease, indicating a conversion of ThDP to HEThDP and the accumulation of HEThDP in the E1p active-sites.

Integration of the signals and a correction for fraction unbound ThDP determined using the equation 2.1 at various time points yields fraction of relative abundance of HEThDP plotted as a kinetic trace in Figure 2.8. These values were fit to a single exponential process as described by equation 2.2 to yield an apparent first-order rate constant of $117 \pm 25\ s^{-1}$ for the formation of HEThDP in E1p active-sites as compared to the overall k_{cat} of $95 \pm 12\ s^{-1}$ determined from V_{max} (57 ± 7 activity units per E1 active-center) for 1-lip PDHc enzymes purified during the course of these studies. Similar apparent rates of HEThDP formation during the E1p reaction and PDHc reactions indicate that the complex assembly has no major effect on the reactions in E1p active-sites. The net forward rates are optimized in the E1p active-sites to decarboxylation of pyruvate to enamine; hence the rates are not affected upon reconstitution of E1p into PDHc. E1p is not the locus of the rate-determining steps in PDHc catalysis.

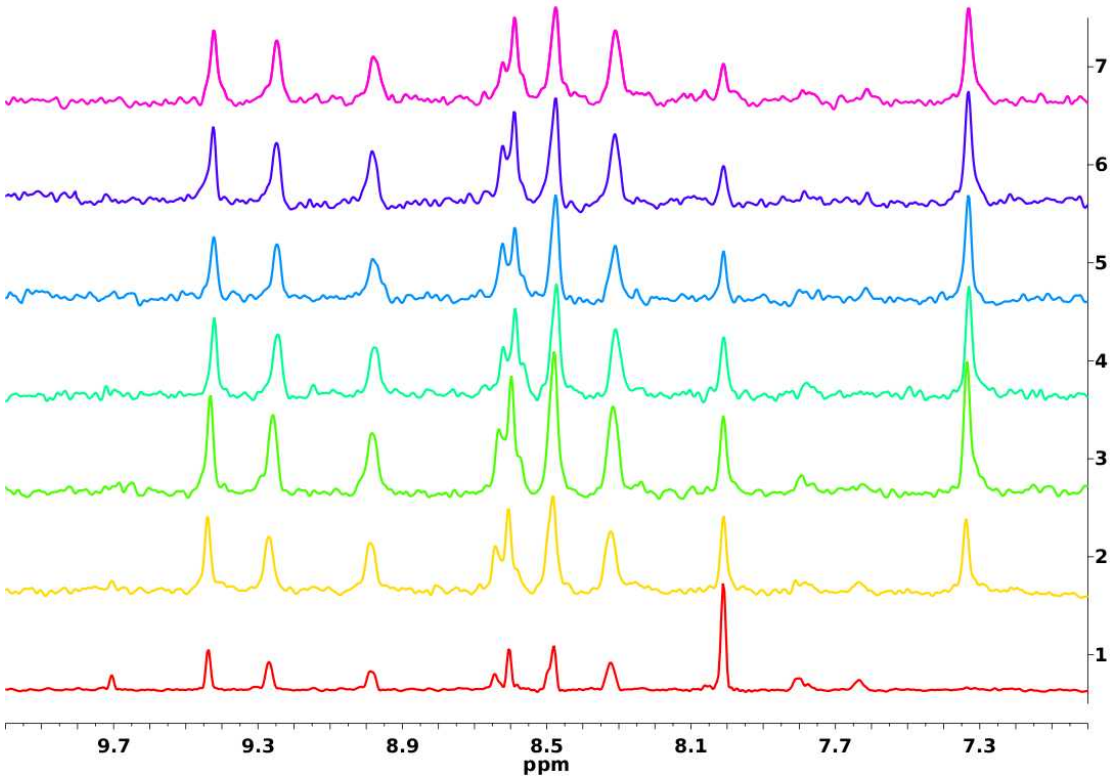

Figure 2.7 Distribution of covalent ThDP intermediates during PDHc reaction

C6'-H ThDP intermediates fingerprint region (7.0 – 10.0 ppm) in 1D ^{1}H-^{13}C HSQC NMR spectra. Overall reaction of PDH multi-enzyme complex was quenched in acid at various time points to obtain supernatant containing ThDP intermediates. (1) Control sample: PDHc and cofactors without pyruvate (2) 0.02 s (3) 0.05 s (4) 0.1 s (5) 0.5 s (6) 5 s (7) 30 s. ThDP (C6'-H): δ 8.01 ppm; HEThDP (C6'-H): δ 7.34 ppm. The other peaks are due to the substrates NAD^{+}, coenzyme A, and the products NADH and S-acetylcoenzyme A.

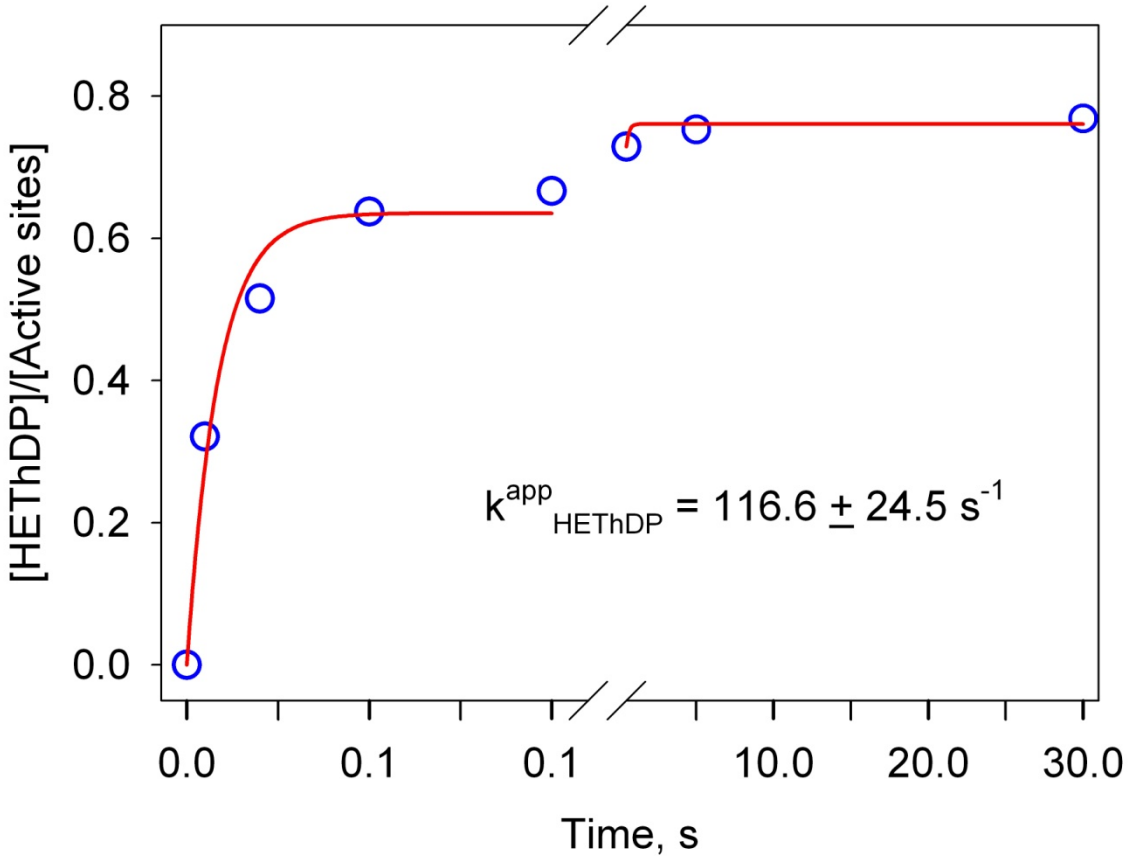

Figure 2.8 Time dependence of HEThDP formation during PDHc reaction

Fraction HEThDP (blue) calculated using ratio of C6'-H signal of HEThDP to total C6'-H signals from HEThDP and ThDP determined at various time points (0, 0.005, 0.02, 0.05, 0.1, 0.5, 5, 30 s) during the PDHc overall reaction. The red trace is the regression fit line.

2.3.5 Covalent ThDP intermediates on the inner loop variant E401K- E1p

Active-site loops spanning residues 401 – 413 (inner loop) and 541 – 557 (outer loop) were shown previously to modulate E1p catalysis. The E401K, H407A, and D549A substitutions were shown to affect E1p catalysis by slowing down pre-decarboxylation steps (Scheme 2.1) and also affecting the rate of reductive acetylation of the lipoyl domain of E2p. These active-site loop variants were also shown to produce acetolactate a carboligase side-reaction product. Y177A an active-site variant, is also included in this study to test the effect of active-site substitutions. These variants were tested with the NMR method to determine the effect of these substitutions on the individual catalytic steps and to detect intermediates in the carboligase reaction steps.

E401K E1p with pyruvate

To determine the formation of the ThDP covalent intermediates in presence of pyruvate, E401K E1p reconstituted with [C2, C6' – $^{13}C_2$]ThDP was mixed with pyruvate and the reaction was stopped at various time points (0.8 to 300 s). Samples collected were analyzed by 1D-^{1}H gCHSQC NMR experiment and the data processed as described earlier for E1p and PDHc. Only resonances at 7.34 ppm pertaining to the HEThDP intermediate could be detected during various time scales on all the variants tested. Similar to the parental E1p, the decarboxylation of LThDP is much faster than its formation in all of the variants. The signal corresponding to the HEThDP intermediate at 7.34 ppm shows a time-dependent increase reaching a steady-state while the signal corresponding to ThDP at 8.01 ppm shows a time-dependent decrease, indicating a conversion of ThDP to HEThDP and the accumulation of HEThDP in E1p active-sites.

Integration of the signals and a correction for fraction unbound ThDP determined using the equation 2.1 at various time points yields the fraction of relative abundance of HEThDP which were plotted as kinetic traces for each variant. These values were fit to a single exponential process as described by equation 2.2 to yield an apparent first-order rate constant for the formation of HEThDP in E1p variant(s) active-sites (Figure 2.9 A). The rate of formation of HEThDP was found to be 0.12 s^{-1}, which is 1000 fold lower compared to parental E1p. Earlier findings with this variant suggested that steps through formation of the pre-decarboxylation intermediate were slowed by this substitution. Also, the E1p-pyruvate Michaelis complex was shown to accumulate during steady-state CD experiments, whereas the rate of formation of the Michaelis complex itself was very fast (within the dead-time of the Pi* Stopped-flow CD instrument). These results taken collectively suggest that the first C-C bond formation is the slowest step for this variant in its reaction with pyruvate. While, the residue is not in close proximity to the ThDP molecule bound at the active-site, its critical location at the hinge of the inner-loop means severe perturbations at this position lead to improper closing of the active-site loops which are necessary for sequestration of the chemistry within the active-site. Specifically reactive nucleophilic intermediates like the Ylide and the enamine need to be sequestered within hydrophobic pockets to prevent protonation or other side reactions. The enamine on this variant reacts with another molecule of pyruvate producing acetolactate as a consequence of improper loop function. Similarly, during the pre-steady state phase, water molecules could thwart ylide formation, thus slowing down the next step, formation of the first C-C bond.

E401K E1p with DCPIP reaction

In the presence of DCPIP, the only intermediate detected was HEThDP unlike the parental E1p. The rate of enamine formation in this variant (0.12 s^{-1}) is within range of the rate of hydrolysis of 2-acetylThDP (0.23 s^{-1}). The rate of formation of 2-acetylThDP being lower than its hydrolysis, this intermediate does not accumulate during the reaction in this variant. The apparent rate of HEThDP formation of 0.016 s^{-1}, is much lower due to the conversion of the enamine to 2-acetylThDP and its hydrolysis (Figure 2.9 B).

E401K E1p PDHc reaction

Next, the effect of reconstitution with E2p-E3p sub-complex on catalysis by the E1p component was determined for this variant by generating PDHc containing E401K E1p variant and performing the overall PDHc reaction in the presence of pyruvate, NAD^+ and coenzyme A. Only HEThDP could be detected during the various time scales monitored for this variant. The fraction HEThDP in the active-sites was determined and the data were fit to a bi-exponential equation 2.3 as shown in Figure 2.9 C. The rate of HEThDP formation was 0.6 $\pm$ 0.07 s^{-1} which is 5-fold higher than the rate in the E1p component by itself. These results suggest that complex formation has a moderate effect on catalysis by the E1p component; presumably the lipoyl domain interaction orders the loop over the E1p active-site leading to a modest recovery in the active-site sequestration.

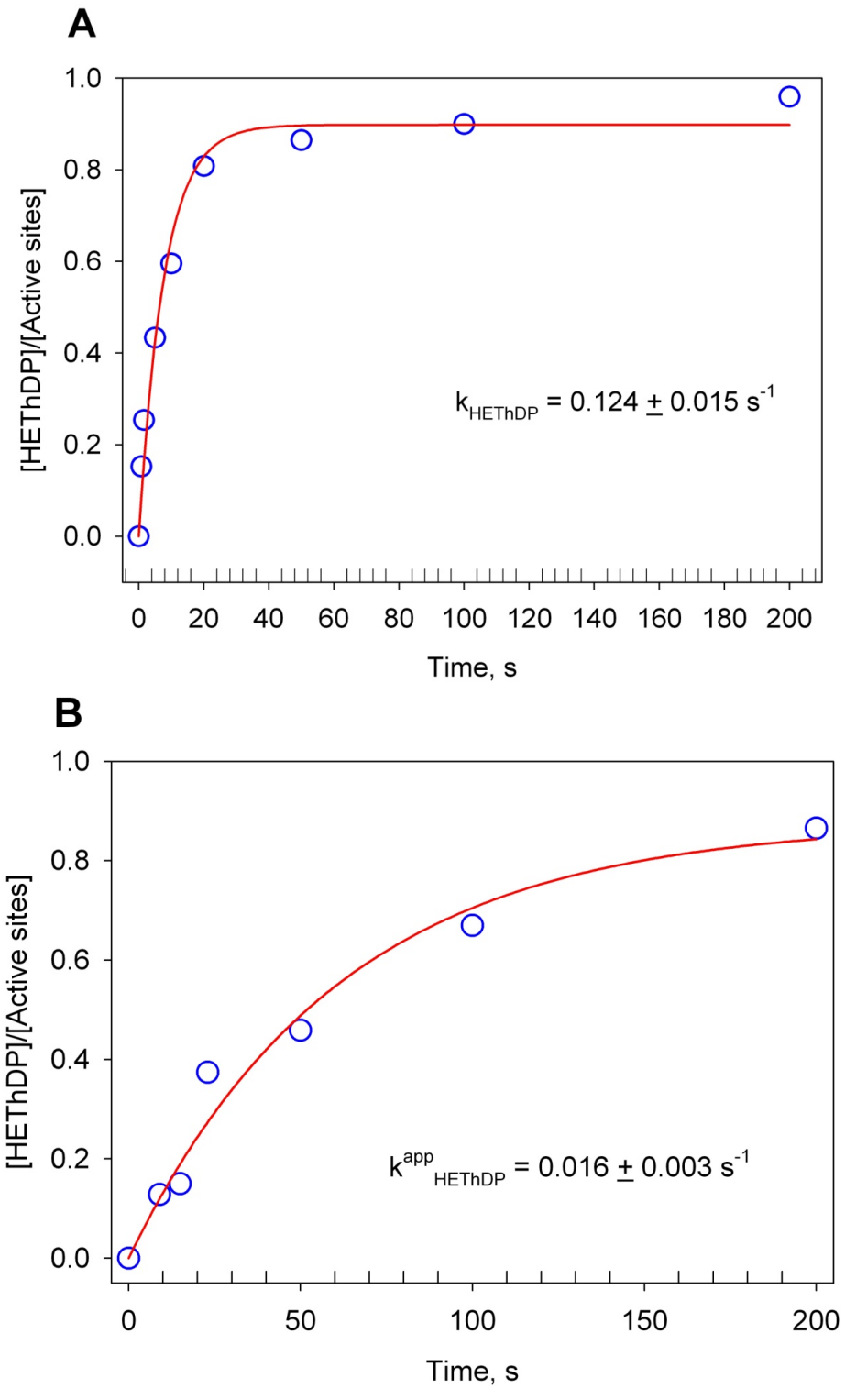
A
1.0
0.8
0.6
0.4
0.2
0.0
[HEThDP]/[Active sites]
k_{HEThDP} = 0.124 ± 0.015 s^{-1}
0
20
40
60
80
100
120
140
160
180
200
Time, s
B
1.0
0.8
0.6
0.4
0.2
0.0
[HEThDP]/[Active sites]
k^{app}_{HEThDP} = 0.016 ± 0.003 s^{-1}
0
50
100
150
200
Time, s

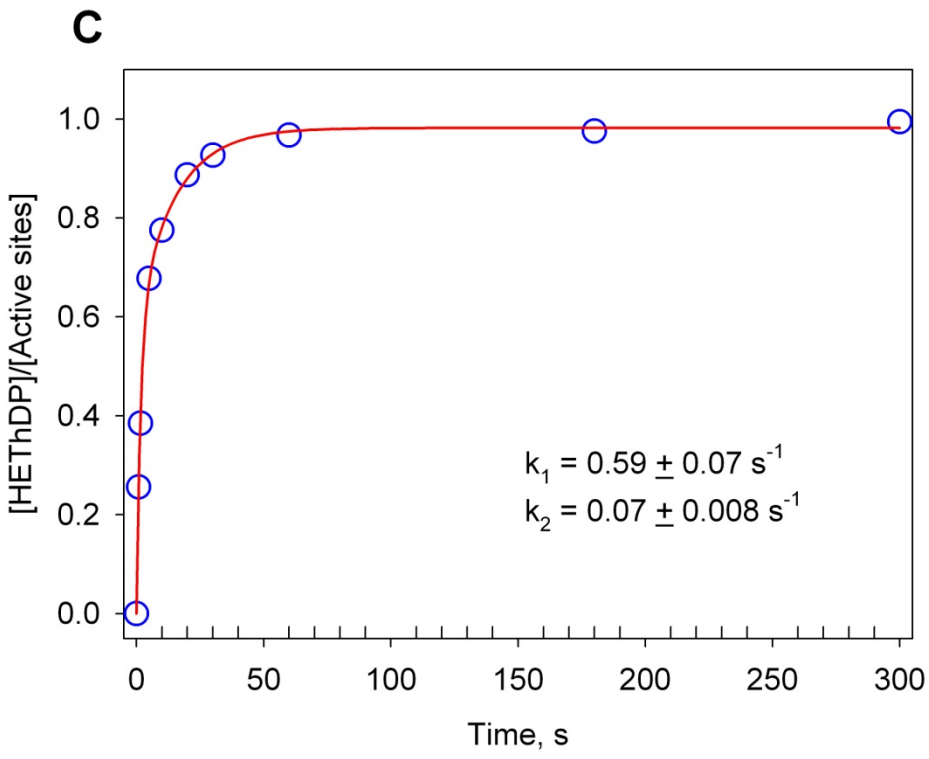

Figure 2.9 Time dependence of HEThDP during various reactions of E401K E1p

Fraction HEThDP (blue) calculated using ratio of C6'-H signal of HEThDP to total C6'-H signals from HEThDP and ThDP determined at various time points during **(A)** E401K E1p reaction with pyruvate (0, 0.8, 1.6, 5, 10, 20, 50, 100, 200 s). **(B)** E401K E1p with pyruvate and DCPIP (0, 9, 15, 23, 50, 100, 200 s) **(C)** E401K E1 PDHc overall reaction (0, 0.8, 1.6, 5, 10, 20, 30, 60, 180, 300 s). The red trace is the regression fit line.

2.3.6 Covalent ThDP intermediates on the inner loop variant H407A- E1p

X-ray structural evidence suggests that the His407 residue participates in catalysis by forming a hydrogen bond with the intermediate analog, PLThDP. During catalysis, this event could trigger closing of the inner-loop and lead to a series of interactions between the inner and outer loops leading to the closing of the outer-loop (Figure 2.1).

H407A E1p with pyruvate

Similar to the earlier cases, in the NMR spectra of samples collected at various time points, no evidence could be found for the accumulation of the LThDP intermediate. Only resonances at 7.34 ppm pertaining to the HEThDP intermediate could be detected during various time scales on all the variants tested. The signal corresponding to the HEThDP intermediate at 7.34 ppm shows a time-dependent increase reaching a steady-state while the signal corresponding to ThDP at 8.01 ppm shows a time-dependent decrease, indicating a conversion of ThDP to HEThDP and the accumulation of HEThDP in H407A E1p active-sites. The data were fit to a bi-exponential equation (2.3) and yielded a rate of 1.15 ± 0.05 s^{-1} for HEThDP formation in this variant (Figure 2.10 A). Similar to the E401K E1p variant, this 100 fold reduction could correspond to a 100-fold slower rate of formation of the first C-C bond. However, this inner-loop variant is 10-fold faster than E401K E1p during the same step. The substitution at the loop hinge has a more severe effect in the proper functioning of the loop, affecting the initial steps of the catalytic cycle.

H407A E1p with DCPIP reaction

In the presence of DCPIP, the only intermediate detected was HEThDP unlike the parental E1p. The rate of enamine formation in this variant (1.15 s^{-1}) is within range of the rate of hydrolysis of 2-acetylThDP (0.23 s^{-1}). Possibly the lower rate of formation of enamine in-turn means lowered rate of formation of 2-acetylThDP, and since the rates of formation and decomposition are similar this intermediate does not accumulate during the reaction in this variant. The apparent rate of HEThDP formation of 0.06 s^{-1} is much lower due to the conversion of enamine to 2-acetylThDP and its hydrolysis (Figure 2.10 B).

H407A E1p PDHc reaction

Next, the effect of reconstitution with E2p-E3p sub-complex on the E1 component catalysis was determined for this variant by generating PDHc containing H407A E1p variant and performing the overall PDHc reaction in the presence of pyruvate, NAD^+ and coenzyme A. Only HEThDP could be detected during the various time scales monitored for this variant. The fraction of HEThDP in the active sites was determined and the data were fit to a bi-exponential equation 2.3 as shown in Figure 2.10 C. The rate of HEThDP formation was 2.53 ± 0.11 s^{-1} which is only 2-fold higher than the rate in the E1p component by itself. These results suggest that complex formation has a moderate effect on the E1p component catalysis, presumably the lipoyl domain interaction orders the loop over the E1p active site leading to a modest recovery in active-site sequestration. However, this effect is not as pronounced as observed with the E401K E1p variant.

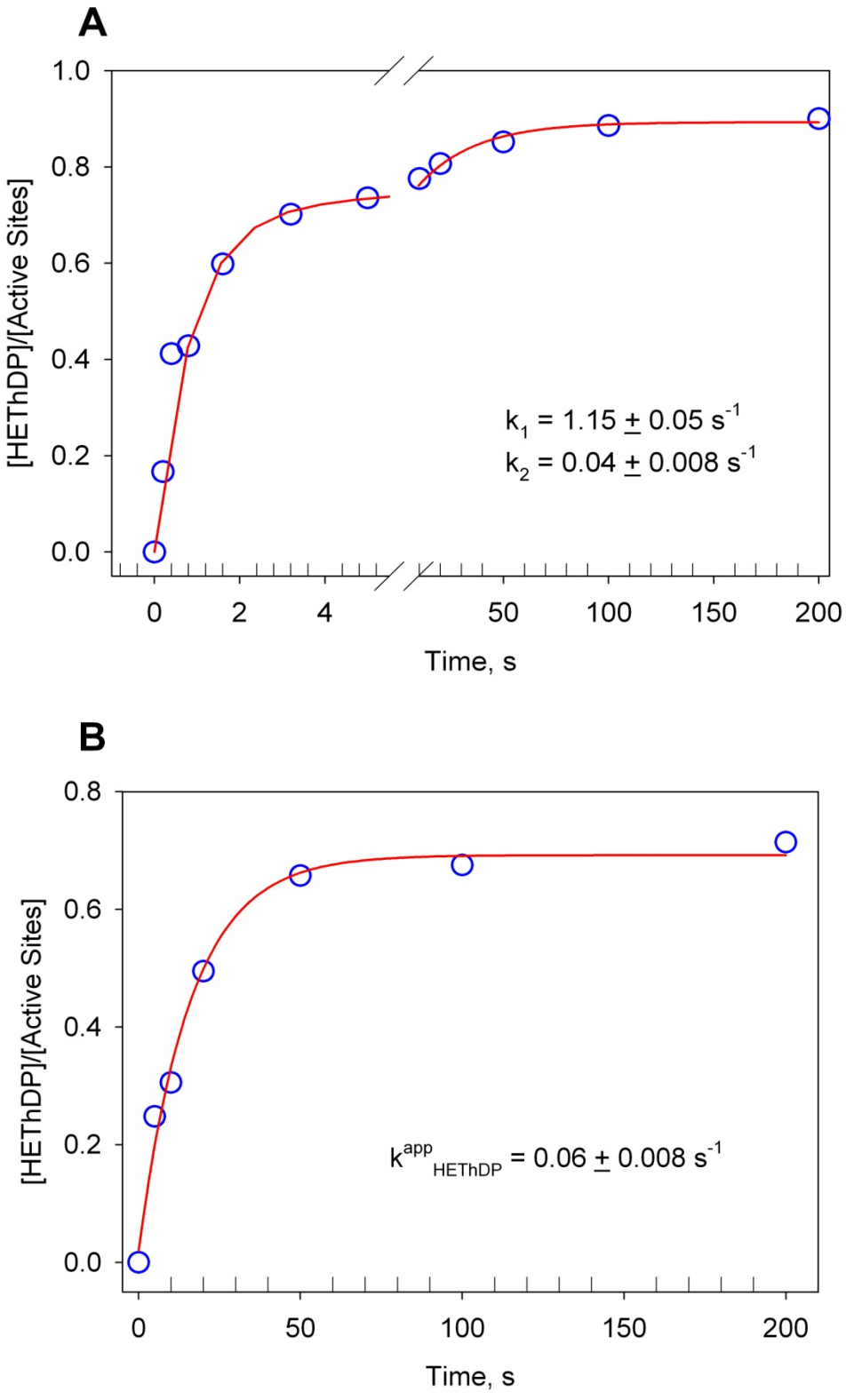
A
1.0
0.8
0.6
0.4
0.2
0.0
[HEThDP]/[Active Sites]
k_1 = 1.15 ± 0.05 s^{-1}
k_2 = 0.04 ± 0.008 s^{-1}
0
2
4
50
100
150
200
Time, s
B
0.8
0.6
0.4
0.2
0.0
[HEThDP]/[Active Sites]
k^{app}_{HEThDP} = 0.06 ± 0.008 s^{-1}
0
50
100
150
200
Time, s

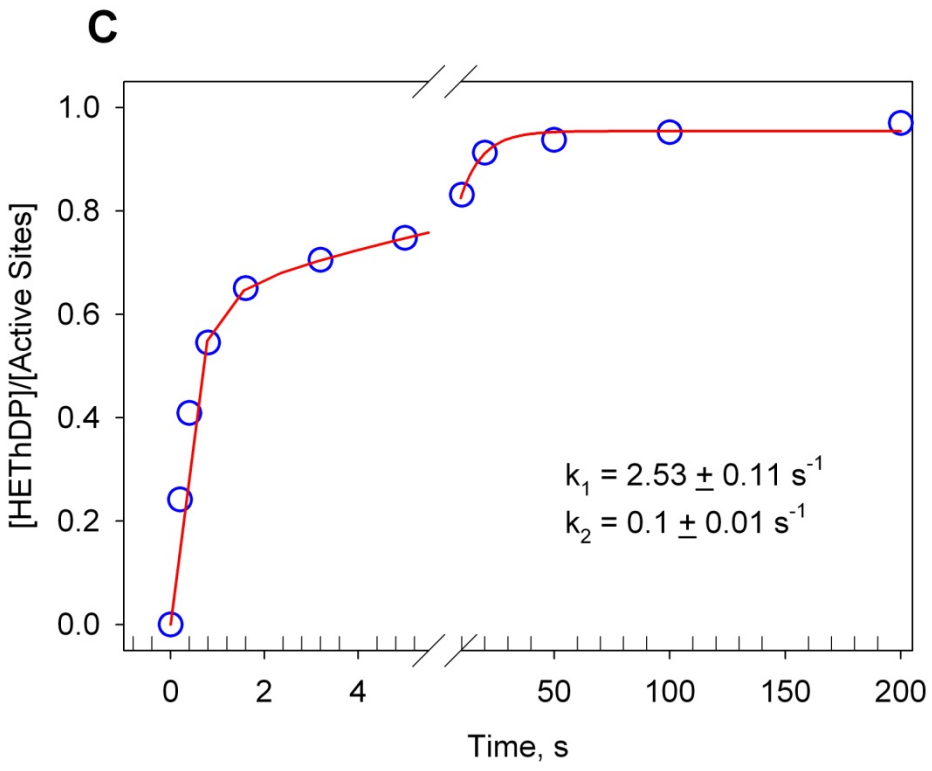

Figure 2.10 Time dependence of HEThDP during various reactions of H407A E1p

Fraction HEThDP (blue) calculated using ratio of C6'-H signal of HEThDP to total C6'-H signals from HEThDP and ThDP determined at various time points during **(A)** H407A E1p reaction with pyruvate (0, 0.2, 0.4, 0.8, 1.6, 3.2, 5, 10, 20, 50, 100, 200 s). **(B)** H407A E1p with pyruvate and DCPIP (0, 5, 10, 20, 50, 100, 200 s) **(C)** H407A E1 PDHc overall reaction (0, 0.2, 0.4, 0.8, 1.6, 3.2, 5, 10, 20, 50, 100, 200 s). The red trace is the regression fit line.

2.3.7 Covalent ThDP intermediates on the outer-loop variant D549A- E1p

According to the X-ray structure of E1p containing PLThDP, a phosphonate analog of C2-α-lactylThDP, in the active sites, residue Asp549 interacts with the inner-loop residue Asn404 and these interactions help in ordering the outer loop over the inner loop (Figure 2.1). To test the effect of substitutions in the outer loop NMR experiments as discussed earlier were performed with the D549A E1p variant, and with PDHc reconstituted with this variant.

D549A E1p with pyruvate

Similar to the earlier cases, in NMR spectra of samples collected at various time points, no evidence could be found for accumulation of the LThDP intermediate. Only resonances at 7.34 ppm pertaining to the HEThDP intermediate could be detected during various time scales on all the variants tested. The signal corresponding to the HEThDP intermediate at 7.34 ppm shows a time-dependent increase reaching a steady state while the signal corresponding to ThDP at 8.01 ppm shows a time-dependent decrease, indicating a conversion of ThDP to HEThDP and the accumulation of HEThDP in the D549A E1p active-sites. The data were fit to a mono-exponential equation (2.2) and yielded a rate of $12.9 \pm 1.0\ s^{-1}$ for HEThDP formation in this variant (Figure 2.11 A). Unlike the inner-loop substitutions, this substitution elicits only a 10-fold rate reduction compared to the parental E1p. However, this rate reduction could correspond to the first step since the decarboxylation step is not rate limiting for this variant.

D549A E1p PDHc reaction

Next, the effect of reconstitution with E2p-E3p sub-complex on the E1 component catalysis was determined for this variant by generating PDHc containing D549A E1p variant and performing the overall PDHc reaction in the presence of pyruvate, NAD^+ and coenzyme A. Only HEThDP could be detected during the various time scales monitored for this variant. The fraction HEThDP in the active sites was determined and the data were fit to a bi-exponential equation 2.3 as shown in Figure 2.11 B. The rate of HEThDP formation was $12.1 \pm 0.5\ s^{-1}$ which is similar to the rate in the E1p component by itself. These results suggest that complex formation has no detectable effect on the E1p component catalysis.

Considering the rates from the parental E1p, the inner-loop variants and the D549A variant *in toto*, a general trend is observed with respect to the disruption caused to the loop motion by these substitutions (Table 2.3). The rate of HEThDP formation follows parental PDHc > D549A E1p PDHc > H407A E1p PDHc > E401K E1p PDHc. The disruption to loop motion follows the following order from minimal to maximal disruption E1p < D549A E1p < H407A E1p < E401K E1p based on their positions in the quaternary structure of the enzyme. The E401K substitution being a charge-reversal (assuming the Lys terminal NH_2 is protonated at pH 7.0) at a hinge residue would produce the maximum disruption. The residues His407 and Asp549, while probably crucial for interactions, their substitution to Ala does not elicit major structural disruptions considering these residues are on flexible regions. These results point to a ping-pong mechanism for loop closure, whereby the inner-loop has to close first providing a new surface for interactions and closing of the outer-loop. In such a mechanism, affecting the inner-loop would have strong detrimental effects on catalysis while the effect due to disruptions of the outer-loop will be of lesser importance.

The effect of complex assembly in the presence of E2p and E3p components, which can be interpreted as recovery of E1p active-site sequestration, also follows a general trend. The recovery seen is of the order E401K E1p (5-fold) > H407A E1p (2-fold) > D549A E1p = parental E1p (no change) from minimal to maximal recovery. Complex assembly helps maximally disrupted variants while it has minimal effect on the outer-loop variant and parental E1p. Presumably, the effect of loop disruption on catalysis has been optimized by evolution for the parental E1p.

Y177A E1p with pyruvate

As a control experiment for the non-specific effects of disruptions to the active-site due to the various substitutions, an active-site variant Y177A was used.

Similar to the earlier cases, in NMR spectra of samples collected at various time points, no evidence could be found for accumulation of the LThDP intermediate. Only resonances at 7.34 ppm pertaining to the HEThDP intermediate could be detected during various time scales on all variants tested. The data were fit to a mono-exponential equation (2.2) and yielded a rate of 26 $\pm$ 1.2 s^{-1} for HEThDP formation in this variant (Figure 2.12). Unlike the active-site loop substitutions, this substitution elicits only a 4-fold rate reduction compared to the parental E1p. This rate reduction could correspond to the pre-decarboxylation steps since the decarboxylation step is not rate limiting for this variant. Since the reduction in rate of HEThDP formation observed in this variant is much less when compared to the loop variants, the non specific effects of substitutions can be assumed to be minimal. The rate reductions observed in the case of loop variants are due to altered dynamics of the loops.

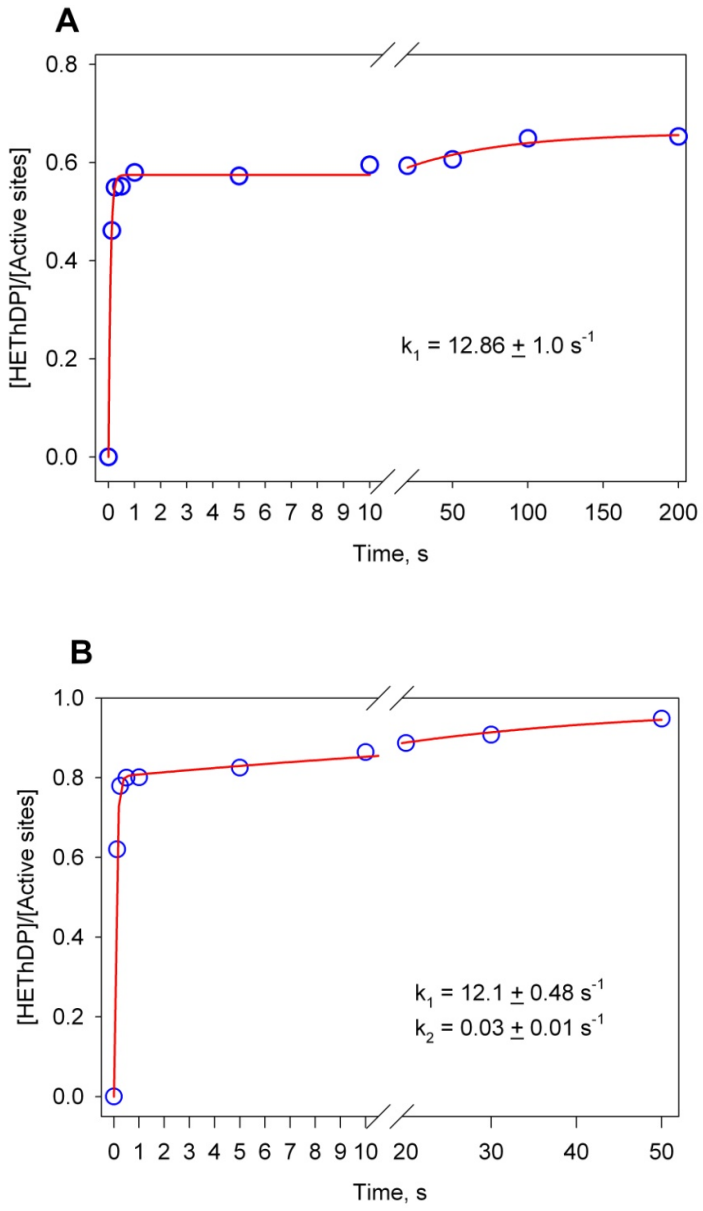

Figure 2.11 Time dependence of HEThDP formation during various reactions of D549A E1p

Fraction HEThDP (blue) calculated using ratio of C6'-H signal of HEThDP to total C6'-H signals from HEThDP and ThDP determined at various time points during **(A)** D549A E1p reaction with pyruvate (0, 0.125, 0.25, 0.5, 1.0, 5.0, 10, 20, 50, 100, 200 s). **(B)** D549A E1 PDHc overall reaction (0, 0.125, 0.25, 0.5, 1.0, 5.0, 10, 20, 30, 50 s). The red trace is the regression fit line.

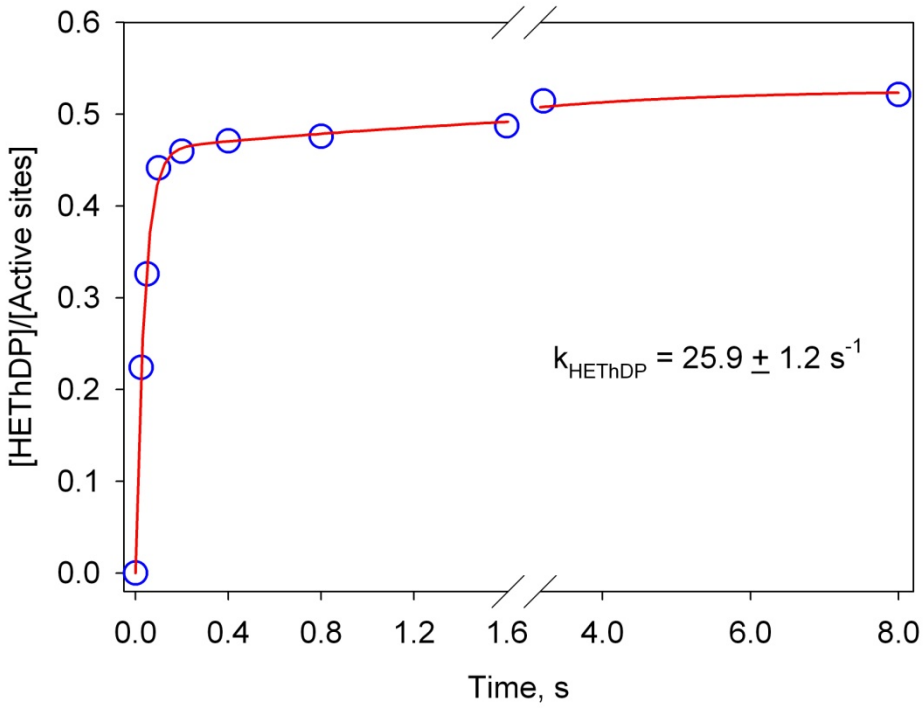

Figure 2.12 Time dependence of HEThDP in reaction of Y177A E1p with pyruvate

Fraction HEThDP (blue) calculated using ratio of C6'-H signal of HEThDP to total C6'-H signals from HEThDP and ThDP determined at various time points during Y177A E1p reaction with pyruvate (0, 0.025, 0.5, 0.1, 0.2, 0.4, 0.8, 1.6, 3.2, 8.0 s).

Table 2.3 Comparision of rates for E1p and variants

	k_{cat}, s^{-1}	k_{HEThDP}, s^{-1}			k_{AcThDP}, s^{-1}
E1 variant		Pyruvate	PDHc reaction	DCPIP	DCPIP reaction
E1p	95.0 ± 12	117 ± 14	116.6 ± 25	73.2 ± 8.8	57 ± 6
E401K	0.83 ± 0.05	0.13 ± 0 .02	0.59 ± 0.05	0.016 ± 0.003	Not detected
H407A	0.08 ± 0.01	1.16 ± 0.05	2.1 ± 0.19	0.06 ± 0.01	Not detected
D549A	0.7 ± 0.1	12.9 ± 1.0	12.1 ± 0.5	--	--
Y177A	3.31 ± 0.3	25.9 ± 1.2			

2.3.8 Reductive acetylation of lipoyl moiety – the final ThDP catalysed step

The reductive acetylation of the lipoyl moiety covalently bound to the lipoyl domain is the final step catalyzed by E1p. The enamine covalently bound to ThDP is oxidized and an acetyl group is transferred to the lipoyl moiety within the E1p active-site. While in the PDH multienzyme complex, the lipoyl domain carrying the lipoyl group shuttles the acetyl group to the catalytic domain of E2p where it is transferred to coenzyme A and the dihydrolipoyl moiety thus generated is reoxidized in the E3p active-sites, E1p has been shown to successfully acetylate the lipoyl domain construct in isolation, without the need for the total complex. This provides a good model reaction to study the final step in E1p catalysis while conserving both the chemistry and structural dynamics involved in this step.

Detection of different forms of Lipoyl domain

The different forms of lipoyl domain could be successfully detected using Electro-Spray Ionization Mass Spectrometry (ESI-MS) and some spectra collected under various reaction conditions are shown in Figure 2.13.

Steady state kinetics of reductive acetylation

The reductive acetylation reaction was monitored at varying concentrations of lipoyl domain in the presence of catalytic E1p and 2 mM pyruvate. Under these conditions the lipoyl domain is a substrate for E1p and during multiple turn-overs the acetylated lipoyl domain accumulates as the product of the reaction (Figure 2.14). Fitting the data to a Hill equation yielded a K_m for the lipoyl domain of 0.8 ± 0.12 μM.

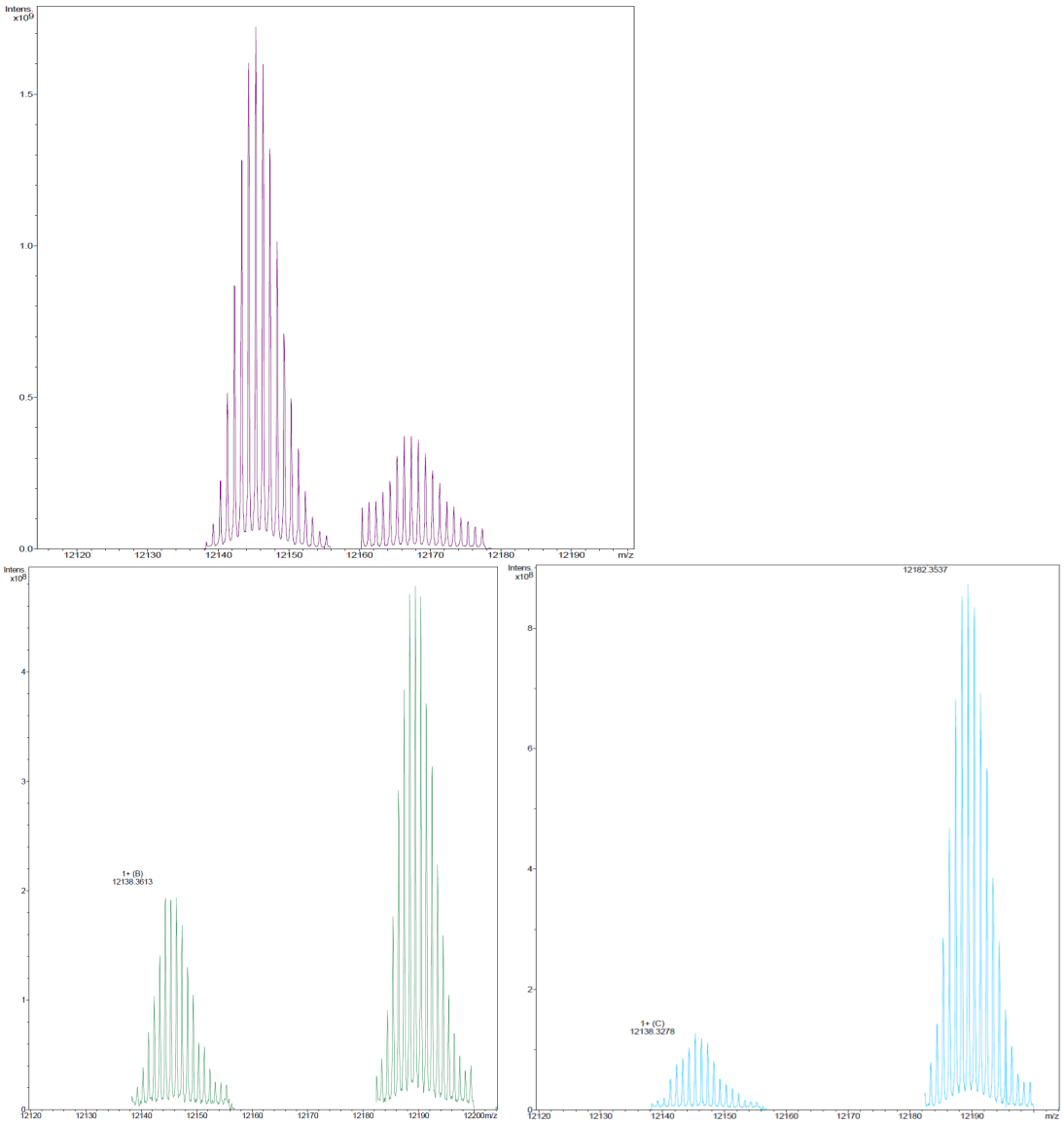

Figure 2.13 Lipoyl domain and its acetylated form detected using ESI-MS

Deconvoluted ESI –MS spectrum of RED: lipoyl domain (LD), (Mass determined by Experiment: 12,145.34; Calculated: 12,144.7). GREEN: of sample obtained at 15 s in a reaction of E1p (0.1 μM), LD (10 μM), and pyruvate (2 mM). BLUE: of sample obtained at 60 s in a reaction of E1p (0.1 μM), LD (20 μM) and pyruvate (2 mM). The acetylated form is seen in the latter two spectra. (Experimental: 12,189.35; Calculated: 12,188.6).

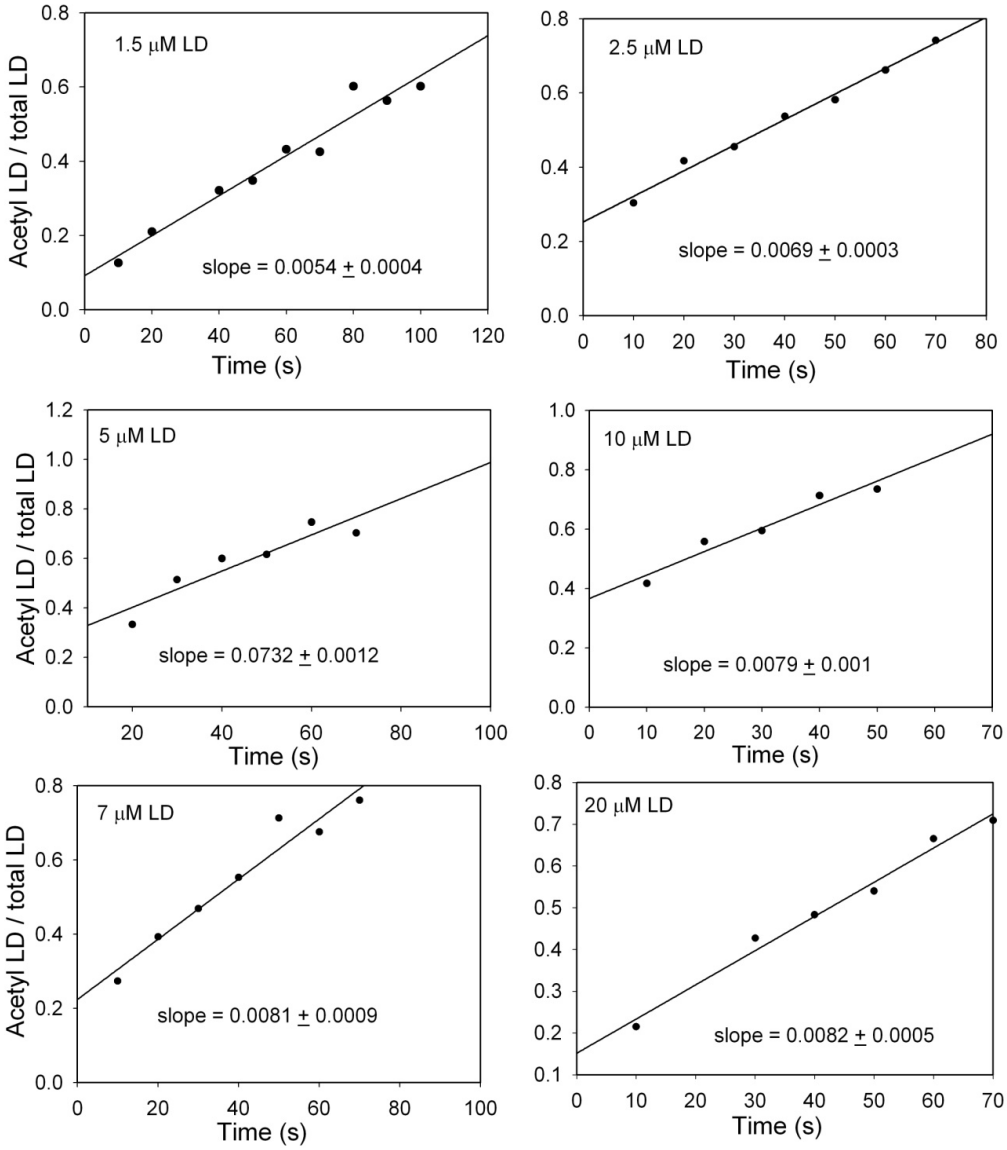

Figure 2.14 Progress curves of reductive acetylation reaction at various concentrations of lipoyl domain.

Reaction of E1p (0.1 μM active centers) with varying concentrations of LD (0 – 20 μM) in the presence of 2 mM pyruvate in 50 mM $(NH_4)_2CO_3$ pH 7.0 was monitored by a discontinuous assay method. Relative intensity of the two forms yields fraction acetylated. Time dependence of this fraction is plotted and the linear slope represents initial rate of fraction acetylation of LD (units: fraction/s).

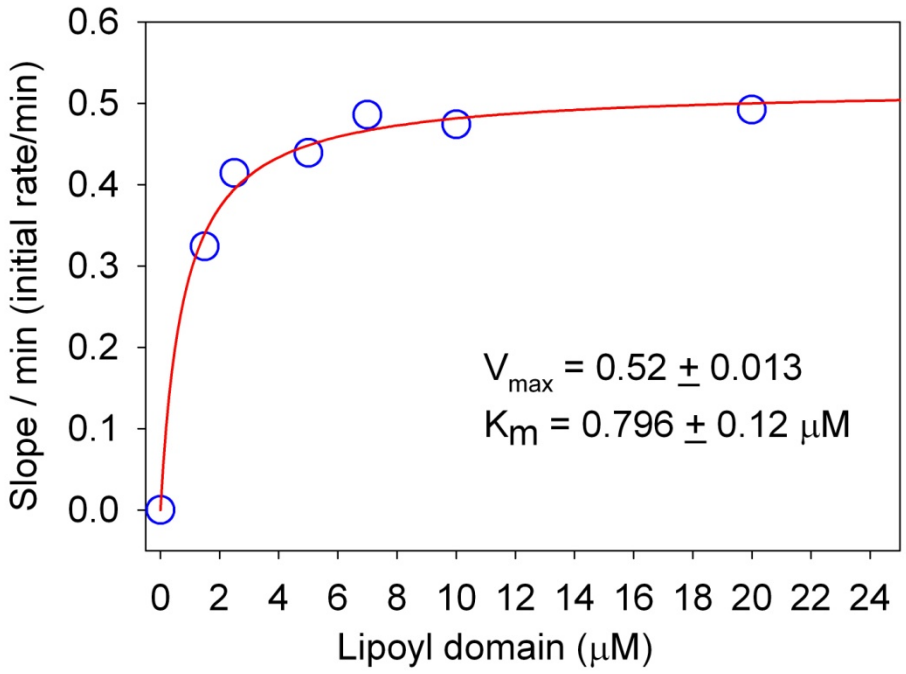

Figure 2.15 Michaelis-Menten plot for reaction of E1p and lipoyl domain as substrate

The initial rates (linear slope) determined using varying concentrations of lipoyl domain as noted were converted to min^{-1} basis and plotted against the lipoyl domain concentration (blue circles). The data were fit to a Hill equation and the red trace is the regression fit line. The V_{max} determined from the plot corresponds to the maximal initial rate min^{-1} .

Pre-steady state kinetics of reductive acetylation of lipoyl domain by E1p

Determination of the K_m for lipoyl domain allowed determination of conditions for a single turnover pre-steady state kinetic experiment which could better mimic the reductive acetylation reaction as it occurs during PDHc catalysis. At high concentrations of E1p (20 μM) and lipoyl domain (20 μM, well over the K_m of 0.8 μM), the E1p – LD complex formation is ensured to be spontaneous, i.e., binding steps are not rate-limiting. Using equal concentration of E1p and the lipoyl domain ensures single turnover conditions, under which the chemistry i.e., transfer of acetyl moiety from E1p to the lipoyl domain becomes the rate limiting step, in a pseudo first-order type process, rather than the dissociation of the product from E1p during longer time points when excess product can be expected to accumulate.

Samples collected at various time points (0.005 – 0.15 s) using a rapid chemical quench instrument were analyzed using ESI-MS. The fraction of lipoyl domain acetylated at different time points was determined by taking a ratio of the relative intensity of the acetylated form to the total relative intensity (sum of lipoyl domain and acetylated lipoyl domain). Time dependence of this fraction was plotted and the data were fit to a mono-exponential equation (2.2) yielding a rate of reductive acetylation of $51.7 \pm 5.4\ s^{-1}$ (Figure 2.16). This pseudo first-order rate constant is composed of the rates including conversion of pyruvate to the enamine and the reductive acetylation of the lipoyl domain by the enamine.

Considering the rates of formation of the enamine from NMR methods and the rate of reductive acetylation and applying Cleland's transit-time model would yield net individual rate constants for the various steps.

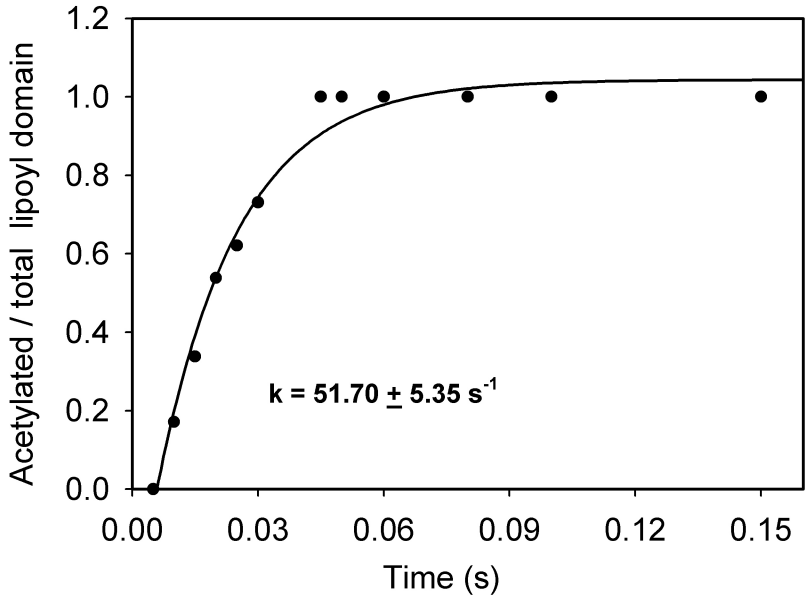

Figure 2.16 Time dependence of fraction acetylated lipoyl domain during single turnover reaction

2.3.9 Determination of net forward rate constants

Following Cleland's net rate constants model (*113*) a similar model can be built for the E1p catalysis in PDHc, substituting net rate constants (denoted with prime) for individual forward and reverse rate constants. Here the net rate constants denote the flux through each step, and in case of irreversible steps the net rate constants would be identical to the true forward rate constants (Scheme 2.5). For a series of reactions, the reciprocal of the net rate constant for any individual step is its transit time. The total time for one molecule of pyruvate to be converted to product is given by the sum of the transit times for each step (*114*). For example for acetate production in the DCPIP reaction

$$\frac{[E]_0}{v} = \frac{1}{k_{cat}} = \frac{1}{k'_1} + \frac{1}{k'_2} + \frac{1}{k'_3} + \frac{1}{k'_4} + \frac{1}{k'_5} \tag{2.9}$$

Where $$k_1' = \frac{k_1 \times [\text{pyruvate}] \times k_2'}{k_{-1} + k_2'}$$

And k_4' represents a net rate constant for formation of E1p-enamine DCPIP complex and the oxidation of this complex to 2-acetylThDP.

This transit time model can be applied to determine any net rate constant as a summation of transit times of the previous steps under substrate saturation conditions.

$$\frac{1}{k_{HEThDP}} = \frac{1}{k'_1} + \frac{1}{k'_2} + \frac{1}{k'_3} \tag{2.10}$$

$$\frac{1}{k_{AcThDP}} = \frac{1}{k_{HEThDP}} + \frac{1}{k'_4} \tag{2.11}$$

Similarly,

$$\frac{1}{k_{\text{reductive acetylation}}} = \frac{1}{k_{\text{HEThDP}}} + \frac{1}{k'_4} \tag{2.12}$$

The Michaelis complex was shown to accumulate within the dead-time (2.5 ms) of the Pi* stopped-flow CD instrument (*16, 99*), and since decarboxylation is not rate limiting in any of the experiments with E1p or variants in equation (2.10) k_2', the net rate constant for formation of LThDP approximates to $k_{HEThDP.}$

From equation 2.11 k_4' can be determined directly by substitution of the rate of formation of AcThDP and HEThDP. Similarly, from equation 2.12, k_4' for the reductive acetylation of the lipoyl domain by the enamine can be determined directly by substitution of the rate of formation of acetyl lipoyl domain and HEThDP (refer to Scheme 2.5 B for net rate constants). The net forward rate constants are summarized in Table 2.4.

While the k_4' represent net rate constant for binding and oxidation of the enamine by either DCPIP or the lipoyl domain, under the saturating conditions used in the experiments, the binding events do not have a major contribution toward this composite net rate constant. Assuming these numbers for both reactions represent the chemical transformations only, a significant finding is that the enamine is similarly susceptible to oxidation by either oxidizing agents.

Scheme 2.5 Transit time model of E1p with net rate constants

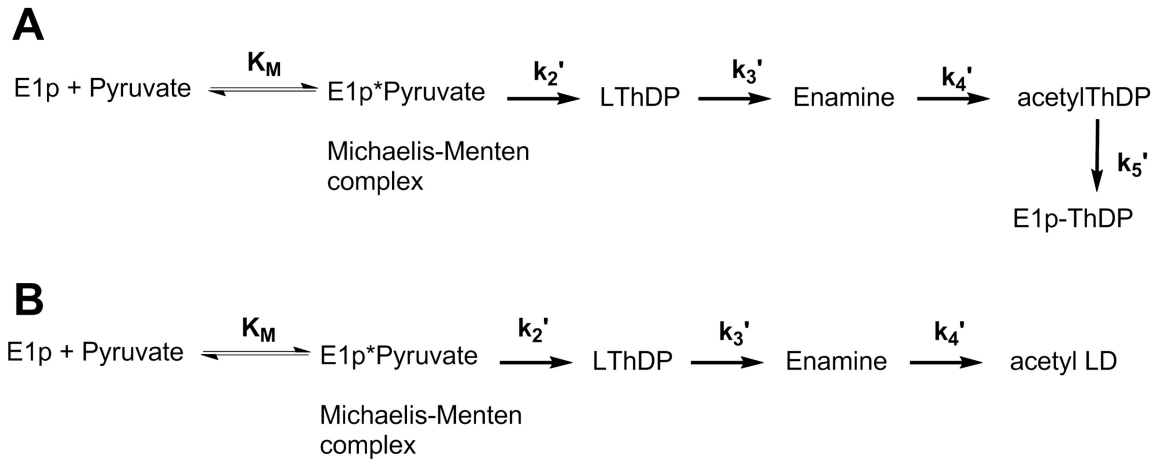

Table 2.4 Net forward rate constants for individual steps in oxidative decarboxylation reactions of E1p

Reaction	k_1', s^{-1}	k_2', s^{-1}	k_3', s^{-1}	k_4', s^{-1}	k_5', s^{-1}
PDH complex	> 600†	117 $\pm$ 25	fast	93.6	--
E1p DCPIP	> 600†	117 $\pm$ 25	fast	111.2	0.23 $\pm$ 0.05

†The MM complex accumulation is completed within 2.5 ms. k_4' is the composite net rate constant involving binding of (DCPIP or lipoyl domain) and reaction with enamine. k_5' is the forward rate constant for hydrolysis of 2-acetylThDP in DCPIP reaction.

2.3.10 Monitoring [C2 – ^{13}C] S-acetyl coenzyme A production by NMR

Conversion of [C3 – ^{13}C]pyruvate to [C2 – ^{13}C]S-acetyl coenzyme A during catalysis of PDH complex was monitored selectively using the 1D-^{1}H gCHSQC NMR filter experiment. In the ^{1}H dimension, only resonances pertaining to ^{1}H attached to ^{13}C3 atom of pyruvate in its keto and hydrate forms and ^{13}C2 atom of S-acetyl coenzyme A were detected. A minor resonance corresponding to [C2 – ^{13}C] acetate at 1.48 ppm was found to be constant at all time points and was found in the control spectrum, indicating that it could be a contamination from the commercial [C3 – ^{13}C]pyruvate (Figure 2.17). No other resonances pertaining to the carboligase side-products (*97*), acetolactate and acetoin, could be detected during the various time scales shown and at longer time scales (200 s). This experiment also confirms that the carboligase side-reactions are considerably slower than the physiological reaction and their effect on the ThDP covalent intermediates accumulation is negligible.

Quantification using integration of ^{1}H signals yielded relative fraction of product at various time points (Figure 2.18). Plotting the relative fractions and fitting the data to a single-exponential equation (2.5) yielded a pseudo first-order rate constant of 1.8 $\pm$ 0.15 s^{-1} for conversion of pyruvate to S-acetyl coenzyme A by PDHc. Fitting the initial time points to a linear plot yielded an initial velocity of 1219 $\pm$ 66 μM/s acetyl coenzyme A produced for the reaction conditions (10 μM E1p active-centers in reaction loop). Assuming full saturation of all components this initial velocity corresponds to a k_{cat} of 122 $\pm$ 6.6 s^{-1} per E1p active-centers.

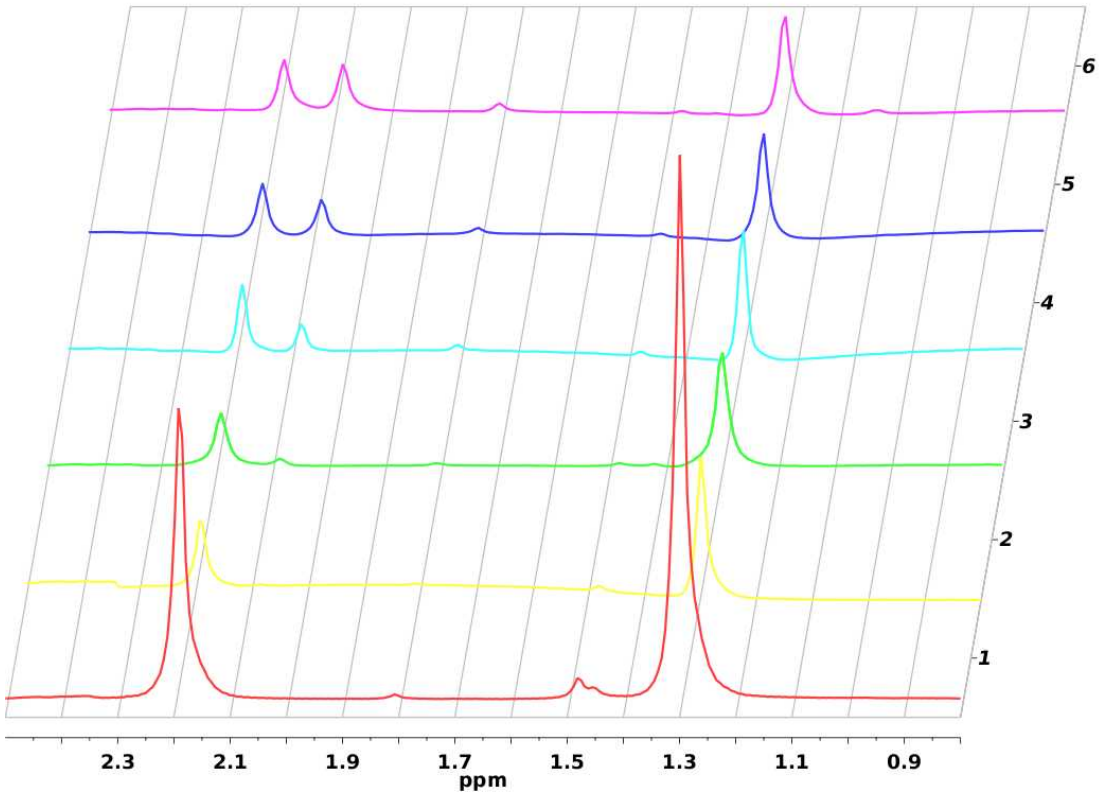

Figure 2.17 Formation of [C2 – ^{13}C] S-acetyl coenzyme A during the overall reaction of PDHc

C3-H acetyl group fingerprint region (0.8 – 2.5 ppm) in 1D ^{1}H-^{13}C HSQC NMR spectra. Reaction of PDHc with [C3 - ^{13}C] pyruvate was quenched in acid at various time points to obtain supernatant containing substrate and products. (1) Control sample: [^{13}C – C3] pyruvate (2) 0.05 s (3) 0.2 s (4) 0.5 s (5) 1.0 s (6) 10 s. pyruvate (C3-H): δ 1.30, 2.19 ppm (keto and hydrate forms); S-acetylcoenzyme A (C2-H): δ 2.08 ppm; acetate (C2-H): δ 1.81 ppm. The peak at 1.48 ppm is of unknown origin.

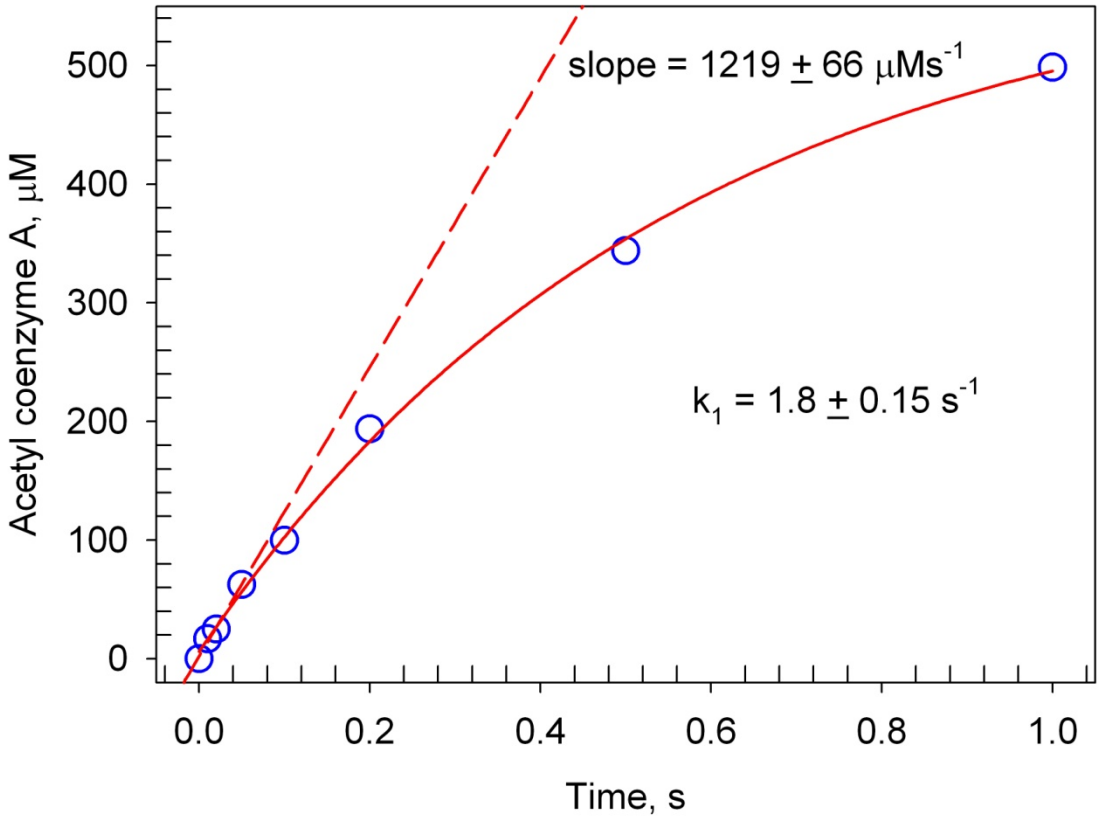

Figure 2.18 Progress curve for S-acetyl coenzyme A production during the overall reaction of PDHc

[C2 - ^{13}C] S-acetylcoenzyme A (blue circles) calculated using ratio of C2-H signal of S-acetyl group to total acetyl groups including pyruvate and acetate determined at various time points during the overall reaction at various time points (0, 0.01, 0.02, 0.05, 0.1, 0.2, 0.5, 1.0 s). Red trace is regression fit to single exponential and red dashed line represents linear fit to initial rate conditions.

2.3.11 Flavin intermediates in PDHc catalysis

The FAD tightly bound to lipoamide dehydrogenase (E3p) component active site which also contains redox active cysteine residues (Cys44 and Cys49) allows direct observation of flavin intermediates during PDHc catalysis (*115, 116*). While the *E. coli* E3p component reaction is known to be very fast and is subject to product inhibition (NADH) leading to complicated kinetics, the peaks with absorbance maxima at 458 nm and 530 nm have been previously assigned, the absorbance at 458 nm to the oxidized form of FAD and the absorbance at 530 nm to a charge transfer band pertaining to the two electron reduced (EH_2) form of the enzyme. Since the rate limiting steps precede the E3p reactions, E3p catalysis in PDHc can be monitored under pre-steady state time scales. Under these conditions, the observed rates for catalytic events in E3p active-sites could provide a lower limit for the turnover number for steps through E1p and E2p, similar to coupled reactions system used for assays.

Firstly, in experiments with PDHc when ThDP or pyruvate or coenzyme A, the essential components for E1p or E2p, were left out, no time-dependent changes could be observed in the E3p active-sites (Figure 2.20 C).

Next, in two experiments with either NAD^+ (substrate for E3p) present or absent, time-dependent changes could be observed in the E3p active-sites (Figure 2.20 A, B). In both cases, decay in the oxidized form of FAD bound to the E3p and a transient build-up and decay in the two-electron reduced form of the enzyme (EH_2) was observed (Figure 2.20 A, B). The decay in oxidized form of FAD corresponds to an accumulation of the $FADH_2$-NAD^+ intermediate. The apparent rate observed was 32 s^{-1} in presence of NAD^+ (Figure

2.20 B) while it was 14.4 s^{-1} in the absence of NAD^+ in presumably a single turnover process as the FAD cannot be regenerated in the absence of NAD^+ (Figure 2.20 A). Comparing the fate of the EH_2 species, generated as an intermediate during reaction of the redox active cysteine residues with the reduced form of the lipoyl moiety, in absence and presence of NAD^+ provides interesting insights.

In the absence of NAD^+, this intermediate forms rapidly at a rate of 50 s^{-1} and then decays in a first-order process with an apparent rate of 4.85 s^{-1} due to the reduction of FAD by this intermediate (Figure 2.20 A). The initial rate of formation of this intermediate could possibly correspond to a lower limit for the PDHc catalysis through E1p and E2p since the reduced lipoyl moiety is produced only after acetyl transfer to coenzyme A in the E2p active site.

In the presence of NAD^+, again this intermediate accumulates rapidly at the rate of 26 s^{-1} but decays slowly in a linear fashion reminiscent of enzyme bound steady-state intermediates (Figure 2.20 B). In pre-steady state experiment to monitor the accumulation of NADH at 360 nm (Figure 2.20 C), a pre-steady state lag phase is observed for approximately 0.08 s correlating to the accumulation of intermediates such as EH_2. Data fit to equation 2.8 yielded a rate of 46.5 s^{-1} during this phase and the amplitude of the phase was 0.1132 absorbance units. Using an extinction coefficient of 4140 M^{-1} cm^{-1} for NADH at 360 nm, this corresponds to 27.4 μM NADH in reaction mixture compared to 20 μM for E3p active sites concentration.

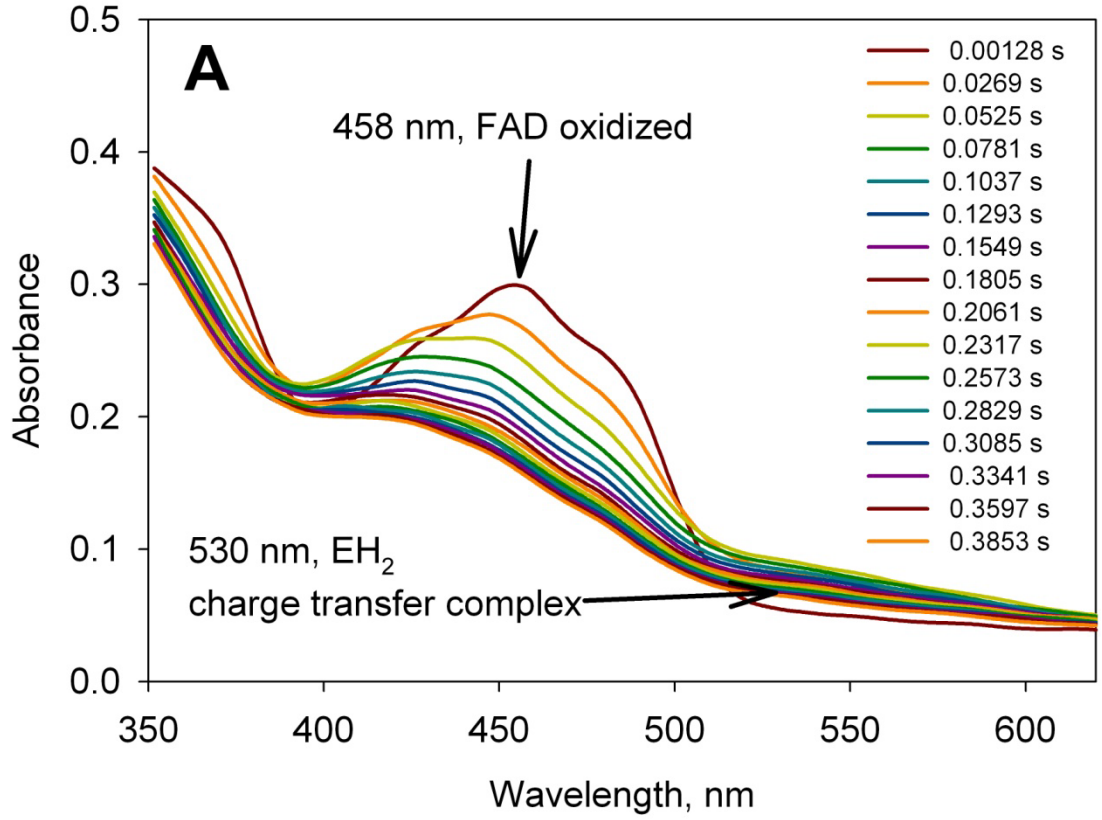
A
458 nm, FAD oxidized
530 nm, EH2
charge transfer complex
0.00128 s
0.0269 s
0.0525 s
0.0781 s
0.1037 s
0.1293 s
0.1549 s
0.1805 s
0.2061 s
0.2317 s
0.2573 s
0.2829 s
0.3085 s
0.3341 s
0.3597 s
0.3853 s
Absorbance
Wavelength, nm
0.0
0.1
0.2
0.3
0.4
0.5
350
400
450
500
550
600

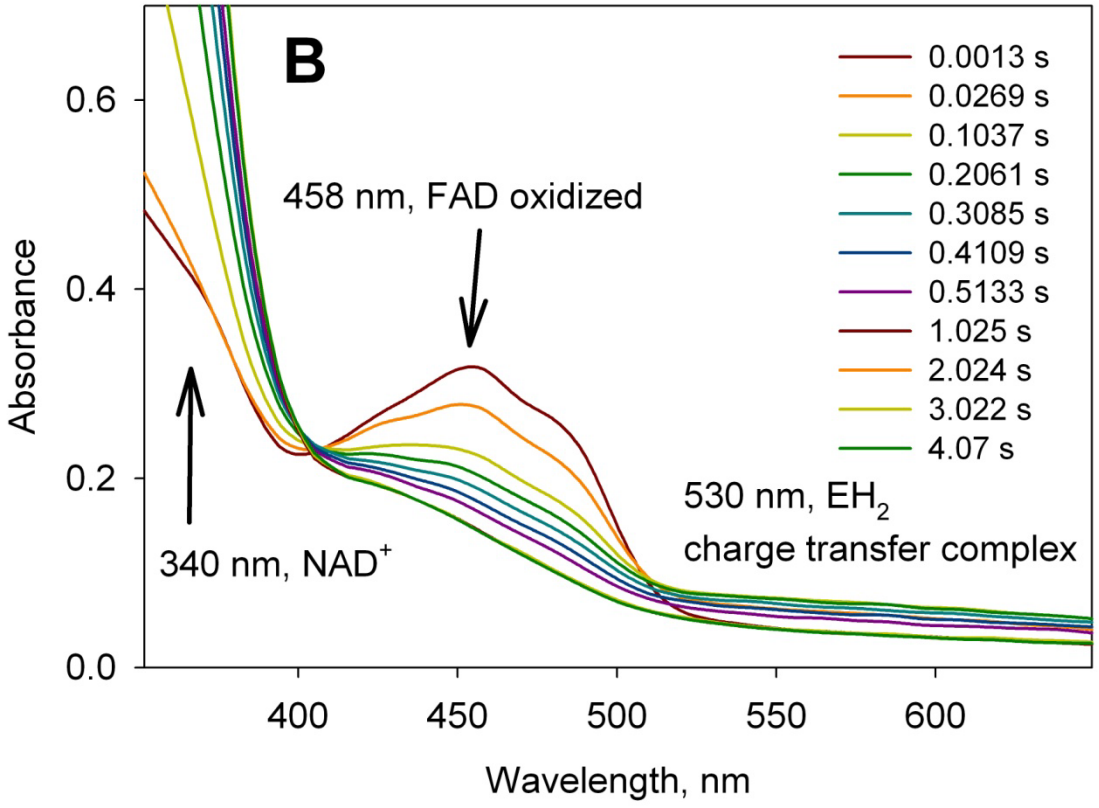
B
458 nm, FAD oxidized
340 nm, NAD+
530 nm, EH2
charge transfer complex
0.0013 s
0.0269 s
0.1037 s
0.2061 s
0.3085 s
0.4109 s
0.5133 s
1.025 s
2.024 s
3.022 s
4.07 s
Absorbance
Wavelength, nm
0.0
0.2
0.4
0.6
400
450
500
550
600

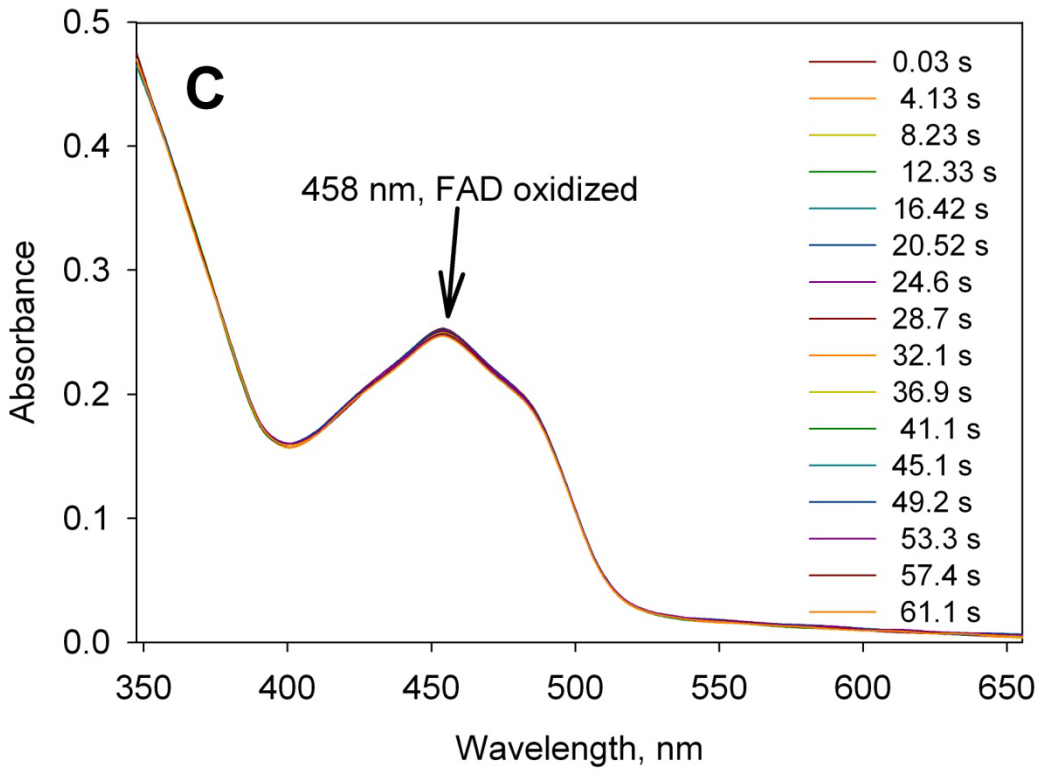

Figure 2.19 Stopped-flow absorbance traces during the reaction of PDHc showing changes in the FAD bound E3p active-sites

(A) Spectra obtained after mixing contents of syringe A, 20 μM PDHc in PDHc reaction medium containing 2 mM ThDP, 2.5 mM Mg^{2+}, and 2 mM coenzyme A and 20 mM KH_2PO_4 buffer pH 7.0, (NAD^+ left out) with syringe B (20 mM pyruvate) and collecting traces at time points noted. (B) Reaction medium including 5 mM NAD^+. (C) Reaction medium does not include coenzyme A. Similar spectra were obtained upon omitting either ThDP or pyruvate from the reaction medium.

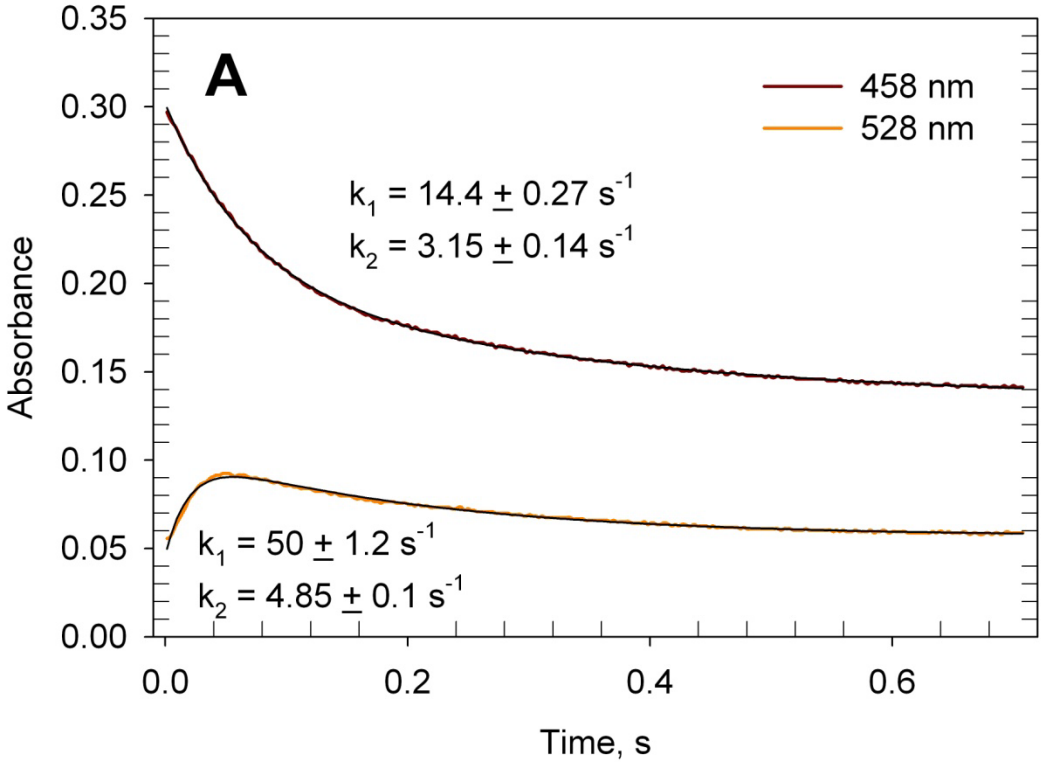
A
458 nm
528 nm
k_1 = 14.4 ± 0.27 s^{-1}
k_2 = 3.15 ± 0.14 s^{-1}
k_1 = 50 ± 1.2 s^{-1}
k_2 = 4.85 ± 0.1 s^{-1}
Absorbance
Time, s
0.00
0.05
0.10
0.15
0.20
0.25
0.30
0.35
0.0
0.2
0.4
0.6

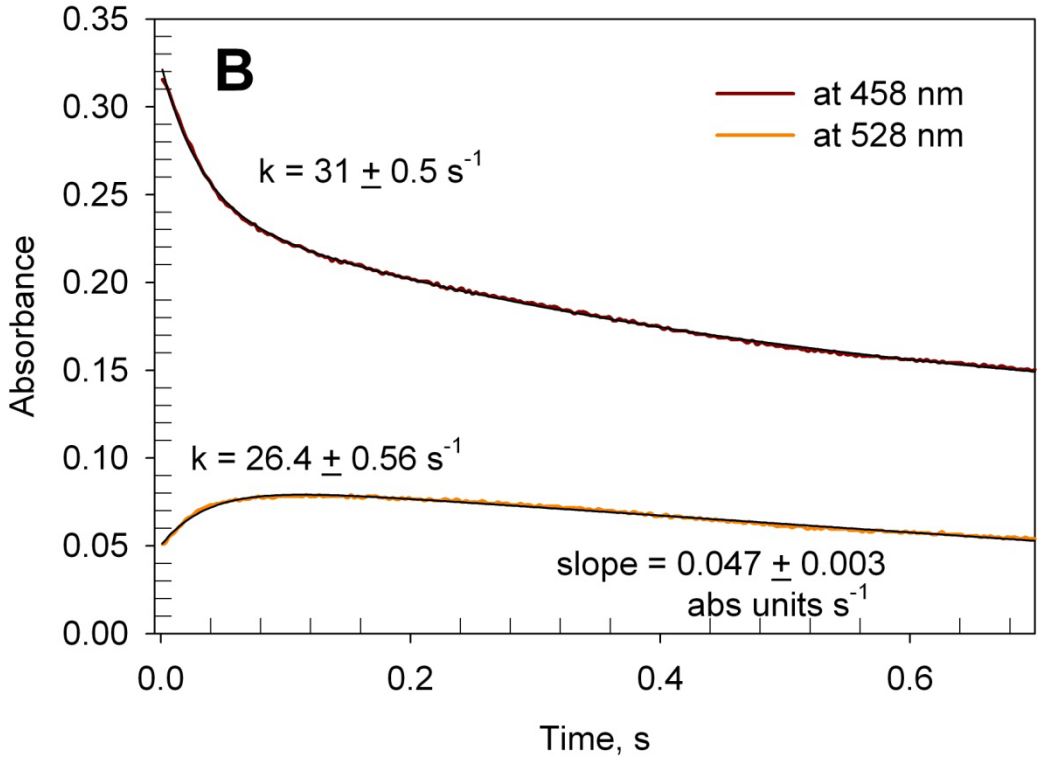
B
at 458 nm
at 528 nm
k = 31 ± 0.5 s^{-1}
k = 26.4 ± 0.56 s^{-1}
slope = 0.047 ± 0.003
abs units s^{-1}
Absorbance
Time, s
0.00
0.05
0.10
0.15
0.20
0.25
0.30
0.35
0.0
0.2
0.4
0.6

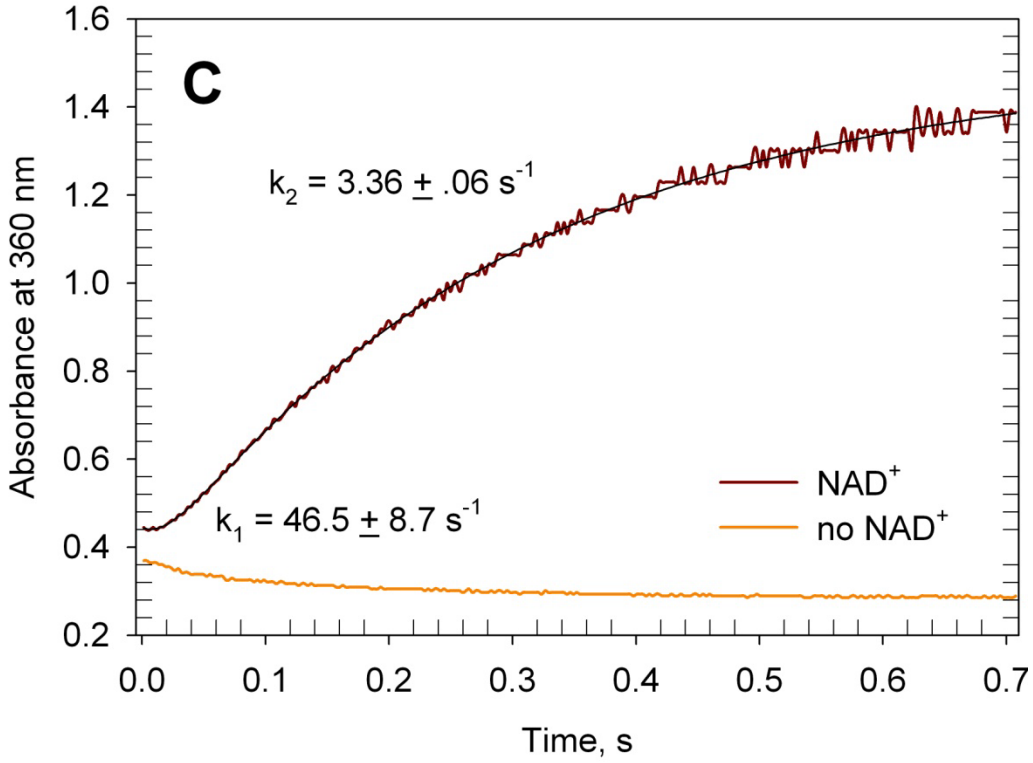

Figure 2.20 Transient state kinetics of flavin intermediates during PDHc catalysis

Kinetic profile of FAD intermediates in the overall reaction of PDHc. The absorbance at 458 nm pertains to the oxidized form of FAD bound to E3p, and the absorbance at 528 nm pertains to a charge transfer complex between the oxidized form of FAD and a two-electron reduced form of the enzyme. **(A)** PDHc in absence of NAD^+ **(B)** PDHc in presence of NAD^+ **(C)** Changes in absorbance at 360 nm pertaining to NADH production. The black traces overlaid on the spectra are the regression fit lines.

2. 4 CONCLUSIONS

This study provides the first observation by NMR of the fate of covalent ThDP intermediates during pyruvate dehydrogenase multienzyme complex catalysis. The decarboxylation of C2-α-lactylThDP, the first covalent intermediate, was a fast step under the various conditions tested. In model studies with this intermediate, Zhang et al. showed the rate of decarboxylation increased with decreasing solvent polarity from water to THF, and in THF, the first order rate constant exceeds 50 s^{-1} (*12*). Presumably, the E1p active site provides such a hydrophobic environment. This environment also stabilizes the enamine by 10 kcal/mole (*110*) and thus channels this electron rich intermediate toward oxidation by the lipoyl moiety on E2p. The net rate constants for oxidation of the enzyme bound enamine indicate interesting biological consequences for the functioning of the PDH multienzyme complex in aerobic oxygen rich environments. The net rate constants for reductive acetylation from this study provide a lower limit for the physiological reaction, since the attachment of the lipoyl domain by the flexible linker could provide added rate enhancement by providing stringent diffusion limitations (*117*).

While reductive acetylation was proposed to be the rate-limiting step in PDHc catalysis based on experiments monitoring [C2 -^{14}C]acetyl group incorporation into PDHc (*118*), the current study provides similar net rate constants for many steps which are within range of the overall k_{cat} pointing toward the possibility of a equalizing of barriers for the interconversion of these intermediates by evolutionary optimization for substrate channeling (*119*). Evidence for such a phenomenon also comes from the observation of the coupling of the dynamics of two active site loops to catalysis.

While substitutions at these positions were previously shown to affect E1p-E2p interactions and consequently the rate of reductive acetylation (for H407A, the k_{cat} is 0.08 s^{-1} while k_{HEThDP} is 1.16 s^{-1}, Table 2.3), they also dramatically impact the first C-C bond formation step in the catalysis, with the most disruptive substitutions producing up to a 1000 fold rate reduction. The E1p active centers are partially rescued in these cases upon assembly to complex formation evidenced by a rate enhancement for C-C bond formation in reconstituted complexes of the most disrupted E1p variants whereas the parental enzyme shows no such changes upon complex formation. The dynamic active center loops presumably play a prominent role in this regard.

CHAPTER 3 Tautomeric and Ionization States of ThDP Illuminate Functions of Key Acidic Residues in YPDC Catalysis

3. 1 INTRODUCTION

Yeast pyruvate decarboxylase (YPDC, EC 4.1.1.1), a thiamin diphosphate (ThDP) and Mg^{2+} dependent decarboxylase catalyses the non-oxidative decarboxylation of pyruvate to acetaldehyde. YPDC is an α4 homotetramer of Mr 250,000 and is subject to substrate activation (*120*) and activation by the substrate surrogate pyruvamide (*121*). The cofactor ThDP is bound at the interface created by two monomers that form a tight dimer. This tight dimer known as the 'functional dimer' is the minimal catalytically active unit and (*122-124*). Two of these functional dimers assemble into a loose tetramer in the quaternary structure.

Thiamin diphosphate catalysis

Role of ThDP in YPDC catalysis has been extensively studied over the past five decades. X-ray crystallography studies showed the coenzyme ThDP bound in the "V" conformation in the active-sites of YPDC (*125, 126*). This unusual conformation of the ThDP brings the C2 and N4' atoms within close contact to each other (3.4 – 3.5 Å) (65). Chemical steps in the ThDP catalysed decarboxylation of pyruvate in YPDC active-site are shown in Scheme 3.1. The role of the 4'-aminopyrimidine ring in acid-base catalysis and activation of the thiazolium C2-H bond has been elucidated (5) and recent advances in application of

circular dichroism (CD) spectroscopy to study enzyme bound chiral intermediates has provided evidence for the presence of the 1',4'-iminopyrimidine tautomeric form in YPDC catalysis, leading to the understanding that C2-α tetrahederal intermediates exist in the 1',4'-iminopyrimidine tautomeric form (16-20, 24). A method which uses rapid chemical quench of reaction mixtures and ^{1}H NMR for detection of covalent ThDP intermediates based on the C6'-H ^{1}H chemical shifts developed at Halle has been useful in studying the catalytic cycle by monitoring the relative amounts of covalent C2-α intermediates directly (4). Both methods have their limitations, for instance - CD methods are limited by need of absorption spectroscopic signatures for pyruvate derived ThDP covalent intermediates and chemical quench NMR method does not provide information about the enzyme bound tautomeric form of the 4'-aminopyrimidine ring and cannot differentiate between the enamine and C2-α-hydroxyethylThDP intermediate. However, the two methods are complementary, the CD methods provide information about the 4'-aminopyrimidine ring and the NMR methods provide information about the covalent adducts to the thiazolium ring. Steady state and pre-steady state experiments which combine these two methods could provide an inclusive representation of ThDP covalent intermediates encapsulated by the current view (represented in Scheme 3.1) that both 4'-aminopyrimidine and thiazolium rings are necessary for ThDP catalysis in enzymes.

Role of enzyme active-site residues

The pH range for YPDC activity is between 5 - 7 units with optimal activity at pH 6.0. YPDC active-site contains residues Asp28, Glu51, His114, His115 and Glu477 with

potential acid-base properties in this range (*127, 128*) and these residues are within close distance of the ThDP cofactor as shown in Figure 3.1. Site-specific substitutions produced variants with very low activity (as determined by steady-state kinetic assays) compared to YPDC. These results point toward the important catalytic acid-base role of these enzyme residues, in particular, the glutamate and aspartate residues are proposed to be involved in essential proton transfer steps. Glu51 a residue within hydrogen bonding distance to the N1' of the 4'-aminopyrimidine ring is a conserved residue among the ThDP superfamily of enzymes and is crucial in the protonation/deprotonation of the N1' atom of the 4'-aminopyrimidine moiety (*86*). The mechanism as shown in Scheme 3.1 also calls for an obligatory general acid for protonation of the central reactive enamine intermediate. Carboligase side reactions ensue when the enamine is trapped by other electrophiles such as pyruvate or acetaldehyde (*129*). Site-specific substitution of Asp28 and Glu477 produced variants with 500-1000 fold reduced activity and showed higher catalytic fidelity toward carboligase reactions compared to YPDC (*122, 130*). These observations point toward the role of these residues in the protonation of the enamine.

Scheme 3.1 Mechanism of YPDC.

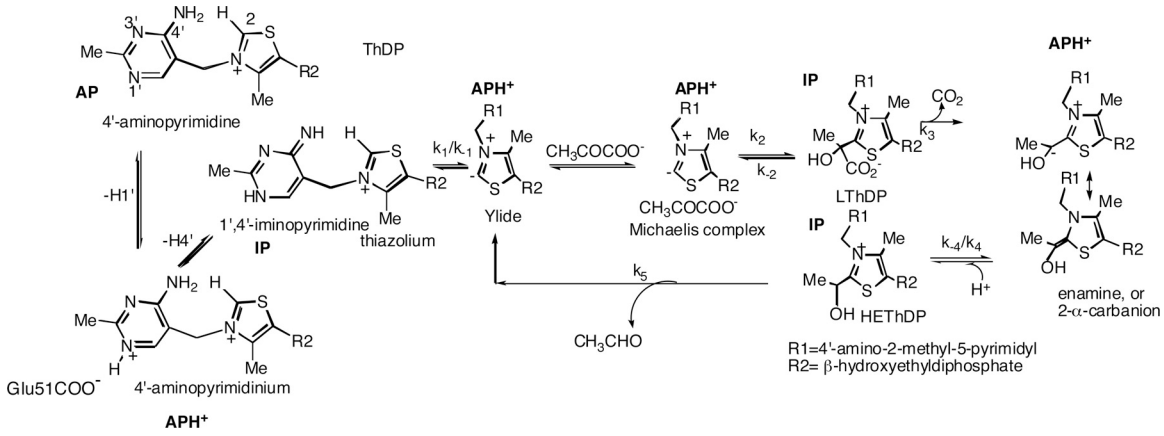

The proposed ionization/tautomeric states of the 4'-aminopyrimidine ring are indicated in bold typeface.

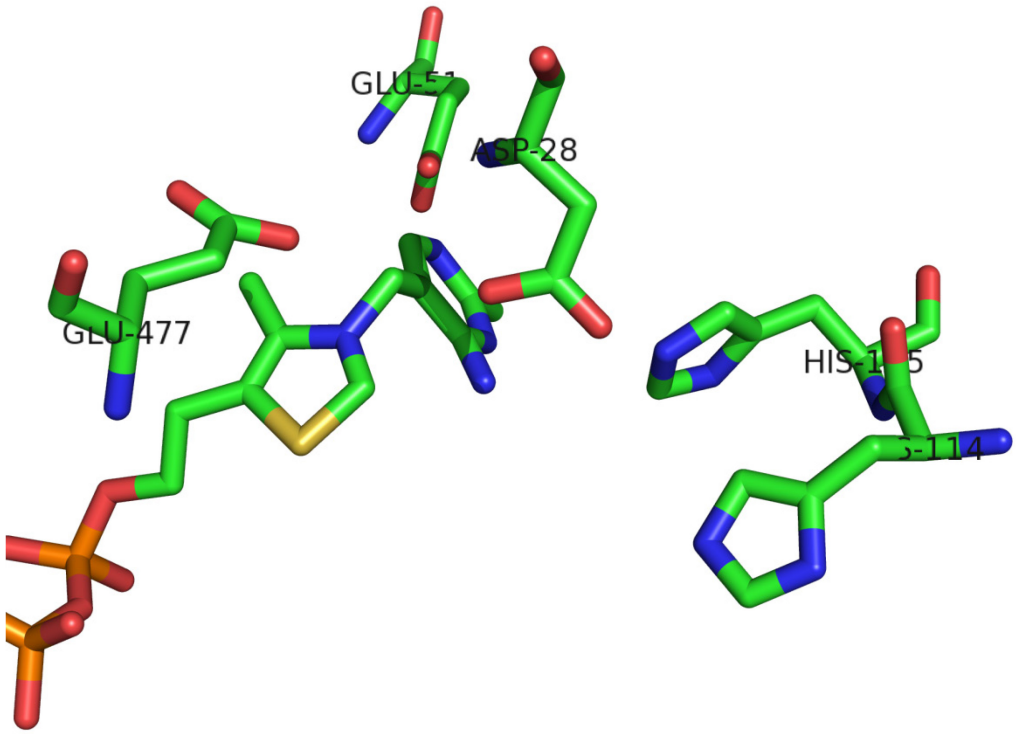

Figure 3.1 Active site acid-base residues near ThDP in YPDC

Role of Cys221 and Glu91

The residue Cys221 at the regulatory site was shown to be the locus of substrate activation by hemithioketal formation with pyruvate. Chemical modification targeted at the reactive Cys221 and site-specific mutagenesis at Cys221 produced variants of YPDC where the allosteric substrate activation was abolished whilst the activity was reduced only 2-5 fold (*75, 76*). Recent X-ray structures with the D28A-YPDC variant and pyruvate and *Kl*PDC with methyl acetylphosphonate provide physical evidence for such an adduct formation (*26, 131*). The structures also reveal large scale reorganization of loops 104-113 and 290-304, which were missing in the unactivated YPDC crystal structure, thus leading to formation of a compact tetramer and a sequestered active-site in the activated state. Alongside this mechanism of activation, site-directed mutagenesis and steady-state kinetic studies point to the other pathways which connect the Cys221 residue to the ThDP binding loop 410-415 residues (*74, 132-134*). The loop residues Gly413, Ile415 make H-bond contacts with N4' and N3' atoms of the 4'-aminopyrimidine ring in addition to contact with His115 residue in the active-site. Ile415 also sustains ThDP in its catalytically active "V" conformation (Figure 3.2). Glu91 present at the interface of the three domains plays a central role in this setup by connecting His92 in the α domain in the vicinity of Cys221with the ThDP binding loop. Substitution at this position produced variants exhibiting slightly lower substrate activation and weakened binding of ThDP compared to YPDC (*61, 133*).

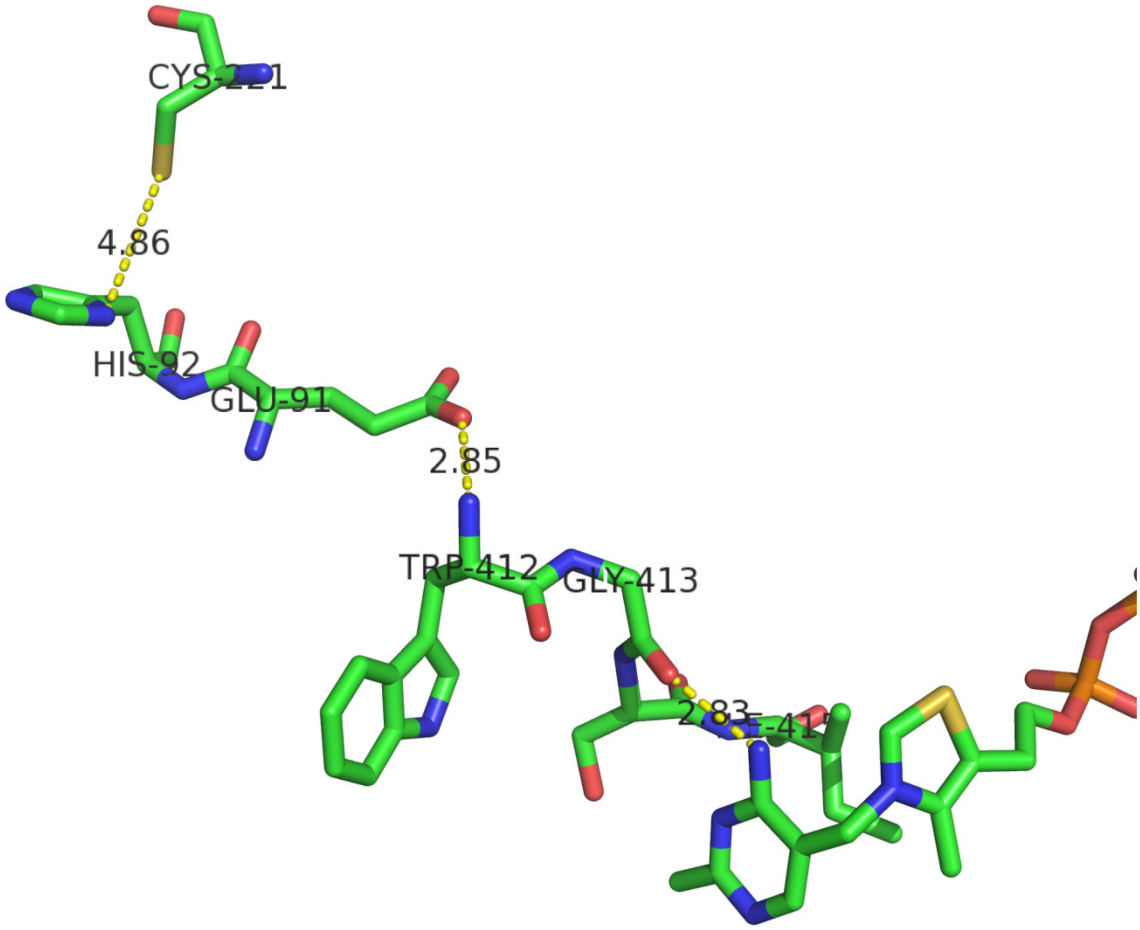

Figure 3.2 Connectivity between the regulatory site and ThDP binding loop (410 – 415)

Residues in the pathway include Cys221, His92, Glu91, Trp412, Gly413, Ser414, and Ile415

To date, most of the information gathered on the YPDC variants discussed above has been derived from steady-state Michaelis-Menten kinetics and chemical quench NMR studies. Recently, phosphinate analogs of pyruvate have been shown to be better steric mimics of pyruvate and most potent inhibitors of the pyruvate dependent E1p component of pyruvate dehydrogenase complexes (*80*). In conjunction with CD spectroscopy experiments, detailed insights into the tautomeric states of intermediate analogs bound to YPDC under steady-state conditions and the rates of formation of such intermediates under pre-steady state conditions were obtained (*16, 55, 105*). The current study aims to apply these steady-state and pre-steady state CD spectroscopy methods to elucidate the tautomeric and ionization states of enzyme-bound ThDP intermediates on these YPDC variants (Scheme 3.2). Since the current methods allow us to study the events in the active-sites containing ThDP, effect of these substitutions on individual catalytic steps can be determined, and the role of these residues in YPDC catalysis can be assigned.

Scheme 3.2 Formation of the 1',4'-iminopyrimidine form of ThDP in tetrahederal intermediates

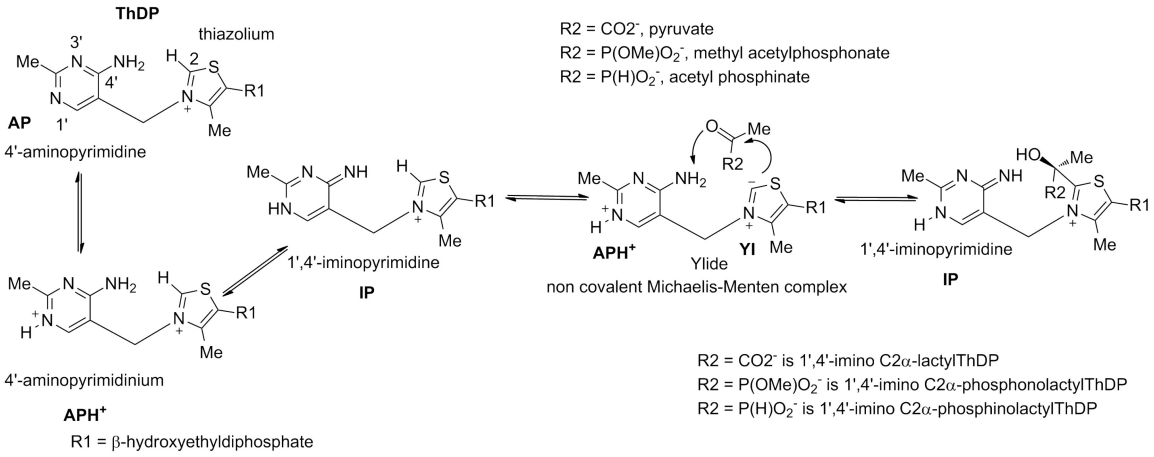

3. 2 MATERIALS AND METHODS

3.2.1 Materials

Triethyl orthopropionate and hypophosphorous acid were purchased from Aldrich and used without further purification. Anhydrous acetone was purchased from Acros Organics. NaI was dried at 70 ^{o}C under 0.1 mm/Hg overnight. Small quantities of anhydrous NaI could be prepared with anhydrous acetone according to the literature procedure (*135*). All NMR spectra were recorded on a 500 MHz Varian INOVA spectrometer.

Thiamin diphosphate ThDP, NAD^{+}, coenzyme A, dithiothreitol (DTT) and isopropyl β-D-1-thiogalactopyranoside (IPTG) were from USB (Cleveland, OH); dichlorophenol-indophenol (DCPIP) from Sigma (St.Louis, MO). Wizard® *Plus* Miniprep DNA Purification System was from Promega (Madison, WI).

3.2.2 Synthesis of Sodium propionyl phosphinate (PP)

Sodium propionyl phosphinate was synthesized using modifications to the procedure for synthesis of Sodium acetylphosphinate described earlier by Baillie et al. (*136*).

Synthesis of sodium (1,1-diethoxypropyl)phosphinate

Hypophosphorous acid (50% w/v in H_2O) (6.6 mL, 0.05 mol) was evaporated at 0.01 mm Hg to remove water using a 50 mL Schlenk flask kept in an ice bath connected to a trap kept at – 70 ^{o}C. Triethyl orthopropionate (20.5 g, 0.12 mol) was added in a drop-wise

manner to the anhydrous acid under N_2 kept on ice bath. Under vigorous stirring dry HCl was passed through until the solution became cloudy. The resulting mixture was allowed to warm to room temperature and stirred overnight under N_2. To remove the volatiles the reaction mixture was evaporated under reduced pressure. After complete removal of all the volatile material a solution of NaOH (3 g, 0.15 mol) in 30 mL degassed water was added in a drop-wise manner to the reaction mixture kept on ice bath. The reaction mixture was then refluxed under N_2 for 2 h. Then the reaction mixture was allowed to cool down and the solution was adjusted to pH 8.0 with conc. HCl on ice bath. The solution was evaporated to dryness and the residue was triturated with 60 mL of boiling absolute ethanol. After filtration, ethanol was evaporated and the residue was recrystallized in absolute ethanol. Yield (1.35 g, 14.1 %). ^{1}H NMR (500 MHz, D_2O-DSS): δ 6.934 (d, J = 515.5 Hz, 1 H), 3.689 (q, J = 6.5 Hz, 4 H), 1.831 (q, J = 6.5 Hz, 2H), 1.173 (t, J = 7 Hz, 6 H), 0.957 (t, J = 7 Hz, 3 H).

Synthesis of Sodium propionyl phosphinate (PP)

Sodium (1,1-diethoxyethyl)phosphinate (1.0 g, 5.2 mmol) was dissolved in a mixture of 9.5 mL of glacial acetic acid and 0.5 mL of water. The solution was stirred at room temperature for 24 h. After removing the solvent in vacuo the residue was triturated with acetone and the resulting white solid was recrystallized from methanol/acetone. Yield (245 mg, 36.2 %). ^{1}H NMR (500 MHz, D_2O-DSS): δ 6.789 (d, J = 544 Hz, 1 H), 2.809 (m, J = 6 Hz, 3 Hz, 2 H), 1.035 (t, J = 7 Hz, 3 H).

3.2.3 Bacteria and Plasmids

BL21(DE3) cells transformed with plasmid encoding for YPDC or the variants E91D YPDC, E51D YPDC and E477Q YPDC with a His6 tag attached to C-terminus (*86, 127, 137*) were used for overexpression. The BL21 (DE3) cells with plasmid encoding for the D28A and D28N variants of YPDC (*127*) were used for overexpression of these variants.

3.2.4 Protein Overexpression

The BL21 (DE3) cells were grown overnight in LB agar plates (Bactotryptone 10 g/L, yeast extract 10 g/L, sodium chloride 10 g/L, agar 15 g/L) in the presence of ampicillin (50 mg/L) at 37 °C. The best looking single colonies were transferred to 15 mL LB medium (Bactotryptone 10 g/L, yeast extract 10 g/L, NaCl 10 g/L, ampicillin 50 mg/L) and grown overnight at 37 °C with shaking at 240 rpm. The cells were then transferred to 700 mL LB medium and grown at 37 °C to an A_{600} of 0.7. Over-expression of the YPDC was induced with 0.5 mM IPTG, 0.5 mM thiamin chloride hydrochloride and 1 mM $MgCl_2$. The cells were further grown at 37°C for an additional 6 h with constant shaking at 240 rpm. The cells were harvested at 6000 rpm for 10 min. at 4 °C and washed with Buffer WB (20 mM NaH_2PO_4, 0.5 mM EDTA-2Na, pH 6.8). The cells were stored frozen at -80 °C.

3.2.5 Protein Purification – YPDC, E51D, E477Q, and E91D YPDC variants

The frozen cells were thawed and the cell pellet was resuspended in (40 mL/L of cell culture) sonication buffer (50 mM NaH_2PO_4, 100 mM NaCl, 2 mM $MgCl_2$ and 1 mM

ThDP, pH 7.5). The cells were disrupted at 20 kHz at 4 °C for 4 min (10 s on, 10 s off) on a Model 500 Sonic Dismembrator (Fisher Scientific). The yellowish suspension was centrifuged at 17,000 rpm at 4 °C for 30 min. The clear yellow supernatant was applied to 5 mL Ni Sepharose 6 Fast Flow (GE Healthcare, NJ) column in gravity flow mode equilibrated with sonication buffer. The protein bound to the column was washed with 50 mL sonication buffer and 50 mL binding buffer (50 mM MES, 100 mM NaCl, 2 mM $MgCl_2$, 1 mM ThDP, 5 mM imidazole, pH 6.0) consecutively. YPDC was eluted using 100 mL of elution buffer (200 mM imidazole, 50 mM NaH_2PO_4, 2 mM $MgCl_2$, 1 mM ThDP, pH 7.5). 0.5 mL fractions were collected and checked for protein content using the Bradford reagent (Bradford et al., 1976). The purity of the fractions was checked by SDS-PAGE. Fractions containing considerable amount of YPDC were combined and dialyzed against dialysis buffer (20 mM MES, 20 mM NaH_2PO_4, 5 mM $MgCl_2$, 1 mM ThDP, 0.1 mM EDTA, pH 6.0) at 4 °C overnight. After dialysis the protein was concentrated to less than 1 mL using an Amicon Centriprep-30 device. Glycerol was added to a final concentration of 30-50% for long-term storage at -20 °C.

3.2.6 Protein Purification – YPDC variants expressed without $(His)_6$ -tag

The frozen cells were thawed and the cell pellet was resuspended in (40 mL/L of cell culture) sonication buffer (50 mM NaH_2PO_4, 100 mM NaCl, 2 mM $MgCl_2$ and 1 mM ThDP, pH 7.5). The cells were disrupted at 20 kHz at 4 °C for 4 min (10 s on, 10 s off) on a Model 500 Sonic Dismembrator (Fisher Scientific). The yellowish suspension was centrifuged at 17,000 rpm at 4 °C for 30 min. The clear yellow supernatant was collected

and ammonium sulfate was added to a final concentration of 1.5 M and the mixture was allowed to stand in ice bath for 15 min. The resulting suspension was centrifuged at 17000 rpm at 4 °C for 15 min. The supernatant was collected and ammonium sulfate was added to a final concentration of 2.8 M. The suspension was allowed to stand for 15 min at ice bath temperature and was centrifuged at 17,000 rpm for 15 min. The pellet containing the crude protein was dissolved in 10 mL of dialysis buffer (20 mM Bis-Tris, 0.5 M EDTA, 2 mM $MgCl_2$, 1 mM ThDP, 0.5 mM PMSF pH 6.8) and dialyzed against the same buffer at 4 °C overnight. The desalted protein was applied to a Pharmacia Hiload Q Sep (HP) column equilibrated with 20 mM Bis-Tris, 0.5 M EDTA, 2 mM $MgCl_2$, pH 6.8 and the protein was eluted by a linear gradient with 2 M NaCl in the same buffer at a flow rate of 5.0 mL/min. 4 mL fractions were collected and the purity of the fractions was checked by SDS-PAGE. The fractions containing considerable amount of YPDC were combined and dialyzed against dialysis buffer (20 mM MES, 20 mM NaH_2PO_4, 5 mM $MgCl_2$, 1 mM ThDP, 0.1 mM EDTA, pH 6.0.) at 4 °C overnight. After dialysis the protein was concentrated to less than 1 mL using an Amicon Centriprep-30 device. Glycerol was added to a final concentration of 30-50% for long-term storage at - 20 °C.

3.2.7 Estimation of protein content

Protein concentrations were determined by the method described by Bradford et al. (*62*). Dilutions of proteins were added to 1X Bradford reagent (BioRad, CA) and the absorbance at 595 nm was used to estimate the concentration from a standard curve prepared with BSA.

3.2.8 Enzyme activity measurements

The enzyme activity was determined using NADH/ADH coupled assay (*63*). Conversion of acetaldehyde to ethanol by yeast alcohol dehydrogenase in the presence of NADH was coupled to YPDC catalyzed production of acetaldehyde from sodium pyruvate. The disappearance of NADH is monitored at 340 nm using a Varian DMS 300 spectrophotometer. The activity was measured in the presence of 20 mM pyruvate in standard assay buffer (50 mM MES, 1 mM ThDP, 2 mM $MgCl_2$, 0.2 mg/mL NADH, 0.08 mg/mL ADH, pH 6.0) at 30°C. The reaction was started with addition of 3 μg/mL YPDC. For the variants higher concentration of enzyme was used.

3.2.9 Circular Dichroism spectroscopy (CD) titration experiments

All CD spectra were recorded on a Chirascan CD Spectrometer from Applied Photophysics (U.K.) in a 1 cm path length cell in the near–UV (280-400) wavelength region.

Titration experiments with propionyl phosphinate (PP)

To 2.4 mL of YPDC or its variants in 20 mM MES buffer (pH 6.0) containing 0.5 mM ThDP and 2.5 mM $MgCl_2$, an aliquot of PP from a 1M stock solution was added to achieve the desired concentration. The mixture was allowed to equilibrate for 1 min and the CD spectrum was recorded at 25 °C. The titration was performed over a range of (0.5 - 40 mM) PP concentration. For quantitative analysis, the CD signal intensity of the IP and Michaelis complex bands corrected for dilution was plotted against PP concentration. Apparent

dissociation constants (K_D^{app}) were calculated by fitting the data to a Hill function described in equation (3.1) using Sigmaplot v.7.0.

$$CD_{297} = CD_0 + \frac{CD_{297}^{max} \bullet [PP]^{n_H}}{(K_D^{app})^{n_H} + [PP]^{n_H}} \quad (3.1)$$

In this expression CD_{297} is the observed CD signal at the given wavelength, CD_0 the CD signal of the protein at this wavelength in the absence of PP, CD_{297}^{max} the maximum CD signal at saturation with PP, [PP] the concentration of substrate analog, and n_H the Hill coefficient.

Titration experiments with pyruvate

Experiments were performed with low activity variants and at 5 °C to slow down side reactions leading to carboligase products. To 2.4 mL of YPDC variants (2.75 mg/mL) at 5 °C in 20 mM MES buffer (pH 6.0) containing 0.5 mM ThDP and 2.5 mM $MgCl_2$, an aliquot of pyruvate from a 1M stock solution was added to achieve the desired concentration. The mixture was stirred for 30 s and the CD spectrum was recorded at 5 °C. Additional aliquots of pyruvate were added until no further changes in CD spectra were observed.

3.2.10 Stopped-flow Circular Dichroism spectroscopy

Kinetic traces were recorded on a Pi*-180 stopped-flow CD spectrometer from Applied Photophysics (U.K.) using 10 mm path length at the specified wavelengths. Data were recorded at 302 nm for the PP experiments and at 313 nm for the pyruvate experiment. Temperature was maintained at 10 °C for YPDC with pyruvate experiment and at 30 °C for YPDC variants with pyruvate experiments.

Pre-steady state kinetics of formation of 1',4'-iminophosphinolactylThDP

A solution of YPDC (8 mg/mL) in 20 mM MES buffer (pH 6.0) containing 0.5 mM ThDP and 2.5 mM $MgCl_2$ in one syringe was mixed rapidly with an equal volume of PP (40 mM) in the same buffer placed in another syringe. 20,000 data points were recorded over a period of 90 s. Data from six shots were averaged and the raw data were smoothed using Savitsky-Golay function provided by the accompanying software and fit to a single-exponential model as in equation (3.2 using Sigmaplot v.7.0.

$$\mathrm{CD}_{302}(t) = CD_1 \bullet e^{-k_1 t} + c \qquad (3.2)$$

Pre-steady state kinetics of formation of 1'4'-iminoC2-α-lactylThDP and 1'4'-iminoC2-α-hydroxyethylThDP

A solution of YPDC (8 mg/mL) or variants in 20 mM MES buffer (pH 6.0) containing 0.5 mM ThDP and 2.5 mM $MgCl_2$ in one syringe was mixed rapidly with an equal volume of

pyruvate (40 mM) in the same buffer placed in another syringe. 20,000 data points (2000 for wild-type) were recorded over a period of 0.2, 20 and 50 s for YPDC, E51D and E477Q variants, respectively. Data from ten shots were averaged and fit to a single-exponential model (wild-type) or double-exponential model (variants) as in equation (3.3 using Sigmaplot v.7.0.

$$\mathrm{CD}_{313}(t) = CD_1 \bullet e^{-k_1 t} + CD_2 \bullet e^{-k_2 t} + c \tag{3.3}$$

3.2.11 Distribution of covalent ThDP intermediates

400 µL of YPDC variants (25 mg/mL) in 20 mM MES buffer pH 6.0 containing 1 mM ThDP and 5 mM $MgCl_2$ was mixed with 50 µL of pyruvate (0.1 M). The reaction was incubated at 5 °C for 180 seconds and quenched with 200 µL of 12.5% TCA in 1M DCl/D_2O. The mixture was centrifuged at 14000 rpm for 30 min. and the supernatant was filtered through a Gelman Nylon Acrodisc (0.45 µm). The filtrate was used for ^1H NMR analysis as reported initially by Tittmann et al. (*4*) and on YPDC by Joseph et al. (*138*). ThDP and ThDP covalent intermediates are stable under acid conditions employed in the experiments (pH = 0.75). The C6'-H resonances in ^1H NMR spectra of ThDP covalent intermediates show different chemical shifts and thus in a reaction mixture can be identified unambiguously. Relative integrals of the C6'-H resonances provide a quantitative estimate of the relative abundance of the intermediates. Under steady-state conditions, applying the steady-state assumption, ratio of relative amount of intermediates approximates to the ratio of individual forward rate constants.

3. 3 RESULTS AND DISCUSSION

YPDC is a homotetrameric substrate activated enzyme with 4 active-sites situated at the interface of monomeric chains and 4 regulatory sites. The dimeric form containing two active sites at the interface of the two interacting chains and two regulatory sites has been earlier shown to be the minimal catalytically active form. Hence, the enzyme can be thought of as a symmetric dimer of catalytically active dimers. In a binding equilibrium model for this catalytic dimer, from symmetry considerations, the two regulatory sites can be assumed to have same substrate affinities and the two active-sites to have similar substrate affinities. This simplified model represents a regulatory site and an active-site with different binding affinities toward the substrate as first developed by Schowen and co-workers (*139*) for treatment of steady-state analysis. Attempts at fitting data to an equation describing this model yielded parameters with large standard errors. Hence, data were fit to the simplified Hill equation. While both models fit the data with comparable goodness of fit, presumably the sample size is not large enough to determine accurately the values of parameters as described by the SHS model. (Refer to Figure A4 in Appendix)

3.3.1 Tautomeric state of ThDP in YPDC variants during pre-decarboxylation steps

YPDC

Upon titration with PP, two CD bands developed simultaneously (i) a positive band at 297 nm and (ii) a negative CD band at 330 nm and (Figure 3.3). The experiment was reminiscent of an analogous experiment with acetylphosphinate reported earlier (*16*).

In this experiment, the two observed changes in CD spectra can be assigned to (i) positive CD band at 297 nm to the 1',4'-iminophosphinolactyl ThDP (IP) (ii) and the negative CD band at 330 nm to a Michaelis complex (MC) consisting of enzyme, substrate analog and ThDP (refer to Scheme 3.2 for chemical structures). Simultaneous development of both bands indicates that the active-sites reside in two distinct tautomeric states in the presence of PP i.e., they are asymmetric. The titration data fit to the Hill equation ((3.1) revealed sigmoidal binding characteristics with Hill coefficients of 2.63 for the IP form and 2.13 for the MC (Figure 3.4) indicating that PP also binds at the regulatory site and this binding event is recognized by both of the active sites. The sigmoidal binding characteristics and the n_H value indicate relay of information regarding substrate binding at the regulatory-site to the active-site, i.e., cooperativity. Importantly, this information is relayed to the 4'-aminopyrimidine ring, and consequently can be detected by CD during intermediate formation. Regulation is achieved by controlling intermediate steps involved in substrate processing including formation of the Michaelis complex.

Attempts to address the question of whether asymmetric active-sites add any degree of complexity to binding events, X-ray structures of YPDC show no significant differences between the active-sites. Experimental results here and elsewhere suggest that the asymmetry is induced only in the presence of substrate in the active-sites. Since this asymmetry is a post substrate binding event it can be assumed to have minimal effect on the affinity of either active-site for substrate. The K_d^{app} for MC and IP forms for YPDC are indeed comparable.

E91D YPDC

With the E91D variant, again the two bands developed simultaneously upon titration with PP (Figure 3.5). However, the titration data fit to the Hill equation ((3.1) revealed hyperbolic binding characteristics with a Hill coefficient of 1.08 for IP form (Figure 3.6) and 1.5 for the MC (Figure 3.6). The K_D^{app} values – estimate of affinity of enzyme active-sites for propionyl phosphinate- for this variant and YPDC were similar and indicate that the E91D variant retains its affinity for the molecule at the asymmetric active-sites notwithstanding partly disrupted communication with the regulatory site (Table 3.1). Similar effect on the Hill coefficient was observed in the Michaelis-Menten kinetics for this variant. The residue Glu91 at the interface of three domains is a part of the proposed communication pathway between the cysteine 221 residue at the regulatory site and the ThDP at the active site.

C221E YPDC

In the C221E variant, the substitution to glutamate mimics pyruvate bound to Cys221 and hyperbolic Michaelis-Menten kinetics was observed (*140*). Also, the activity was reduced by only 2 - 5 fold as compared to YPDC during its activated state. In the titration experiments of the regulatory site variant C221E with PP, again both CD bands were observed but with reduced intensities (Figure 3.7). The titration data fit to the Hill equation revealed hyperbolic binding characteristics with a Hill coefficient of 1.0 for the IP form. Clearly since PP cannot bind at the regulatory site of the enzyme allosteric activation is completely abolished.

Taken together, these experiments suggest that (i) substrate analogs such as phosphonate and phosphinate mimics of pyruvate can also bind at the regulatory site and elucidate a response similar to pyruvate. (ii) Substrate regulation, or substrate analog regulation in the present case, can be detected during individual catalytic steps at the active-site. (iii) Overall, the binding of substrate analog i.e., formation of Michaelis complex is subject to allosteric regulation in YPDC. The formation of Michaelis complex with pyruvate could be subject to allosteric regulation in the corresponding reaction of YPDC with pyruvate.

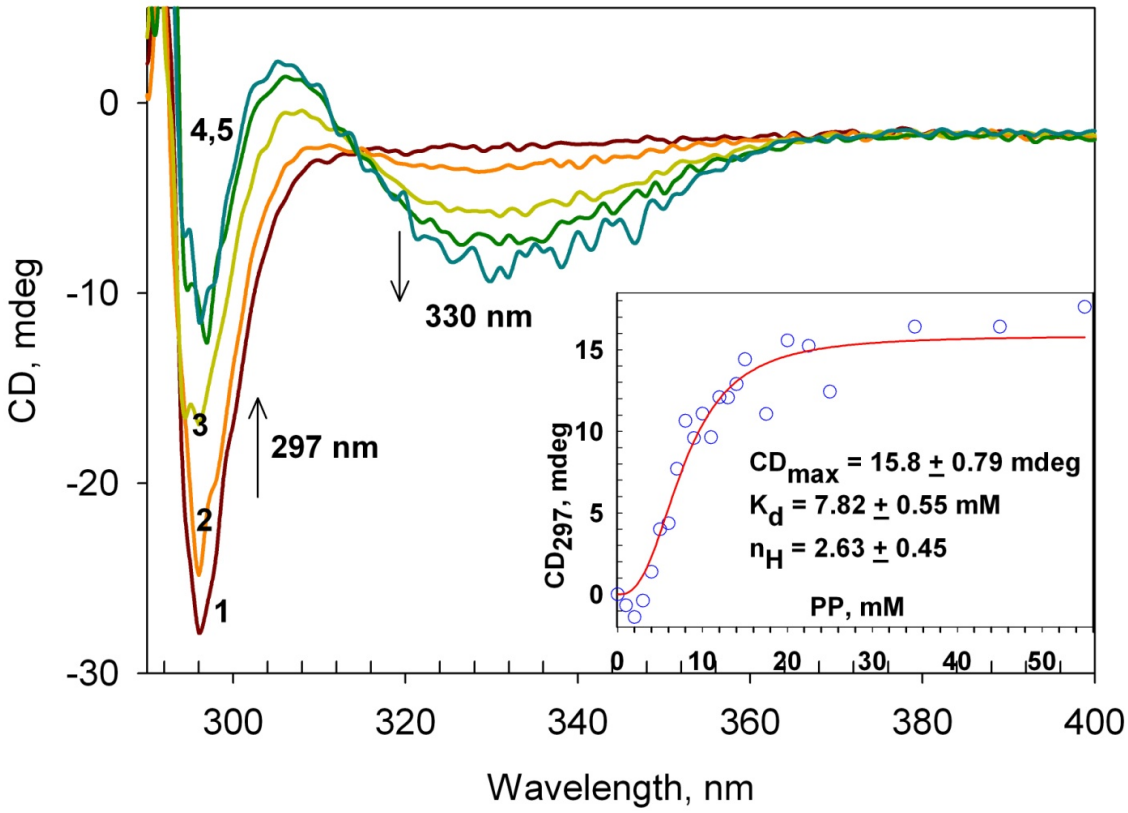

Figure 3.3 Formation of 1', 4'-iminophosphinolactyl-ThDP on YPDC

Near UV (290- 400 nm) CD spectra of wild-type YPDC (5.0 mg/mL) in absence of (1) and in presence of varying amounts: (2) 5 mM PP (3) 10 mM PP (4) 20 mM PP (5) 40 mM PP. The 1',4'- iminoPLThDP species (Scheme 1) is seen accumulating at 297 nm and the Michaelis complex (Enzyme + PP) is seen accumulating at 330 nm. (Inset) Dependence of signal amplitude at 297 nm with PP concentration. The data points (blue circles) were fit to a Hill equation ((3.1, see text) and the regression fit line (red) is displayed.

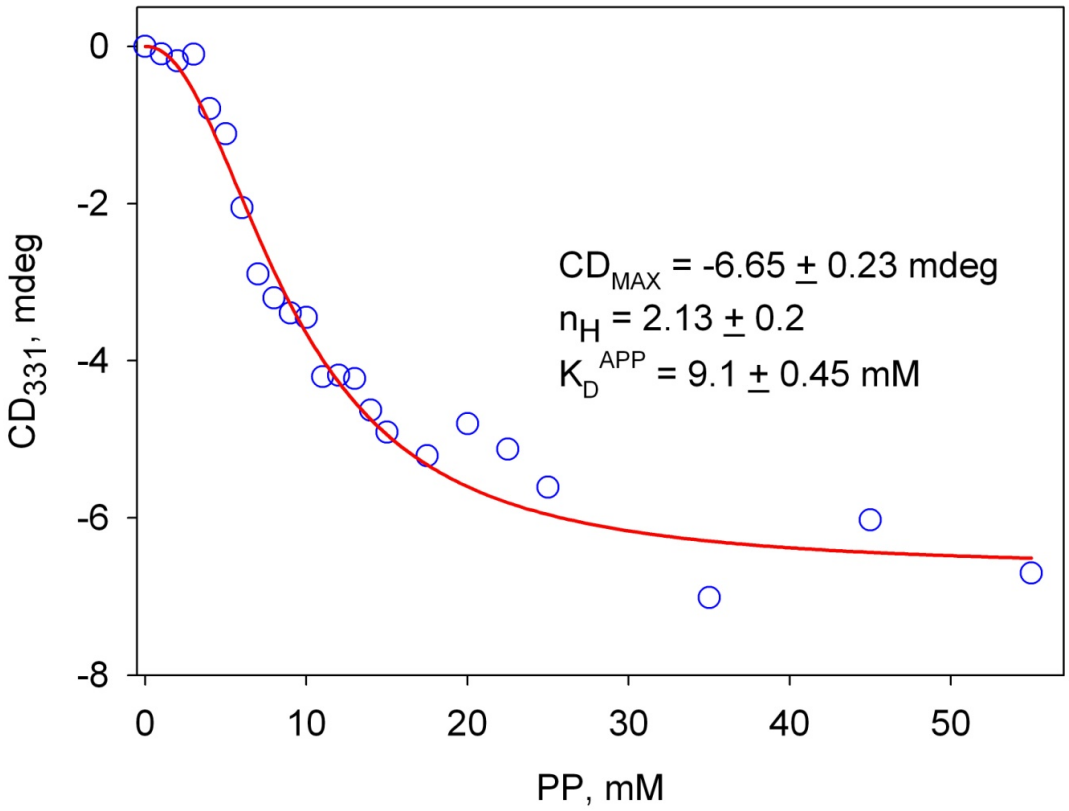

Figure 3.4 Binding parameters of PP to YPDC (MC) as determined by CD titration

CD mdeg at maxima 331 nm obtained over the course of titration (Figure 3.3) plotted against concentration of PP (mM). The data points (blue circles) were fit to the Hill equation ((3.1, see text) and the regression fit line (red) is displayed.

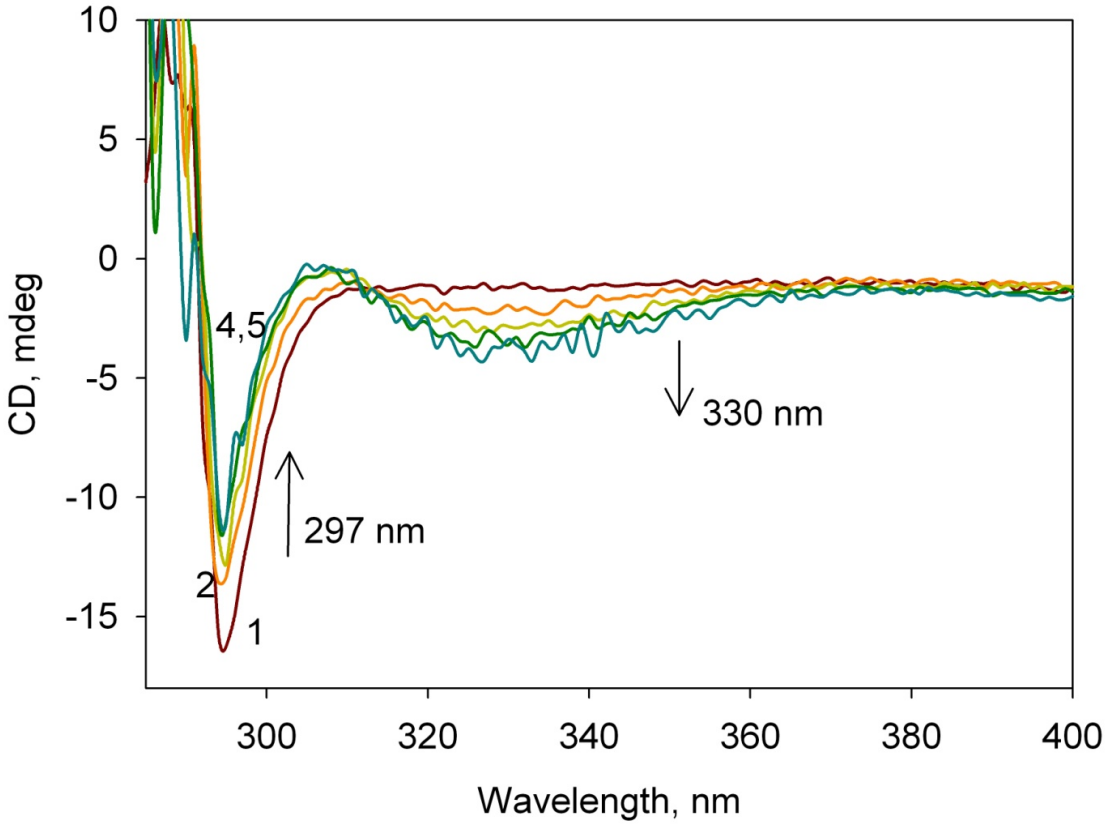

Figure 3.5 Formation of 1', 4'-iminophosphinolactyl-ThDP on E91D YPDC

Near UV (290 - 400 nm) CD spectra of titration of E91D YPDC (2.75mg/mL) (1) in presence of varying amounts: (2) 5 mM PP (3) 10 mM PP (4) 20 mM PP (5) 35 mM PP. The 1', 4'- iminoPLThDP species is seen accumulating at 297 nm and the Michaelis complex at 330 nm.

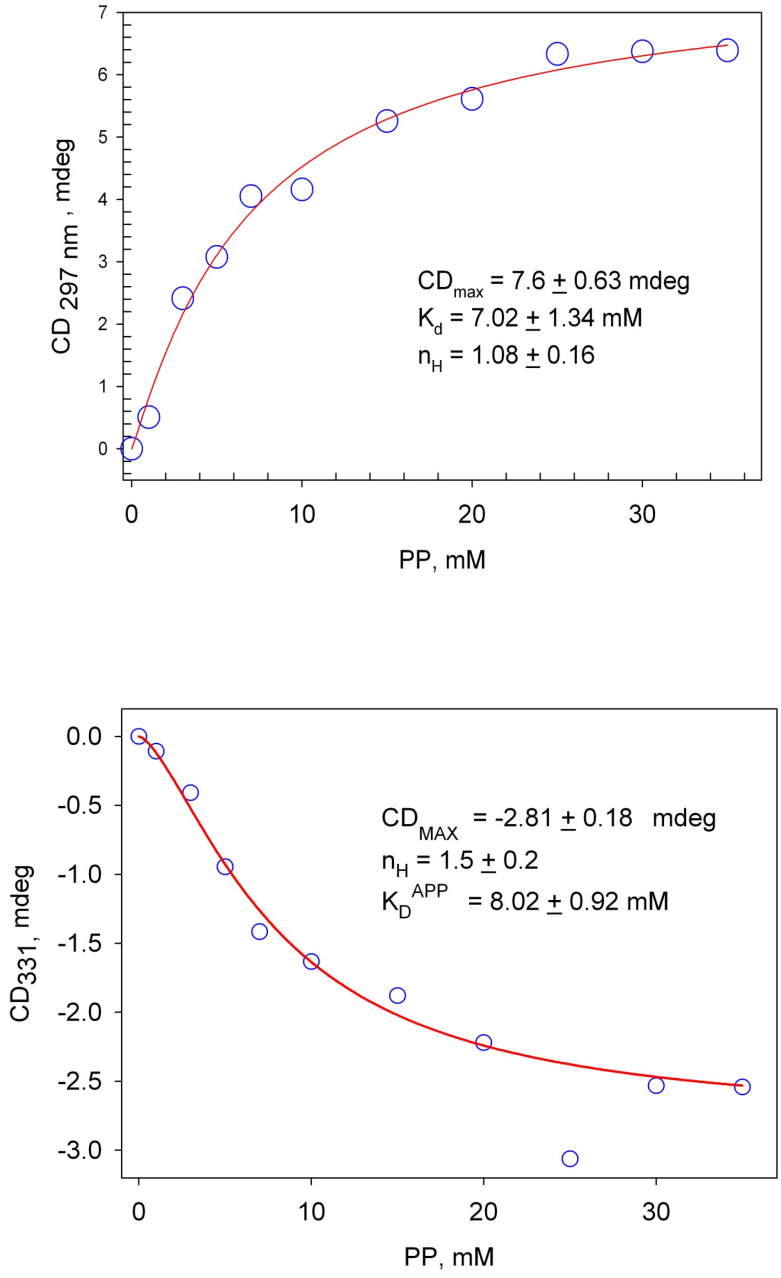

Figure 3.6 Binding parameters of PP to E91D (IP & MC) as determined by CD titration

CD mdeg of IP form at maxima 297 nm (Top) and CD mdeg of MC form at minima 331 nm (Bottom) obtained over the course of titration (Figure 3.5) plotted against concentration of PP (mM). The data points (blue circles) were fit to the Hill equation ((3.1, see text) and the regression fit line (red) is displayed.

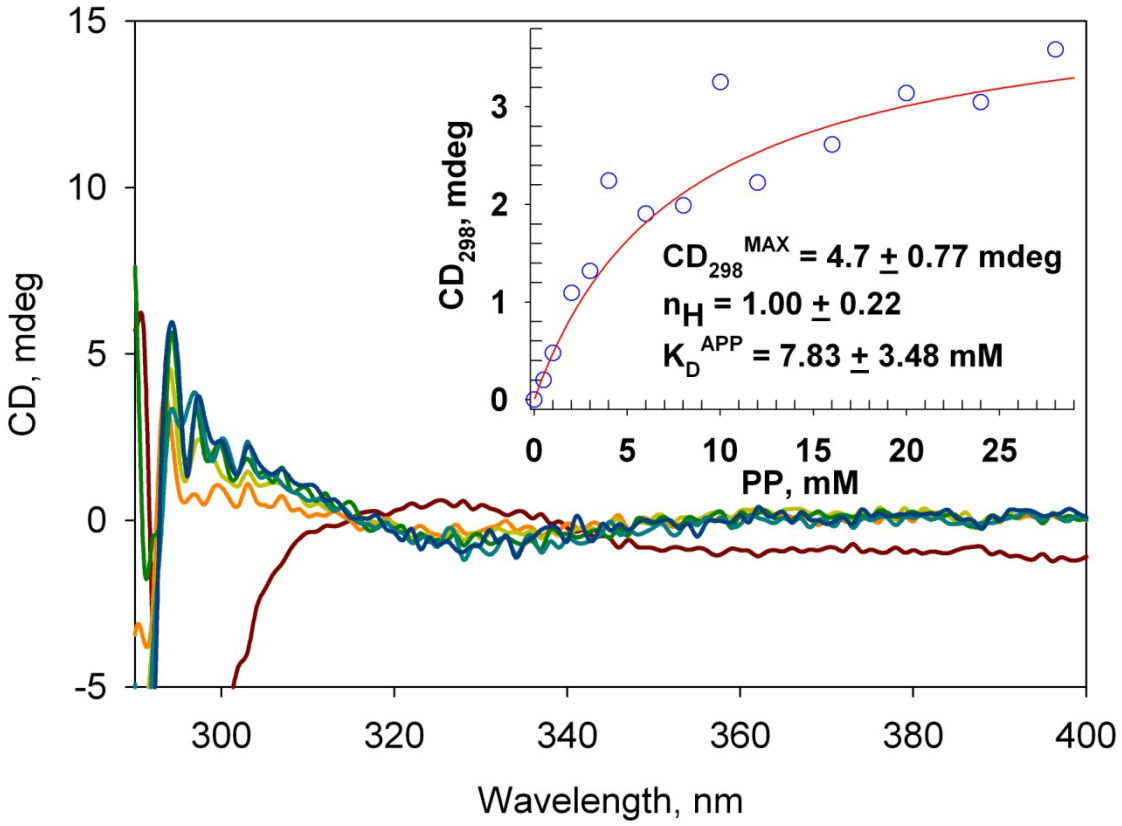

Figure 3.7 Formation of 1', 4'-iminophosphinolactylThDP on C221E YPDC

Near UV (290- 400 nm) CD spectra of C221E YPDC (2.75 mg/mL) (brown). Difference spectra obtained after subtraction of (1) in presence of varying amounts (1 – 28 mM) of PP. The 1',4'- iminoPLThDP species is seen accumulating at 297 nm. (Inset) Dependence of signal amplitude at 297 nm with PP concentration. The data points (blue circles) were fit to a Hill equation ((3.1, see text) and the regression fit line (red) is displayed.

Table 3.1 Binding constant (K_D^{app}) of PP as determined by monitoring Michaelis complex and/or 1',4'-iminophosphinolactylThDP formation

Enzyme Variant	K_D^{app} , (mM)	Hill coefficient	CD max, (mdeg)
YPDC	9.1 ± 0.45 **(MC)**	2.13 ± 0.2 **(MC)**	- 6.65 + 0.23 **(MC)**
	7.82 ± 0.55 **(IP)**	2.63 ± 0.45 **(IP)**	15.8 ± 0.79 **(IP)**
E91D	8.02 ± 0.92 **(MC)**	1.5 ± 0.2 **(MC)**	-2.85 + 0.18 **(MC)**
	7.02 ± 1.34 **(IP)**	1.08 ± 0.16 **(IP)**	7.6 ± 0.63 **(IP)**
C221E	7.83 ± 3.48 **(IP)**	1.0 ± 0.22 **(IP)**	4.7 ± 0.77 **(IP)**
E51D	13.6 + 0.35 **(IP)**	2.74 + 0.2 **(IP)**	21.6 + 0.54 **(IP)**

E51D YPDC

The E51D substitution has an unusual effect: addition of PP produces only the positive CD band at 297 nm (Figure 3.8) pertaining to the enzyme bound 1',4'-iminophosphinolactyl ThDP intermediate. The negative CD band at 330 nm pertaining to the Michaelis complex does not develop. Apparently, E51D YPDC variant can still protonate the N1' atom, a necessary step enroute to formation of the first tetrahederal adduct and stabilization of the IP tautomer, however the stabilization of the Michaelis complex observed in presence of substrate analog in YPDC is disrupted in this variant. Titration data fit to the Hill equation revealed sigmoidal binding characteristics and the Hill coefficient was 2.74, similar to the value observed with YPDC. Allosteric regulation of the enzyme catalysis by PP is still seen in the formation of the tetrahederal intermediate analog.

E477Q YPDC and D28A YPDC

Upon titration of E477Q and D28A active-site variants with PP no CD bands were observed. The positive band at 297 nm was very weak in both cases (Figure 3.9, Figure 3.10). The negative band at 330 nm is absent in both cases. These active site substitutions severely affect the (i) binding (Michaelis complex formation) and (ii) formation of the intermediate 1',4'-iminophosphinolactyl-ThDP with propionyl phosphinate. These residues are situated above the thiazolium ring in position to interact with the substrate carboxylate. Substitutions at these positions thus affect the binding of substrate in a productive conformation which facilitates addition of thiazolium C2 to carbonyl group of the substrate.

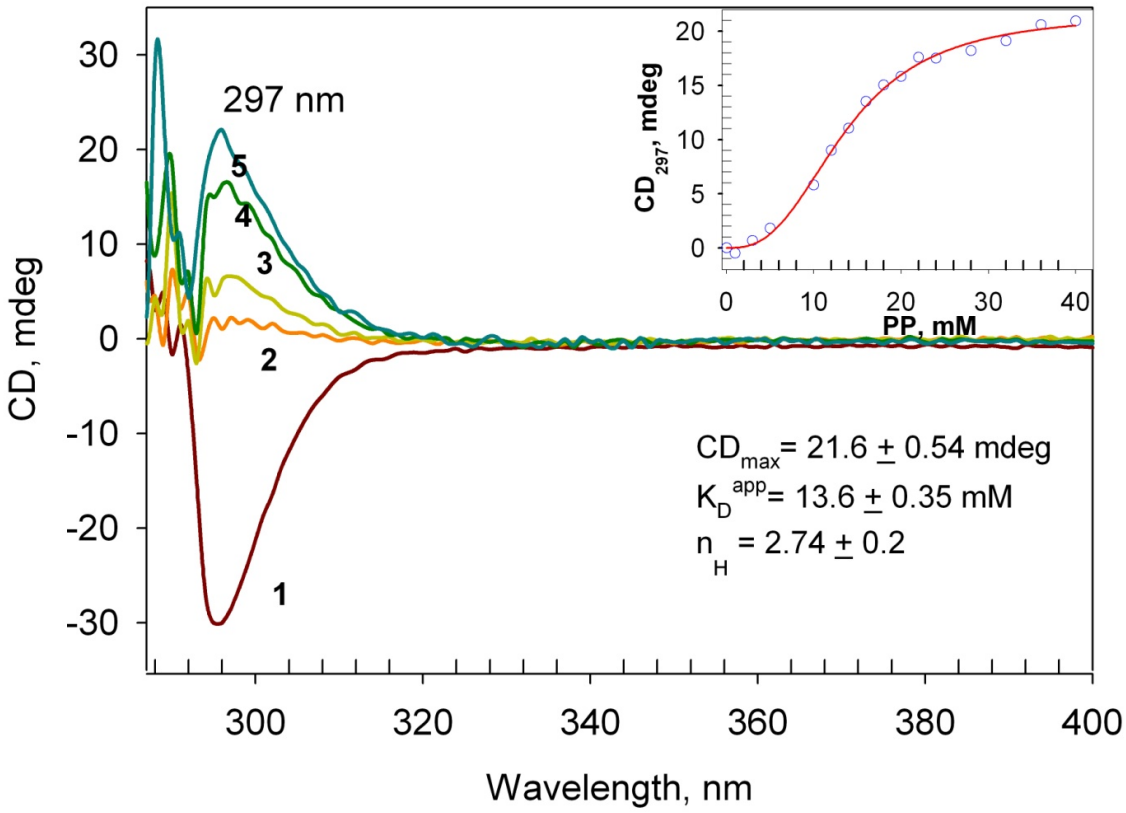

Figure 3.8 Formation of 1', 4'-iminophosphinolactyl-ThDP on E51D YPDC

Near UV (290- 400 nm) CD spectra of E51D YPDC (5.0 mg/mL) (1). Difference spectra obtained after subtraction of (1) in presence of varying amounts: (2) 5 mM PP (3) 10 mM PP (4) 20 mM PP (5) 40 mM PP. The 1',4'- iminoPLThDP species is seen accumulating at 297 nm. (Inset) Dependence of signal amplitude at 297 nm with PP concentration. The data points (blue circles) were fit to a Hill equation ((3.1, see text) and the regression fit line (red) is displayed.

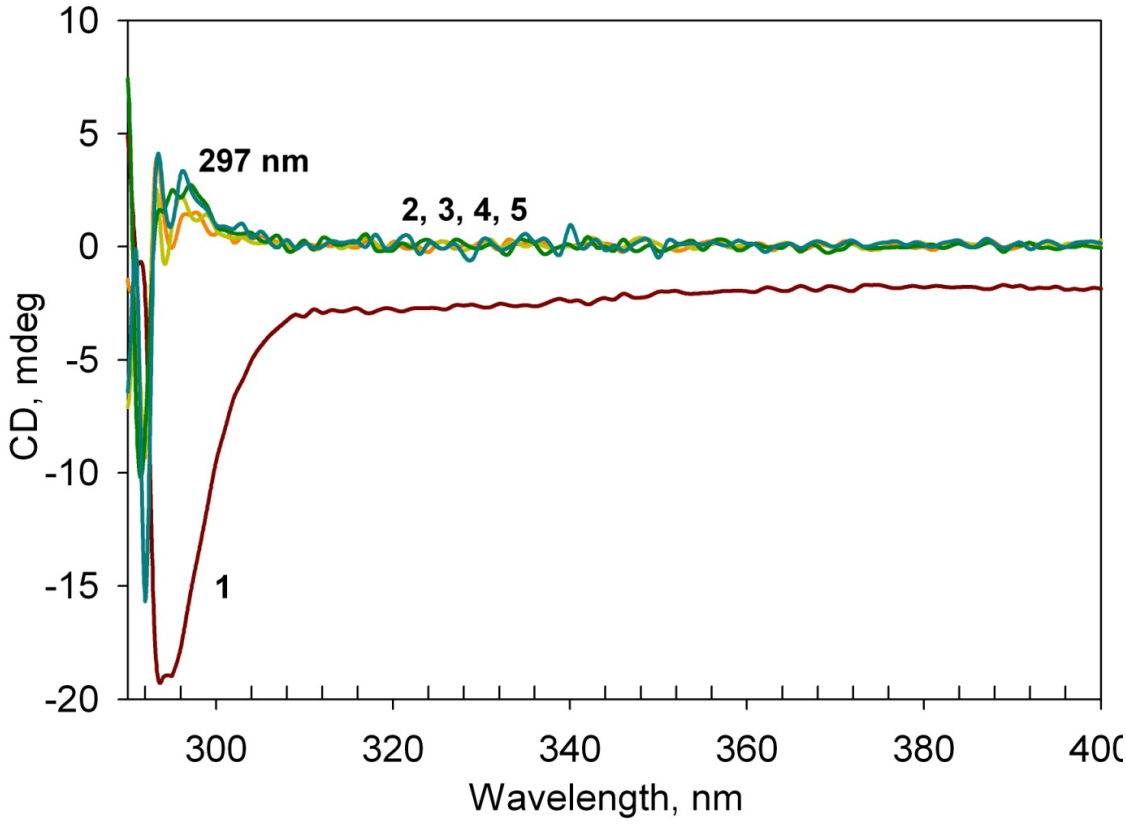

Figure 3.9 Formation of 1', 4'-iminophosphinolactyl-ThDP on E477Q YPDC

Near UV (290- 400 nm) CD spectra of E477Q YPDC (2.75mg/mL) (1). Difference spectra obtained after subtraction of (1) in presence of varying amounts: (2) 5 mM PP (3) 10 mM PP (4) 20 mM PP (5) 40 mM PP. The 1', 4'- iminoPLThDP species is seen accumulating in very little amount at 297 nm.

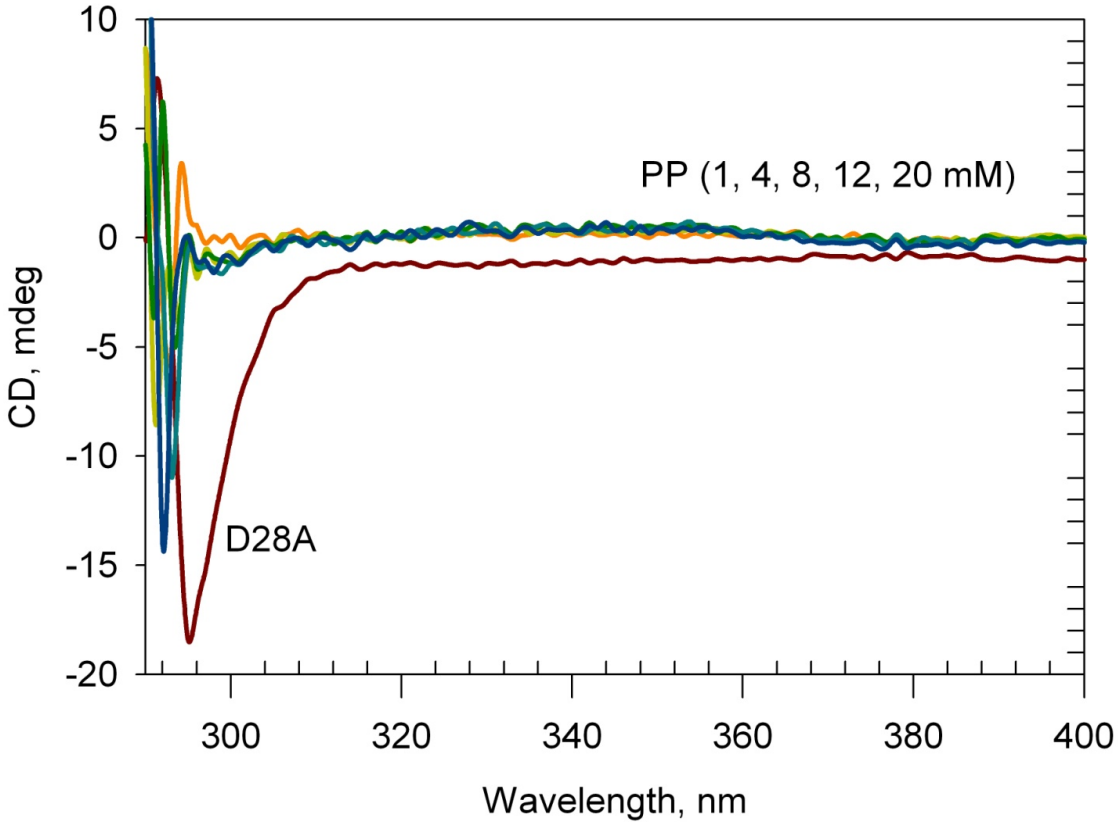

Figure 3.10 Titration of D28A YPDC with PP

Near UV (290- 400 nm) CD spectra of D28A YPDC (2.75mg/mL) (brown). Difference spectra obtained after subtraction of D28A YPDC (brown) in presence of varying amounts of PP.

3.3.2 Tautomeric state of ThDP during catalytic cycle of YPDC variants

Some low activity variants of YPDC (E51D, D28A, and E477Q) accumulate intermediates under steady-state conditions and conversion between intermediates is slow. These variants could be used to determine the tautomeric and ionization states of enzyme bound ThDP intermediates. At low temperatures and using low concentrations of pyruvate, carboligase side reactions which produce chiral acetoin or acetolactate in enantiomeric excess can also be minimized. CD titration experiments were performed at 5 ºC and pyruvate concentrations were controlled in the range 1 mM – 7 mM, which is the typical $S_{0.5}$ range for these variants.

E477Q YPDC

Addition of 1 mM pyruvate to the E477Q YPDC variant produced two CD bands: (i) broad positive band with CD_{max} at 297 nm and (ii) broad negative band centered on 340 nm developed (Figure 3.11). With further addition of pyruvate, the bands showed minor changes, suggestive of saturated active sites. The enzyme could bind pyruvate even at low concentrations ($S_{0.5}^{E477Q}$ = 3.0 mM). The induced active-site asymmetry observed in these spectra are very similar to those observed on addition of PP or acetylphosphinate to YPDC. This experiment provides clear evidence for substrate induced asymmetry of YPDC active-sites in the presence of pyruvate. The detection of active-site bound intermediates also provides support for the notion that YPDC is catalytically active during the low substrate concentration regime where mostly the unactivated form (regulatory site is unfilled) predominates.

Chemical quench and NMR analysis of a sample treated similarly revealed presence of only the HEThDP covalent intermediate in approximately half of the active-sites under steady-state conditions (Figure 3.13). These results are consistent with the alternating active-sites mechanism proposed by Sergienko et al. (*141*). In a corresponding pre-steady state experiment where E477Q was mixed with saturating amounts of pyruvate (20 mM), a time-dependent change was observed in the positive direction for the CD signal pertaining to the IP form at 313 nm (Figure 3.12). Based on evidence from chemical quench/NMR experiments and steady-state CD spectroscopy experiments, the observed rate of formation obtained from fitting the data to equation (3.3 is the apparent rate of formation of the HEThDP intermediate.

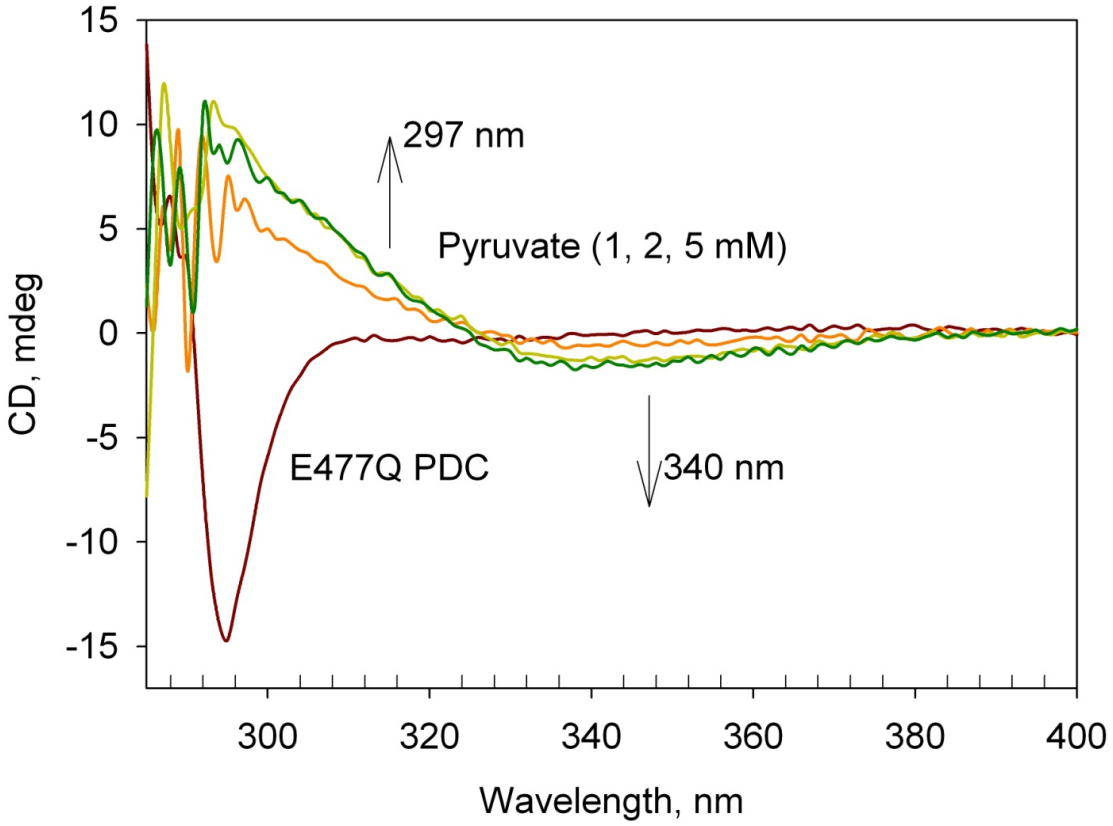

Figure 3.11 IP form of ThDP and Michaelis complex of E477Q YPDC in presence of pyruvate

Near UV (290- 400 nm) CD spectra of E477Q YPDC (2.75mg/mL) (brown) and difference spectra of enzyme in presence of different amounts of pyruvate (1 mM, 2 mM, and 5mM). A positive CD band with maxima at 297 nm pertaining to the 1', 4' imino tautomer of tetrahedral HEThDP intermediate and a negative CD band centered around 340 nm pertaining to the Michaelis complex formed immediately and showed small pyruvate concentration dependence.

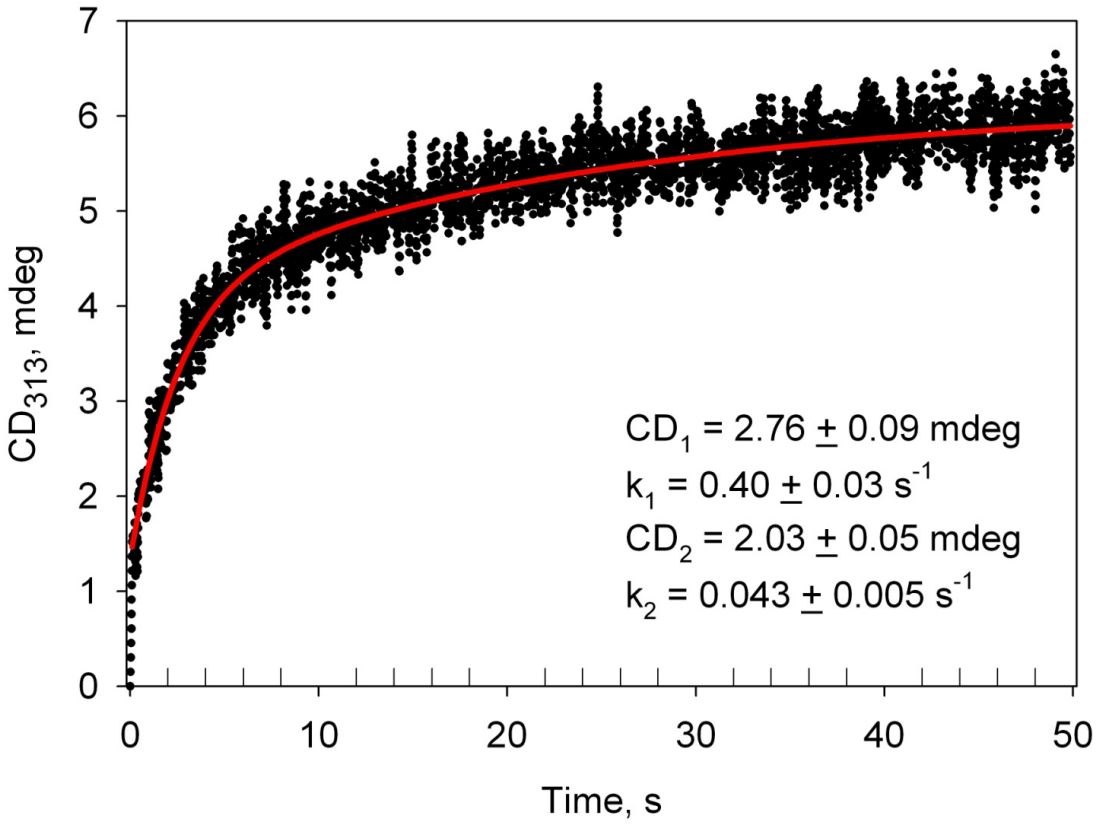

Figure 3.12 Time course of formation of IP tautomer of ThDP on E477Q YPDC in presence of pyruvate

E477Q YPDC (8 mg/mL) was rapidly mixed with 40 mM Pyruvate in a Pi*-180 stopped-flow CD spectrometer and the CD signal at 313 nm was monitored over a period of 50 seconds at 30 °C. Data from 10 shots were averaged and the average was fit to a double-exponential model ((3.3, see text). The red trace is the regression fit line.

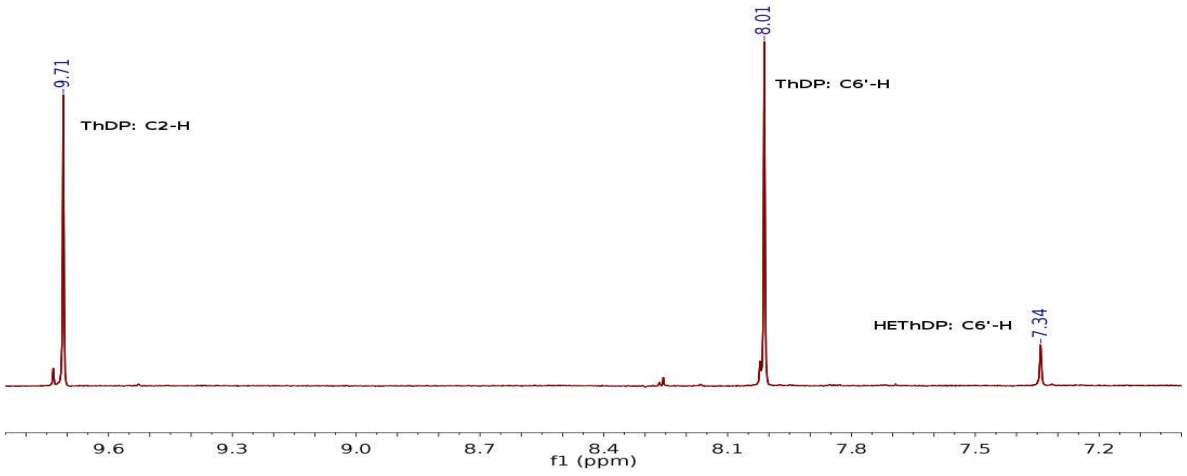

Figure 3.13 Steady-state covalent ThDP intermediate distribution in E477Q YPDC

Reaction of E477Q YPDC (25 mg/mL) with pyruvate (11 mM) at 5 °C was quenched with acid after 3 min. After centrifugation, the supernatant containing the ThDP intermediates was analyzed by ^{1}H NMR using the characteristic C6'-H chemical shifts. The relative abundance of intermediates was determined from relative integrals of the corresponding signals after correction for excess ThDP from buffer. (51.4%)

D28A YPDC

Upon addition of 1 mM pyruvate to the D28A YPDC variant, the CD bands did not show as strong a development as in the other YPDC variants. Upon further addition of pyruvate reaching final concentrations of 10 mM weak bands - positive band at 297 nm and a negative band at 328 nm - develop (Figure 3.14). For this variant, pyruvate dependent acetaldehyde production plot exhibited remarkable characteristics. The rate of acetaldehyde production follows a sharp rise reaching maxima at 2.5 – 3 mM pyruvate concentration followed by a dramatic decrease, attributed to apparent substrate inhibition (*130*). This variant produces acetolactate predominantly and C2-α-acetolactyl-ThDP (ALThDP) is the major intermediate under steady-state conditions as determined by chemical quench/NMR previously (*4*). To place these results into context, at low pyruvate concentrations, due to the low population of tetrahedral intermediates (alternatively, MC and the enamine predominate), the CD band at 297 nm could not be observed, but at high concentrations ALThDP builds up; this is reflected at 297 nm the wavelength at which the ThDP-bound tetrahedral intermediates are seen in their IP form. While (S)-acetolactate the predominant enantiomer produced by this variant shows a positive CD band with CD_{max} at 300 nm, no time dependence could be observed in the signal shown in the figure during course of the experiment at low pyruvate concentrations. Upon overnight incubation of the reaction mixture at 4 °C with 20 mM pyruvate, chiral acetolactate accumulation could be detected as positive CD band with CD_{max} at 300 nm. The D28N variant, in contrast, showed no CD bands in the regions 297 nm and 340 nm upon addition of pyruvate even at concentrations as high as 20 mM (Figure 3.15). On this variant, presumably the intermediates do not accumulate at detectable levels due to distortion of the active-site by the D28N substitution.

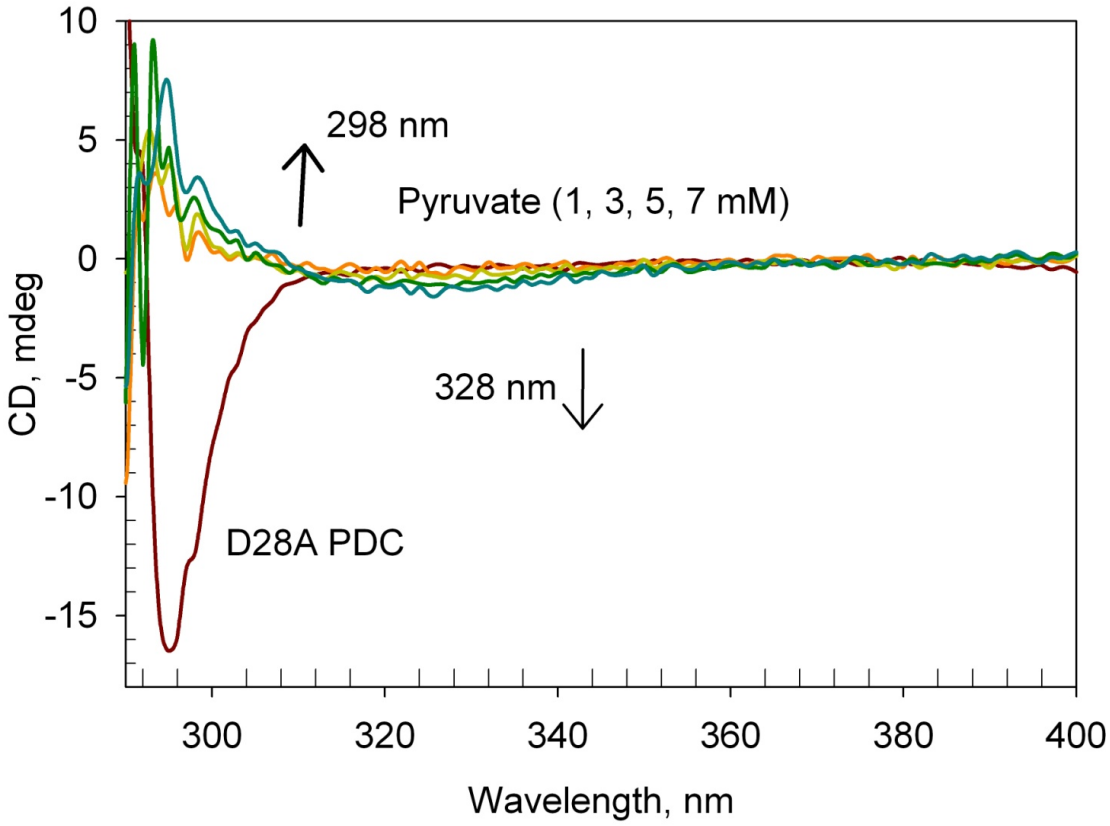

Figure 3.14 IP form of ThDP and Michaelis complex of D28A YPDC in presence of pyruvate

Near UV (290- 400 nm) CD spectra of D28A YPDC (2.75mg/mL) (brown) and difference spectra of enzyme in presence of different amounts of pyruvate (1 mM, 3 mM, 5mM, and 7 mM). A positive CD band with maxima at 297 nm pertaining to the 1', 4' imino tautomer of a tetrahedral ThDP intermediate and a negative CD band centered on 328 nm pertaining to the Michaelis complex are seen.

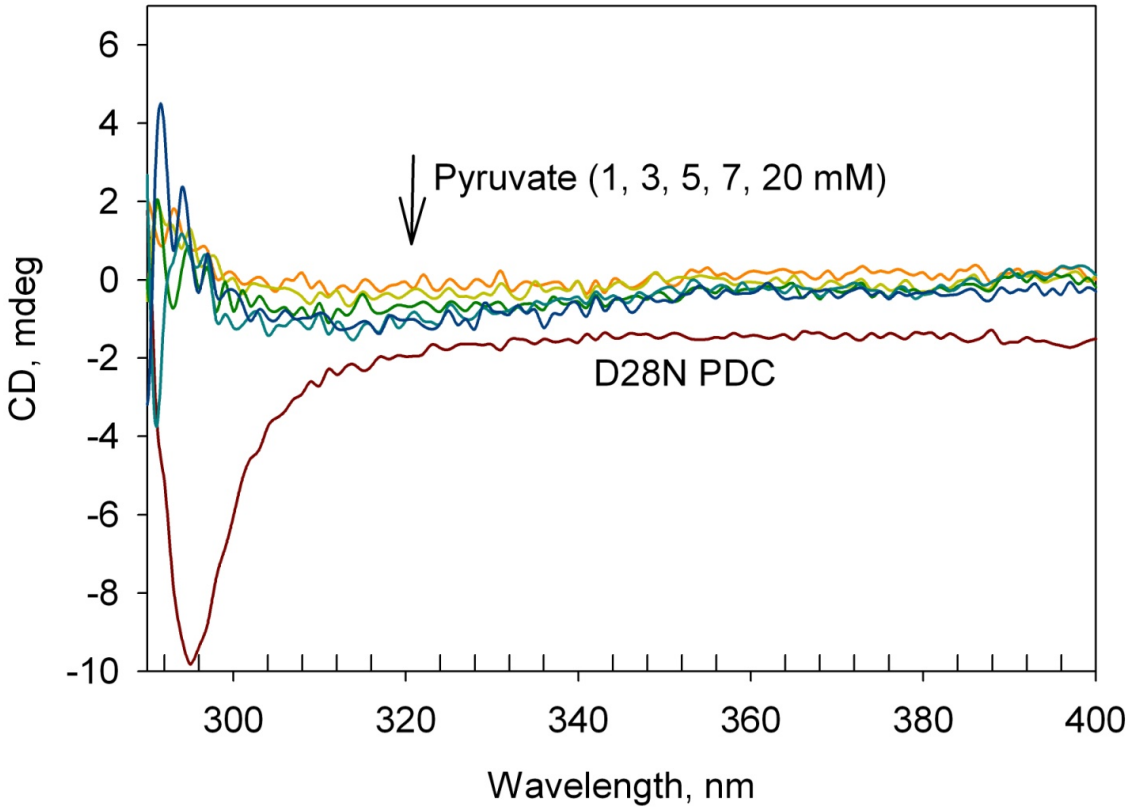

Figure 3.15 Titration of D28N YPDC with pyruvate

Near UV (290- 400 nm) CD spectra of D28N YPDC (2.0 mg/mL) and difference spectra of enzyme in presence of different amounts of pyruvate (1 mM, 3 mM, 5mM, 7 mM, and 20 mM). No positive changes are seen in the 295-310 nm region, but a weak negative band centered around 318-320 nm develops with increasing amounts of pyruvate.

E51D YPDC

Upon addition of 1 mM pyruvate to the E51D YPDC variant, a positive CD band with CD_{max} at 297 nm was evident (Figure 3.16). Little further change in the amplitude could be seen upon addition of 5 mM and 20 mM pyruvate. The intermediates saturated the active-site at concentrations as low as 1 mM ($S_{0.5}^{E51D}$ = 1.6 mM). Chemical quench and NMR analysis of a sample treated similarly revealed presence of only the HEThDP covalent intermediate in approximately half of the active-sites under steady-state conditions (Figure 3.18). However, under pre-steady state conditions both LThDP and HEThDP were observed (Figure A5 in Appendix). Again, approximately half of the active-sites were filled with both covalent intermediates (LThDP & HEThDP). In a corresponding pre-steady state experiment where E51D YPDC was mixed with saturating amounts of pyruvate (40 mM), a time-dependent biphasic change was observed in the positive direction for the CD signal pertaining to the IP form at 313 nm (Figure 3.17). Based on evidence from chemical quench/NMR experiments and steady-state CD spectroscopy experiments, during pre-steady state, decarboxylation of LThDP is one of the rate-limiting steps, and therefore LThDP accumulates, during steady state product release and C-C bond formation are the slow steps and only HEThDP is detected during the steady-state. The fast phase observed in time-dependent changes in the positive CD signal at 313 nm can be assigned to the apparent rate of formation of LThDP.

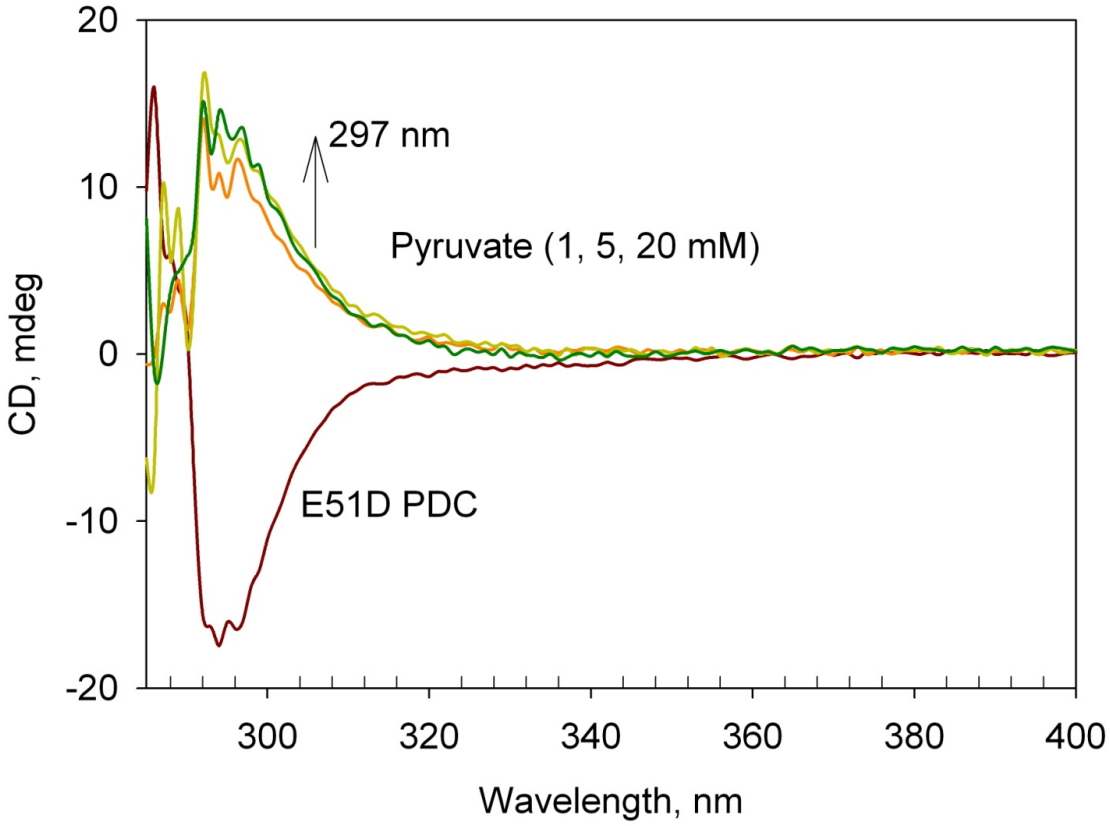

Figure 3.16 IP form of ThDP on E51D YPDC in presence of pyruvate

Near UV (290- 400 nm) CD spectra of E51D YPDC (2.75mg/mL) and difference spectra of enzyme in presence of different amounts of pyruvate (1 mM, 5mM, 20 mM). A positive CD band with maxima at 297 nm pertaining to the 1', 4' imino tautomer of a tetrahedral ThDP intermediate formed immediately and showed negligible pyruvate concentration dependence.

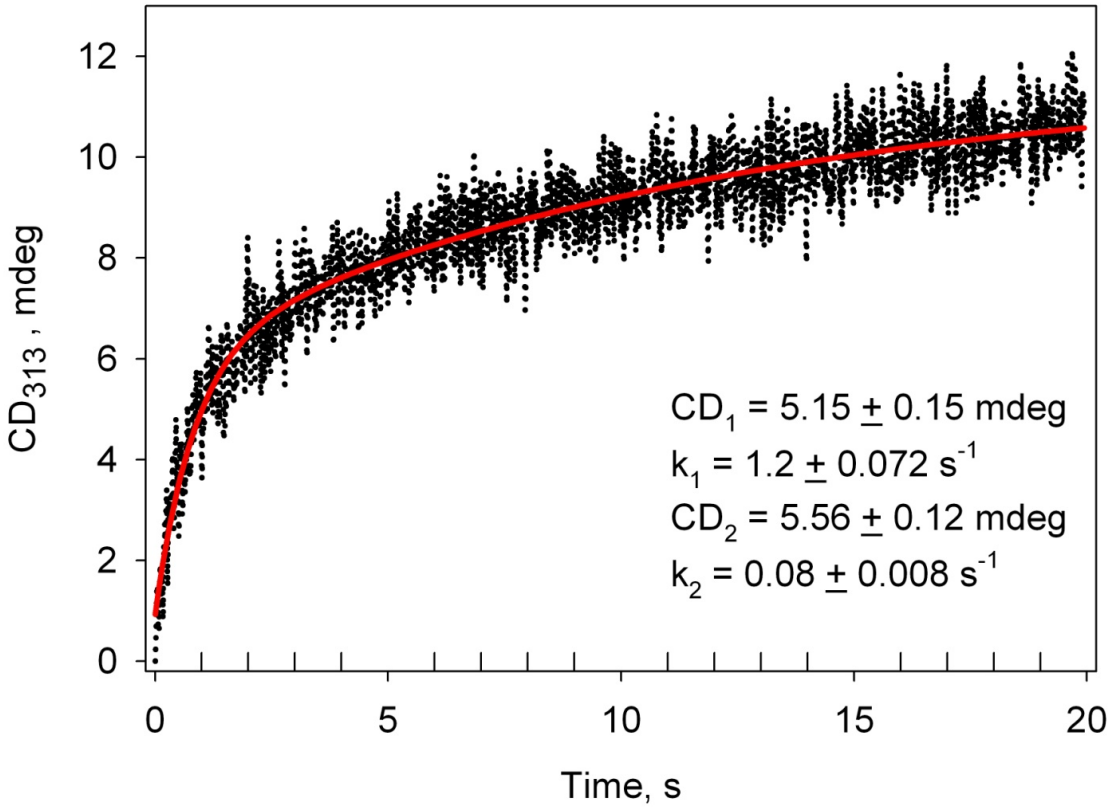

Figure 3.17 Time course of formation of IP tautomer of ThDP on E51D YPDC in presence of pyruvate

E51D YPDC (8 mg/mL) was rapidly mixed with 40 mM Pyruvate in a Pi*-180 stopped-flow CD spectrometer and the CD signal at 313 nm was monitored over a period of 20 seconds at 30 °C. Data from 10 shots were averaged and the average was fit to a double-exponential model ((3.3, see text). The red trace is regression fit line.

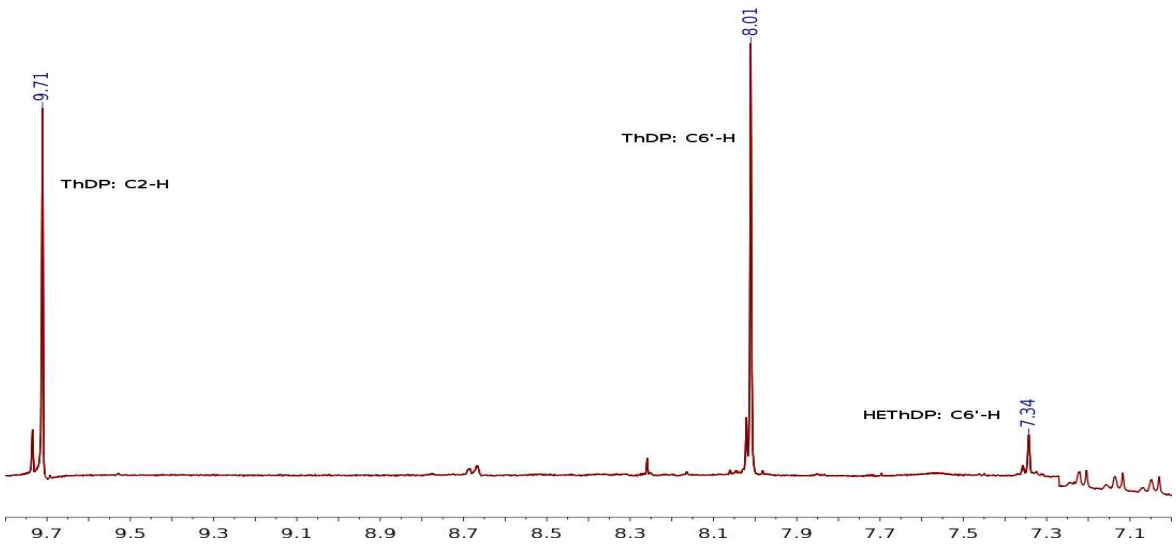

Figure 3.18 Steady-state covalent ThDP intermediate distribution in E51D YPDC

Reaction of E51D YPDC (25 mg/mL) with pyruvate (11 mM) at 5 °C was quenched with acid after 3 min. After centrifugation, the supernatant containing the ThDP intermediates was analyzed by ^{1}H NMR using the characteristic C6'-H chemical shifts. The relative abundance of intermediates was determined from relative integrals of the corresponding signals after correction for excess ThDP from buffer. (51.4%)

3.3.3 Presteady state rate of formation of 1', 4'-iminotautomer of ThDP covalent intermediates

The rate of formation of 1', 4'-imino-C2α-phosphinolactyl-ThDP from PP and wild-type YPDC as monitored at 302 nm was 0.06 s^{-1} (Figure 3.19), while the Michaelis complex observed at 330 nm during titration experiments was formed within the dead-time (1.5 msec) of the stop-flow instrument under saturating conditions of PP (40 mM).

While the high turn-over rate of pyruvate precluded any steady-state CD experiments, pre-steady state experiments enabled detection of IP tautomer at 313 nm upon mixing of YPDC with saturating concentrations of pyruvate (20 mM). Unlike with PP, accumulation of species with positive CD signal at 313 nm was very fast and the process reached a steady state within 0.2 s (Figure 3.20). In previous chemical quench NMR studies with YPDC, under steady state conditions the active-sites were shown to be mostly filled with HEThDP intermediate. However, under pre-steady state conditions (at 0.035 s time-point) pyruvamide activated YPDC active-sites contain both LThDP and HEThDP (Figure A7 in Appendix). During the pre-steady state phase, both decarboxylation of LThDP and product release are the slow steps, however during the steady state phase product release is the slowest step. Based on NMR experiments, the observed pre-steady state rate of formation can be assigned to the apparent rate of formation of the LThDP intermediate. Under substrate saturating conditions when the rate of formation of Michaelis complex is very fast, the apparent rate of formation of LThDP intermediate approximates to the net forward rate constant k_2 in Scheme 3.1. This observation is in very good agreement with the previously determined k_2 for YPDC reaction with pyruvate (*4*). The rates of formation of covalent ThDP intermediates on some YPDC variants are summarized in Table 3.2.

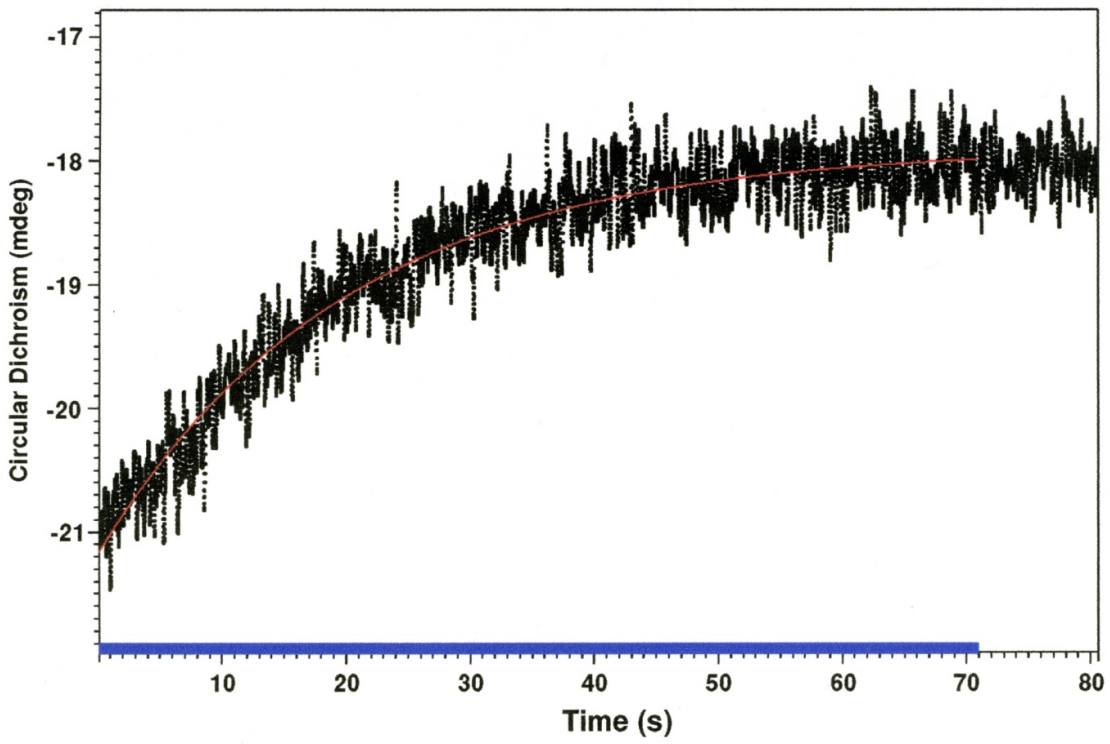

Figure 3.19 Time course of formation of 1',4' iminoPLThDP on YPDC

YPDC (8mg/mL) was rapidly mixed with 40 mM PP in a Pi*-180 stopped-flow CD spectrometer and the CD signal at 302 nm was monitored over a period of 90 seconds. Data from 6 shots were averaged and smoothing the raw data was performed using Savitsky-Golay function provided by the accompanying software and fit to a single-exponential model. The red trace is regression fit line.

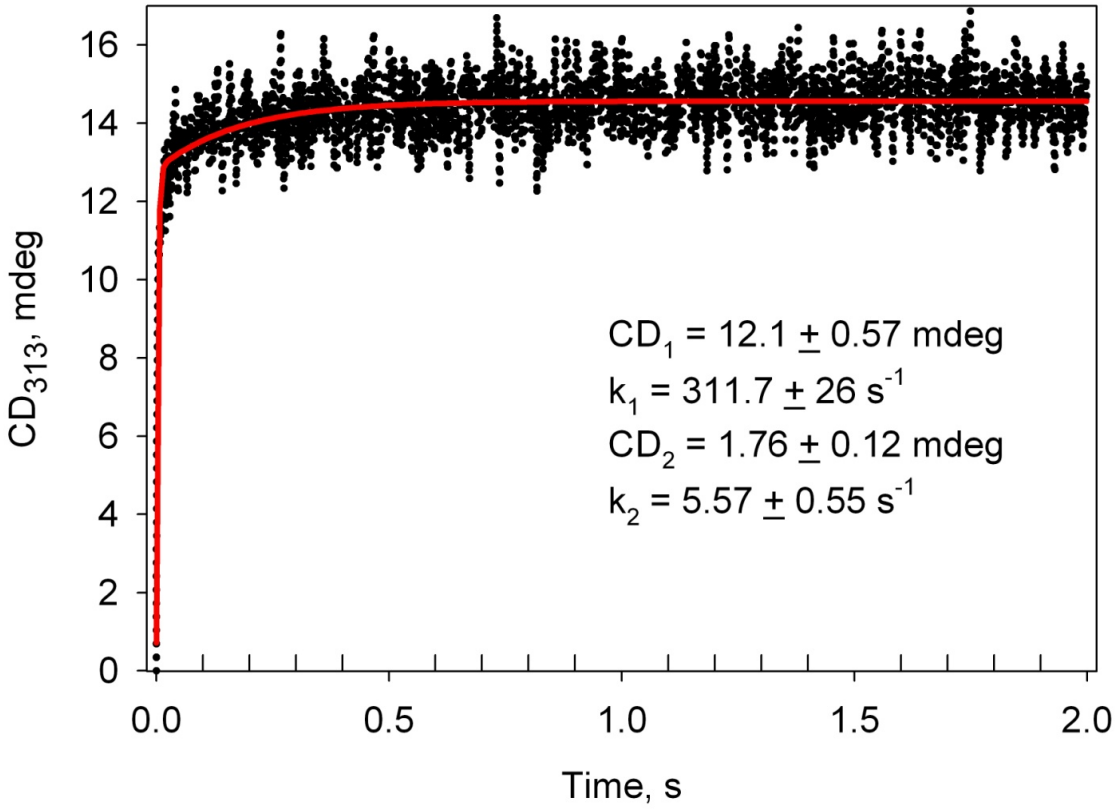

Figure 3.20 Time course of formation of IP tautomer of ThDP on YPDC in presence of pyruvate

YPDC (8 mg/mL) was rapidly mixed with 40 mM Pyruvate in a Pi*-180 stopped-flow CD spectrometer and the CD signal at 313 nm was monitored over a period of 50 seconds at 10 °C. Data from 10 shots were averaged and the average was fit to a single-exponential model. The red trace is regression fit line.

Table 3.2 Apparent rate of formation of IP tautomer of ThDP in presence of substrates

Enzyme	**Substrate**	**Apparent rate of IP formation (s^{-1})**
YPDC	Propionyl phosphinate	0.06
YPDC	Pyruvate	312 $\pm$ 26; 1.76 $\pm$ 0.12
E51D YPDC	Pyruvate	1.2 $\pm$ 0.07; 0.08 $\pm$ 0.01
E477Q YPDC	Pyruvate	0.4 $\pm$ 0.03; 0.04 $\pm$ 0.005

3. 4 CONCLUSIONS

Allosteric substrate regulation and co-operativity

While X ray structures provided direct evidence for large scale rearrangements in the quaternary and tertiary structures of activated YPDC and related non-oxidative decarboxylases (*26, 134, 142*), the current study probes the effect of these changes in the individual active-sites. The findings suggest that the catalytic regulation is achieved via control of individual steps in the multi-step non-oxidative decarboxylation involving 3 covalent intermediates undertaken by the enzyme. While a model for active-site communication in presence of substrate and substrate analogs was been proposed earlier for YPDC, this study provides the first instance for direct detection of this phenomenon in presence of pyruvate. Effort to answer questions regarding the pathway for such a communication did not provide unambiguous results. According to the 'proton-wire mechanism for thiamin enzymes' initially proposed by Frank et al. (*143*) and recent experiments on E1p (*85*) a direct pathway connects the N1' atoms of ThDP and the Glu51 residue plays a central role in shuttling of a proton between the two connected active-centers. Substitution of this residue in the E51D variant, while producing CD spectra reminiscent of other ThDP enzymes with non-communicating active-sites, does not provide any hints since the physical origins of the Michaelis complex CD band necessitates presence of a charged residue close to the N1' atom of ThDP.

Michaelis complex in YPDC catalysis

The Michaelis complex observed as a negative CD band at 330 nm in the presence of pyruvate or PP is the non-covalent enzyme substrate/substrate analog intermediate in YPDC catalysis (Scheme 3.1 and Scheme 3.2). The charge-transfer CD band of this intermediate is proposed to be composed of the enzyme bound ThDP and a pyruvate molecule bound to the active-site in a near attack conformation as also detected on some slow variants of the E1p component of *E. coli* pyruvate dehydrogenase complex (*17, 101, 144*). However, this intermediate does not accumulate upon titration of either E1p or pyruvate oxidase with PP (Figure A8 in Appendix). The present study with YPDC variants provides some insight into the minimal conditions necessary for accumulation of the Michaelis complex at levels detectable by CD spectroscopy.

YPDC, E91D and C221E variants stabilize the Michaelis complex in the presence of acetyl phosphinate, methyl acetylphosphonate (*16, 17*) and PP. However, substitutions at the active-site perturb the stabilization of this intermediate. The residue Glu51 appears to be necessary for stabilization of the enzyme-ThDP-pyruvate or enzyme-ThDP- PP Michaelis complex. Considering the conserved role of this residue in protonation of the N1' position of the 4'-aminopyrimidine ring, it can be concluded that the APH^+ form of ThDP is an essential component of the Michaelis complex. The D28A and E477Q variants failed to accumulate the Michaelis complex upon titration with PP. These residues are located closer to the pyruvate binding site and positioned above the thiazolium ring. Perturbations at these positions possibly affect optimal binding of PP in the active-site and thus preclude formation of the Michaelis complex. These results point toward the optimal positioning of PP in the active-site as another necessary component.

Solid state NMR studies discussed in Chapter 1 provide evidence for activation of the C2-H bond of the thiazolium ring in enzyme bound YPDC. Together, these observations provide a situation where the ThDP is activated via protonation at N1' and PP is bound in a favorable orientation presumably dictated by residues Asp28 and Glu477 for the Michaelis complex to be stabilized. This situation could possibly be the near attack conformation.

With pyruvate however, the E477Q and D28A variants do stabilize the Michaelis complex indicating that pyruvate binds to the active-site in the near attack conformation in these variants albeit with perturbations. Possibly the tetrahederal stereochemistry at the phosphorous center in PP, in addition to the substitutions at these positions precludes such binding as observed with pyruvate. Approximately 50% of the active-sites in E477Q YPDC and 10-15% active-sites in D28A YPDC are in the Michaelis complex form in a reaction with pyruvate according to NMR analysis of steady-state intermediate distribution.

1',4'-Iminopyrimidine tautomer of ThDP in YPDC catalysis

The 1',4'-iminopyrimidine tautomeric form of ThDP has been shown to accompany tetrahederal pre-decarboxylation intermediate analogs in 10 different members of the ThDP superfamily of enzymes. Also, the 1',4'-iminopyrimidine tautomeric form of ThDP was previously shown to accumulate during HEThDP formation in the reversible reaction with acetaldehyde on YPDC. The current study for the first time provides evidence for formation of such intermediate in the forward direction of catalysis with pyruvate. While the steady-state CD spectroscopy experiments pointed toward accumulation of 1',4'-imino-HEThDP in E51D and E477Q variants, chemical quench/ NMR analysis at various time

scales afforded snapshots of tetrahederal intermediate distribution during both steady-state and pre-steady state phases. Rate constants for LThDP formation on YPDC from NMR analysis and rate constant for formation of 1',4'-imino-LThDP from pre-steady state CD spectroscopy are in very good agreement within experimental error, during short time-scales the 1',4'-imino-LThDP can also be detected and kinetically characterized during the forward reaction.

Conclusions for 1',4'-imino-C2α-LThDP detection with YPDC can also be extended to experiments with E51D variant where both LThDP and HEThDP are detected by NMR analysis during pre-steady state and HEThDP is detected during steady-state. Interestingly, perturbation of the conserved acidic residue does not affect accumulation of the IP tautomer in contrast to the Michaelis complex accumulation. The environment around N1' still favors protonation but at a slower rate compared to YPDC. However, abolishing the acid residue as in the case of E51A produced a variant which does not accumulate tetrahederal intermediates to detectable levels at steady-state in reaction with pyruvate (Figure A6 in Appendix). In this case, the N1' protonation step is severely compromised thus slowing down the YI formation.

Evidence for active-site asymmetry in the presence of pyruvate was gathered from experiments with E477Q YPDC and D28A YPDC during steady-state. The co-existence of both pre-decarboxylation and post-decarboxylation intermediates in YPDC active-sites are in agreement with a previous prediction by a model for alternating sites mechanism of catalysis of YPDC (*141*). Moreover, detection of the IP form of ThDP in the presence of C2-α-acetolactylThDP in D28A YPDC active-sites provides further support for the notion that 'all C2-α-ThDP tetrahederal intermediates are in the IP form.'

REFERENCES

1. Breslow, R. (1958) On the Mechanism of Thiamine Action. IV.1 Evidence from Studies on Model Systems, *J. Am. Chem. Soc. 80*, 3719-3726.

2. Frey, P. A. (1989) 2-Acetylthiamin pyrophosphate: an enzyme-bound intermediate in thiamin pyrophosphate-dependent reactions, *Biofactors 2*, 1-9.

3. Schellenberger, A., Hubner, G., and Neef, H. (1997) Cofactor designing in functional analysis of thiamin diphosphate enzymes, *Methods Enzymol 279*, 131-146.

4. Tittmann, K., Golbik, R., Uhlemann, K., Khailova, L., Schneider, G., Patel, M., Jordan, F., Chipman, D. M., Duggleby, R. G., and Hubner, G. (2003) NMR analysis of covalent intermediates in thiamin diphosphate enzymes, *Biochemistry 42*, 7885-7891.

5. Schellenberger, A. (1998) Sixty years of thiamin diphosphate biochemistry, *Biochim. Biophys. Acta 1385*, 177-186.

6. Wille, G., Meyer, D., Steinmetz, A., Hinze, E., Golbik, R., and Tittmann, K. (2006) The catalytic cycle of a thiamin diphosphate enzyme examined by cryocrystallography, *Nat. Chem. Biol. 2*, 324-328.

7. Chipman, D. M., Duggleby, R. G., and Tittmann, K. (2005) Mechanisms of acetohydroxyacid synthases, *Curr Opin Chem Biol 9*, 475-481.

8. Kluger, R., and Tittmann, K. (2008) Thiamin diphosphate catalysis: enzymic and nonenzymic covalent intermediates, *Chem Rev 108*, 1797-1833.

9. Kluger, R., and Rathgeber, S. (2008) Catalyzing separation of carbon dioxide in thiamin diphosphate-promoted decarboxylation, *FEBS J 275*, 6089-6100.

10. Kluger, R., Ikeda, G., Hu, Q., Cao, P., and Drewry, J. (2006) Accelerating unimolecular decarboxylation by preassociated acid catalysis in thiamin-derived intermediates: implicating Bronsted acids as carbanion traps in enzymes, *J Am Chem Soc 128*, 15856-15864.

11. Jordan, F., Li, H., and Brown, A. (1999) Remarkable stabilization of zwitterionic intermediates may account for a billion-fold rate acceleration by thiamin diphosphate-dependent decarboxylases, *Biochemistry 38*, 6369-6373.

12. Zhang, S., Liu, M., Yan, Y., Zhang, Z., and Jordan, F. (2004) C2-alpha-lactylthiamin diphosphate is an intermediate on the pathway of thiamin diphosphate-dependent pyruvate decarboxylation. Evidence on enzymes and models, *J Biol Chem 279*, 54312-54318.

13. Brandt, G. S., Nemeria, N., Chakraborty, S., McLeish, M. J., Yep, A., Kenyon, G. L., Petsko, G. A., Jordan, F., and Ringe, D. (2008) Probing the active center of benzaldehyde lyase with substitutions and the pseudosubstrate analogue benzoylphosphonic acid methyl ester, *Biochemistry 47*, 7734-7743.

14. Merski, M., and Townsend, C. A. (2007) Observation of an acryloyl-thiamin diphosphate adduct in the first step of clavulanic acid biosynthesis, *J Am Chem Soc 129*, 15750-15751.

15. Nemeria, N., Korotchkina, L., McLeish, M. J., Kenyon, G. L., Patel, M. S., and Jordan, F. (2007) Elucidation of the chemistry of enzyme-bound thiamin diphosphate prior to substrate binding: defining internal equilibria among tautomeric and ionization states, *Biochemistry 46*, 10739-10744.

16. Nemeria, N., Chakraborty, S., Baykal, A., Korotchkina, L. G., Patel, M. S., and Jordan, F. (2007) The 1',4'-iminopyrimidine tautomer of thiamin diphosphate is poised for catalysis in asymmetric active centers on enzymes, *PNAS 104*, 78-82.

17. Nemeria, N., Baykal, A., Joseph, E., Zhang, S., Yan, Y., Furey, W., and Jordan, F. (2004) Tetrahedral intermediates in thiamin diphosphate-dependent decarboxylations exist as a 1',4'-imino tautomeric form of the coenzyme, unlike the michaelis complex or the free coenzyme, *Biochemistry 43*, 6565-6575.

18. Jordan, F., Nemeria, N. S., Zhang, S., Yan, Y., Arjunan, P., and Furey, W. (2003) Dual catalytic apparatus of the thiamin diphosphate coenzyme: acid-base via the 1',4'-iminopyrimidine tautomer along with its electrophilic role, *J. Am. Chem. Soc. 125*, 12732-12738.

19. Baykal, A. T., Kakalis, L., and Jordan, F. (2006) Electronic and nuclear magnetic resonance spectroscopic features of the 1',4'-iminopyrimidine tautomeric form of thiamin diphosphate, a novel intermediate on enzymes requiring this coenzyme, *Biochemistry 45*, 7522-7528.

20. Jordan, F., Zhang, Z., and Sergienko, E. (2002) Spectroscopic evidence for participation of the 1',4'-imino tautomer of thiamin diphosphate in catalysis by yeast pyruvate decarboxylase, *Bioorg Chem 30*, 188-198.

21. Cain, A. H., Sullivan, G. R., and Roberts, J. D. (1977) The protonation site of vitamin B1 as determined from natural-abundance nitrogen-15 nuclear magnetic resonance spectra, *J. Am. Chem. Soc. 99*, 6423-6425.

22. Arjunan, P., Sax, M., Brunskill, A., Chandrasekhar, K., Nemeria, N., Zhang, S., Jordan, F., and Furey, W. (2006) A thiamin-bound, pre-decarboxylation reaction intermediate analogue in the pyruvate dehydrogenase E1 subunit induces large scale disorder-to-order transformations in the enzyme and reveals novel structural features in the covalently bound adduct, *J Biol Chem 281*, 15296-15303.

23. Brandt, G. S., Kneen, M. M., Chakraborty, S., Baykal, A. T., Nemeria, N., Yep, A., Ruby, D. I., Petsko, G. A., Kenyon, G. L., McLeish, M. J., Jordan, F., and Ringe, D. (2009) Snapshot of a reaction intermediate: analysis of benzoylformate decarboxylase in complex with a benzoylphosphonate inhibitor, *Biochemistry 48*, 3247-3257.

24. Nemeria, N. S., Chakraborty, S., Balakrishnan, A., and Jordan, F. (2009) Reaction mechanisms of thiamin diphosphate enzymes: defining states of ionization and tautomerization of the cofactor at individual steps, *FEBS J 276*, 2432-2446.

25. Chakraborty, S., Nemeria, N. S., Balakrishnan, A., Brandt, G. S., Kneen, M. M., Yep, A., McLeish, M. J., Kenyon, G. L., Petsko, G. A., Ringe, D., and Jordan, F. (2009) Detection and time course of formation of major thiamin diphosphate-bound covalent intermediates derived from a chromophoric substrate analogue on benzoylformate decarboxylase, *Biochemistry 48*, 981-994.

26. Kutter, S., Weiss, M. S., Wille, G., Golbik, R., Spinka, M., and Konig, S. (2009) Covalently bound substrate at the regulatory site of yeast pyruvate decarboxylases triggers allosteric enzyme activation, *J Biol Chem 284*, 12136-12144.

27. Reynolds, W. F., Peat, I. R., Freedman, M. H., and Lyerla, J. R. (1973) Determination of the tautomeric form of the imidazole ring of L-histidine in basic solution by carbon-13 magnetic resonance spectroscopy, *J. Am. Chem. Soc. 95*, 328-331.

28. Rabenstein, D. L., and Sayer, T. L. (1976) Carbon-13 chemical shift parameters for amines, carboxylic acids, and amino acids, *J. Magn. Reson. 24*, 27-39.

29. Surprenant, H. L., Sarneski, J. E., Key, R. R., Byrd, J. T., and Reilley, C. N. (1980) Carbon-13 NMR studies of amino acids: Chemical shifts, protonation shifts, microscopic protonation behavior, *J. Magn. Reson. 40*, 231-243.

30. Bachovchin, W. W., and Roberts, J. D. (1978) Nitrogen-15 nuclear magnetic resonance spectroscopy. The state of histidine in the catalytic triad of .alpha.-lytic protease. Implications for the charge-relay mechanism of peptide-bond cleavage by serine proteases, *J. Am. Chem. Soc. 100*, 8041-8047.

31. Sudmeier, J. L., Bradshaw, E. M., Haddad, K. E. C., Day, R. M., Thalhauser, C. J., Bullock, P. A., and Bachovchin, W. W. (2003) Identification of Histidine Tautomers in Proteins by 2D 1H/13CŒ¥2 One-Bond Correlated NMR, *J. Am. Chem. Soc. 125*, 8430-8431.

32. Naito, A., Ganapathy, S., Akasaka, K., and McDowell, C. A. (1981) Chemical shielding tensor and [sup 13]C--[sup 14]N dipolar splitting in single crystals of L-alanine, *J. Chem. Phys. 74*, 3190-3197.

33. Haberkorn, R. A., Stark, R. E., Van Willigen, H., and Griffin, R. G. (1981) Determination of bond distances and bond angles by solid-state nuclear magnetic resonance. Carbon-13 and nitrogen-14 NMR study of glycine, *J. Am. Chem. Soc. 103*, 2534-2539.

34. Smith, S. O., Farr-Jones, S., Griffin, R. G., and Bachovchin, W. W. (1989) Crystal Versus Solution Structures of Enzymes NMR Spectroscopy of a Crystalline Serine Protease, *Science 244*, 961-964.

35. Gu, Z., and McDermott, A. (1993) Chemical shielding anisotropy of protonated and deprotonated carboxylates in amino acids, *J. Am. Chem. Soc. 115*, 4282-4285.

36. Gu, Z., Zambrano, R., and McDermott, A. (1994) Hydrogen Bonding of Carboxyl Groups in Solid-State Amino Acids and Peptides: Comparison of Carbon Chemical Shielding, Infrared Frequencies, and Structures, *J. Am. Chem. Soc. 116*, 6368-6372.

37. Bagno, A., and Scorrano, G. (1996) Site of Ionization of Polyfunctional Bases and Acids. 2. Ab Initio Electric Field Gradients at Nitrogen, Oxygen, Phosphorus, and Sulfur in Neutral and Ionized Forms, *J. Phys. Chem. 100*, 1545-1553.

38. Ooms, K. J., Bolte, S. E., Smee, J. J., Baruah, B., Crans, D. C., and Polenova, T. (2007) Investigating the Vanadium Environments in Hydroxylamido V(V)

Dipicolinate Complexes Using 51V NMR Spectroscopy and Density Functional Theory, *Inorg. Chem. 46*, 9285-9293.

39. Ooms, K., Polenova, T., Shough, A.-M., Doren, D. J., Nash, M. J., and Lobo, R. F. (2009) Identification of Mixed Valence Vanadium in ETS-10 Using Electron Paramagnetic Resonance, 51V Solid-State Nuclear Magnetic Resonance, and Density Functional Theory Studies, *J. Phys. Chem. C 113*, 10477-10484.

40. McDermott, A., and Polenova, T. (2007) Solid state NMR: new tools for insight into enzyme function, *Curr Opin Struct Biol 17*, 617-622.

41. McDermott, A., and Polenova, T. (2010) *Solid State NMR Studies of Biopolymers*, John Wiley & Sons Ltd, Chichester, West Sussex, U.K.

42. Yang, J., Tasayco, M. L., and Polenova, T. (2008) Magic angle spinning NMR experiments for structural studies of differentially enriched protein interfaces and protein assemblies, *J Am Chem Soc 130*, 5798-5807.

43. Sun, S., Siglin, A., Williams, J. C., and Polenova, T. (2009) Solid-state and solution NMR studies of the CAP-Gly domain of mammalian dynactin and its interaction with microtubules, *J Am Chem Soc 131*, 10113-10126.

44. Han, Y., Ahn, J., Concel, J., Byeon, I. J., Gronenborn, A. M., Yang, J., and Polenova, T. (2010) Solid-state NMR studies of HIV-1 capsid protein assemblies, *J Am Chem Soc 132*, 1976-1987.

45. Pooransingh-Margolis, N., Renirie, R., Hasan, Z., Wever, R., Vega, A. J., and Polenova, T. (2006) 51V solid-state magic angle spinning NMR spectroscopy of vanadium chloroperoxidase, *J Am Chem Soc 128*, 5190-5208.

46. Rozovsky, S., and McDermott, A. E. (2007) Substrate product equilibrium on a reversible enzyme, triosephosphate isomerase, *PNAS 104*, 2080-2085.

47. Farr-Jones, S., Smith, S. O., Kettner, C. A., Griffin, R. G., and Bachovchin, W. W. (1989) Crystal versus solution structure of enzymes: NMR spectroscopy of a peptide boronic acid-serine protease complex in the crystalline state, *PNAS 86*, 6922-6924.

48. Smith, S. O., Farr-Jones, S., Griffin, R. G., and Bachovchin, W. W. (1989) Crystal versus solution structures of enzymes: NMR spectroscopy of a crystalline serine protease, *Science 244*, 961-964.

49. Bachovchin, W. W., Kanamori, K., Vallee, B. L., and Roberts, J. D. (1982) Nitrogen-15 nuclear magnetic resonance of arsanilazotyrosine-248 carboxypeptidase A and its complex with beta-phenylpropionate. Structure and dynamics in solution, *Biochemistry 21*, 2885-2892.

50. Bachovchin, W. W., Kaiser, R., Richards, J. H., and Roberts, J. D. (1981) Catalytic mechanism of serine proteases: reexamination of the pH dependence of the histidyl 1J13C2-H coupling constant in the catalytic triad of alpha-lytic protease, *PNAS 78*, 7323-7326.

51. Chan-Huot, M., Sharif, S., Tolstoy, P. M., Toney, M. D., and Limbach, H. H. (2010) NMR studies of the stability, protonation States, and tautomerism of (13)c- and (15)n-labeled aldimines of the coenzyme pyridoxal 5'-phosphate in water, *Biochemistry 49*, 10818-10830.

52. Lai, J., Niks, D., Wang, Y., Domratcheva, T., Barends, T. R., Schwarz, F., Olsen, R. A., Elliott, D. W., Fatmi, M. Q., Chang, C. E., Schlichting, I., Dunn, M. F., and Mueller, L. J. (2010) X-ray and NMR Crystallography in an Enzyme Active Site: The Indoline Quinonoid Intermediate in Tryptophan Synthase, *J Am Chem Soc*.

53. Kern, D., Kern, G., Neef, H., Tittmann, K., Killenberg-Jabs, M., Wikner, C., Schneider, G., and Hubner, G. (1997) How thiamine diphosphate is activated in enzymes, *Science 275*, 67-70.

54. Perrin, D. D., Armarego, W. L. F., and Perrin, D. R. (1980) *Purification of Laboratory Chemicals*, 2nd ed., Pergamon Press Inc., Elmsford, N.Y.

55. Chakraborty, S. (2006) Spectroscopic detection and kinetic charecterization of thiamin-bound intermediates on enzymes., In *Chemistry*, p 318, Rutgers, the State University of New Jersey, Newark, NJ.

56. Todd, A. R., and Bergel, F. (1937) 73. Aneurin. Part VII. A synthesis of aneurin, *Journal of the Chemical Society (Resumed)*, 364-367.

57. Uray, G., Celotto, C., Ibovnik, A., and Zoltewicz, J. A. (1989) Secondary deuterium kinetic isotope effects in the cleavage of thiamin and N-methylthiaminium ion: first

evidence to identify the rate-limiting step, *The Journal of Organic Chemistry 54*, 3941-3945.

58. Contant, P., Forzy, L., Hengartner, U., and Moine, G. (1990) A New Convergent Synthesis of Thiamine Hydrochloride, *Helvetica Chimica Acta 73*, 1300-1305.

59. Nicewonger, R., Costello, C. A., and Begley, T. P. (1996) Mechanistic Studies on Thiaminase I. 3. Stereochemistry of the Thiaminase I and the Bisulfite-Catalyzed Degradation of Chiral Monodeuteriothiamin, *The Journal of Organic Chemistry 61*, 4172-4174.

60. Timm, D. E., Liu, J., Baker, L. J., and Harris, R. A. (2001) Crystal structure of thiamin pyrophosphokinase, *J Mol Biol 310*, 195-204.

61. Li, H. (1999) Studies on the regulatory mechanism of substrate activation in yeast pyruvate decarboxylase., In *Chemitry*, p 274, Rutgers, the State University of New Jersey, Newark, NJ.

62. Bradford, M. M. (1976) A rapid and sensitive method for the quantitation of microgram quantities of protein utilizing the principle of protein-dye binding, *Anal Biochem 72*, 248-254.

63. Holzer, H., Schultz, G., Villar-Palasi, C., and Juntgen-Sell, J. (1956) [Isolation of yeast carboxylase, and study on the activity of the enzyme in the living cell.], *Biochem Z 327*, 331-344.

64. Arjunan, P., Nemeria, N., Brunskill, A., Chandrasekhar, K., Sax, M., Yan, Y., Jordan, F., Guest, J. R., and Furey, W. (2002) Structure of the pyruvate dehydrogenase multienzyme complex E1 component from Escherichia coli at 1.85 A resolution, *Biochemistry 41*, 5213-5221.

65. Arjunan, P., Umland, T., Dyda, F., Swaminathan, S., Furey, W., Sax, M., Farrenkopf, B., Gao, Y., Zhang, D., and Jordan, F. (1996) Crystal structure of the thiamin diphosphate-dependent enzyme pyruvate decarboxylase from the yeast Saccharomyces cerevisiae at 2.3 A resolution, *J Mol Biol 256*, 590-600.

66. Frank, R. A., Price, A. J., Northrop, F. D., Perham, R. N., and Luisi, B. F. (2007) Crystal structure of the E1 component of the Escherichia coli 2-oxoglutarate dehydrogenase multienzyme complex, *J Mol Biol 368*, 639-651.

67. Neue, G., and Dybowski, C. (1997) Determining temperature in a magic-angle spinning probe using the temperature dependence of the isotropic chemical shift of lead nitrate, *Solid State Nucl. Magn. Reson. 7*, 333-336.

68. Bennett, A. E., Rienstra, C. M., Auger, M., Lakshmi, K. V., and Griffin, R. G. (1995) Heteronuclear decoupling in rotating solids, *J. Chem. Phys. 103*, 6951-6958.

69. Herzfeld, J., and Berger, A. E. (1980) Sideband intensities in NMR spectra of samples spinning at the magic angle, *J. Chem. Phys. 73*, 6021-6030.

70. Chan, J. C. C., and Tycko, R. (2003) Recoupling of chemical shift anisotropies in solid-state NMR under high-speed magic-angle spinning and in uniformly C-13-labeled systems, *Journal of Chemical Physics 118*, 8378-8389.

71. States, D. J., Haberkorn, R. A., and Ruben, D. J. (1982) A Two-Dimensional Nuclear Overhauser Experiment with Pure Absorption Phase in 4 Quadrants, *J. Magn. Reson. 48*, 286-292.

72. Wylie, B. J., Franks, W. T., and Rienstra, C. M. (2006) Determinations of N-15 chemical shift anisotropy magnitudes in a uniformly N-15, C-13-labeled microcrystalline protein by three-dimensional magic-angle spinning nuclear magnetic resonance spectroscopy, *J. Phys. Chem. B 110*, 10926-10936.

73. Arduengo, A. J., Goerlich, J. R., and Marshall, W. J. (1997) A Stable Thiazol-2-ylidene and Its Dimer, *Liebigs Annalen 1997*, 365-374.

74. Baburina, I., Li, H., Bennion, B., Furey, W., and Jordan, F. (1998) Interdomain information transfer during substrate activation of yeast pyruvate decarboxylase: the interaction between cysteine 221 and histidine 92, *Biochemistry 37*, 1235-1244.

75. Baburina, I., Gao, Y., Hu, Z., Jordan, F., Hohmann, S., and Furey, W. (1994) Substrate activation of brewers' yeast pyruvate decarboxylase is abolished by mutation of cysteine 221 to serine, *Biochemistry 33*, 5630-5635.

76. Baburina, I., Dikdan, G., Guo, F., Tous, G. I., Root, B., and Jordan, F. (1998) Reactivity at the substrate activation site of yeast pyruvate decarboxylase: inhibition by distortion of domain interactions, *Biochemistry 37*, 1245-1255.

77. Hubner, G., Weidhase, R., and Schellenberger, A. (1978) The mechanism of substrate activation of pyruvate decarboxylase: a first approach, *Eur J Biochem 92*, 175-181.

78. O'Brien, T. A., Kluger, R., Pike, D. C., and Gennis, R. B. (1980) Phosphonate analogues of pyruvate. Probes of substrate binding to pyruvate oxidase and other thiamin pyrophosphate-dependent decarboxylases, *Biochim Biophys Acta 613*, 10-17.

79. Kluger, R., and Pike, D. C. (1977) Active site generated analogues of reactive intermediates in enzymic reactions. Potent inhibition of pyruvate dehydrogenase by a phosphonate analogue of pyruvate1, *J Am Chem Soc 99*, 4504-4506.

80. Nemeria, N. S., Korotchkina, L. G., Chakraborty, S., Patel, M. S., and Jordan, F. (2006) Acetylphosphinate is the most potent mechanism-based substrate-like inhibitor of both the human and Escherichia coli pyruvate dehydrogenase components of the pyruvate dehydrogenase complex, *Bioorg Chem 34*, 362-379.

81. Gallo, A. A., and Sable, H. Z. (1976) Carbon 13 magnetic resonance studies of DL-2-(alpha-hydroxyethyl) thiamin and related compounds. Relation of kinetic acidity to electronic factors in thiamin catalysis, *J Biol Chem 251*, 2564-2570.

82. Sharif, S., Fogle, E., Toney, M. D., Denisov, G. S., Shenderovich, I. G., Buntkowsky, G., Tolstoy, P. M., Huot, M. C., and Limbach, H. H. (2007) NMR localization of protons in critical enzyme hydrogen bonds, *J Am Chem Soc 129*, 9558-9559.

83. Sharif, S., Denisov, G. S., Toney, M. D., and Limbach, H. H. (2007) NMR studies of coupled low- and high-barrier hydrogen bonds in pyridoxal-5'-phosphate model systems in polar solution, *J Am Chem Soc 129*, 6313-6327.

84. Sharif, S., Schagen, D., Toney, M. D., and Limbach, H. H. (2007) Coupling of functional hydrogen bonds in pyridoxal-5'-phosphate-enzyme model systems observed by solid-state NMR spectroscopy, *J Am Chem Soc 129*, 4440-4455.

85. Nemeria, N. S., Arjunan, P., Chandrasekhar, K., Mossad, M., Tittmann, K., Furey, W., and Jordan, F. (2010) Communication between thiamin cofactors in the Escherichia coli pyruvate dehydrogenase complex E1 component active centers: evidence for a "direct pathway" between the 4'-aminopyrimidine N1' atoms, *J Biol Chem 285*, 11197-11209.

86. Gao, Y. (2000) Mechanism of pyruvate decarboxylase: site-directed mutagenesis studies on Glu51, In *Department of Chemistry*, p 159, Rutgers University, Newark, NJ.

87. Jordan, F., Adams, J., Farzami, B., and Kudzin, Z. H. (1986) Conjugated α-Keto Acids as Mechanism-Based Inactivators of Brewer's Yeast Pyruvate Decarboxylase Electronic effects of Substituents and Detection of a Long-Lived Intermediate, *Journal of Enzyme Inhibition and Medicinal Chemistry 1*, 139-149.

88. Stephens, P., Darlison, M., Lewis, H., and Guest, J. (1983) The pyruvate dehydrogenase complex of Escherichia coli K12. Nucleotide sequence encoding the pyruvate dehydrogenase component, *Eur J Biochem 133*, 155-162.

89. Stephens, P., Darlison, M., Lewis, H., and Guest, J. (1983) The pyruvate dehydrogenase complex of Escherichia coli K12. Nucleotide sequence encoding the dihydrolipoamide acetyltransferase component, *Eur J Biochem 133*, 481-489.

90. Stephens, P., Lewis, H., Darlison, M., and Guest, J. (1983) Nucleotide sequence of the lipoamide dehydrogenase gene of Escherichia coli K12, *Eur J Biochem 135*, 519-527.

91. Koike, M., Reed, L. J., and Carroll, W. R. (1960) alpha-Keto acid dehydrogenation complexes. I. Purification and properties of pyruvate and alpha-ketoglutarate dehydrogenation complexes of Escherichia coli, *J Biol Chem 235*, 1924-1930.

92. Gunsalus, I. C. (1954) *in The Mechanism of Enzyme Action (McElvoy, W. D., and Glass, B., eds) The Johns Hopkins University Press, Baltimore, MD*, pp. 545-580.

93. Massey, V. (1963) *in The Enzymes (Boyer, P. D., Lardy, H., and Myrback, K., eds) Academic Press, New York 2nd Ed*, pp. 275-305.

94. Reed, L. J. (1974) Multienzyme complexes, *Acc. Chem. Res. 7*, 40-46.

95. Seifert, F., Ciszak, E., Korotchkina, L., Golbik, R., Spinka, M., Dominiak, P., Sidhu, S., Brauer, J., Patel, M. S., and Tittmann, K. (2007) Phosphorylation of serine 264 impedes active site accessibility in the E1 component of the human pyruvate dehydrogenase multienzyme complex, *Biochemistry 46*, 6277-6287.

96. Seifert, F., Golbik, R., Brauer, J., Lilie, H., Schroder-Tittmann, K., Hinze, E., Korotchkina, L. G., Patel, M. S., and Tittmann, K. (2006) Direct kinetic evidence for half-of-the-sites reactivity in the E1 component of the human pyruvate dehydrogenase multienzyme complex through alternating sites cofactor activation, *Biochemistry 45*, 12775-12785.

97. Nemeria, N., Tittmann, K., Joseph, E., Zhou, L., Vazquez-Coll, M. B., Arjunan, P., Hubner, G., Furey, W., and Jordan, F. (2005) Glutamate 636 of the Escherichia coli pyruvate dehydrogenase-E1 participates in active center communication and behaves as an engineered acetolactate synthase with unusual stereoselectivity, *J Biol Chem 280*, 21473-21482.

98. Nemeria, N., Arjunan, P., Brunskill, A., Sheibani, F., Wei, W., Yan, Y., Zhang, S., Jordan, F., and Furey, W. (2002) Histidine 407, a phantom residue in the E1 subunit of the Escherichia coli pyruvate dehydrogenase complex, activates reductive acetylation of lipoamide on the E2 subunit. An explanation for conservation of active sites between the E1 subunit and transketolase, *Biochemistry 41*, 15459-15467.

99. Kale, S., and Jordan, F. (2009) Conformational ensemble modulates cooperativity in the rate-determining catalytic step in the E1 component of the Escherichia coli pyruvate dehydrogenase multienzyme complex, *J Biol Chem 284*, 33122-33129.

100. Kale, S., Ulas, G., Song, J., Brudvig, G. W., Furey, W., and Jordan, F. (2008) Efficient coupling of catalysis and dynamics in the E1 component of Escherichia coli pyruvate dehydrogenase multienzyme complex, *PNAS 105*, 1158-1163.

101. Kale, S., Arjunan, P., Furey, W., and Jordan, F. (2007) A dynamic loop at the active center of the Escherichia coli pyruvate dehydrogenase complex E1 component modulates substrate utilization and chemical communication with the E2 component, *J Biol Chem 282*, 28106-28116.

102. Wei, W., Li, H., Nemeria, N., and Jordan, F. (2003) Expression and purification of the dihydrolipoamide acetyltransferase and dihydrolipoamide dehydrogenase subunits of the Escherichia coli pyruvate dehydrogenase multienzyme complex: a mass spectrometric assay for reductive acetylation of dihydrolipoamide acetyltransferase, *Protein Expression and Purification 28*, 140-150.

103. Nemeria, N., Volkov, A., Brown, A., Yi, J., Zipper, L., Guest, J. R., and Jordan, F. (1998) Systematic study of the six cysteines of the E1 subunit of the pyruvate

dehydrogenase multienzyme complex from Escherichia coli: none is essential for activity, *Biochemistry 37*, 911-922.

104. Nemeria, N., Yan, Y., Zhang, Z., Brown, A. M., Arjunan, P., Furey, W., Guest, J. R., and Jordan, F. (2001) Inhibition of the Escherichia coli pyruvate dehydrogenase complex E1 subunit and its tyrosine 177 variants by thiamin 2-thiazolone and thiamin 2-thiothiazolone diphosphates. Evidence for reversible tight-binding inhibition, *J Biol Chem 276*, 45969-45978.

105. Meyer, D., Neumann, P., Parthier, C., Friedemann, R., Nemeria, N., Jordan, F., and Tittmann, K. (2010) Double duty for a conserved glutamate in pyruvate decarboxylase: evidence of the participation in stereoelectronically controlled decarboxylation and in protonation of the nascent carbanion/enamine intermediate, *Biochemistry 49*, 8197-8212.

106. Asztalos, P., Parthier, C., Golbik, R., Kleinschmidt, M., Hubner, G., Weiss, M. S., Friedemann, R., Wille, G., and Tittmann, K. (2007) Strain and near attack conformers in enzymic thiamin catalysis: X-ray crystallographic snapshots of bacterial transketolase in covalent complex with donor ketoses xylulose 5-phosphate and fructose 6-phosphate, and in noncovalent complex with acceptor aldose ribose 5-phosphate, *Biochemistry 46*, 12037-12052.

107. Tittmann, K., Vyazmensky, M., Hubner, G., Barak, Z., and Chipman, D. M. (2005) The carboligation reaction of acetohydroxyacid synthase II: steady-state intermediate distributions in wild type and mutants by NMR, *PNAS 102*, 553-558.

108. Zhang, S. (2003) In *Graduate School Newark* Rutgers, the State University of New Jersey, Newark, NJ.

109. Tittmann, K., Proske, D., Spinka, M., Ghisla, S., Rudolph, R., Hubner, G., and Kern, G. (1998) Activation of thiamin diphosphate and FAD in the phosphatedependent pyruvate oxidase from Lactobacillus plantarum, *J Biol Chem 273*, 12929-12934.

110. Zhang, S., Zhou, L., Nemeria, N., Yan, Y., Zhang, Z., Zou, Y., and Jordan, F. (2005) Evidence for dramatic acceleration of a C-H bond ionization rate in thiamin diphosphate enzymes by the protein environment, *Biochemistry 44*, 2237-2243.

111. Gruys, K. J., Datta, A., and Frey, P. A. (1989) 2-Acetylthiamin pyrophosphate (acetyl-TPP) pH-rate profile for hydrolysis of acetyl-TPP and isolation of acetyl-TPP as a transient species in pyruvate dehydrogenase catalyzed reactions, *Biochemistry 28*, 9071-9080.

112. Flournoy, D. S., and Frey, P. A. (1986) Pyruvate dehydrogenase and 3-fluoropyruvate: chemical competence of 2-acetylthiamin pyrophosphate as an acetyl group donor to dihydrolipoamide, *Biochemistry 25*, 6036-6043.

113. Cleland, W. W. (1975) Partition analysis and the concept of net rate constants as tools in enzyme kinetics, *Biochemistry 14*, 3220-3224.

114. Fersht, A. (1998) In *Structure and mechanism in protein science: a guide to enzyme catalysis and protein folding*, pp 123-125, W.H. Freeman and Company, New York.

115. Argyrou, A., Blanchard, J. S., and Palfey, B. A. (2002) The lipoamide dehydrogenase from Mycobacterium tuberculosis permits the direct observation of flavin intermediates in catalysis, *Biochemistry 41*, 14580-14590.

116. Sahlman, L., and Williams, C. H., Jr. (1989) Lipoamide dehydrogenase from Escherichia coli. Steady-state kinetics of the physiological reaction, *J Biol Chem 264*, 8039-8045.

117. Jones, D. D., Stott, K. M., Howard, M. J., and Perham, R. N. (2000) Restricted motion of the lipoyl-lysine swinging arm in the pyruvate dehydrogenase complex of Escherichia coli, *Biochemistry 39*, 8448-8459.

118. Berg, A., Westphal, A. H., Bosma, H. J., and de Kok, A. (1998) Kinetics and specificity of reductive acylation of wild-type and mutated lipoyl domains of 2-oxo-acid dehydrogenase complexes from Azotobacter vinelandii, *Eur J Biochem 252*, 45-50.

119. Burbaum, J. J., Raines, R. T., Albery, W. J., and Knowles, J. R. (1989) Evolutionary optimization of the catalytic effectiveness of an enzyme, *Biochemistry 28*, 9293-9305.

120. Boiteux, A., and Hess, B. (1970) Allosteric properties of yeast pyruvate decarboxylase, *FEBS Lett 9*, 293-296.

121. Hubner, G., Konig, S., and Schellenberger, A. (1988) The functional role of thiol groups of pyruvate decarboxylase from brewer's yeast, *Biomed Biochim Acta 47*, 9-18.

122. Sergienko, E. A., and Jordan, F. (2002) Yeast pyruvate decarboxylase tetramers can dissociate into dimers along two interfaces. Hybrids of low-activity D28A (or D28N) and E477Q variants, with substitution of adjacent active center acidic groups from different subunits, display restored activity, *Biochemistry 41*, 6164-6169.

123. Konig, S., Svergun, D., Koch, M. H., Hubner, G., and Schellenberger, A. (1993) The influence of the effectors of yeast pyruvate decarboxylase (PDC) on the conformation of the dimers and tetramers and their pH-dependent equilibrium, *Eur Biophys J 22*, 185-194.

124. Killenberg-Jabs, M., Jabs, A., Lilie, H., Golbik, R., and Hubner, G. (2001) Active oligomeric states of pyruvate decarboxylase and their functional characterization, *Eur J Biochem 268*, 1698-1704.

125. Muller, Y. A., Lindqvist, Y., Furey, W., Schulz, G. E., Jordan, F., and Schneider, G. (1993) A thiamin diphosphate binding fold revealed by comparison of the crystal structures of transketolase, pyruvate oxidase and pyruvate decarboxylase, *Structure 1*, 95-103.

126. Dyda, F., Furey, W., Swaminathan, S., Sax, M., Farrenkopf, B., and Jordan, F. (1993) Catalytic centers in the thiamin diphosphate dependent enzyme pyruvate decarboxylase at 2.4-A resolution, *Biochemistry 32*, 6165-6170.

127. Liu, M., Sergienko, E. A., Guo, F., Wang, J., Tittmann, K., Hubner, G., Furey, W., and Jordan, F. (2001) Catalytic acid-base groups in yeast pyruvate decarboxylase. 1. Site-directed mutagenesis and steady-state kinetic studies on the enzyme with the D28A, H114F, H115F, and E477Q substitutions, *Biochemistry 40*, 7355-7368.

128. Sergienko, E. A., and Jordan, F. (2001) Catalytic acid-base groups in yeast pyruvate decarboxylase. 3. A steady-state kinetic model consistent with the behavior of both wild-type and variant enzymes at all relevant pH values, *Biochemistry 40*, 7382-7403.

129. Baykal, A., Chakraborty, S., Dodoo, A., and Jordan, F. (2006) Synthesis with good enantiomeric excess of both enantiomers of alpha-ketols and acetolactates by two thiamin diphosphate-dependent decarboxylases, *Bioorg Chem 34*, 380-393.

130. Sergienko, E. A., and Jordan, F. (2001) Catalytic acid-base groups in yeast pyruvate decarboxylase. 2. Insights into the specific roles of D28 and E477 from the rates and stereospecificity of formation of carboligase side products, *Biochemistry 40*, 7369-7381.

131. Kutter, S., Wille, G., Relle, S., Weiss, M. S., Hubner, G., and Konig, S. (2006) The crystal structure of pyruvate decarboxylase from Kluyveromyces lactis. Implications for the substrate activation mechanism of this enzyme, *FEBS J 273*, 4199-4209.

132. Li, H., and Jordan, F. (1999) Effects of substitution of tryptophan 412 in the substrate activation pathway of yeast pyruvate decarboxylase, *Biochemistry 38*, 10004-10012.

133. Li, H., Furey, W., and Jordan, F. (1999) Role of glutamate 91 in information transfer during substrate activation of yeast pyruvate decarboxylase, *Biochemistry 38*, 9992-10003.

134. Jordan, F., Nemeria, N., Guo, F., Baburina, I., Gao, Y., Kahyaoglu, A., Li, H., Wang, J., Yi, J., Guest, J. R., and Furey, W. (1998) Regulation of thiamin diphosphate-dependent 2-oxo acid decarboxylases by substrate and thiamin diphosphate.Mg(II) - evidence for tertiary and quaternary interactions, *Biochim Biophys Acta 1385*, 287-306.

135. Perrin, D. D., Armarego, W.L.F., and Perrin, D.R. (1980) *Purification of Laboratory Chemicals*, 2nd ed., Pergamon Press, New York.

136. Baillie, A. C., Wright, B.J., Wright, K. (1982) Process for preparing new herbicidally, fungicidally or insecticidally active compounds, FBC Limited (Cambridge, GB2), United States.

137. Wang, J., Golbik, R., Seliger, B., Spinka, M., Tittmann, K., Hubner, G., and Jordan, F. (2001) Consequences of a modified putative substrate-activation site on catalysis by yeast pyruvate decarboxylase, *Biochemistry 40*, 1755-1763.

138. Joseph, E., Wei, W., Tittmann, K., and Jordan, F. (2006) Function of a conserved loop of the beta-domain, not involved in thiamin diphosphate binding, in catalysis and substrate activation in yeast pyruvate decarboxylase, *Biochemistry 45*, 13517-13527.

139. Alvarez, F. J., Ermer, J., Huebner, G., Schellenberger, A., and Schowen, R. L. (1991) Catalytic power of pyruvate decarboxylase. Rate-limiting events and microscopic rate constants from primary carbon and secondary hydrogen isotope effects, *J. Am. Chem. Soc. 113*, 8402-8409.

140. Wei, W., Liu, M., and Jordan, F. (2002) Solvent kinetic isotope effects monitor changes in hydrogen bonding at the active center of yeast pyruvate decarboxylase concomitant with substrate activation: the substituent at position 221 can control the state of activation, *Biochemistry 41*, 451-461.

141. Sergienko, E. A., and Jordan, F. (2002) New model for activation of yeast pyruvate decarboxylase by substrate consistent with the alternating sites mechanism: demonstration of the existence of two active forms of the enzyme, *Biochemistry 41*, 3952-3967.

142. Versees, W., Spaepen, S., Wood, M. D., Leeper, F. J., Vanderleyden, J., and Steyaert, J. (2007) Molecular mechanism of allosteric substrate activation in a thiamine diphosphate-dependent decarboxylase, *J Biol Chem 282*, 35269-35278.

143. Frank, R. A., Titman, C. M., Pratap, J. V., Luisi, B. F., and Perham, R. N. (2004) A molecular switch and proton wire synchronize the active sites in thiamine enzymes, *Science 306*, 872-876.

144. Jordan, F., Arjunan, P., Kale, S., Nemeria, N. S., and Furey, W. (2009) Multiple roles of mobile active center loops in the E1 component of the Escherichia coli pyruvate dehydrogenase complex - Linkage of protein dynamics to catalysis, *J Mol Catal B Enzym 61*, 14-22.

145. System, W. P. M. D. P. (2005) *T e c h n i c a l B u l l e t i n TB117*.

APPENDIX

CHAPTER 1

RESULTS

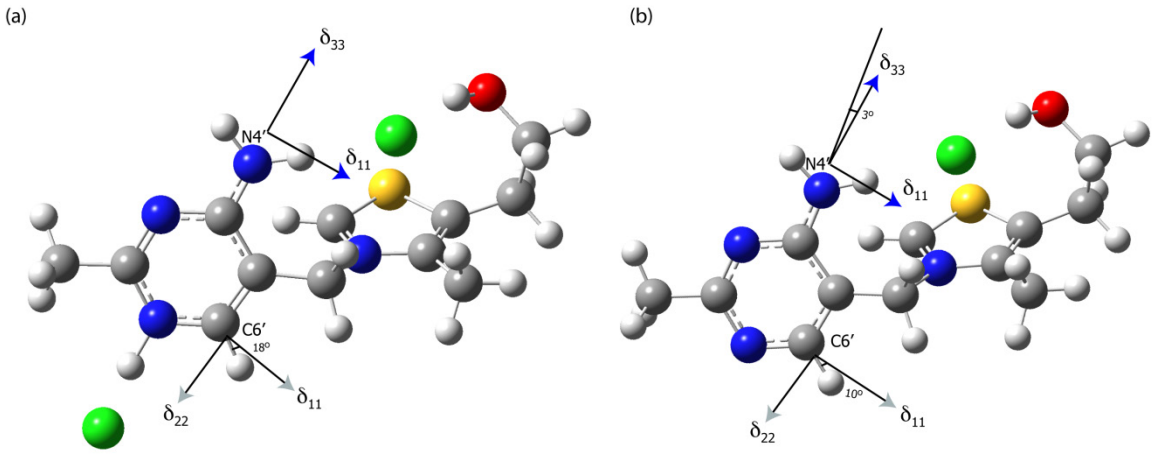

Figure A1. Structures of Th•HCl (a) and Th (b) used for DFT calculations and depicting orientations of C6' and N4' CSA tensors. For both atoms, the third principal component (δ_{33} for C6', δ_{22} for N4') is perpendicular to the 4'-aminopyrimidine plane.

Table A1. Experimental and Computed ^{13}C and ^{15}N CSA Parameters for 2,6'-^{13}C/4'-^{15}N Th•HCl and Th. (next page). Experiment performed by Dr. Olga Dmitrenko and Mr. Sivakumar Paramasivam at the Department of Chemistry & Biochemistry, University of Delaware, Newark, DE. Data reproduced here with permission.

Sample	Atom	Method	δ_{iso} (ppm	δ_σ (ppm)	η_σ	δ_{11} (ppm	δ_{22} (ppm	δ_{33} (ppm
Th•HCl	C2	Slow-MAS	153.4	-98.5 ± 1.6	0.59 ± 0.0	231.7	173.6	54.9
		ROCSA	153.4	-103.8 ± 5.(	0.61 ± 0.0	237.0	173.6	49.6
		DFT/with Cl^-	154.9	-105.9	0.80	250.2	165.5	49.0
		DFT/without Cl	158.7	110.3	1.00	269.0	158.7	48.4
	C6’	Slow-MAS	147.8	-109.6 ± 4.:	0.78 ± 0.0	245.3	159.9	38.2
		ROCSA	147.8	-111.3 ± 7.:	0.81 ± 0.0	248.5	158.4	36.5
		DFT/with Cl^-	153.7	-114.0	0.87	260.3	161.1	39.7
		DFT/without Cl	149.7	-110.2	0.88	253.3	156.3	39.5
	N4’	ROCSA	116.5	74.9 ± 3.5	0.27 ± 0.0	191.4	89.2	68.9
		DFT/with Cl^-	113.1	70.8	0.11	183.9	81.6	73.8
		DFT/without Cl	103.8	78.4	0.25	182.2	74.4	54.8
Th	C2	Slow-MAS	156.5	-100.8 ± 1.:	0.66 ± 0.0	240.2	173.6	55.7
		ROCSA	156.5	-103.1 ± 6.(	0.62 ± 0.0	240.0	176.1	53.4
		DFT/with Cl^-	155.6	-107.0	0.75	249.2	169.0	48.6
		DFT/without Cl	162.8	-114.9	0.80	266.2	174.3	47.9
	C6’	Slow-MAS	160.4	-107.8 ± 2.:	0.92 ± 0.0	263.9	164.7	52.6
		ROCSA	160.4	-108.7 ± 5.(	0.93 ± 0.0	265.3	164.2	51.7
		DFT/with Cl^-	162.2	109.2	0.90	271.4	156.7	58.5
		DFT/without Cl	163.4	-108.6	0.99	271.5	163.9	54.8
	N4’	ROCSA	91.2	59.6 ± 2.6	0.28 ± 0.0	150.8	69.7	53.1
		DFT/with Cl^-	98.2	59.5	0.51	157.7	83.6	53.3
		DFT/without Cl	70.2	-56.2	0.90	123.5	73.0	14.0

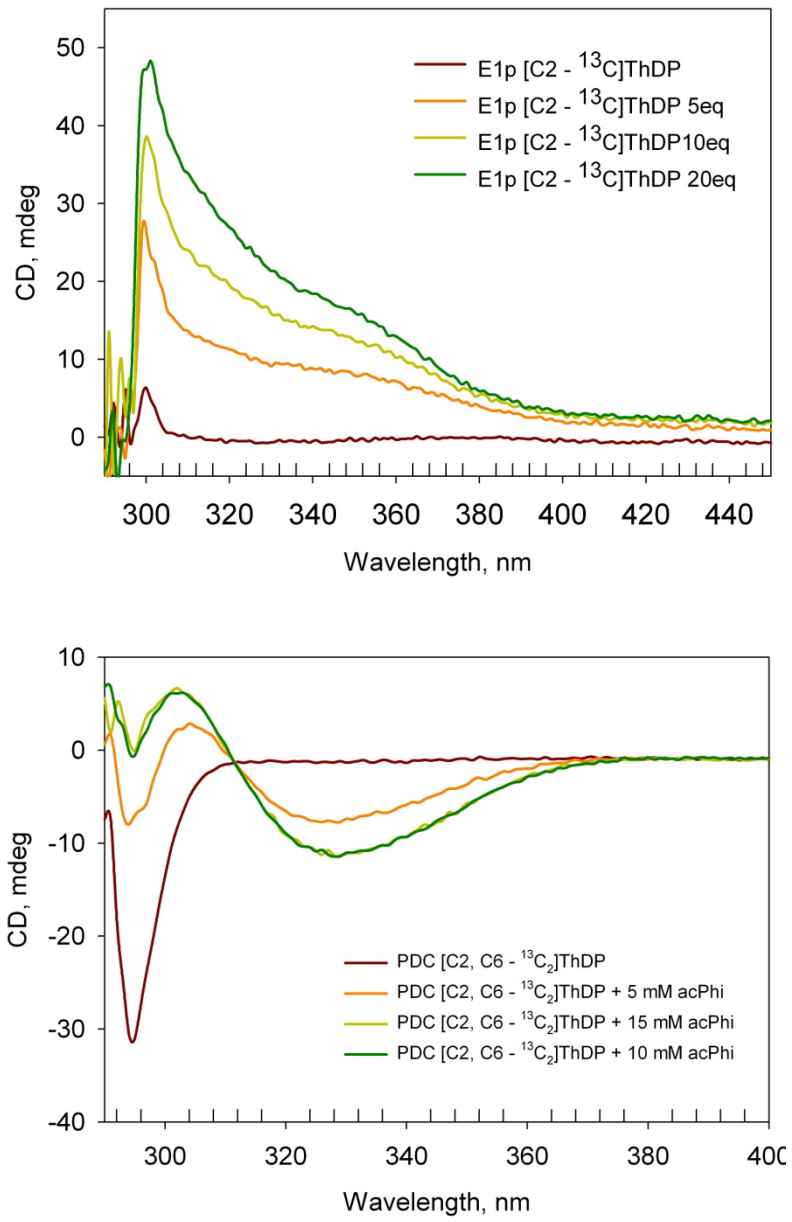

Figure A2. Representative CD spectra of E1p and YPDC SSNMR samples

CD spectra of titration of (Top) E1p (15 mg/mL, 0.15 mM active centers) reconstituted with [C2 – ^{13}C]ThDP titrated with MAP (0.15 – 10 mM) in 20 mM KH_2PO_4 pH 7.0 buffer containing additional 10 mM Mg^{2+}. (Bottom) YPDC (15 mg/mL) reconstituted wit [C2, C6' – $^{13}C_2$]ThDP titrated with acetylphosphinate (5 – 15 mM) in 20 mM MES pH 6.0 buffer containing additional 20 mM Mg^{2+}.

CHAPTER 2

MATERIALS AND METHODS

Calibration and Test reaction of Kintek Rapid Chemical Quench Flow-3 (RQF-3)

All loop volumes were calibrated using Bromophenol Blue following a protocol for calibration using an absorbance standard as described in the manual accompanying the instrument. (Chemical Quench Flow Instruction Manual, Version 6.4, Published on April 1, 2008 by KinTek Corporation, Austin, TX). The calibrations were further tested by performing a test reaction recommended by the manufacturer. The reaction involved base catalysed pseudo first decay of Benzimidinemalanonitrile (BMN; λ_{max} = 310 nm). The test reaction was performed using RQF-3 for two quench methods: (i) constant quench method and (ii) large volume quench method. The decay rates were comparable to rates determined independently for the same reaction on SX-20MV Stopped-flow PDA instrument (Applied Photophysics, Leatherhead, U.K.) and to rate reported in the literature (140 s^{-1}).

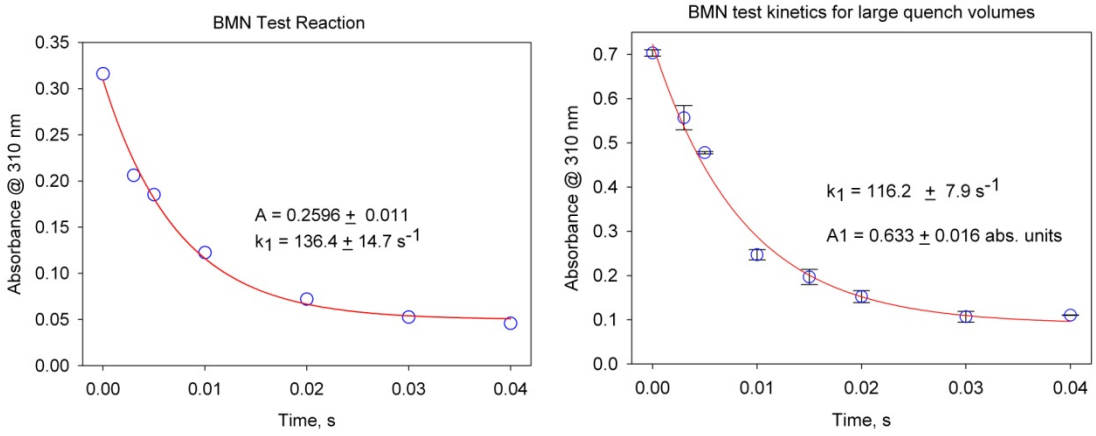

Figure A3. Kinetics of base catalysed decomposition of BMN. Left: Constant quench, Right: Large quench volumes (reagents are loaded into drive syringes directly).

Plasmid Isolation

Plasmid purification was carried out as per protocol for Wizard® *Plus* Minipreps DNA purification system (*145*).

1. Pellet 5-10 ml of cells by centrifugation at 1,400 × g for 10 min. Pour off the supernatant and blot the tube upside-down on a paper towel to remove excess media.

2. Completely resuspend the cell pellet in 400 µl of Cell Resuspension Solution. Transfer the resuspended cells to a 1.5 ml microcentrifuge tube.

3. Add 400 µl of Cell Lysis Solution and mix by inverting the tube 4 times. The cell suspension should clear immediately.

4. Add 400 µl of Neutralization Solution and mix by inverting the tube several times. Alternatively, if using an EndA+ strain, add 800 µl of Neutralization Solution, mix by inverting the tube 4 times and incubate at room temperature for 10 min.

5. Centrifuge the lysate at 10,000 × g in a microcentrifuge for 5 min. If a pellet has not formed by the end of the centrifugation, centrifuge an additional 15 min.

6. Pipet 1ml of the resuspended resin into each barrel of the Minicolumn/ syringe assembly. (If crystals or aggregates are present, dissolve by warming the resin to 25-37°C for 10 min. Cool to 30°C before use). Thoroughly mix the Wizard® Minipreps DNA Purification Resin before removing an aliquot.

7. Carefully remove all the cleared lysate from each miniprep and transfer it to the barrel of the Minicolumn/syringe assembly containing the resin. No mixing is required at this stage. The resin and lysate should be in contact only for the time it takes to load the Minicolumns.

8. Open the stopcocks and apply a vacuum of at least 15 inches of Hg to pull the resin/lysate mix into the Minicolumn. When the entire sample has completely passed through the column, break the vacuum at the source.

If using an EndA+ strain, add 2ml of 40% isopropanol/4.2M guanidine hydrochloride solution to each column. Apply a vacuum and continue it for 30 s after all of the solution has flowed through the columns. Note that this solution will flow through the column more slowly than the standard Column Wash Solution. After this wash proceed with the standard column wash procedure (Step 9).

9. Add 2 ml of the Column Wash Solution (containing 95% ethanol) to the Syringe Barrel and reapply the vacuum to draw the solution through the Minicolumn.

10. Dry the resin by continuing to draw a vacuum for 30 s after the solution has been pulled through the column. Do not dry the resin for more than 30 s. Remove the Syringe Barrel and transfer the Minicolumn to a 1.5 ml microcentrifuge tube. Centrifuge the Minicolumn at 10,000 × *g* in a microcentrifuge for 2 min to remove any residual Column Wash Solution.

11. Transfer the Minicolumn to a new microcentrifuge tube. Add 50 µl of nuclease-free water to the Minicolumn and wait 1 min. Centrifuge the tube at 10,000 × *g* in a microcentrifuge for 20 s to elute the DNA. The DNA will remain intact on the Minicolumn for up to 30 min; however, prompt elution will minimize nicking of plasmids in the range of 20kb. For elution of large plasmids (≥10kb), the use of water preheated to 65-70°C may increase yields. For plasmids ≥20kb, use water preheated to 80°C.

7. Remove and discard the Minicolumn. DNA is stable in water without addition of buffer if stored at -20°C or below. DNA is stable at 4°C in TE buffer. To store the DNA in TE buffer, add 5 µl of 10X TE buffer to the 50 µl of eluted DNA.

8. Concentration of plasmids was estimated using ε= 0.050 at 260nm.

Transformation

1. The required number of competent cell tubes from *Singles*™ *Kits* previously stored at -80 °C were thawed on ice.

2. After the cells thawed each tube was flicked 1–2 times to evenly resuspend the cells. The cells are then ready for the addition of the DNA.

3. To each tube containing competent cells, 1-2 µL of purified plasmid DNA was directly added. After gentle stirring, the mix was incubated on ice for 5 minutes. This procedure was repeated for all samples.

4. Now, the samples were warmed on 42 °C water bath for 30 seconds with no shaking. This "heat shock" step is most easily accomplished if the tubes are in a floating rack in which the lower half of the tubes is exposed. The rack is placed in the water bath so that the lower half of the tubes are submerged for 30 s, and then replaced on ice.

5. The tubes were returned to ice for 2 minutes.

6. 250 µL SOC medium thawed at room temperature was added to each sample.

7. The samples were now incubated at 37°C while shaking at 250 rpm for 60 min prior to plating on selective media.

7. Selection for transformants was accomplished by plating on LB medium containing ampicillin. Since the appropriate amount of transformation mixture to plate varies with the efficiency of both the ligation and the competent cells, 5–100 µl of each transformation was plated on LB medium containing ampicillin (50 µg/mL). When plating less than 25 µl, first, 40–60 µl SOC was transferred onto the plate and then the cells were transferred into the SOC.

8. The plating spreader (bent glass rod or equivalent) was immersed into ethanol and flamed to sterilize. After the flame is extinguished, the spreader was allowed to cool for approximately 10 seconds. To further cool the spreader, it was brought into contact with the inside of the plate cover.

9. Now, the spreader was brought into contact with the pool of cells and the plate was rotated slowly.

10. The sample was evenly distributed on the plate. Care was taken not to spread to dryness as it could be lethal to cells, instead, after spreading briefly, the plates were set on the bench for several minutes to allow excess liquid to be absorbed, and then inverted and incubated overnight at 37°C.

Expression control

For efficient target protein purification it is desirable to have working cell banks which express the target protein in abundance and under tight control of the inducer. The induction period also has to be optimized to avoid damage to the expressed target protein within the cells upon prolonged incubation.

1. An isolated single colony was picked with a sterilized tooth pick from fresh plates containing cells freshly transformed with plasmid DNA of interest and a copy was made

by touching onto a fresh LB plate containing ampicillin (50 µg/mL). The tooth pick was now introduced into 2 mL of LB medium containing ampicillin (50 µg/mL) in a 15 mL tube. The procedure was repeated for multiple colonies.

2. The culture was grown for 14-16 hours at 37 °C while shaking in an incubator at 250 rpm.

3. 10 mL of fresh LB medium was inoculated with 200 µL of this overnight culture and incubated at 37 °C while shaking in at 250 rpm. After the culture reached early log phase (O.D. = 0.6-0.8) target protein overexpression was induced by adding 1.0 mM IPTG and incubated for another 8 hours.

4. Samples of 1 mL each were taken from the cultures at 0, 2, 4, 6, and 8 hours for analysis by SDS-PAGE.

5. The samples were centrifuged at 5000 rpm, the supernatant discarded and the cell pellets were resuspended in 1 mL de-ionized water and centrifuged again. The washed cell pellet was now resuspended in 200 µL de-ionized water.

6. To this suspension, equal volume of SDS sample buffer was added and the samples were boiled at 95 °C for 4 minutes. After cooling the samples were centrifuged at 14000 rpm to remove insoluble material, and the supernatant was collected.

7. The supernatant was applied on SDS-PAGE gel and colonies corresponding to samples showing good expression of target protein were used for further cell bank preparation. Also, the overexpression time was noted for sample corresponding to best expression of target protein.

8. 10 mL cultures in LB medium containing ampicillin (50 µg/mL) were inoculated from copies of best colonies as determined above. The cultures were incubated with

shaking at 250 rpm overnight at 37 °C. 100 µL aliquots from these cultures were mixed with 100 µL glycerol and stored frozen at -80 °C.

SDS PAGE

Determination of the purity of the FPLC and HPLC protein fractions was done using SDS PAGE. The procedure for gel casting was essentially similar to that described in Mini-PROTEAN® 3 Cell Instruction Manual (www.biorad.com, bulletin # 4006157B). Briefly, separations were done on a 7.5 % Laemmli Buffer System. Separating gel was prepared by combining 2.50 ml of 30 % acrylamide/ Bis stock solution in 4.85 ml of deionized water, 2.50 ml of 1.5 M Tris-HCl (pH 8.8), 100 µl of 10 % SDS and 50 µl of 10% APS. Polymerization was initiated by adding 5.0 µl of TEMED. The resulting solution was added immediately to the preassembled cast, overlaid with 1 ml DI water and allowed to solidify for 20 min at room temperature The stacking gel was prepared by combining 1.33 ml of 30 % acrylamide/ Bis stock solution in 6.10 ml of deionized water, 2.50 ml of 0.5 M Tris-HCl (pH 6.8), 100 µl of 10 % SDS and 50 µl of 10% APS. Polymerization was initiated by adding 10.0 µl of TEMED. This solution was poured on the top of solidified separating gel and allowed to gel after adding sample combs.

Samples were prepared by appropriately diluting the fractions so that maximum sample concentration is less than 3 µg/ml. To 10 µl of this sample 20 µl each of DI water and sample buffer were added and heated for 3 min in boiling water bath. 40 µl of this sample was then applied to the gel and allowed to run for 15 min at 80 volts initially and then for 40 min at 160 volts. Subsequently, the gel was stained with staining solution for 20 min and destained for 40 min.

Acrylamide/Bis (30% T, 2.67% C)

87.6 g acrylamide (29.2 g/100 mL) 0.24 g N'N'-bis-methylene-acrylamide (0.8 g/100 mL)

Make to 300 mL with deionized water. Filter and store at 4 °C in the dark (30 days maximum.)

Sample Buffer (SDS Reducing Buffer)

Note: Store at room temperature

3.8 mL deionized water, 1.0 mL 0.5 M Tris-HCl, pH 6.8, 0.8 mL glycerol, 1.6 mL 10% (w/v) SDS 0.4 mL 2- Mercaptoethanol, 0.4 mL 1.0 % (w/v) bromophenol blue, 8.0 mL total volume.

Dilute the sample at least 1:4 with sample buffer, and heat at 95 °C for 4 minutes.

5X Electrode (Running) Buffer, pH 8.3

30.3 g Tris base, 144.0 g Glycine, 10.0 g SDS

Dissolve and bring total volume up to 1,000 mL with deionized water. Do not adjust pH with acid or base. Store at 4 °C. If precipitation occurs, warm to room temperature before use. Use: Dilute 50 mL of 10x stock with 450 mL deionized water for each electrophoresis run. Mix thoroughly before use.

10% APS (fresh daily) Dissolve 100 mg ammonium persulfate in 1 mL of deionized water.

CHAPTER 3

RESULTS

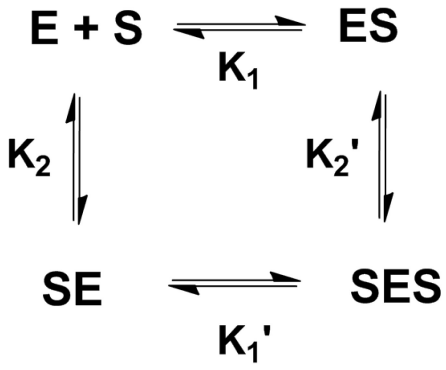

Scheme A1. Kinetic model for substrate analog (S) binding at the regulatory and active sites of YPDC (E). Species SE represents fraction enzyme with S bound at the regulatory site. Species ES represents fraction enzyme with S bound at the active site. Species SES represents fraction enzyme with S bound at both sites. This model yields the following equation:

$$CD = \frac{CD_{max} \bullet (K_2^{'}S + S^2)}{S^2 + (\frac{K_2^{'}K_1}{K_2} + K_2^{'})S + K_1K_2^{'}} \qquad (A.1)$$

Titration data can be fit to the following parametric equation

$$CD = \frac{CD_{max} \bullet (\alpha \times S + \beta \times S^2)}{S^2 + \gamma \times S + \delta} \qquad (A.2)$$

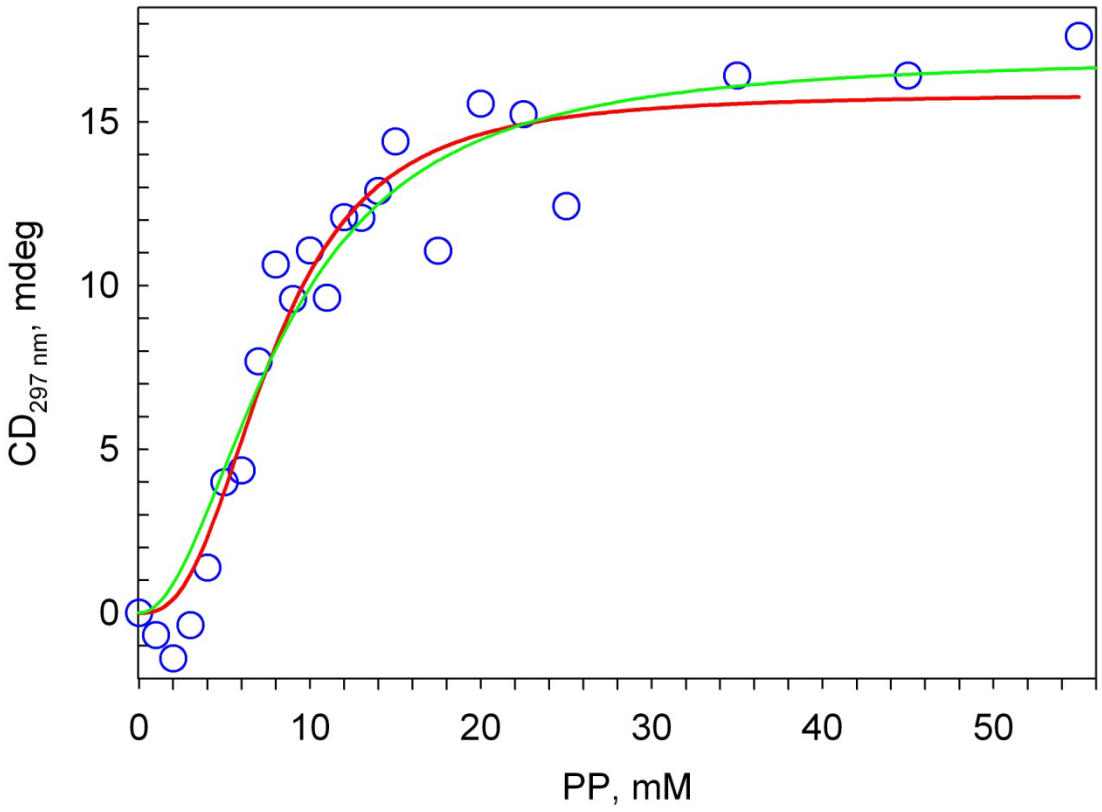

Figure A4. CD titration data pertaining to formation of 1',4'-iminophosphinolactylThDP fit to two different models. Blue circles: CD titration data. Red: Regression fit trace of data fit to Hill equation (R^2 = 0.9493). Green: Regression fit trace data fit to equation A.2 representing binding model described in Scheme A1 (R^2 = 0.9429).

While both models fit the data with comparable goodness of fit, fitting the data to equation A.2 yielded parameters with large standard errors. This indicates that while both models fit the experimentally observed data, the sample size is not large enough to determine accurately the values of parameters in equation A.2.

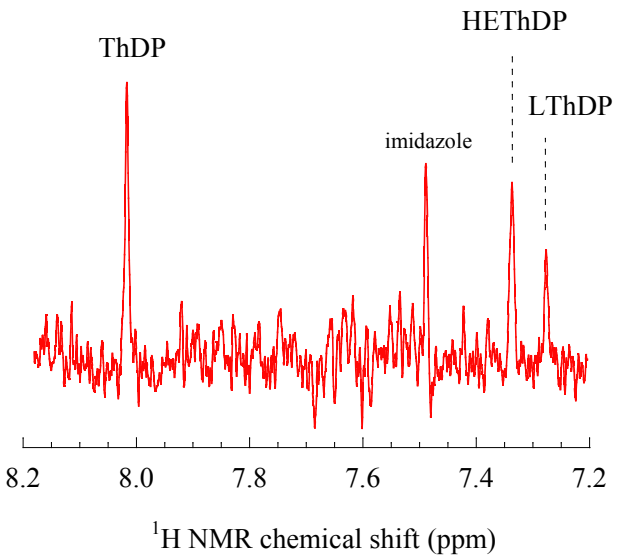

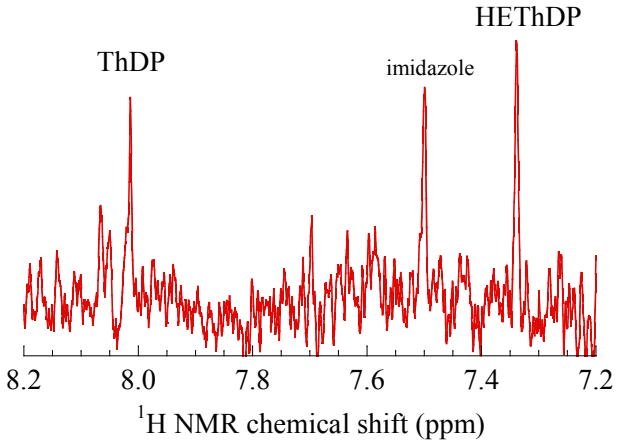

Figure A5. C6' – H fingerprint region in 1H NMR spectra.ThDP covalent intermediate distribution during pre-steady state (Top) and steady state (Bottom) regimes of the reaction of E51D YPDC(20 mg/mL) with pyruvate (20 mM). Experiment performed by Dr. Kai Tittmann at Martin-Luther University, Halle. Figure reproduced here with permission.

Intermediate distribution E51A YPDC pre-steady-state (2 sec)

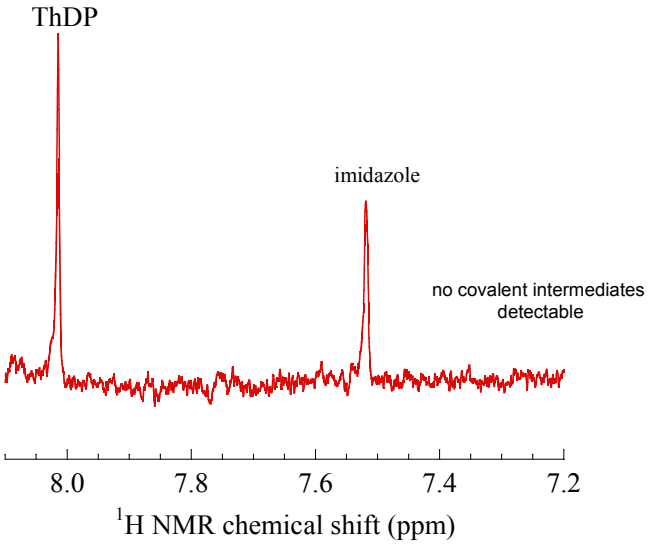

Intermediate distribution E51A YPDC steady-state

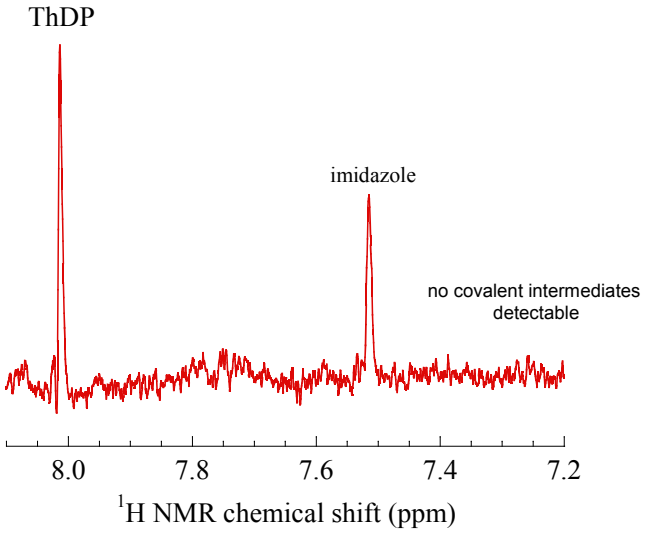

Figure A6. C6' – H fingerprint region in 1H NMR spectra. ThDP covalent intermediate distribution during pre-steady state (Top) and steady state (Bottom) regimes of the reaction of E51A YPDC(20 mg/mL) with pyruvate (20 mM). Experiment performed by Dr. Kai Tittmann at Martin-Luther University, Halle. Figure reproduced here with permission.

Intermediate distribution of YPDC wild-type under different conditions

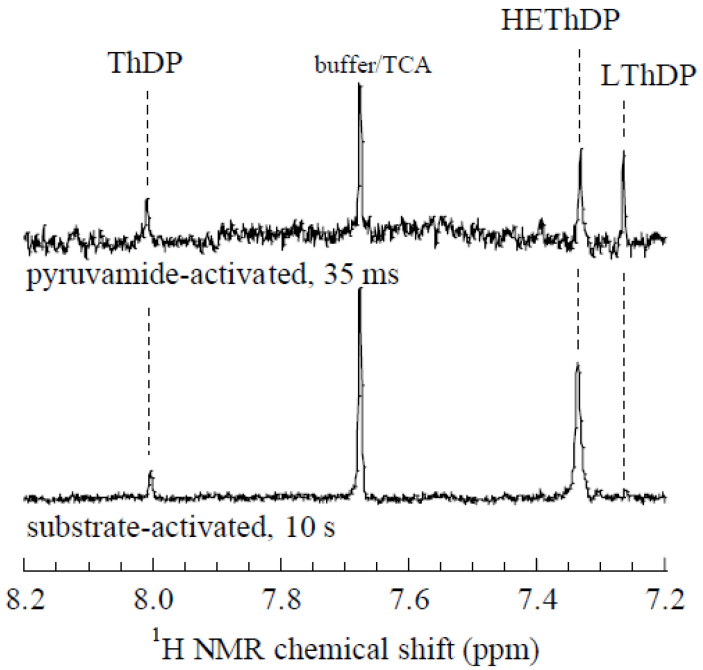

Figure A7. C6' – H fingerprint region in 1H NMR spectra. ThDP covalent intermediate distribution during pre-steady state under pyruvamide activation (Top) and steady state (Bottom) regimes of the reaction of YPDC(20 mg/mL) with pyruvate (20 mM). Experiment performed by Dr. Kai Tittmann at Martin-Luther University, Halle. Figure reproduced here with permission.

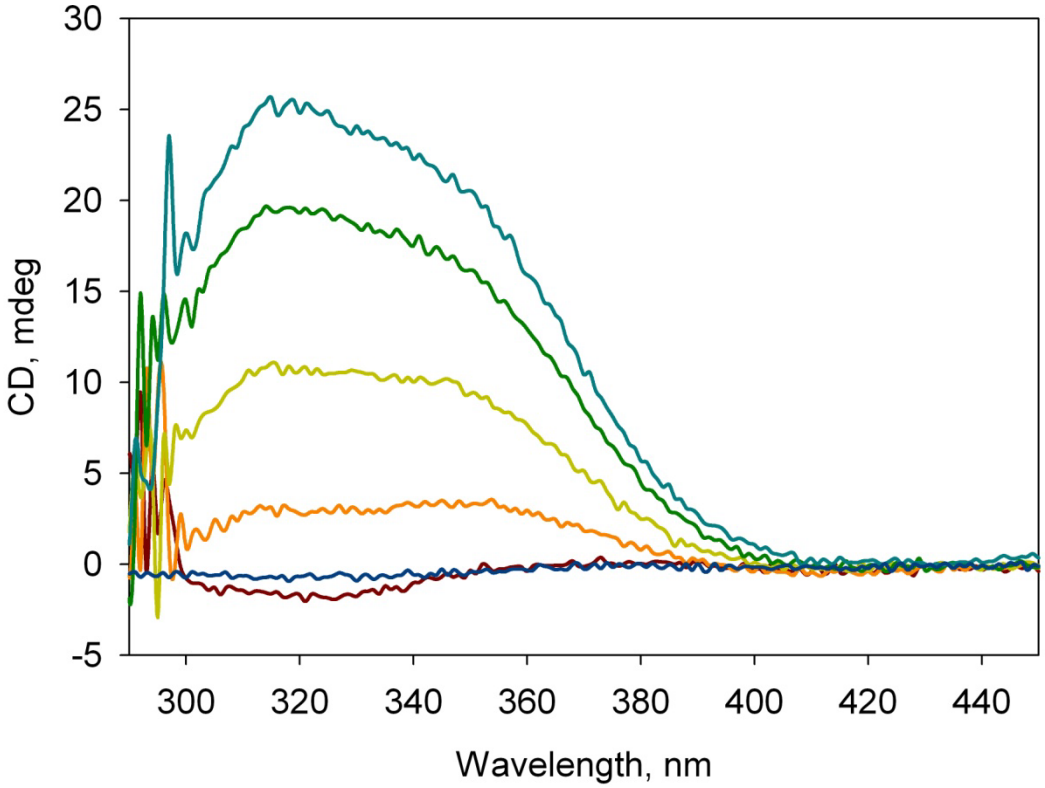

Figure A8. Representative CD spectra of E1p titration with propionylphosphinate (PP). E1p (5 mg/mL) was titrated with varying amounts of PP (1 μM – 500 μM) in 20 mM KH_2PO_4 buffer pH 7.0 containing 0.5 mM ThDP and 2.5 mM Mg^{2+} at 25 ºC. A positive CD band pertaining to 1',4'-imino-C2α-phosphinolactylThDP formed in the active sites is seen developing at 320 nm with increasing PP concentrations.

VITA

Anand Balakrishnan

1982 Born September 13 in Salem, India.

2000 Graduated from Gautami Junior College, Hyderabad, India.

2000-04 Attended Birla Institute of Technology & Science (BITS), Pilani, India.

2004 B.Pharm., (Hons.) First Class, BITS, Pilani, India.

2004-11 Graduate work in Chemistry, Rutgers University, Newark, New Jersey.

2004-08 Teaching Assistantship, Department of Chemistry.

2008-11 Graduate Assistantship, Department of Chemistry.

2009 Article: Chakraborty, S., Nemeria, N. S., Balakrishnan, A., Brandt, G. S., Kneen, M. M., Yep, A., McLeish, M. J., Kenyon, G. L., Petsko, G. A., Ringe, D., and Jordan, F. (2009) Detection and time course of formation of major thiamin diphosphate-bound covalent intermediates derived from a chromophoric substrate analogue on benzoylformate decarboxylase, *Biochemistry 48*, 981-994.

2009 Article: Nemeria, N. S., Chakraborty, S., Balakrishnan, A., and Jordan, F. (2009) Reaction mechanisms of thiamin diphosphate enzymes: defining states of ionization and tautomerization of the cofactor at individual steps, *FEBS J 276*, 2432-2446.

2011 Article: Paramasivam, S., Balakrishnan, A., Dmitrenko, O., Godert, A., Begley, T.P., Jordan, F., Polenova, T. (2011) Solid-state NMR identification and density functional theory studies of ionization states of thiamin, *J. Phys. Chem. B. 115(4), 730-736.*

2011 Ph.D. in Chemistry.